

Fifth International Conference

MMM 2010

Multiscale Materials Modeling

October 04 - 08, 2010, Freiburg, Germany

CONFERENCE PROCEEDINGS

Editors:
Peter Gumbsch
Erik van der Giessen

FRAUNHOFER VERLAG

Organized by Fraunhofer Institute
for Mechanics of Materials IWM.
Hosted by University of Freiburg.



Supported by



Micromechanics

Twin toughening in ferroelectric materials: effect of microstructure on the fracture process

Amir Abdollahi, Irene Arias

**Laboratori de Càlcul Numéric
Departament de Matemàtica Aplicada III
Universitat Politècnica de Catalunya
Jordi Girona 1-3 E-08034 Barcelona, Spain
e-mail: irene.arias@upc.edu**

ABSTRACT

We present a phase field model for the coupled simulation of microstructure formation and evolution and the nucleation and propagation of cracks in single crystal ferroelectric materials. Based on variational approaches, the total energy of a ferroelectric material considering brittle fracture is introduced. Simulation results show a twin formation during crack propagation. Interactions between the twins and the crack are investigated under mechanical and electro-mechanical loads. Various effects of these interactions on the crack propagation such as the fracture toughening are also evaluated. The results prove the capabilities of the proposed model to establish a link between the material microstructure and the crack propagation.

1. Introduction

Ferroelectric ceramics are a family of brittle and multi-phase materials possessing unique electromechanical coupling properties. These materials are employed commonly as sensors, actuators and transducers. The microstructure of these materials is strongly dependent on the loading conditions. Microstructural changes also happen around pre-existing or propagating cracks due to interactions between the crack tip stress fields and the localized switching phenomena in this zone. This suggests that these microscopic phenomena should be taken into account in the analysis of the fracture behavior of ferroelectrics. One important aspect is the fracture toughening governed by ferroelectric twins or domains. The formation and arrangement of the twins around the crack can inhibit the crack propagation. To simulate this phenomenon, a mathematical model is proposed based on phase field, variational approaches to ferroelectric domain evolution and crack propagation [1]. To derive the microstructural evolution, we follow the phase field model based on a Ginsburg-Landau description of ferroelectric materials [2]. This family of continuum models explicitly describes the formation and evolution of individual ferroelectric domains in single crystals. Regarding the model of brittle fracture, we follow a regularized variational formulation of brittle fracture, which allows crack nucleation, branching, path identification, and interaction between multiple cracks without remeshing [3]. This formulation involves the minimization of a total energy with respect to any admissible crack set and displacement field, which can be efficiently performed with specialized numerical algorithms. The variational character of these two distinct theories allows for a natural coupling. The general form of the total energy is introduced in the next section. Simulation results are also presented to investigate interactions between the material microstructure and the crack propagation.

2. Coupled Model

The total energy of a ferroelectric body occupying a region Ω may be written as

$$H_\kappa[\mathbf{u}, \mathbf{p}, \phi, v] = \int_\Omega [(v^2 + \eta_\kappa)F[\mathbf{u}, \mathbf{p}] + H_{es}(\mathbf{p}, \nabla\phi)] \, d\Omega + G_c \int_\Omega \left[\frac{(1-v)^2}{4\kappa} + \kappa|\nabla v|^2 \right] \, d\Omega, \quad (1)$$

where \mathbf{u} is mechanical displacement, \mathbf{p} is polarization, ϕ is electric potential, F is the electro-elastic energy density and G_c is the critical energy release rate or the surface energy density in Griffith's theory. The scalar field v provides a diffuse representation of the fracture zone, κ is a positive regularization constant to regulate the diffusion of the fracture zone and η_κ is a positive small value to avoid the singularity of the first part of the energy. This functional is minimized in subsequent load increments, imposing additionally an irreversibility condition, namely that the field v (informally, a measure of the *integrity* of the material) can only decrease at any point in space during the incremental process. It has been shown that, as long as η_κ converges to zero faster than κ , this regularized theory converges to the sharp theory of brittle fracture. This means that the minimizers of this energy will develop localized features, in particular localized regions with low or zero values of v , where the smeared crack is located. Indeed, for sufficiently small κ , the value of v becomes close to zero in a neighborhood of the fracture zone, and close to one outside. The multi-well energy density F for ferroelectric materials is defined such that it has four minima corresponding to the four variants of the tetragonal phase with normalized polarization $\mathbf{p}' = (1,0), (0,1), (-1,0)$ and $(0,-1)$. The electro-static energy density H_{es} is associated with the polarization and the electric field $\mathbf{E} = -\nabla\phi$ and it is defined according to the crack face boundary conditions we want to model. Here we consider permeable conditions, which assume that the crack is electrically perfect. The first and second parts of the total energy in Eqn. (1) represent the bulk and surface energy contributions, respectively. The proposed algorithm to minimize the total energy performs alternating energy minimizations with respect to polarization, mechanical displacement, electric potential and v subsequently. Iterating this algorithm until convergence leads to a steady state formation of ferroelectric domains and the fracture zone for each load step, which physically means that the load is applied much slower than the relaxation time of the microstructure.

3. Numerical Simulations

The model has been exercised with different electro-mechanical loads and different initial polarization orientations [1]. Here, we show a set of representative simulations. A square cell is discretized with finite elements and a monotonically increasing mechanical displacement is applied on the top and bottom sides of the square to pull both sides gradually with time. This mechanical load effectively guarantees the initiation and evolution of a crack through the model. The top and bottom sides of the model are fixed at zero electric potential. The model is polarized with an initial horizontal polarization. Four steps of ferroelectric domains evolution and crack propagation are presented in Fig. 1. Switched polarization vectors form a wing-shaped twins in front of the crack tip in Fig.1(a). These twins grow with the load until they reach the boundary of the model at top and bottom sides. Further growth of these twins are accommodated by a formation of multiple twins presented in Fig.1(b). This kind of twinning resembles a process zone where multiple twins interact with the crack tip. To evaluate the effects of twinning on the crack propagation, the evolution of the normalized surface energy as a function of the load step is presented in Fig.2. This graph is also obtained for a single-phase material by running

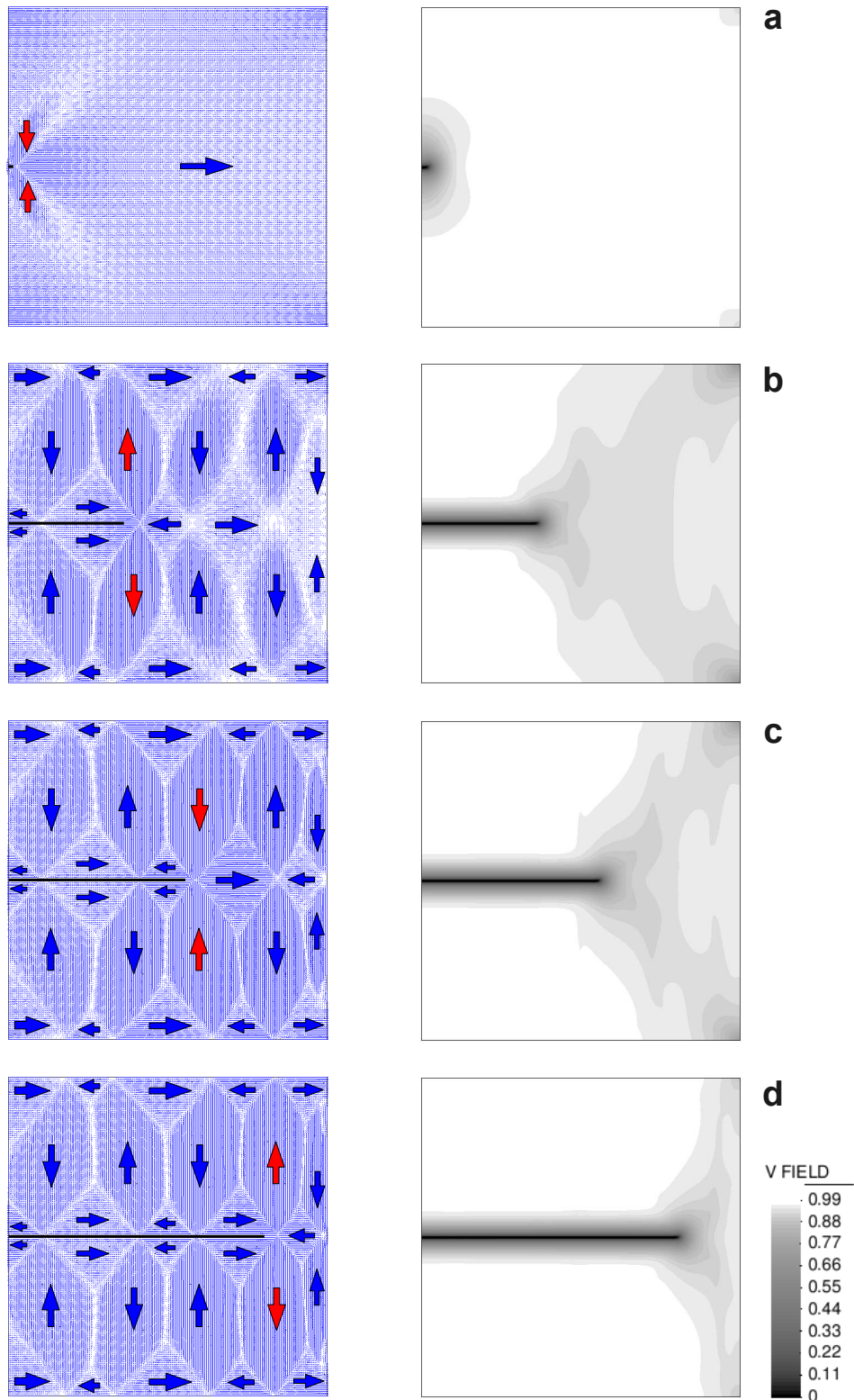


Figure 1: Microstructure fracture evolution at four load steps. The left column is the evolution steps of domains or microstructure and the right column is the corresponding steps of fracture propagation. Domains orientations are indicated with arrows and the fracture zone is presented with the contour of v field. The filtered area of the v field ($v = 0$) is the black line which shows the crack position in each step. The red arrows represent the twins in front of the crack tip.

the simulation with the fixed polarization. Since twinning does not happen in the single-phase model, its surface energy evolution is considered as a reference graph to be compared with the multi-phase one. The four steps presented in Fig.1 are marked with the points in Fig.2. It is obvious in this figure that the energy of multi-phase model is gradually separated from the single-phase graph and it shows slower evolution rate. This is a retarding effect of the 90° ferroelastic domain switching on the crack propagation. This effect becomes more pronounced as the switched zone grows and wing-shaped twins appear in front of the crack tip in Fig.1(a). The energy evolution during the following load steps shows a slow-fast crack propagation. This is due to the formation of multiple twins in front of the crack presented in Fig.1(b)-(d). The corresponding points b, c and d in Fig.2 indicate the starting points of the slow crack propagation. Owing to the longer c axis, compressive stresses in the y direction are induced by the vertical twins, leading to this strong toughening effect.

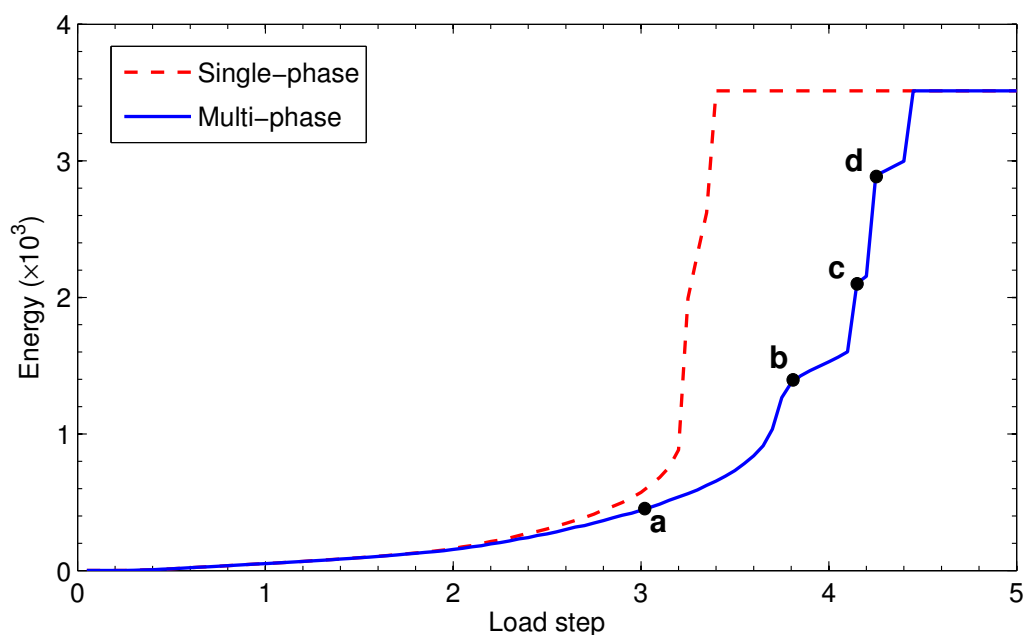


Figure 2: Evolution of the surface energy as a function of the load step. The graphs are obtained considering single and multi-phase models. The points correspond to the load steps in Fig.1.

Acknowledgements

The support of the Ministerio de Ciencia e Innovación (DPI2007-61054) is gratefully acknowledged.

References

- [1] A. Abdollahi and I. Arias. *Submitted for publication*, 2010.
- [2] W. Zhang and K. Bhattacharya. A computational model of ferroelectric domains. Part I: model formulation and domain switching. *Acta Materialia*, **53**, 185–198, 2005.
- [3] G.A. Francfort and J.-J. Marigo. Revisiting brittle fracture as an energy minimization problem. *Journal of the Mechanics and Physics of Solids*, **46**(8), 1319–1342, 1998.

Interplay between fast crack dynamics and surface reconstructions in Silicon brittle fracture

Tristan Albaret¹, Delia Fernandez-Torre² and Alessandro De Vita³

¹Laboratoire de Physique de la Matière Condensée et Nanostructures, Université Lyon 1/CNRS UMR 5586, 43 Bld du 11 Novembre, 69622 Villeurbanne, France

²Instituto de Estructura de la Materia, Madrid, Spain

³Kings College London, Department of Physics, London, UK
(contact : tristan.albaret@lpmcn.univ-lyon1.fr)

Brittle fracture has long been a system of choice to develop multi-scale modeling schemes for material science. However, despite number of theoretical simulations approaches (ref. 1,2,3) many intriguing experimental observations are still not satisfactorily explained, especially because they may depend on the detailed dynamical behaviour of the advancing tip.

This is for instance the case of fast Silicon cracks travelling along the [-211] direction and opening (111) surfaces. Post-mortem *STM* experiments have shown that a majority of steps on the cleaved surface do have a specific symmetry ([2-1-1] steps) while the atomic structures observed on the terraces are (2x1) π -bonded reconstructions (ref. 4). At first sight this propensity to form steps seems to be in contradiction with the stability of the same crack system under loading conditions that include a large shear component (ref. 5,6).

To disentangle these questions we have used the *LOTf* ("learn on the fly") *QM/MM* scheme to study the Si(111)[-211] crack system (ref. 7,8). The simulations consist in molecular dynamics runs including $\sim 200\,000$ silicon atoms among which only a few hundreds around the crack tip are treated at the quantum level while the rest of the system is described with empirical classical potentials.

Our results highlight the interplay between the dynamics of the π -bonded surface reconstructions and the fracture process itself. Namely, calculations under mixed mode I-II loading (tensile + shear) suggest that the apparent contradiction between the above mentioned experimental results could be explained by the structural asymmetry between the π -bonded reconstructions on the opposite cleavage surfaces. Following our analysis we finally draw some predictions concerning the atomic structures of the (111) facets obtained under mixed mode I-II loading.

References :

- 1) G. S. Smith, E. B. Tadmor, N. Bernstein and E. Kaxiras *Acta mater.* 49 (4089) 2001
- 2) N. Bernstein, D. W. Hess *Phys. Rev. Lett.* 91 (02501) 2003
- 3) T. Hoshi, Y. Iguchi and T. Fujiwara *Phys. Rev. B* 72 (075323) 2005
- 4) R.M. Feenstra and J. A. Stroscio, *Phys. Rev. Lett.* 59 (2173) 1987
- 5) D. Sherman and I. Be'ery, *Scripta Materialia* 49 (551) 2003
- 6) R. Pérez and P. Gumbsch, *Phys. Rev. Lett.* 84 (5347) 2000
- 7) G. Csányi, T. Albaret, M. C. Payne and A. De Vita *Phys. Rev. Lett.* 93 (175503) 2005
- 8) J. Kermode, T. Albaret, D. Sherman, N. Bernstein, P. Gumbsch, M. C. Payne, G. Csányi and A. De Vita *Nature* 455 (1224) 2008

A damage-coupled material law for semicrystalline polyethylene

José A. Alvarado-Contreras¹, Maria Anna Polak² and Alexander Penlidis³

¹Machine Design and Modelling Group, University of the Andes, Mérida, Venezuela

²Department of Civil and Environmental Engineering, University of Waterloo, Canada

³Department of Chemical Engineering, University of Waterloo, Canada
ajose@ula.ve

This work presents a novel damage-coupled micromechanical formulation for semicrystalline polyethylene. The model describes the deformation and degradation processes in polyethylene under uniaxial tension considering the interplay between the amorphous and crystalline phases and following a Continuum Damage Mechanics approach from a microstructural viewpoint. The material morphology is modelled as a collection of inclusions consisting of crystalline material attached to an amorphous layer. The interface region interconnecting the two phases is the plane through which loads are carried. It is assumed that the constitutive model contains complete information about the mechanical behaviour and degradation processes of each constituent. After modelling the two phases independently, the inclusion behaviour is found by applying some compatibility and equilibrium restrictions along the interface plane. The model provides a rational representation of the damage process of the intermolecular bonds holding crystals and of the tie-molecules connecting neighbouring crystallites. For the crystalline phase, the proposed model considers the deformation mechanisms by the theory of crystallographic slip and incorporates the effects of intracrystalline debonding and fragmentation. For the amorphous phase, the model is developed within a thermodynamic framework able to describe the features of the material behavior. Amorphous phase hardening is considered into the model and associated to the molecular configurations arising during the deformation process. The equation governing damage evolution is obtained by choosing a particular form based on internal energy and entropy. The predicted stress-strain behavior and texture evolution are compared with experimental results and numerical simulations from the literature. The proposed model predicts the progressive loss of material stiffness attributed to the crystal fragmentation and molecular debonding of the crystal-amorphous interfaces.

Dilute Discrete Dislocation Dynamics in BCC Crystals

Tellechea E.¹, Ariza M.P.¹, Ortiz M.²

¹Universidad de Sevilla. Camino de los descubrimientos, s.n. 41092-Sevilla, Spain (etellechea@us.es, mpariza@us.es)

²California Institute of Technology, 1200 E. California Blvd. Pasadena, CA 91125 (ortiz@aero.caltech.edu)

ABSTRACT

We present a study of 3D dilute dislocation dynamics in BCC crystals based on discrete crystal elasticity. Ideas are borrowed from discrete differential calculus and algebraic geometry to construct a mechanics of discrete lattices. Stored energy of discrete dislocation loops of increasing size are evaluated as part of discrete dislocation dynamics simulations with fully atomistic resolution.

1. Introduction

The notion of lattice complexes provides a convenient means of manipulating forms and fields defined over the crystal. Atomic interactions are accounted for via linearized embedded atom potentials thus allowing for the application of efficient fast Fourier transform. Dislocations are treated within the theory as energy minimizing structures that lead to locally lattice-invariant but globally incompatible eigendeformations. The discrete nature of the theory automatically eliminates the need for core cutoffs. In order to avoid inordinate computational effort that does not lead to explicit laws of macroscopic behavior, in this work we compute the limiting form of the stored energy in the dilute limit. This limit can be characterized explicitly in terms of key material properties such as the prelogarithmic factor of the discrete dislocation cores, and can be evaluated in $O(N)$ time, in contrast to conventional dislocation dynamics approaches where the calculation of stored energies requires $O(N^2)$ time, thus effectively supply a Fast Multiscale Model of dislocation dynamics.

2. Stored Energy of Discrete Dislocations

Within the harmonic approach, the energy of a crystal is a convex function of the displacement field. The underlying crystalline structure, however, allows for displacements that leave the lattice-invariant. In this way, the total energy of a crystal is a non-convex function of the displacements when crystallographic slip is allowed. In this context we apply the theory of eigendeformations¹. The plastic distortion in a slipped crystal may be written as

$$\beta_{ij} = \sum_{\alpha=1}^N \gamma^\alpha s_i^\alpha m_j^\alpha \quad (1)$$

the sum runs over all the available slip systems in the crystals. The energy of the crystal, as a functional of the displacement field and the eigendeformation, is given by

$$E(u, \beta) = \int_V \frac{1}{2} C_{ijkl} (u_{i,j} - \beta_{ij})(u_{k,l} - \beta_{kl}) dV \quad (2)$$

which is now quadratic in the elastic distortion field $\beta_{ij}^e = u_{i,j} - \beta_{ij}$ and piecewise quadratic in $u_{i,j}$ where C_{ijkl} are the usual elastic moduli.

2.1 Eigendeformations in Discrete Lattices

Analogously, within the discrete formulation, the energy of a harmonic crystal admits the representation³

$$E(\mathbf{u}) = \frac{1}{2\pi} \int_{[-\pi,\pi]^n} \frac{1}{2} \langle \hat{\Psi}(\theta) \widehat{d\mathbf{u}}(\theta), \widehat{d\mathbf{u}}^*(\theta) \rangle d^n \theta \quad (3)$$

$$E(\mathbf{u}) = \frac{1}{2\pi} \int_{[-\pi,\pi]^n} \frac{1}{2} \langle \hat{\Phi}(\theta) \hat{\mathbf{u}}(\theta), \hat{\mathbf{u}}^*(\theta) \rangle d^n \theta \quad (4)$$

where Ψ and Φ are the force-constant fields of the lattice and $*$ denotes the convolution operation. The force-constant fields are related as

$$\hat{\Phi} = \mathbf{Q}_1^T \hat{\Psi} \mathbf{Q}_1^* \quad (5)$$

where \mathbf{Q}_1 is the matrix that provides the Discrete Fourier Transform (DFT) representation of the differential operator for 1-forms³. In the spirit of the eigendeformation theory, the elastic energy may be assumed to be of the form

$$E(\mathbf{u}, \beta) = \frac{1}{2} \langle \mathbf{B}(d\mathbf{u} - \beta), d\mathbf{u} - \beta \rangle \quad (6)$$

which replaces representation (3) in the presence of eigendeformations. The equilibrium problem is given by

$$\mathbf{A}\mathbf{u} = \mathbf{f} + \delta\mathbf{B}\beta \quad (7)$$

where $\delta\mathbf{B}\beta$ may be regarded as a distribution of eigenforces corresponding to the eigendeformations β . Provided that the lattice is stable, the equilibrium displacements follow as

$$\mathbf{u} = \mathbf{A}^{-1}(\mathbf{f} + \delta\mathbf{B}\beta) \quad (8)$$

Finally, the corresponding minimum potential energy is

$$F(\beta) = \frac{1}{2} \langle \mathbf{B}\beta, \beta \rangle - \frac{1}{2} \langle \mathbf{A}^{-1} \delta\mathbf{B}\beta, \delta\mathbf{B}\beta \rangle \quad (9)$$

In the theory of continuously distributed elastic dislocations, a result of Mura¹ shows that the energy $E(\beta)$ can in fact be expressed directly as a function $E(\alpha)$ of the dislocation density field α and is independent of the choice of slip distribution β used to define α . By virtue of the discrete Hodge-Helmholtz decomposition for perfect lattices³, the energy in function of density dislocation can be written as

$$E(\alpha) = \frac{1}{2} \langle \mathbf{B}\delta\Delta^{-1}\alpha, \delta\Delta^{-1}\alpha \rangle - \frac{1}{2} \langle \mathbf{A}^{-1} \delta\mathbf{B}\delta\Delta^{-1}\alpha, \delta\mathbf{B}\delta\Delta^{-1}\alpha \rangle \equiv \frac{1}{2} \langle \Gamma * \alpha, \alpha \rangle \quad (10)$$

where Γ is twice the interaction energy between two unit dislocations. In applications we shall work often with the DFT representation

$$E(\alpha) = \frac{1}{(2\pi)^3} \int_{-\pi}^{\pi} \int_{-\pi}^{\pi} \int_{-\pi}^{\pi} \frac{1}{2} \langle \hat{\Gamma}(\theta) \hat{\alpha}(\theta), \hat{\alpha}(\theta)^* \rangle d\theta_1 d\theta_2 \quad (11)$$

where

$$\hat{\Gamma}(\theta) = \hat{\Delta}_2^{-T} \mathbf{Q}_2^* (\hat{\Psi} - \hat{\Psi} \mathbf{Q}_1^* \hat{\Phi}^{-1} \mathbf{Q}_1^T \hat{\Psi}) \mathbf{Q}_2^T \hat{\Delta}_2^{-1} \quad (12)$$

If the force constants are of finite range, i. e., if Φ and Ψ vanish for all but a finite number of sites, then the sum that gives their DFT is finite and it follows that $\hat{\Phi}, \hat{\Psi} \in C^\infty([-\pi, \pi]^3)$. If, in addition, the lattice is stable and has no soft modes, then $\hat{\Phi}$ and $\hat{\Psi}$ are invertible in the perforated Brillouin zone $[-\pi, \pi]^3 \setminus \{0\}$ and, hence, $\hat{\Phi}^{-1}, \hat{\Psi}^{-1}$ and, by extension, $\hat{\Gamma}(\theta)$ are likewise smooth in that set. Since the set E_2 of 2-cells in BCC defines a Bravais lattice, it follows that $\hat{\Gamma}(-\theta) = \hat{\Gamma}(\theta)$, i. e., $\hat{\Gamma}(\theta)$ is even. In addition, since $\hat{\Gamma}(\theta)$ is the DFT of a real-valued function we have $\hat{\Gamma}^*(\theta) = \hat{\Gamma}(-\theta) = \hat{\Gamma}(\theta)$, whence it follows that $\hat{\Gamma}(\theta)$ is itself real valued.

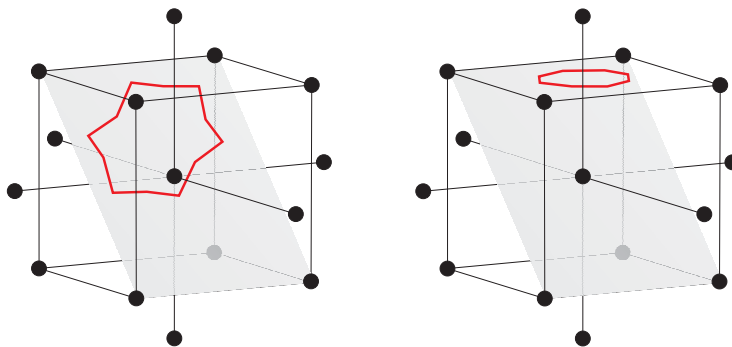


Figure 1: Elementary dislocation loops (generators of the group B^2) for the body-centered cubic lattice. Elementary loop on a cartesian segment (right) and elementary loop on a diagonal segment (left).

3. Applications

As a first illustration of the theory, we have computed the stored energy of dislocation loops of increasing size embedded in periodic cells in a BCC crystal. Within the dual space we can define a dislocation line as an ordered sequence of elementary dual segments. In the present work we have studied different configurations corresponding to closed dislocation lines obtained as a sum of elementary dislocation loops (Fig. 2). In all cases, the simulation cells contain 1 million molybdenum atoms ($N = 100$). The computed stored energy values are listed in Table 1.

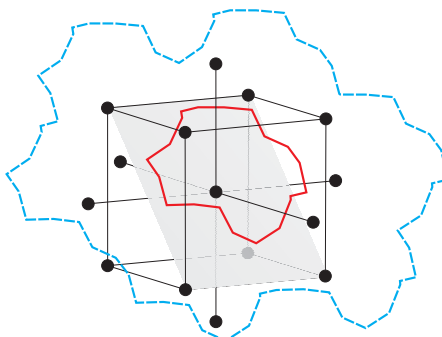


Figure 2: Dislocation lines as a sum of 4 (continuous line) and 28 (dashed line) elementary dislocation loops.

Table 1: Stored energy values obtained for dislocation loops of increasing size.

Elementary loops	Stored Energy [eV]
1	1.92
4	4.76
28	23.52

4. Summary and conclusions

We have presented an application of the discrete theory of dislocations of Ariza and Ortiz³ to the analysis of dislocations in BCC crystals. We have presented a discrete model for the calculation of the stored energy in a crystal containing a closed dislocation loop as part of a Fast Multiscale Model of dislocation dynamics leading to the explicit characterization of work hardening.

Acknowledgements

We gratefully acknowledge the support of the Ministerio de Educación y Ciencia of Spain (DPI2009-14305-C02-01), the support of the Consejería de Innovación of Junta de Andalucía (P09-TEP-4493) and the support of the Department of Energy National Nuclear Security Administration under Award Number DE-FC52-08NA28613 through Caltech's ASC/PSAAP Center for the Predictive Modeling and Simulation of High Energy Density Dynamic Response of Materials.

References

- [1] Mura, T. Micromechanics of defects in solids. *Kluwer Academic Publishers*, Boston, 1987.
- [2] Hirth, J.P., Lothe, J. Theory of Dislocations. *Wiley*, Florida, 1982.
- [3] Ariza, M.P., Ortiz, M. Discrete crystal elasticity and discrete dislocations in crystals. *Arch. Ration. Mech. Anal.*, **178**, 149–226, 2005.
- [4] Ramasubramanian, A., Ariza, M.P., Ortiz, M. A discrete mechanics approach to dislocation dynamics in BCC crystal. *Arch. Ration. Mech. Anal.*, **55**, 615–647, 2007.

Dislocation densities and size dependent deformation of polycrystals

Swantje Bargmann, Bob Svendsen

Institute of Mechanics
Dortmund University of Technology
44221 Dortmund
Germany

swantje.bargmann@tu-dortmund.de
bob.svendsen@tu-dortmund.de

ABSTRACT

The purpose of this work is the formulation of models for extended or gradient crystal plasticity via the application of a recently developed rate variational approach to the formulation of continuum thermodynamic models for history-dependent, inelastic systems. The approach is based on the formulation of rate potentials whose form is determined by (i) energetic processes via the free energy, (ii) kinetic processes via the dissipation potential, and (iii) the form of the evolution relations for the internal-variable-like quantities upon which the free energy and dissipation potential depend. For the case of extended crystal plasticity, these latter quantities include for example the inelastic local deformation, or dislocation densities. In the current work, two classes of dislocation densities are considered.

1. Continuum thermodynamic framework

To begin, we summarize briefly the results of the continuum thermodynamic rate variational formulation of Svendsen and Bargmann [15] to multiscale crystal plasticity based on [14, 12]. For simplicity, attention is restricted to quasi-static, isothermal processes. Let B_r be a reference configuration of the material in question with boundary ∂B_r and outward unit normal \mathbf{n}_r . Further, let $\boldsymbol{\chi}$ be the time-dependent deformation field of the material with respect to B_r , $\mathbf{F} := \nabla^r \boldsymbol{\chi}$ the local deformation or deformation gradient with respect to B_r . The inelastic part \mathbf{F}_P of \mathbf{F} is modeled as usual via the flow rule $\dot{\mathbf{F}}_P = \mathbf{L}_P \mathbf{F}_P$ in terms of $\mathbf{L}_P = \sum_a (\mathbf{s}_a \otimes \mathbf{n}_a) \dot{\gamma}_a$ and the set $\gamma = \{\gamma_1, \dots\}$ of scalar-valued glide-system slip fields. Here, \mathbf{s}_a and \mathbf{n}_a represent the glide direction and glide normal, respectively, of glide-system a . The direction $\mathbf{t}_a = \mathbf{n}_a \times \mathbf{s}_a$ transverse to \mathbf{s}_a in the glide plane is also used in what follows.

The thermodynamic formulation here is restricted to (metallic) crystal plasticity as based on the common constitutive split $\psi_r(\nabla^r \boldsymbol{\chi}, \mathbf{F}_P, \boldsymbol{\epsilon}) = \psi_{E_r}(\mathbf{F}_E(\nabla^r \boldsymbol{\chi}, \mathbf{F}_P)) + \psi_{P_r}(\mathbf{F}_P, \boldsymbol{\epsilon})$ of the referential free energy density ψ_r into elastic ψ_{E_r} and inelastic ψ_{P_r} parts. Here, $\mathbf{F}_E = \nabla^r \boldsymbol{\chi} \mathbf{F}_P^{-1} = \nabla^i \boldsymbol{\chi}$ represents the elastic local deformation, and $\boldsymbol{\epsilon}$ is a set of dislocation densities. The evolution of these is modeled by a relation of the form $\dot{\boldsymbol{\epsilon}}(\dots, \dot{\gamma}, \nabla^r \dot{\gamma})$ quasi-linear in $\dot{\gamma}$ and $\nabla^r \dot{\gamma}$. Together, the constitutive forms of ψ_r , $\dot{\mathbf{F}}_P$ and $\dot{\boldsymbol{\epsilon}}$ determine that $\zeta_r(\dots, \nabla^r \boldsymbol{\chi}, \dot{\gamma}, \nabla^r \dot{\gamma})$ of the energy storage rate density ζ_r . Kinetics-controlled inelastic processes, e.g., dislocation activation, are accounted for in the current approach via a dissipation potential $\chi_r = \chi_r(\dots, \dot{\gamma}, \nabla^r \dot{\gamma})$ for the current isothermal case including lengthscale-dependent activation of dislocation processes [16, 1, 3]. Besides the momentum balance, the stationarity conditions of the rate functional with volume density $\zeta_r + \chi_r$ yield a generalized glide-system flow rule $\sigma_a = \partial_{\dot{\gamma}_a} \chi_r - \text{div}_r(\partial_{\nabla^r \dot{\gamma}_a} \chi_r)$ in B_r in terms of the generalized thermodynamic conjugate $\sigma_a = -\partial_{\dot{\gamma}_a} \zeta_r + \text{div}_r(\partial_{\nabla^r \dot{\gamma}_a} \zeta_r)$ to $\dot{\gamma}_a$.

Here, $-\partial_{\dot{\gamma}_a} \zeta_r$ depends in particular on the Schmid stress $\tau_a = \mathbf{s}_a \cdot \mathbf{F}_E^T \partial_{\mathbf{F}_E} \psi_{Er} \mathbf{n}_a$. In addition, $x_a = -\text{div}_r(\partial_{\nabla^r \dot{\gamma}_a} \zeta_r)$ is the glide-system back stress. For more details, the interested reader is referred to Svendsen and Bargmann [15]. For brevity, attention is focused in the remainder of this work on models for the dislocation densities composing ϵ and the corresponding form of $\psi_{Pr}(\mathbf{F}_P, \epsilon)$. These determine in turn ζ_r , and so σ_a as well as the glide-system back stress x_a .

2. Model examples

A common model class in the literature [e.g., 7, 5, 9, 11, 10, 6, 4] is based on the choice $\epsilon \equiv (\varrho_1^{ss}, \varrho_2^{ss}, \dots, \varrho_1^{gn}, \varrho_2^{gn}, \dots)$ depending on the sets $\varrho_1^{ss}, \varrho_2^{ss}, \dots$ and $\varrho_1^{gn}, \varrho_2^{gn}, \dots$ of scalar dislocation densities¹ for statistically-stored (ss) dislocations (SSDs) and geometrically-necessary (gn) dislocations (GNDs), respectively. As shown in detail in Svendsen and Bargmann [15], the GND models in [7, 5, 9, 11, 10, 6, 4] are all based on generalizations of the Ashby model [2]. For example, the models of Gurtin [10] and Kuroda and Tvergaard [11] are based on the large-deformation generalizations $\dot{\varrho}_a^{ge} = -\mathbf{F}_P^{-1} \bar{\mathbf{s}}_a \cdot \nabla^r \dot{\gamma}_a$ and $\dot{\varrho}_a^{gs} = \mathbf{F}_P^{-1} \bar{\mathbf{t}}_a \cdot \nabla^r \dot{\gamma}_a$ of the Ashby model for pure-edge and pure-screw GND densities, respectively, with $\bar{\mathbf{s}}_a = b \mathbf{s}_a$, $\bar{\mathbf{t}}_a = b \mathbf{t}_a$ and $\bar{\mathbf{n}}_a = b \mathbf{n}_a$. The formulation of this model in the current context is based on the constitutive forms $\psi_{Pr}(\epsilon) = \sum_a \frac{1}{2} h_0^g (|\varrho_a^{ge}|^2 + |\varrho_a^{gs}|^2)$ of the inelastic free energy density in terms of the hardening modulus h_0^g . Then

$$\zeta_{vr} = \partial_{\mathbf{F}_E} \psi_{Er} \mathbf{F}_P^{-T} \cdot \nabla^r \dot{\chi} - \sum_a \tau_a \dot{\gamma}_a - \sum_a h_0^g \varrho_a^{ge} \mathbf{F}_P^{-1} \bar{\mathbf{s}}_a \cdot \nabla^r \dot{\gamma}_a + \sum_a h_0^g \varrho_a^{gs} \mathbf{F}_P^{-1} \bar{\mathbf{t}}_a \cdot \nabla^r \dot{\gamma}_a \quad (1)$$

follows for the stored energy rate density, and so

$$\begin{aligned} \sigma_a &= \tau_a - x_a, \\ x_a &= h_0^g \mathbf{F}_P^{-1} \bar{\mathbf{s}}_a \cdot \nabla^r \varrho_a^{ge} - h_0^g \mathbf{F}_P^{-1} \bar{\mathbf{t}}_a \cdot \nabla^r \varrho_a^{gs} + (h_0^g \varrho_a^{ge} \bar{\mathbf{s}}_a - h_0^g \varrho_a^{gs} \bar{\mathbf{t}}_a) \cdot \mathbf{f}_P, \end{aligned} \quad (2)$$

in terms of the large-deformation-based quantity $\mathbf{f}_P = \text{div}_r \mathbf{F}_P^{-T}$ model by

$$\dot{\mathbf{f}}_P = - \sum_a \{ (\mathbf{s}_a \cdot \mathbf{f}_P) \dot{\gamma}_a + \mathbf{F}_P^{-1} \mathbf{s}_a \cdot \nabla^r \dot{\gamma}_a \} \mathbf{n}_a. \quad (3)$$

For more details, the reader is referred to Svendsen and Bargmann [15].

In a sense, the models of the above class represent GNDs as being of pure edge, or pure screw, character. In general, however, GNDs will be of mixed character. A step in this direction for large deformation is given by the non-dimensional vector-valued measure ϱ_{ia} with $\dot{\varrho}_{ia} = \dot{\varrho}_a^{ge} \mathbf{s}_a + \dot{\varrho}_a^{gs} \mathbf{t}_a$, representing a direct generalization of the Ashby model. Indeed, this is related to the vector-valued (non-dimensional) dislocation density \mathbf{g}_{ra} determining the glide-system-based form $\mathbf{G}_r = \sum_a \mathbf{s}_a \otimes \mathbf{g}_{ra}$ [e.g., 14, 12] of the non-dimensional generalized Nye dislocation tensor \mathbf{G}_r in the context of plastic incompressibility. We have

$$\dot{\mathbf{g}}_{ra} = \mathbf{F}_P^{-1} \dot{\varrho}_{ia} + \dot{\gamma}_a \mathbf{G}_r^T \mathbf{n}_a = \nabla^r \dot{\gamma}_a \times \mathbf{F}_P^T \bar{\mathbf{n}}_a + \dot{\gamma}_a \mathbf{G}_r^T \mathbf{n}_a. \quad (4)$$

Note that $\mathbf{g}_{ia} = \mathbf{F}_P \mathbf{g}_{ra}$ is indeed of mixed character. In particular, $\mathbf{s}_a \cdot \mathbf{g}_{ia}$ represents its screw part, $\mathbf{t}_a \cdot \mathbf{g}_{ia}$ its in-plane edge part, and $\mathbf{n}_a \cdot \mathbf{g}_{ia}$ its out-of-plane edge part. Since $\dot{\varrho}_{ia}$ is perpendicular to \mathbf{n}_a , the evolution of the out-of-plane component $\mathbf{n}_a \cdot \mathbf{g}_{ia}$ of \mathbf{g}_{ia} is not influence by

¹Here in non-dimensional form $\varrho := b^2 \rho$, where b is the Burgers vector magnitude, and ρ the dimensional dislocation density.

the inhomogeneity of $\dot{\gamma}_a$. In this sense, the evolution relation for \mathbf{g}_{ia} is in qualitative agreement with the GND concept of Ashby [2].

Assume now that the dislocation tensor, or its glide-system projection, is a reasonable measure of energy storage due to excess dislocation development in the system. Then $\boldsymbol{\epsilon} \equiv (\mathbf{g}_{r1}, \dots)$ and $\psi_{Pr}(\mathbf{F}_P, \boldsymbol{\epsilon}) = \psi_{Pr}(\mathbf{F}_P, \mathbf{g}_{r1}, \dots)$, yielding

$$\begin{aligned} \zeta_r &= \partial_{\mathbf{F}_E} \psi_{Er} \mathbf{F}_P^{-T} \cdot \nabla^r \dot{\boldsymbol{\chi}} \\ &- \sum_a \{ \tau_a - \mathbf{G}_r \partial_{\mathbf{g}_{ra}} \psi_{Pr} \cdot \mathbf{n}_a - \mathbf{s}_a \cdot \partial_{\mathbf{F}_P} \psi_{Pr} \mathbf{F}_P^T \mathbf{n}_a \} \dot{\gamma}_a \\ &+ \sum_a \mathbf{F}_P^T \bar{\mathbf{n}}_a \times \partial_{\mathbf{g}_{ra}} \psi_{Pr} \cdot \nabla^r \dot{\gamma}_a \end{aligned} \quad (5)$$

and

$$\begin{aligned} \sigma_a &= \tau_a - \mathbf{G}_r \partial_{\mathbf{g}_{ra}} \psi_{Pr} \cdot \mathbf{n}_a - \mathbf{s}_a \cdot \partial_{\mathbf{F}_P} \psi_{Pr} \mathbf{F}_P^T \mathbf{n}_a - x_a, \\ x_a &= \{ \mathbf{F}_P \text{curl}_r \partial_{\mathbf{g}_{ra}} \psi_{Pr} - \mathbf{G}_r \partial_{\mathbf{g}_{ra}} \psi_{Pr} \} \cdot \mathbf{n}_a. \end{aligned} \quad (6)$$

The standard example of $\psi_{Pr}(\mathbf{F}_P, \mathbf{g}_{r1}, \dots)$ is the ubiquitous quasi-quadratic form

$$\psi_{Pr}(\mathbf{F}_P, \mathbf{g}_{r1}, \dots) = \sum_a \sum_b \frac{1}{2} h_{ab} \mathbf{F}_P \mathbf{g}_{ra} \cdot \mathbf{F}_P \mathbf{g}_{rb} \quad (7)$$

formally analogous to such relations for SSD-based hardening [e.g., 8]. Such a form is obtained for example from that

$$\psi_{Pr} = \frac{1}{2} h_0^g |\mathbf{G}_i|^2 = \frac{1}{2} \sum_a \sum_b h_0^g (\mathbf{s}_a \cdot \mathbf{s}_b) \mathbf{g}_{ia} \cdot \mathbf{g}_{ib} \quad (8)$$

with $\mathbf{G}_i = \mathbf{G}_r \mathbf{F}_P^T$ and

$$|\mathbf{G}_i| = \sqrt{\sum_a \sum_b (\mathbf{s}_a \cdot \mathbf{s}_b) \mathbf{g}_{ia} \cdot \mathbf{g}_{ib}}. \quad (9)$$

Then $h_{ab} = h_0^g (\mathbf{s}_a \cdot \mathbf{s}_b)$ is symmetric. Note the role of the direction cosines $\mathbf{s}_a \cdot \mathbf{s}_b$, $a, b = 1, 2, \dots$, between the various glide directions as weighting factors in the form for ψ_{Pr} based on $|\mathbf{G}_i|$. Exactly this type of weighting factor has been derived on the basis of statistical mechanical considerations by Limkumnerd and van der Giessen [13].

Further such considerations as well as additional model examples will be given at the meeting.

Acknowledgements. Partial financial support for this work from the German National Science Foundation (DFG) is gratefully acknowledged.

References

- [1] Anand, L., Gurtin, M., Lele, S.P., Gething, C., 2005. A one-dimensional theory of strain-gradient plasticity: Formulation, analysis, numerical results. *Journal of the Mechanics and Physics of Solids* 53, 1789–1826.
- [2] Ashby, M. F., 1970. The deformation of plastically non-homogeneous materials. *Philosophical Magazine* 21, 399–424.

- [3] Bardella, L., 2006. A deformation theory of strain gradient crystal plasticity that accounts for geometrically necessary dislocations. *Journal of the Mechanics and Physics of Solids* 54, 128–160.
- [4] Bargmann, S., Ekh, M., Runesson, K., Svendsen, B., 2010. Modeling of polycrystals with gradient crystal plasticity: A comparison of strategies. *Philosophical Magazine* 90, 1263–1288.
- [5] Bayley, C.J., Brekelmans, W.A.M., Geers, M.G.D., 2006. A comparison of dislocation induced back stress formulations in strain gradient crystal plasticity. *International Journal of Solids and Structure* 43, 7268–7286.
- [6] Ertürk, I., van Dommelen, J.A.W., Geers, M.G.D., 2009. Energetic dislocation interactions and thermodynamical aspects of strain gradient crystal plasticity theories. *Journal of the Mechanics and Physics of Solids* 57, 1801–1814.
- [7] Evers, L.P., Brekelmanns, W.A.M., Geers, M.G.D., 2004. Non-local crystal plasticity model with intrinsic SSD and GND effects. *Journal of the Mechanics and Physics of Solids* 52, 2379–2401.
- [8] Franciosi, P., Zaoui, A., 1982. Multislip in f.c.c. crystals a theoretical approach compared with experimental data. *Acta Metallurgica* 30, 1627–1637.
- [9] Geers, M.G.D., Brekelmans, W.A.M., Bayley, C.J., 2007. Second-order crystal plasticity: internal stress effects and cyclic loading. *Modeling and Simulation in Material Science and Engineering* 15, S133–S145.
- [10] Gurtin, M.E., 2008. A finite-deformation, gradient theory of single-crystal plasticity with free energy dependent on densities of geometrically necessary dislocations. *International Journal of Plasticity* 24, 702–725.
- [11] Kuroda, M., Tvergaard, V., 2008. A finite deformation theory of higher-order gradient crystal plasticity. *Journal of the Mechanics and Physics of Solids* 56, 2573–2584.
- [12] Levkovitch, V., Svendsen, B., 2006. On the large-deformation- and continuum-based formulation of models for extended crystal plasticity. *International Journal of Solids and Structures* 43, 7246–7267.
- [13] S. Limkumnerd, E. van der Giessen, 2008. Statistical approach to dislocation dynamics: From dislocation correlations to a multiple-slip continuum theory of plasticity. *Physical Review B* 77, 184111-1–184111-12
- [14] Svendsen, B., 2002. Continuum thermodynamic models for crystal plasticity including the effects of geometrically-necessary dislocations. *Journal of the Mechanics and Physics of Solids* 50, 1297–1329.
- [15] Svendsen, B., Bargmann, S., 2010. On the continuum thermodynamic rate variational formulation of models for extended crystal plasticity at large deformation, *Journal of the Mechanics and Physics of Solids* online, doi:10.1016/j.jmps.2010.06.005.
- [16] Uchic, M.D., Dimiduk, D.M., Florando, J.N., Nix, W.D., 2004. Sample dimensions influence strength and crystal plasticity. *Science* 305, 986–989.

Role of discrete intra-granular slip bands on the plastic behavior of poly-crystals

Stéphane Berbenni^{1*}, Camille Perrin^{1,2}, Christophe Collard¹, Horst Vehoff² and Marcel Berveiller¹

¹ Laboratory of Physics and Mechanics of Materials, LPMM, CNRS, Arts et Métiers, Technopole, 57078, Metz Cedex 03, France

² Department of Materials Science, Saarland University, Bldg D22, P.O. Box 151150, D-66041 Saarbruecken, Germany

*Corresponding author: Tel.: +33 3 5500 4034; Fax: +33 3 8737 4284;
Email address: Stephane.Berbenni@metz.ensam.fr (S. Berbenni)

A breakthrough in the general hypothesis of *spatially homogeneous intra-granular fields* accepted in mean field approaches based on the classic Eshelby's inclusion problem is proposed. Intra-granular slip patterns (slip bands...) are modeled in single slip configurations both by distributions of *coaxial circular glide loops* [1] and *flat ellipsoids* (also called *oblate spheroids*) [2] constrained by spherical grain boundaries. The mechanical interactions between slip bands are taken into account to obtain the mechanical fields and the free energy. It is then found that intra-granular mechanical fields strongly depend on the grain size and the slip line spacing. In addition, in the case of glide loops, the modeling is able to capture different behaviors between near grain boundary regions and grain interiors. In particular, a grain boundary layer containing strong gradients of internal stresses and lattice rotations is found. These results are confirmed quantitatively by EBSD measurements of intra-granular misorientations carried out with orientation imaging mapping (OIM) on deformed Ni poly-crystals and on specific grains undergoing "quasi" single slip [3]. Furthermore, as a result of the computation of the free energy, an average back-stress over the grain (in the case of loops) or over slip bands (in the case of oblate spheroids) can be derived so that it is possible to define *new interaction laws for poly-crystal's behavior* which are naturally dependent on internal lengths [2,4]. Hence, using a "diluted" model in terms of concentration of plastic grains, the macroscopic deformation of fcc poly-crystals at very low plastic strains are computed either in rate-independent or rate-dependent plasticity. Contrary to conventional mean-field approaches, internal length scale effects on the initial strain hardening stage are reported for both types of configurations.

References

- [1] S. Berbenni, M. Berveiller, T. Richeton. Int. J. Solids Struct. 45 (2008), 4147.
- [2] C. Collard, V. Favier, S. Berbenni, M. Berveiller. Int. J. Plast. 26 (2010), 310.
- [3] C. Perrin, S. Berbenni, H. Vehoff, M. Berveiller. Acta Mater. (2009), submitted.
- [4] T. Richeton, S. Berbenni, M. Berveiller. Acta Mater. 57 (2009), 1347.

Directional Deformation Memory in Metallic Glasses: Insights from Atomistic Simulations for Mesoscale Modeling

Erik Bitzek¹ and Ju Li²

¹Department of Materials Science and Engineering, University Erlangen-Nürnberg, Martensstr. 5, Erlangen 91058, Germany, erik.bitzek@ww.uni-erlangen.de

²Department of Materials Science and Engineering, University of Pennsylvania, Philadelphia, Pennsylvania 19104, USA

A fundamental difficulty for modeling in metallic glasses (MGs) is the inherent multi-scale nature of the involved processes. For example, the activation of shear transformation zones (STZs), the smallest flow defects in MGs, takes place on a timescale of tens of picoseconds, whereas the formation of shear bands (SBs) occurs over periods up to milliseconds. Similarly, the SB thickness can exceed hundreds of nanometers, and the produced shear offset can be in the micron range, whereas the sizes of STZs are of the order of nanometers.

In contrast to crystalline materials, where the multiscale modeling approach has been well established by passing information between atomistic simulations, dislocation dynamics and crystal plasticity models, the development of mesoscale and constitutive models of MG plasticity is still in its infancy. This is in part due to the lack of an adequate description of deformation induced structural damage, and of how this damage affects mechanical softening and STZ operation. In particular, the homogeneous deformation of MGs is currently believed to be isotropic and damage due to prior deformation is usually characterized by scalar variables like the generation of excess free volume or the decrease in topological short range order.

Here we show evidence for the need of directional state variables to model appropriately MG deformation. Molecular dynamics (MD) simulations and experiments using elastostatic compression on CuZr-based MGs show that homogeneous deformation by uniaxial compression affects the subsequent deformation in the directions *orthogonal* to the initial loading direction. A detailed analysis of the simulations results relates this behavior to irreversible structural changes during the initial deformation. The implications for mesoscopic modeling of MGs are discussed, and an STZ based computational model is presented which utilizes statistical information about shear transformations and damage accumulation from atomistic simulations.

Plastic deformation mechanisms in nanocrystalline FCC metals: A Molecular Dynamics Study

C Brandl¹, H. Van Swygenhoven¹

¹Paul Scherrer Institute, NUM/ASQ, Materials Science and Simulation, CH-5232 Villigen
PSI, Switzerland
christian.brandl@psi.ch

Large scale molecular dynamics studies of FCC nanocrystalline (nc) metals provide an approach to relate the atomic-scale processes to the mechanical response in the high strain-rate / stress regime at room temperature. Simulations revealed two major deformation mechanisms: intergranular processes (grain boundary sliding and migration) and intragranular processes involving partial dislocation activity. In particular grain boundaries can act as source and sink for partial and perfect dislocations. Moreover, dislocation propagation can be significantly affected by the surrounding grain boundary structure in terms of dislocation pinning and dislocation cross-slip.

A parameter study on the temperature, applied stress, strain rate and grain size dependence indicates that the deformation behavior is related to the rate dependence of the dislocation activity and the disorder effect of different dislocation environments. Moreover, the high stress regime forces a subset of dislocation processes to operate beyond the rate-dependent regime, which indicates once more the difficulty to extrapolate from the molecular dynamics simulations to usual experimental conditions. More generally, the parameter dependence (stress, temperature and grain size) of the flow stress will be discussed in terms of thermally activated dislocation processes and the therein lying implications on a grain size dependence.

Towards combining Molecular Dynamics and Dislocation Dynamics to study Fatigue Crack Propagation

Steffen Brinckmann¹, Dhiraj K. Mahajan¹ and Alexander Hartmaier¹

¹Interdisciplinary Centre for Advanced Materials Simulation (ICAMS),
Stiepel Str. 129, Ruhr-Universität Bochum, Germany
Steffen.Brinckmann@rub.de

Near-threshold fatigue crack propagation is fatal for many engineering applications ranging from train wheels to sensing devices on the micrometer scale. During this failure mechanism only a small material domain deforms plastically and the crack growth takes place on a scale of Angstroms per cycle. Although the crack advance per load-cycle is minute, structures fail due to this mechanism by accumulation of crack advance during many million cycles. This study aims at understanding the fatigue crack propagation mechanisms. It will investigate small-scale dislocation activity in the proximity of the crack tip and crack advance.

To accomplish this, a multiscale model using Molecular Dynamics (MD) and Discrete Dislocation Dynamics (DDD) is being established. The domain around the crack tip, in which dislocations nucleate and the crack grows, is simulated by MD and thus free of phenomenological rules and assumptions. However, the spatial domain of the MD domain is small due to the computational expense of the model. To overcome this limitation, in our model the MD domain is surrounded by a numerically efficient DDD domain, in which the motion of discrete dislocations is studied. We make sure that dislocations can move from the MD domain into the DDD domain and do not pile up at the interface. The multiscale model uses the concept of point-forces to glue both models of different spatial scales.

In this contribution, we introduce this novel model and discuss its benefits and limitations. A short overview will focus on some of the main obstacles in developing this multiscale model: computational architecture, strong fluctuations in atomic forces, etc. Examples of applications will be given, demonstrating how dislocations that are generated in the MD domain move into the DDD domain.

Investigation of the onset of plasticity in silicon nanostructures by molecular dynamics simulations

Julien Godet¹, Julien Guénoles¹, Sandrine Brochard¹, Laurent Pizzagalli¹

¹Institut Pprime, CNRS - Université de Poitiers - ENSMA, UPR 3346
Département de Physique et Mécanique des Matériaux
Bvd M. & P. Curie, SP2MI, BP 30179
86962 Futuroscope Chasseneuil Cedex, FRANCE
Email: sandrine.brochard@univ-poitiers.fr

The mechanical properties of semiconductor nanostructures are currently attracting considerable interest, not only because of potential applications in electronic devices, but also because these nanostructures are model systems for studying the elementary mechanisms of plasticity. Besides, their mechanical properties characterisation has revealed very different behaviours compared to what is known in bulk materials. For example, experimental observations in semiconductor nanopillars show that they could be ductile at room temperature whereas their bulk form is brittle. The explanation for such behaviours probably lies in the origin of the plasticity in these systems. In this work, we focused on the onset of plasticity in silicon thin films and nanowires free of any initial defect. Molecular dynamics simulations with well-tested potentials are used for this study.

For thin films we observed dislocation nucleation from $\{100\}$ surface irregularities when submitted to stress. According to the temperature and the stress magnitude, two distinct regimes of plasticity have been observed: one at high temperature and low stress where partial dislocations propagate in the glide set planes, and one at low temperature and high stress where dislocations propagate in the shuffle set planes.

For nanowires with $[001]$ axis and square section, stresses have been applied along the nanowire axis to investigate the elastic limit as a function of the temperature, the strain rate and the nanowire diameter. For almost all tests, we have observed dislocation nucleation from lateral surface or corner of the nanowire. In particular in compression, a unusual glide system, $[10\ -1](101)$, have been activated. This unexpected behaviour may be rationalised by considering the generalised stacking fault energy surface along the (101) plane, determined for the different potentials and from *ab initio* calculations.

On the J and M integrals during the crack-crazing patterns interactions

Seddiki, H¹, Chabaat, M²

¹Doctorate student, ²Professor

Built Environment Research Laboratory, Civil Engineering Faculty, University of Sciences and Technology Houari Boumediene, B.P. 32 El Alia, Bab Ezzouar, Algiers 16111, Algeria

This paper addresses an analysis of the stress field as well as the Energy Release Rates (ERR) associated with the main crack propagating into its surrounding Damage Zone (DZ) or the so-called Fracture Process Zone (FPZ) composed mainly of crazing patterns. Expressions for translation (J) and isotrope expansion (M) representing the active parts of crack driving forces ERR are formulated in a purely theoretical context. These elementary movements correspond to the active parts of crack driving forces occurring during the interactions of the DZ with the main crack. In the study, J and M integrals are the ERR due to the translational of both the crack and the DZ and the ERR due to the expansion energy of the DZ, respectively. Even though, a study that the crazes growth occurs along directions parallel to the minor principal stress axis and constitutes an important toughening mechanism. Thus, the mode I Stress Intensity Factor (SIF) is employed to quantify effects of this damage on the main crack. Therefore, a relation between the J-integral and the M-integral are established under the assumption mentioned above. It is also proven that the M-integral is equivalent to the decrease of the total potential energy of the microcracking solids although the strongly interacting situations are taken into account. On the other hands, the J-integral due to the linear propagation of the crack and also due to the translational change in the growth of the damage is used to confirm that crazes closer to the main crack dominate the resulting interaction effect and reflect an anti-shielding of the damage while a reduction constitutes a material toughness.

Influence of the Vacancy on Dislocation Mobility in BCC Metals

Zhiming Chen¹, Matous Mrovec^{1,2}, Peter Gumbsch^{1,2}

¹ Institut für Zuverlässigkeit von Bauteilen und Systemen, Karlsruher Institut für Technologie, Kaiserstr 12, 76131 Karlsruhe, Germany

² Fraunhofer-Institute Für Werkstoffmechanik, Wöhlerstr 11, 79108 Freiburg, Germany
Zhiming.chen@izbs.uni-karlsruhe.de

The plastic deformation of metals is primarily governed by dislocation generation and motion. While the onset of plastic yield corresponds to triggering of dislocation motion, subsequent hardening is mainly controlled by interaction of gliding dislocations with other lattice defects. Point defects can be considered as the simplest crystal defects that are always present within the material. Experimental results show that if the density of point defects increases, e.g., under irradiation conditions, the yield point and the flow stress also change significantly. These changes of macroscopic properties are directly related to the processes at the atomic scale where the dislocation motion becomes strongly influenced by the numerous point defects.

In the present work we investigate the influence of vacancies on the mobility of dislocations in various body-centered cubic (bcc) metals by means of atomistic simulations. The Nudged Elastic Band (NEB) method has been implemented to determine the changes of the energy barriers for the dislocation motion as well as for the vacancy migration near the dislocation cores. To describe the inter-atomic interactions, we employed the bond-order potentials, which are based on the tight-binding theory and are therefore able to describe correctly directional covalent bonds that are crucial for the cohesion and structure of bcc transition metals.

Our simulation results show that the dislocation mobility may be strongly influenced by the presence of vacancies and the change of the energy barrier depends sensitively on the vacancy position. Additionally, the vacancy diffusion within the dislocation cores can be high compared to that in the bulk. Based on the atomistic results, we will discuss possible influences on the macroscopic mechanical behavior of the investigated materials.

Multi-scale modelling of localization and damage: a computational homogenization approach

E.W.C. Coenen¹, V.G. Kouznetsova² and M.G.D. Geers²

¹Materials innovation institute (M2i), P.O. Box 5008, 2600 GA, Delft,
The Netherlands, E.W.C.Coenen@tue.nl

²Eindhoven University of Technology, Department of Mechanical Engineering,
P.O. Box 513, 5600 MB, Eindhoven, The Netherlands

Simultaneously with the increased utilization of complex materials, the demand for multi-scale modeling has developed. In computational homogenization, the mechanical equilibrium of the macroscale problem is solved in a nested manner with the equilibrium of the underlying microstructure. This technique is very powerful and versatile, especially in the applications where overall material properties are influenced by applied strain paths and microstructural evolution.

However, structural analyses beyond the point of strain localization and up to the point of fracture are not possible with classical computational homogenization scheme. Computational homogenization hinges on a separation of scales for both the characteristic length of microstructural as well as the loading. The development of a strain localization band in the microstructure, inevitably limits the concept of homogenization. This implies that classical computational homogenization schemes are not equipped to handle strain localization at both scales in a consistent way.

In this work, an innovative multi-scale framework has been developed, which correctly upscales the effect of microscale damage on macroscale fracture. The new scheme, divides the microscopic deformation into a bulk and localization type of deformation. The macroscopic continuum is enriched with a cohesive discrete crack, which lumps the microstructural strain localization and the residual load carrying capacity. This overcomes the limitation of classical schemes.

The two-scale framework involves an enhanced equilibrium formulation for the macroscale, dedicated scale transition relations to couple both scales and special boundary conditions for the microstructural volume element to allow the development of microstructural strain localization. This will be presented and illustrated by some numerical examples.

Algorithms for Discrete Dislocation Modeling of Fracture

Srinath S. Chakravarthy and William A. Curtin

182 Hope Street, Division of Engineering, Brown University, Providence Rhode Island
02912, USA

email : srinath_chakravarthy@brown.edu

ABSTRACT

The application of discrete dislocation dynamics methods to study materials with realistic yield stresses and realistic cohesive strengths requires new algorithms. Here, limitations of the standard algorithms are discussed, and then new algorithms to overcome these limitations are presented and their successes demonstrated by example. With these new methods, the stability, accuracy and robustness of the DD methodology for the study of deformation and fracture is greatly improved.

1. Introduction

Discrete dislocation (DD) methods have emerged over the last two decades as a means to study plastic deformation at the sub-continuum scale, providing fundamental understanding of strengthening/hardening phenomena and of size effects in plasticity. Fully three-dimensional DD models have been used primarily to study strain hardening due to dislocation forest interactions in nominally homogeneous blocks of material under uniform loading at the largest scales^{1,2,3,4,5}, individual dislocation/obstacle interactions^{6,7,8,9}, and individual dislocation loop/crack tip interactions¹⁰ at the smallest scales and, most recently, tension, compression and bending in micro/nanoscale pillars or beams^{11,12}. For solving complex boundary value problems, the use of 2d plane-strain DD models¹³ is common due to high computational cost of 3d DD¹⁴. The two-dimensional plane-strain DD method has been used to provide insight into a variety of fracture problems including fatigue crack growth in single crystals¹⁵, crack growth in thin films¹⁶, confined layers¹⁷ and bi-material interfaces¹⁸.

A common approach to modeling crack growth in both DD and continuum plasticity is through the use of a cohesive zone model as a continuum model of the complex non-linear separation of atomic planes. The primary properties of a cohesive zone model in realistic material systems are the cohesive strength σ_{coh} , typically 2-20 GPa, and the fracture energy Γ_0 , typically a few J/m². Two characteristic lengths associated with the cohesive zone are the critical opening $\delta_c \sim \Gamma_0/\sigma_{coh}$, typically 0.1 nm and thus comparable to the dislocation Burgers vector, and the critical cohesive length $\delta_{coh} \sim \mu\Gamma_0/\sigma_{coh}^2$, typically 1 nm. Resolving stress and strain fields over the nanometer scale, capturing the interaction of dislocations with a nanoscale cohesive zone, and modeling crack growth over the several microns needed to establish material fracture resistance, present severe computational challenges. Existing DD studies of deformation and fracture have thus used idealized material systems with low flow stresses ($\sigma_y \leq 100$ MPa) and low cohesive strengths ($\sigma_{coh} \leq 1$ GPa) to extract trends in behavior as a function of σ_{coh}/σ_y and other material parameters. It is thus of great interest to extend the capability of the DD method to encompass a broader and more realistic range of material properties.

Here we present several computational enhancements and modifications to algorithms reported in the literature to enable DD modeling of fracture in realistic material systems. The paper is

organized as follows. In the next section we describe the general framework for DD modeling of deformation and fracture. In Sections 3, 4, 5 and 6, we present the details of the existing algorithms, their limitations, and new algorithms that overcome these limitations. In the last section we present an example of the successful implementation of the set of modified algorithms to a system with material properties corresponding to a realistic material.

2. Discrete Dislocation formulation

The small strain discrete dislocation dynamics (DD) formulation of Van der Giessen and Needleman¹³ treats edge dislocations as line defects with Burgers vector b in a plane strain, isotropic elastic single-crystal material, and the changes in geometry due to slip are neglected. The crystal has three slip systems at angles ϕ_α , $\alpha = 1 \dots 3$ relative to the x_1 axis. Slip planes on each slip system are introduced with a spacing of d along the x_1 axis. Along each slip plane are placed dislocation sources of strength τ_s and dislocation obstacles of strength τ_{obs} . The areal densities of sources and obstacles are denoted as ρ_s and ρ_{obs} respectively. Dislocations nucleated from a source on a given slip plane are constrained to glide on that slip plane. Dislocation nucleation from a source occurs when the resolved shear stress on the source exceeds the critical value τ_s for a time period t_{nuc} . The initial separation L_{nuc} of the dipole is chosen such that the dislocation dipole would be in equilibrium under the stress τ_s . Dislocations of opposite sign on the same slip plane are annihilated if they are within a critical distance $L_e = 6b$. Dislocations pinned at obstacles are released when the resolved shear stress exceeds the strength of the obstacle τ_{obs} . The glide motion of dislocations is controlled by a mobility law, where the dislocation velocity v glide is proportional to the Peach-Koehler force (F_{pk}) on the dislocation as $v = F_{pk}/B$ where B is the mobility coefficient. The Peach-Koehler force is $F_{pk} = \tau_{pk}b$, where τ_{pk} is the total resolved shear stress along the glide plane of the dislocation and is composed of contributions from the applied stress, dislocation/dislocation interactions, and image stresses due to imposed boundary conditions. To compute τ_{pk} , a superposition method is used wherein total fields are decomposed into the sum of (i) an analytic singular (\sim) fields generated by the dislocations in an infinite or semi-infinite space and (ii) a corrective (\wedge) field that accounts for the image forces, the actual problem geometry, and the boundary conditions, which is computed using finite elements¹³.

To model fracture, we insert an initial crack into the material described above such that the initial crack tip is at the origin and introduce a cohesive zone model along the crack line ahead of the initial tip and a remote stress intensity (K) field is imposed (see Fig. 4a). The computational strategy is carried out in an incremental manner. At each time step, (i) the value of the remote K field is increased, (ii) the Peach-Koehler forces F_{pk} on all dislocations are computed, (iii) the dislocation structure is updated by motion of existing dislocations, nucleation of new dislocations, annihilation, pinning at obstacles, and dislocations exiting from free surfaces, and (iv) the stress and strain state for the updated dislocation structure using the superposition scheme is calculated.

In each of the following sections, details of one standard algorithm are described and the shortcomings identified. A new algorithm is then presented that alleviates the shortcomings, as demonstrated by example.

3. Gradient correction to the velocity

The equation of motion for the dislocations along the glide plane is $dx/dt = v = F_{pk}/B$. This equation of motion is typically integrated using the forward Euler (FE) method, so that the new position of the dislocation is given by $x(t + \Delta t) = x(t) + v(x(t))\Delta t$. In most DD simulations, a maximum time step $\Delta t = 5 \times 10^{-10}$ s has been used along with a maximum dislocation velocity 20 m/s¹⁹ along with an additional underrelaxation scheme. Segurado et al.²⁰ have investigated the effects of the velocity cut-off and the time step, showing that the macroscopic uniaxial tensile response and the resulting dislocation structures are significantly influenced. Furthermore, we have found that when the plastic flow stress is controlled mainly by the obstacles, with ensuing pileups, that the time-step, velocity cut-off, and underrelaxation, can unduly influence the dislocation unpinning from obstacles. This is easily seen in the simple problem of a dislocation pileup generated by a single source with strength τ_s surrounded by two obstacles with infinite strength at a distance $L_{obs}/2$ on either side of the source. For an equilibrium pile-up of n dislocations, the stress on the pinned dislocation should be n times the applied stress²¹. Figure 1 shows the stress on the pinned dislocation versus the applied stress as simulated using the standard algorithms. The behavior should be smooth in between successive nucleation events from the source, and show discrete jumps upon each nucleation event. Despite the use of underrelaxation and a velocity cut-off, severe oscillations are observed, which arises from incorrect dislocation positions in the pileup stemming from the numerical algorithms. For a time step of 5×10^{-10} s, oscillations are observed with as few as three dislocations in the pileup. When the obstacle has a finite strength, the oscillations can cause premature unpinning of a pinned dislocation, and lead to a lack of control over the material yield stress. Other artifacts also arise that we will not discuss here.

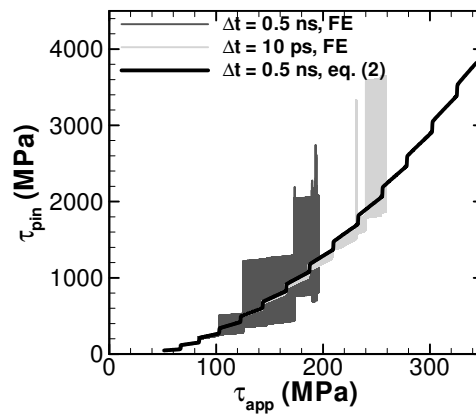


Figure 1: Stress on the pinned dislocation in a symmetric pileup versus applied stress, for a single source with strength $\tau_s = 50$ MPa and obstacle spacing $L_{obs} = 200$ nm. Each step in the curve is associated with the nucleation of a new dislocation dipole. Oscillations with standard forward euler method and its elimination with the gradient velocity correction are shown.

The problems above stem mainly from rapidly varying stress fields due to closely spaced dislocations, particularly in pile-ups. The Backward Euler method, given by

$$x(t + \Delta t) = x(t) + v(x(t + \Delta t))\Delta t \quad (1)$$

has higher order accuracy and stability but requires the velocity at the end of the time step, which usually involves an expensive and cumbersome implicit solution process. However, a simple estimate for $v(x(t + \Delta t))$ can be obtained by expanding it in a Taylor series, using the mobility law, and manipulating to solve for the velocity

$$v(x(t + \Delta t)) = \frac{1}{B} \frac{F_{pk}}{\left(1 - \frac{1}{B} \frac{\partial F_{pk}}{\partial x} \Delta t\right)} \quad (2)$$

The correction in (2) reflects the fact that over the time period Δt the dislocation moves through a spatially-varying force field. When the field gradient is large, the correction improves the net dislocation motion in comparison to the forward Euler scheme, leading to more accurate dislocation positions and avoiding spurious large interaction forces arising when dislocations become too close together. Since the dislocation interactions are available as analytical fields, their spatial derivatives are also available in analytical form and the overall computation effort can be easily minimized when the Fast Multipole method (FMM) is used to accelerate the computation of dislocation interactions. Using the above correction, the velocity cut-off is set to 1000 m/s, which is consistent with the maximum dislocation velocity reported in atomistic simulations²². Results for the single pileup problem simulated using the gradient correction show complete elimination of the oscillations (Figure 1). While some oscillations appear when there are multiple dislocations on multiple slip systems if the time step is too large, a time step of $\Delta t \leq 5 \times 10^{-11}$ s eliminates all oscillations and circumvents the need for any additional underrelaxation algorithms.

4. Dislocation nucleation

In most DD simulations reported to date, a dislocation dipole is instantaneously nucleated at a distance $L_{nuc}/2$ on each side of the source when the stress on the source has been greater than the nucleation stress τ_s for a time period t_{nuc} . For sources located close to the crack plane, the abrupt injection of a dislocation dipole results in a sudden jump in the displacement field on the crack boundary and causes numerical instabilities. In addition, in large pile-up situations (strong obstacles), the abrupt injection of the dipole into the existing pile-up generates spurious forces on the pile-up dislocations, inducing oscillations similar to those seen in Figure 1a.

To minimize the above problems, we introduce a dipole gradually over the nucleation time t_{nuc} , such that Burgers vector and separation increase linearly with time as

$$b^{dipole}(t) = b \frac{t}{t_{nuc}}, 0 < t \leq t_{nuc}, \tau > \tau_s \quad (3)$$

$$x^{dipole}(t) = L_{nuc} \frac{t}{t_{nuc}}, 0 < t \leq t_{nuc}, \tau > \tau_s \quad (4)$$

Equations (3) and (4) ensure that these “latent” dipoles have the correct Burgers vector and are at the proper nucleation distance when $t = t_{nuc}$. Algorithmically, the “latent” dislocations are not subjected to the mobility law until $t = t_{nuc}$, but do contribute to the Peach-Koehler forces on all dislocations, and to the displacements and tractions on the boundaries. If at some time $t_0 < t_{nuc}$ the stress on the source drops below the nucleation stress, the Burgers vector and position of the dipole are then reduced linearly toward zero, i.e. equations (3) and (4) are used with t replaced by $t_0 - t$.

5. Dislocation/Cohesive Zone (CZ) Interactions

For the fracture problem, the cohesive tractions along the crack plane are described by a non-linear traction-separation ($T - \Delta$) law, where Δ depends on the displacement fields u . In accordance with the standard superposition scheme $\Delta = \hat{\Delta} + \tilde{\Delta}$, the cohesive tractions at the end of an increment are $T^{t+\Delta t} = T(\tilde{\Delta}^{t+\Delta t} + \hat{\Delta}^{t+\Delta t})$. However, during the incremental loading procedure, the updated dislocation fields $\tilde{\Delta}^{t+\Delta t}$ are known and $\hat{\Delta}^{t+\Delta t}$ is the quantity that needs to be solved for. Therefore, expanding $\hat{\Delta}^{t+\Delta t}$ into a Taylor series we obtain the linearized traction at the end of the increment as

$$T^{t+\Delta t} = T(\tilde{\Delta}^{t+\Delta t} + \hat{\Delta}^t) - \frac{\partial T(\tilde{\Delta}^{t+\Delta t} + \hat{\Delta}^t)}{\partial \Delta} \dot{\hat{\Delta}} \Delta t \quad (5)$$

where $\frac{\partial T}{\partial \Delta}$ is a cohesive stiffness, the superscript t indicates time and a superposed dot denotes differentiation in time. The incremental traction $T^{t+\Delta t}$ is then imposed on the boundary, the finite element solution for $\hat{\Delta}$ is computed and the field is updated using $\hat{\Delta}^{t+\Delta t} = \hat{\Delta}^t + \dot{\hat{\Delta}} \Delta t$.

The linearization of the CZ tractions and the linear incremental solution process is only valid when the sum ($\tilde{\Delta}_i + \hat{\Delta}_i$) is smaller than δ_c and Δt is small. When $\tilde{\Delta}_i^{t+\Delta t} > \delta_c$, the superposition of the dislocation displacement field in (5) causes an initially closed CZ to open. Since the superposed fields lie in the non-linear portion of the ($T - \Delta$) law, the subsequent FEM solution is incorrect, leading to an incorrect solution for the total opening. With the use of realistic material properties, $\delta_c < b$, dislocation fields of order b , which is equivalent to the interaction of a single dislocation with the cohesive zone, can lead to failure of the superposition scheme. The use of adaptive time stepping and Newton-Raphson iterative schemes do not reliably resolve the issue even for time increments equal to 1×10^{-12} s. This behavior is illustrated in Fig. 2, where upper plots show the dislocation displacement field ($\tilde{\Delta}$) along the crack line while the lower plots show the resulting crack opening profile obtained from the finite element solution, for two different snapshots in time of a DD/CZ simulation. The solution from the standard superposition is smooth (Fig. 2a) when $\tilde{\Delta} < b$ but as $\tilde{\Delta}$ approaches b (Fig. 2b) the numerical solution displays incorrect and extreme oscillatory behavior, illustrating failure of the standard superposition scheme.

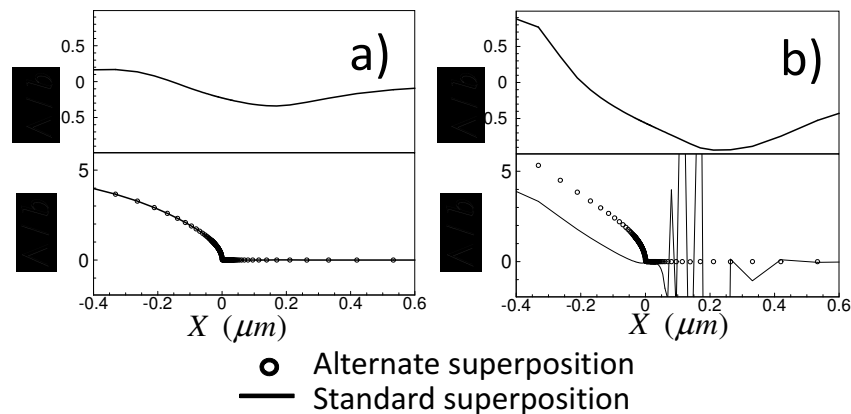


Figure 2: Normalized displacement along the crack line: upper plot shows displacement due to dislocations ($\tilde{\Delta}$); lower plot shows the crack opening profile obtained from FEM solution and DD superposition. a) $\tilde{\Delta} \ll b$, both superposition schemes are nearly identical and the crack opening is smoothly varying. b) $\tilde{\Delta} \sim b$, for which numerical instabilities arise with standard superposition while the alternative approach remains smooth. Material parameters are $\Gamma_0 = 1.1$ J/m², $\sigma_{coh} = 7$ GPa, $\delta_c = 0.059$ nm and $b = 0.25$ nm.

To avoid the above problem, which is fundamentally a failure of the superposition method applied to a non-linear cohesive zone, we use the alternative superposition scheme of O’Day and Curtin²³. The O’Day and Curtin²³ method is similar in spirit to the Eshelby inclusion problem²⁴. Briefly, two problems are solved: (i) a standard DD problem in the domain where DD plasticity is permitted, but subjected to zero traction or zero displacement boundary conditions independent of the actual boundary conditions; and (ii) an elastic/cohesive zone problem of the entire domain without dislocations, with all the desired loading and boundary conditions, and with the negative of the tractions developed along the displacement boundaries of Problem (i) also imposed. Superposition of Problems (i) and (ii) then yields the exact solution of the posed boundary value problem. Problem (i) is solved using the standard DD methodology but with the special boundary conditions while Problem (ii) is solved using standard finite element methodology with a Newton-Raphson (NR) iterative scheme to accurately capture the non-linearity of the cohesive zone model. In this approach, superposition is applied only *within* the DD domain and not along its boundaries. The cohesive zone thus lies *outside* the domain of superposition. Dislocation interactions with the cohesive zone are captured through the tractions developed in the DD Problem (i) that are imposed on the cohesive zone in Problem (ii). Transmission of dislocations into the cohesive zone can still occur, thereby opening the cohesive zone as should occur physically, but without spurious instabilities due to an inappropriate use of superposition. Figure 2 shows that instabilities reported with the standard superposition are eliminated with the use of alternate superposition. We note that this problem does not obviously arise in most prior DD simulations, where $\sigma_{coh} \leq 1$ GPa and $\delta_c \gg b$.

6. Moving Mesh Method

For any problem involving a cohesive zone model, a finite element mesh must resolve the high stresses and stress gradients in the vicinity of the crack tip as it moves. The minimum element size near the crack tip is $\sim \delta_{coh}/3$, as determined via numerical studies. For realistic cohesive zone properties, $\delta_c \sim 0.1$ nm and $\delta_{coh} \sim 1$ nm, requiring a mesh on the Angstrom scale. At the same time, however, fracture toughness in the presence of plasticity is achieved only after significant (1-100 microns) crack growth and development of a plastic wake. Capturing microns of crack growth with sub-Angstrom mesh sizes requires innovative computational methods; a simple uniform sub-Angstrom mesh extending over microns of material is computationally intractable. Previous DD studies have thus used lower cohesive strengths, corresponding to increased $\delta_{coh} > 100$ nm and larger mesh sizes, and have not always investigated crack growth sufficient to establish the entire resistance curve.

Standard adaptive meshing methods involve re-meshing, which requires costly decomposition of the stiffness matrix with every re-meshing operation. For elasticity problems, such as the DD corrective solution, this can be avoided using by using what we term the ”moving mesh” method. The essence of this method is that, in a frame of reference moving with the crack tip, the dislocations, and all field variables including those of the cohesive zone, can be considered as moving in the opposite direction. The moving mesh method allows the crack to grow forward for some distance and then shifts the dislocations, and field variables backward by exactly that amount, re-establishing the crack tip at the original location relative to the original mesh, leaving the stiffness matrix unchanged. A more detailed description is given below.

A uniform mesh of size $\Delta x_{unif} = \delta_{coh}/4$, suitable for resolving the cohesive zone, is placed around the initial crack tip, extending a distance X_{unif} ahead of the crack tip. Further away, the mesh size increases smoothly with increasing distance from the crack tip. During loading, the crack tip position is monitored at each increment. If the crack tip position passes a pre-

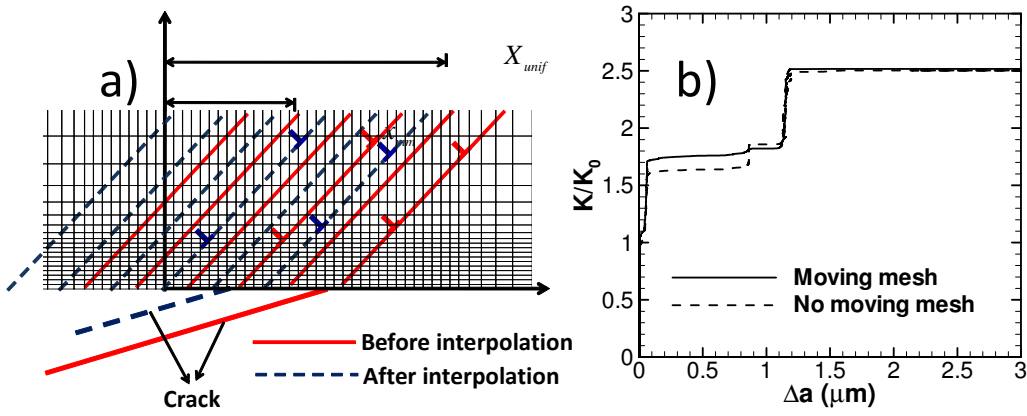


Figure 3: a) Schematic of the moving mesh method, showing the backward translation of all slip planes, dislocations, and field quantities, including crack plane displacements, after the crack has grown forward by some small amount. b) Stress intensity versus crack growth, as computed using the moving mesh method (solid line) with $\Delta X_{unif} = 35\delta_{coh} = 1.1 \mu\text{m}$, $x_{mm} = 20\delta_{coh}$ and a fixed mesh of the same fine-scale resolution (dashed line), $\Delta X_{unif} = 4 \mu\text{m}$, $x_{mm} = 4 \mu\text{m}$. Material properties are $\Gamma_0 = 1.1 \text{ J/m}^2$, $\sigma_{coh} = 1 \text{ GPa}$ and $\sigma_Y = 200 \text{ MPa}$, giving $\delta_{coh} = 32 \text{ nm}$.

selected distance x_{mm} , which is an even integer multiple of Δx_{unif} , then all finite element field quantities (stresses, strains and displacements) are interpolated from any nodal position x to a location $x - x_{mm}/2$. All dislocation slip planes are also moved from positions x_{slip} to $x_{slip} - x_{mm}/2$. Figure 3a shows a typical near tip mesh and schematic of the interpolation process. With x_{mm} and X_{unif} integer multiples of Δx_{unif} , the interpolation in the uniform mesh region around the crack tip is *exact* and is equivalent to transferring field quantities from a nodal position i to a position $i - N_{mm}$, where $N_{mm} = \text{int}(x_{mm}/2\Delta x_{unif})$. Small errors associated with the interpolation of field quantities and evaluation of dislocation stresses outside of the uniform mesh region are then eliminated by performing a new corrective field solution with all dislocations fixed at the new positions. Since the mesh remains fixed, the stiffness matrix remains unchanged during these processes. The method ensures that the crack tip is always located between 0 and x_{mm} , and thus in the regime of full resolution for the cohesive zone.

The extent of the uniform mesh ahead of the crack tip determines the accuracy of the solution. Numerical studies over the parameter range $X_{unif} = 10\delta_{coh}$ to $50\delta_{coh}$ with $x_{mm} \approx X_{unif}/2$ show that $X_{unif} = 20\delta_{coh}$ is sufficient to produce mesh independent results. Figure 3b shows the crack resistance curve as calculated using the moving mesh computation and using a mesh of the same fine-scale resolution but extending over the entire length of the crack growth shown. The results are essentially identical because the precise evolution of the dislocation system and crack growth are sensitive to round-off errors (reflecting the chaotic aspects of dislocation dynamics)²⁵, so that small differences due to the meshing, away from the crack tip region modify the crack growth process.

7. Modeling of Crack Growth

Here, we demonstrate that the collective set of algorithms described above permit for the stable calculation of extensive crack growth in a material with both high yield stress and high cohesive strength. Prior to that demonstration, we comment on other developments that are pertinent to DD modeling of plastic flow and fracture. First, we have recently shown that the DD material properties can be tuned to obtain a desired yield stress²⁶. An analytic model based on the

traditional source/obstacle pile-up model predicts a yield stress of

$$\sigma_Y = \frac{1}{S} \sqrt{\frac{4\mu b}{\pi(1-\nu)} \frac{\tau_{obs}}{1.5L_{obs}} + \tau_s^2} \quad (6)$$

where L_{obs} is the average obstacle spacing in a system with maximum obstacle spacing of $1.5L_{obs}$ and S is the Schmid factor. The high accuracy of this formula has been demonstrated by direct DD simulations for both single source/obstacle configurations and full tension specimens. Those DD studies required use of both the velocity correction and the modified nucleation criterion.

Second, in all DD calculations of the type discussed here, a major fraction of the computational effort is devoted to computing the dislocation-dislocation interactions, the dislocation-boundary corrections, and the source nucleation. As the total number N of dislocations in the computational cell increases, the incremental computational effort using direct methods scales as N^2 and the total effort scales as N^3 . To reduce the computational burden significantly, we have implemented the fast multipole method (FMM)²⁷ which reduces the computational effort to $O(N)$, and has previously been applied to dislocation interactions²⁸. The FMM implementation is relatively standard, and so is not discussed here. We do note, however, that the method is naturally applicable to efficient computation of the derivatives of the dislocation fields, enabling implementation of the velocity correction of (2) with little additional overhead.

Employing all the computational enhancements implemented as described in this paper, Fig. 4b shows the fracture resistance curve of a simulation in which the material yield stress is $\sigma_Y = 700$ MPa, the cohesive strength is $\sigma_{coh} = 7$ GPa, and the cohesive energy is $\Gamma_0 = 1.13$ J/m². Other parameters in the model are a Burgers vector $b = 0.25$ nm, slip plane spacing $d = 100b$, areal density of sources $\rho_s = 66$ μm^{-2} with average source strength $\tau_s = 50$ MPa, and an average obstacle spacing $L_{obs} = 3/\rho_{obs}d = 80$ nm. Figure 4b shows that crack growth starts around the elastic value K_0 , but dislocation activity dissipates energy and stabilizes crack growth. At a critical load K_c , plastic dissipation is insufficient to prevent crack growth and the crack grows with no further increase in load in a brittle manner. It can be seen that 3.2 μm of crack growth is needed to establish K_c and no numerical instabilities or convergence issues were observed, even when the crack grows in a brittle like fashion. Forthcoming publications will present far more extensive results on crack growth as a function of material parameters, with analysis revealing the factors controlling fracture toughness²⁹.

8. Summary

We have presented computational refinements and modifications to the existing DD methodology that enable modeling of fracture, with cohesive and yield strengths representative of real engineering materials. A gradient correction for the dislocation velocity prevents overshoot of dislocations and associated premature unpinning from obstacle. Gradual nucleation of dipoles over the nucleation time t_{nuc} suppresses instabilities. An alternative superposition method accurately captures dislocation/cohesive zone interactions. Finally, a moving mesh method permits modeling of extensive crack growth in spite of sub-Angstrom mesh resolution at the crack tip and at no additional computational cost. These enhancements to the DD method enable the study of crack growth phenomena across a realistic range of material properties, which is uncovering fundamental features of fracture in plastically-deforming materials.

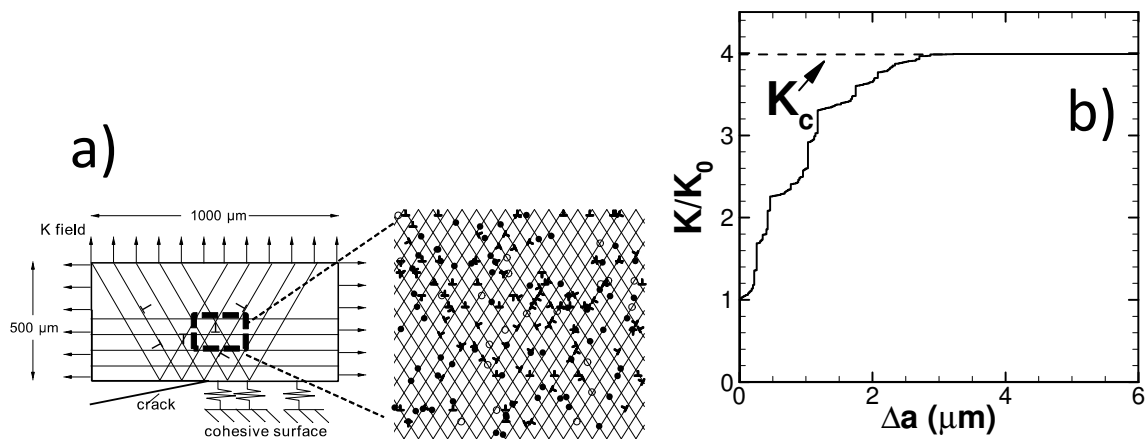


Figure 4: a) Schematic of the top half of a symmetric DD/CZ fracture simulation geometry with DD plasticity model consisting of slip planes, dislocations, dislocation sources (solid circles) and dislocation obstacles (open circles). b) Stress intensity versus crack growth, showing stable growth of the crack with increasing load over several microns, culminating in a final fracture toughness K_c for a material with $\sigma_{coh} = 7$ GPa, $\Gamma_0 = 1.1$ J/m² and $\sigma_Y = 700$ MPa, giving $\delta_c = 0.059$ nm, $\delta_{coh} = 1.6$ nm. Meshing scales are $\Delta x_{unif} = \delta_{coh}/4$, $X_{unif} = 35\delta_{coh}$, $x_{mm} = 20\delta_{coh}$.

Acknowledgements

The authors gratefully acknowledge support from NASA Langley Research Center (Grant # NNX07AU56A) and the NSF Materials Research Science and Engineering Center at Brown on “Micro- and Nano-mechanics of Materials” (DMR-0520651).

References

- [1] L.P. Kubin, B. Devincere, and M. Tang. Mesoscopic modelling and simulation of plasticity in fcc and bcc crystals: Dislocation intersections and mobility. *Journal of Computer-Aided Materials Design*, 5(1):31 – 54, 1998.
- [2] A. Hartmaier, M.C. Fivel, G.R. Canova, and P. Gumbsch. 3d discrete dislocation models of thin-film plasticity. In *Materials Research Society Symposium - Proceedings*, volume 505, pages 539–544, 1998.
- [3] R. Madec, B. Devincere, and L. P. Kubin. From dislocation junctions to forest hardening. *Phys. Rev. Lett.*, 89(25):255–268, 2002.
- [4] Vasily Bulatov, Wei Cai, Jeff Fier, Masato Hiratani, Gregg Hommes, Tim Pierce, Meijie Tang, Moono Rhee, Kim Yates, and Tom Arsenlis. Scalable line dynamics in ParaDiS. In *SC '04: Proceedings of the 2004 ACM/IEEE conference on Supercomputing*, pages 367 – 378, 2004.
- [5] W. Cai, V. Bulatov, T. Pierce, M. Hiratani, M. Rhee, M. Bartlet, and M. Tang. Massively-parallel dislocation dynamics simulations. In *Solid Mechanics and Its Applications*, volume 115. Kluwer, Dordrecht, 2004.
- [6] Y. Wang, D.J. Srolovitz, J.M. Rickman, and R. Lesar. Dislocation motion in the presence of diffusing solutes: a computer simulation study. *Acta Materialia*, 48(9):2163 – 2175, 2000.

- [7] M. Hiratani and H. M. Zbib. On dislocation-defect interactions and patterning: stochastic discrete dislocation dynamics (SDD). *Journal of Nuclear Materials*, 323(2-3):290–303, 2003.
- [8] C.S. Shin, M.C. Fivel, M. Verdier, and C. Robertson. Dislocation dynamics simulations of fatigue of precipitation-hardened materials. *Materials Science and Engineering A*, 400-401:166–169, 2005.
- [9] Y. Xiang and D.J. Srolovitz. Dislocation climb effects on particle bypass mechanisms. *Philosophical Magazine*, 86(25-26):3937 – 3957, 2006.
- [10] I.N. Mastorakos and H.M. Zbib. Shielding and amplification of a penny-shape crack due to the presence of dislocations. *International Journal of Fracture*, 142(1-2):103–117, 2006.
- [11] J. Senger, D. Weygand, P. Gumbsch, and O. Kraft. Discrete dislocation simulations of the plasticity of micro-pillars under uniaxial loading. *Scripta Materialia*, 58(7):587–590, 2008.
- [12] C. Motz, D. Weygand, J. Senger, and P. Gumbsch. Micro-bending tests: A comparison between three-dimensional discrete dislocation dynamics simulations and experiments. *Acta Materialia*, 56(9):1942–1955, 2008.
- [13] E. Van der Giessen and A. Needleman. Discrete dislocation plasticity: a simple planar model. *Modelling and Simulation in Materials Science and Engineering*, 3(5):689–735, 1995.
- [14] Zhiqiang Wang, Nasr Ghoniem, Sriram Swaminarayan, and Richard LeSar. A parallel algorithm for 3D dislocation dynamics. *Journal of Computational Physics*, 219(2):608–621, 2006.
- [15] V. S. Deshpande, A. Needleman, and E. Van der Giessen. Discrete dislocation modeling of fatigue crack propagation. *Acta Materialia*, 50:831–846, 2002.
- [16] M.P. O’Day, P. Nath, and W.A. Curtin. Thin film delamination: A discrete dislocation analysis. *Journal of the Mechanics and Physics of Solids*, 54(10):2214–2234, 2006.
- [17] Nils Broedling, Alexander Hartmaier, and Huajian Gao. A combined dislocation cohesive zone model for fracture in a confined ductile layer. *International Journal of Fracture*, 140(1):169–181, 2006.
- [18] M.P. O’Day and W.A. Curtin. Bimaterial interface fracture: A discrete dislocation model. *Journal of the Mechanics and Physics of Solids*, 53(2):359–382, 2005.
- [19] H. H. M. Cleveringa, E. Van der Giessen, and A. Needleman. A discrete dislocation analysis of bending. *International Journal of Plasticity*, 15(8):837–868, 1999.
- [20] J. Segurado, J. Llorca, and I. Romero. Computational issues in the simulation of two-dimensional discrete dislocation mechanics. *Modelling and Simulation in Materials Science and Engineering*, 15:361–375, 2007.
- [21] J. D. Eshelby and B. A. Bilby. *Fracture*, volume I, chapter Chapter 2. Academic Press, 1968.
- [22] David L. Olmsted, Louis G. Hector Jr., W.A. Curtin, and R.J. Clifton. Atomistic simulations of dislocation mobility in al, ni and al/mg alloys. *Modelling and Simulation in Materials Science and Engineering*, 13(3):371 – 388, 2005.

- [23] M. P. O'Day and W. A. Curtin. A superposition framework for discrete dislocation plasticity. *Journal of Applied Mechanics*, 71:805–815, 2004.
- [24] J. D Eshelby. Elastic inclusions and inhomogeneities. In I.N. Sneddon and R. Hill, editors, *Progress in Solid Mechanics*, volume ii, 1961.
- [25] V. S. Deshpande, A. Needleman, and E. Van der Giessen. Dislocation dynamics is chaotic. *Scripta Materialia*, 45(9):1047–1053, 2001.
- [26] Srinath Chakravarthy and William Curtin. Effect of source and obstacle strengths on yield stress: A discrete dislocation study. *Journal of the Mechanics and Physics of Solids*, 58(5):625–635, 2010.
- [27] L. Greengard and V. Rokhlin. A fast algorithm for particle simulations. *Journal of Computational Physics*, 73(2):325–348, 1987.
- [28] Anders Jonsson. Discrete dislocation dynamics by an $O(N)$ algorithm. *Computational Materials Science*, 27:271–288, 2003.
- [29] Srinath Chakravarthy and William Curtin. Origin of plasticity length-scale effects in fracture. *Physical Review Letters*, Accepted for publication, July 2010.

A New Interpretation of the Haasen Plot for Solute-Strengthened Alloys

W. A. Curtin and Y. Dong

Division of Engineering, Brown University, Providence, RI 02912 USA

The study of strain rate sensitivity and the associated activation volume of thermally-activated phenomena in metals has a long history. Traditional theories of the Haasen plot, i.e. the inverse activation volume $1/\Delta V$ versus $\sigma - \sigma_0$ (σ_0 =initial yield stress), postulate that when multiple strengthening mechanisms (e.g. solutes and forest dislocations) operate that the inverse activation volumes are additive, i.e. $1/\Delta V = 1/\Delta V_s + 1/\Delta V_f$, so that the intercept is non-zero ($=1/\Delta V_s$) while the slope remains the same as in the pure material since $1/\Delta V_f \sim \sigma - \sigma_0$. For solute-strengthened alloys, the slope of the inverse activation volume $1/\Delta V$ versus stress is linear but often with a slope much lower than that found in the pure material, e.g. [1]. In an attempt to rectify this discrepancy, we propose an alternative postulate for solute-strengthened alloys wherein the activation enthalpy equals that of solute strengthening alone. This leads to the prediction $1/\Delta V = 1/\Delta V_s + (1/\sigma_0 \Delta V_s)(\sigma - \sigma_0)$, which remains linear in $\sigma - \sigma_0$ but with a slope controlled by the ratio of the solute inverse activation volume $1/\Delta V_s$ and the solute-strengthening yield stress σ_0 . This parameter-free prediction of the slope of the Haasen plot is compared to literature data [2] and reasonable agreement is obtained. A variety of computational models based on point and extended obstacle pinning, and line tension, are presented to uncover the fundamental origins of the proposed postulate.

[1] R. A. Mulford, *Acta Metall.* 27, 1115-1124 (1979).

[2] B. J. Diak and S. Saimoto, *Mat. Sci. Eng.* A234-236, 1019-1022 (1997).

Solute strengthening in Aluminum alloys

W.A. Curtin, G.P.Leyson, L.G. Hector Jr.

The strengthening of Aluminum by substitutional solute atoms (Li, Mg, Si, Cu, Ge and Cr) on dislocations is predicted using first principles calculations and a new analytic theory. Solute energies in and around the dislocation core are first calculated using density functional theory and flexible boundary condition [1] and/or multiscale methods. An analytic model is then developed that derives from concepts first presented by Labusch to predict the pinning of a dislocation within a random field of solutes but resolves issues concerning the previously-unspecified “range” of solute-dislocation interactions. The theory predicts both the energy barriers to dislocation motion and the zero-temperature flow stress, allowing for predictions of finite-temperature flow stresses. Results show that solutes in the dislocation core dominate the energy contributions. Quantitative comparisons with experimental flow stresses at $T=78\text{K}$ are made for Al-X alloys ($X=\text{Mg, Si, Cu, Cr, Mn, Fe, and Ge}$) and good agreement is obtained.

[1] Woodward, C., Trinkle, D.R., Hector, L.G., Olmsted, D.L., 2008. Phys. Rev. Lett. 100, 045507

[2] Labush, R., 1970. Phys. Status Solidi 41, 659

Multiscale Modeling of Hydrogen Embrittlement

W. A. Curtin and J. Song
Division of Engineering, Brown University, Providence, RI

Hydrogen embrittlement is a pervasive mode of degradation in many metallic systems and a number of mechanisms have been proposed to explain the phenomenon in different material systems. Here, a mechanism related to Hydrogen-Enhanced Decohesion (HEDE) is proposed wherein H accumulation at the crack tip shuts off crack tip dislocation emission, eliminating crack blunting and suppressing ductile failure modes, and causing failure by cleavage of the nanohydride but with surrounding dislocation plasticity providing plastic dissipation. The atomic scale aspects of this mechanism are studied via simulation, with H in single crystal Ni as a model system. Accumulation of H around a crack tip due to the crack tip fields and the indirect interaction between H atoms is modeled atomistically using a new efficient self-consistent procedure and the effects of H accumulation on dislocation emission and/or cleavage fracture are studied. Even at low bulk H concentrations and low applied stress intensities, a nanoscale hydride forms around the crack tip. This nanohydride prevents dislocation emission from the crack tip and then grows as the applied load is increased, eventually cleaving in a brittle manner. The kinetics of H diffusion to the crack tip region is assessed to determine the time required to accumulate the H needed to suppress dislocation emission and drive brittle cleavage. A mechanism map is then generated to predict embrittlement as a function of loading rate, initial crack size, H chemical potential, temperature, effective H diffusion activation enthalpy, and cleavage stress intensity.

Multisite model prediction of twinning induced anisotropy in fcc metals

S. Dancette, L. Delannay

Université Catholique de Louvain (UCL), Department of Mechanical Engineering (iMMC-MEMA), av. G. Lemaître, 4 – B1348, Louvain la Neuve - Belgium
sylvain.dancette@uclouvain.be, laurent.delannay@uclouvain.be

Twinning is commonly observed above a certain level of deformation at room temperature in face centered cubic (fcc) metals with low stacking fault energy (SFE). Twins carry a part of the plastic deformation and they act as barriers to dislocation motion, leading to anisotropic hardening already at the crystal level. Deformation twinning influences strongly the development of texture and, hence, the macroscopic anisotropy.

Twinning of FCC metals is investigated in this study by means of experimental observations as well as an advanced crystal plasticity model. Individual twins, as they are formed, are treated as separate crystal entities co-deforming with the parent grain. A physical law takes account of the reduction of the mean free path of dislocations with the evolving dislocation density and the increasing twin volume fraction, as suggested by Allain et al. [1].

The behavior of the polycrystalline aggregate is assessed by means of a “multisite” model derived from the ALAMEL model [2]. This simplified model of short-range grain interactions is suitable for micro-macro modeling of real-scale forming processes. The main modeling assumption is that each grain interacts exclusively with one of its direct neighbors. The macroscopic strain is achieved, on average, over two subregions lying on either sides of a planar grain boundary. Stress equilibrium and displacement continuity is fulfilled along the interface.

Simulations of various deformation paths, ranging from tensile tests to cold rolling or torsion, have been assessed based on experimental data. A comparison of the multisite model to more classical scale transition schemes demonstrates that the anisotropic material response can be reproduced more accurately when taking proper account of next-neighbor grain interaction.

[1] S. Allain, J.P. Chateau, O. Bouaziz. *Mat. Sci. Eng. A* 2004;387-389:143-147

[2] L. Delannay, M.A. Melchior, J.W. Signorelli, J.-F. Remacle, T. Kuwabara. *Comp. Mat. Sci.* 2009;45:739-743

Multisite modeling of strain heterogeneity in multiphase polycrystals – Evaluation based on CPFEM and experiment

Delannay L.⁽¹⁾, Resk H.⁽¹⁾, Kumar S.⁽¹⁾, Martin G.⁽²⁾, Brassart L.⁽¹⁾, Willemet M.⁽¹⁾ and Pardoën T.⁽¹⁾

⁽¹⁾iMMC, Université catholique de Louvain (UCL), av. G. Lemaître 4,
1348 Louvain-la-Neuve, Belgium, Laurent.Delannay@uclouvain.be

⁽²⁾SIMAP, Groupe Physique du Métal, Domaine Universitaire, 1130 rue de la piscine,
38402 Saint Martin D'Hères, France

In its original version, the multisite model [1,2] proposes a simplified treatment of short-range grain interactions throughout a polycrystalline aggregate, by considering that the macroscopically prescribed deformation is achieved on average within pairs of adjacent (sub-)grains. The model yields valid predictions of texture development [1] and anisotropy [2] in single-phase metallic alloys, but the anisotropy of strain is underestimated in multiphase alloys [3]. Therefore an enhanced version of the model is proposed according to which each pair of grains is treated as an isolated inclusion in a self-consistent scheme. Strain concentration tensors are computed based on isotropic, effective tangent moduli so that the method is suitable also in non-monotonic (or cyclic) loading.

The model is tested and compared to crystal plasticity based finite element modeling (CPFEM) of the strain partitioning in a duplex stainless steel revealing either equiaxed or Widmanstätten microstructure. Strain partitioning is estimated experimentally based on image correlation [4]. Finite element meshes reproducing the undeformed microstructure are used in an inverse analysis of the phase strengths. Then the multisite model is applied on a statistically representative reproduction of the microstructure and the texture and its predictions are compared to the full-field predictions.

- [1] Van Houtte P., Li S., Seefeldt M., Delannay L. (2005) "Deformation texture prediction: from the Taylor model to the advanced Lamel model", *International Journal of Plasticity*, 21, 589-624.
- [2] Delannay L., Melchior M.A., Signorelli J.W., Remacle J.-F., Kuwabara T. (2009) "Influence of grain shape on the planar anisotropy of rolled steel sheets - Evaluation of three models", *Computational Materials Science*, 45, 739-743.
- [3] Delannay L., Melchior M.A., Jacques P.J, Van Houtte P. (2005) "Simulation of the Lattice Strains Developed during a Tensile Test on a Multiphase Steel", *Materials Science Forum*, 495-497, 1627-1632.
- [4] Martin G. et al. "A new technique to determine micro-scale distribution - application to duplex stainless steel", *Proceedings of Duplex World 2010*, Oct. 2010, Baulne, France.

Effect of the stacking-fault energy on dislocation junctions in FCC metals

L. Dupuy¹, M. Blétry², E. Ferrié³, V. Quatela³ and M. Fivel³

¹CEA Saclay, DEN/DANS/DMN/SRMA/LC2M, 91191 Gif-sur-Yvette, France

²ICMPE, CNRS/Paris Est, 94320 Thiais, France

³SIMaP, Grenoble INP/CNRS, 38402 St Martin d'Hères, France

The formation and strength of dislocations junctions in FCC metals has been calculated using a new nodal dislocation dynamics software (Numodis). Following earlier studies, this model explicitly accounts for all slip systems and Burgers vectors observed in FCC metals, including stacking-faults and partial dislocations.

A particular emphasis is given here to the effect of the stacking-fault energy on the properties of these junctions. The structure of the different types of junctions existing in these metals is first examined including the Lomer-Cottrell lock, the collinear junction, the Hirth lock and the glissiles junctions.

We have also determined the 'yield surface' in stress space corresponding to the dissolution of these junctions. These results are compared with other models including line tension model, molecular dynamics simulations and other dislocation dynamics models. The influence of stacking-fault energy is studied as a function of the size of the junction.

Finally, the possibility to incorporate stacking-fault and partial dislocations in dislocation dynamics is critically assessed.

Mesoscale modeling of failure in partially sintered metals and homogenization to macroscale

Authors: Nathanaël Durr, Martin Sauer, Klaus Thoma

Affiliations: Fraunhofer Institute for High-Speed Dynamics
Ernst-Mach Institute
Eckerstraße 4, 79104 Freiburg, Germany
nathanael.durr@emi.fraunhofer.de

ABSTRACT

In this paper, we present a methodology for the multiscale analysis of deformation and failure of partially sintered metals. This methodology is based on experimental investigations, mesoscale modeling with the finite element method (FEM), and transfer of relationships derived at the mesoscale to the macroscale using a homogenization process. It can be used to investigate structure-properties relationships and is illustrated for a specific type of copper. The material is produced from cold-pressed spherical powder sintered at 700°C.

1. Introduction

The ability to predict the influence of manufacturing parameters on the behavior of polygranular materials under impact loads could speed up the material development process in areas such as protective materials. The behavior of such materials is governed by a number of factors. Apart from loading and sample geometry, the mechanical properties of grains and grain interfaces, i.e. the mesoscopic material properties, and the mesoscopic material structure, i.e. grain and pore sizes, shapes and orientations, play an important role. In this paper, we give an overview on the steps that are required for both mesoscale material modeling of partially sintered metals as applied for mesoscopic fragmentation analysis in [1], and the derivation of homogenized material laws. The latter can be used in a dynamic analysis on the macroscopic scale. A methodology similar to the one presented here was used in [2] for an open-cell aluminum foam.

The first steps are the construction of Representative Volume Elements (RVEs) at the mesoscale and the derivation of the required material laws. The third step is the construction of a continuum-mechanical model at the macroscale. For this purpose, different loading states are numerically investigated at the RVE scale using the commercial software LS-DYNA. The analysis of the homogenized results is made possible by using equivalent quantities. The homogenized plastic behavior, a pressure-density relationship and a triaxiality-dependent failure criterion can then be derived. As an example for the last step, model validation, the analysis of a cylinder compression test and the comparison to experimental results are given.

2. Construction of the RVE

Figure 1, left, shows a micrograph obtained by chemical etching of copper after cold-pressing of a spherical powder at 300 MPa and subsequent sintering at 700°C. Pores appear as black areas on the micrograph. The analysis of a set of micrographs allowed the progressive reconstruction of the 3D topology of a mesoscopic volume. The software GEODICT [3] of

Fraunhofer ITWM, Kaiserslautern, was used to generate a voxel-based RVE. A graphical representation of the RVE is given in Figure 1, right.

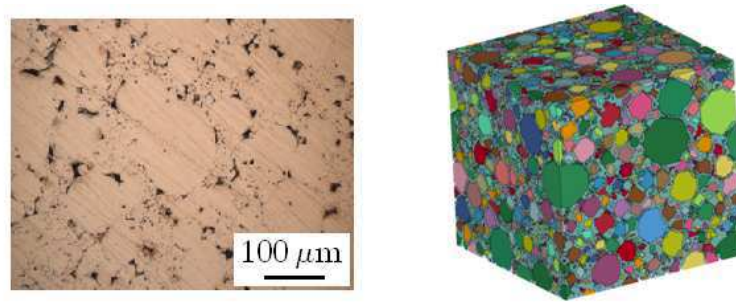


Figure 1. Left: micrograph of copper pressed at 300 MPa and sintered at 700°C; right: computer-generated, voxel-based mesoscopic volume after artificial insertion of border.

To reduce the computational effort, smaller volumes were extracted from the original RVE. Their representativeness was ensured by checking that the material response was conserved as the size of the volume decreased. The most optimal RVE was characterized by a 0.4 mm edge length and about 500 grains. In order to account for grain boundary failure, which is a typical phenomenon in partially sintered metals, an artificial “border” material with a thickness of at least one voxel was inserted between metallic grains, see Figure 1, right.

3. Mesoscale Material and Failure Modeling

Each of the two materials constituting the RVE, bulk copper and grain boundary material, is modeled with a piecewise linear elastic-plastic law. The material data for bulk copper was taken from the literature. Material parameters for the border material, weaker than the metallic grains, were determined by fitting computed homogenized mesoscopic material response to macroscopic experimental tensile test results as shown in Figure 2, left.

Failure of the border material was modeled with the so-called nodesplit method available in LS-DYNA. It is based on a failure criterion at interface nodes. In order to use this method, nodes which are linked to different grains need to be duplicated for each grain. When the failure threshold (effective plastic strain) is reached in adjacent elements, the coincident nodes are permitted to separate from each other. With this failure model, the fragmentation pattern shown in Figure 2, right, can be obtained.

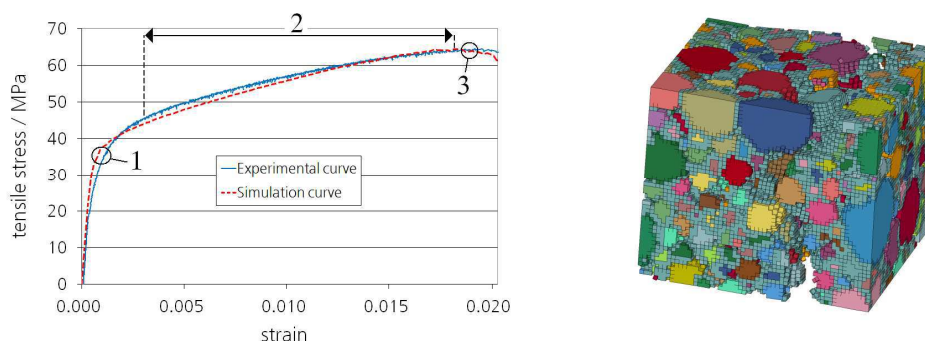


Figure 2. Left: fitting of the experimental and the simulated material responses; right: fragmentation pattern of the RVE as failure point “3” is achieved.

In order to obtain a good fit of experimental and simulated stress-strain curves, three separate aspects of the material response were optimized:

- 1 - The initial yield stress is determined by the initial yield stress of the border material.
- 2 - Optimization of the plasticity curvature: a damage model of the RVE at grain scale was realized. For this purpose, values of critical effective plastic strain within a selected failure interval were uniformly distributed to all inter-granular nodes. This allows the successive birth of cracks in the RVE during the loading and leads to a softened stress increase (concave curvature).
- 3 - Optimization of the global failure point: this point is also coupled to the damage model of the RVE, a global stress decrease occurs when enough nodes have split after the neighboring elements reached the effective plastic strain criterion.

2. Mesoscale Modeling Results, Homogenization and a Simplified Macroscale Model

The heterogeneous mesoscopic model can be used to derive a homogeneous macroscopic model (homogenization). To achieve this, further tests were performed on the RVE that combined uni- and multiaxial loading states, either with traction or compression. Equivalent quantities for stresses and strains are commonly used to analyze different loading states. We used quantities based on the von Mises definition:

$$\sigma_{\text{vM}} = \sqrt{\frac{3}{2} \underline{s}_{ij} : \underline{s}_{ij}} \quad \varepsilon_{\text{eff}}^{\text{pl}} = \sqrt{\frac{3}{2} \underline{\varepsilon}_{ij}^{\text{pl}} : \underline{\varepsilon}_{ij}^{\text{pl}}} \quad (1a-1b)$$

Eqn (1a) and (1b) define the von Mises stress σ_{vM} and the equivalent plastic strain $\varepsilon_{\text{eff}}^{\text{pl}}$, where \underline{s} is the deviatoric component of the stress tensor.

For each loading state, the equivalent stress was plotted over the equivalent strain, as shown in Figure 3, left. The behavior can be described by a Johnson-Cook type yield stress, see Eqn (2). The parameters A, B and n are directly derived from the analysis of the flow curves:

$$\sigma_Y = \left(A + B \left(\varepsilon_{\text{eff}}^{\text{pl dev}} \right)^n \right) \quad (2)$$

Similarly, the representation of the effective plastic deviatoric strain at failure over the triaxiality σ^* , defined by Eqn (3a), allows the definition of a simplified failure law. We used a simplified Johnson-Cook failure law as depicted in Eqn (3b).

$$\sigma^* = \frac{-p}{\sigma_{\text{vM}}} = \frac{(\sigma_{11} + \sigma_{22} + \sigma_{33})}{\sigma_{\text{vM}}} \quad \varepsilon_{\text{eff}}^{\text{pl dev}}(\text{failure}) = (D_1 + D_2 \exp(D_3 \sigma^*)) \quad (3a-3b)$$

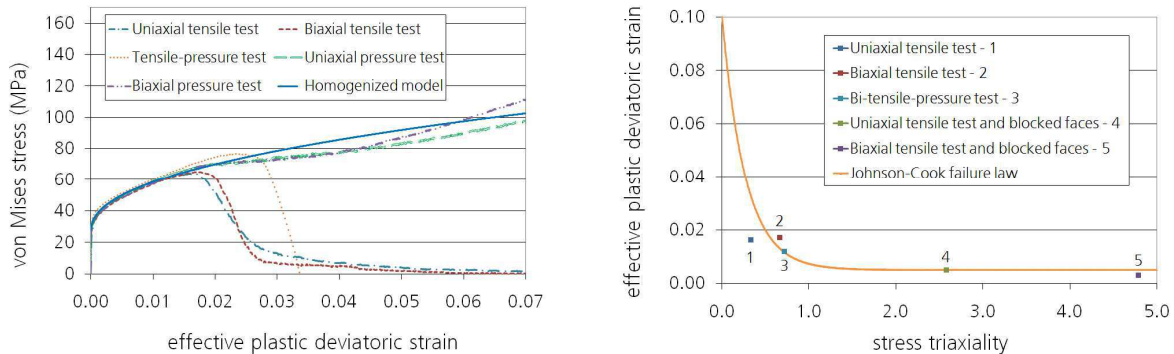


Figure 3. Left: homogenized stress evolution for each loading type and selected Johnson-Cook hardening law; right: triaxiality-dependent failure strain and Johnson-Cook failure law.

A homogenized equation of state, relating pressure and volumetric strain, was also derived but will not be detailed here.

3. Validation of the homogenization: pressure test

An example for the validation of the homogenized model is outlined briefly in the following. In the experiment, a cylindrical sample is pressed between two plates. The experimental result is compared with the simulation of the same test, as shown in Figure 4.

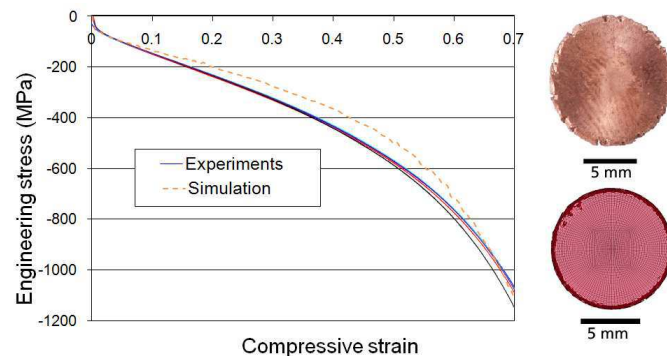


Figure 4. Numerical and experimental stress-strain curves and top view of the compressed sample at the end of experiment and simulation.

Figure 4 shows a very good accordance of the simulated and experimentally observed stress evolution over the strain. The formation of cracks on the periphery of the sample is also similar, see the pictures on the right of Figure 4.

5. Conclusion

The methodology for the multiscale analysis of deformation and failure of partially sintered metals outlined in this paper contains several steps. From microstructure analysis, a RVE that contains material and geometric information was built. Mesoscopic material parameters were determined by fitting homogenized simulation results to results of experimental tensile tests. Further loading cases were simulated to characterize the mesoscopic behavior. The results were aggregated to allow the definition of homogeneous macroscopic material laws. As an example for validation of the macroscopic laws, a compressive test at macroscale confirmed the accordance of numerical and experimental results. The developed model remains open for further improvement, especially in the domain of the behavior under dynamic loading.

Acknowledgements

We thank Frank Bagusat from EMI for conducting the experiments. The project was sponsored by the United States Department of the Navy, Office of Naval Research (ONR), under grant No. N00014-07-1-1053, this support is gratefully acknowledged.

References

- [1] M. Sauer, F. Bagusat, N. Durr, A. Klomfass. Fragmentation of Partially Sintered Materials – Experimental Investigation and Mesoscale Simulation. Proceedings of the 11th Hypervelocity Impact Symposium, Freiburg 2010 (in print).
- [2] Wicklein M, Thoma K. Numerical investigations of the elastic and plastic behavior of an open-cell aluminum foam. *Mat Sc. Eng.*, 2005, A 397: 391-399.
- [3] www.geodict.com

Interaction Between Grain Boundaries and Dislocations: Towards a Cohesive Law for Discrete Dislocation Dynamics

Sebastián ECHEVERRI RESTREPO¹, Barend J. THIJSSSE

Delft University of Technology, Department of Materials Science and Engineering,
Mekelweg 2, 2628CD, Delft, The Netherlands.

¹s.echeverrirestrepo@tudelft.nl

Within the framework of a multiscale project to model the role of interfaces in plasticity of face centered cubic metallic materials, the atomistic behavior of grain boundaries (GB's), dislocations and their different modes of interaction is analyzed by means of molecular dynamics (MD) simulations. The Embedded Atom Method (EAM) potentials developed by Mishin et al. [1,2] and the MD software package Camelion [3] are used.

An algorithm to generate GB's given its 5 macroscopic degrees of freedom (DOFs) [4] was developed. Variations to the 3 additional microscopic DOFs [4] are performed by rigidly translating one of the crystals with respect to the other.

A single full edge dislocation is then artificially inserted by removing two half planes (with a normal parallel to the direction $[110]$) from one of the crystals and displacing the remaining atoms according to the elastic isotropic theory of dislocations [5]. The system is then relaxed at a temperature of 0 K until the inserted dislocation splits into two Shockley partials and equilibrium is reached.

Stress is then applied to the system forcing the dislocation to approach and interact with the grain boundary. With the purpose of generating data to formulate a cohesive law to describe GBs in discrete dislocation dynamics simulations, the stress field and the structural evolution of the GB are measured during the interaction. This is done by keeping track of two sets of planes of atoms parallel to the GB plane. Simulations are performed for GBs with different DOFs and different energies.

References

- [1] Y Mishin, D Farkas, M J Mehl, and D A Papaconstantopoulos. Interatomic potentials for Al and Ni from experimental data and ab initio calculations. In Mat. Res. Soc. Symp. Proc. 538, 535-540, (1999).
- [2] Y. Mishin, M. J. Mehl, D. A. Papaconstantopoulos, A. F. Voter and J. D. Kress, Phys. Rev. B 63, 224106 (2001).
- [3] B. J. Thijssse. Camelion. Virtual Materials Laboratory, Department of Materials Science and Engineering, Delft University of Technology, The Netherlands
- [4] D. Wolf and S. Yip. Materials interfaces: atomic-level structure and properties. Chapman and Hall, (1992).
- [5] D. Hull and D. J. Bacon. Introduction to dislocations. Butterworth Heinemann, fourth edition, (2002).

Non-Uniqueness in Energy Minimization of Atomistic and Multiscale Problems: A Branch-Following and Bifurcation Investigation

Ryan S. Elliott¹, Ellad B. Tadmor¹, and Tsvetanka Sendova²

¹The University of Minnesota
Department of Aerospace Engineering and Mechanics
107 Akerman Hall
110 Union St. S.E.
Minneapolis, Minnesota 55455 USA
elliott@aem.umn.edu

²The University of Minnesota
Institute for Mathematics and its Applications
Minneapolis, Minnesota 55455 USA

Static multiscale and atomistic simulations aim to obtain an equilibrium configuration (local energy minimum) of a body composed of discrete atoms subject to applied loads and/or displacements. Often a system of "proportional loading" is considered and the evolution of the body's equilibrium configuration is determined in an incremental fashion as the scalar "loading parameter" is varied. At each step, a minimization procedure, such as the conjugate gradient method, is employed using the previous relaxed configuration as an initial guess.

A practical problem with such simulations is that due to the highly nonlinear nature of the problem, many equilibrium configurations should be expected. Therefore, the real possibility of multiple competing physical processes is encountered. Unfortunately, the simulation procedure described above provides only one of the possible equilibrium evolutions. Even more troubling is the fact that this particular equilibrium evolution will, generally, depend on the numerical energy minimization method employed and the particular values used for its parameters.

This work takes a different approach to the exploration of the equilibrium behavior of atomistic and multiscale systems. It performs a Branch-Following and Bifurcation (BFB) investigation in order to map out a large number of equilibrium configurations over a wide range of the problem's loading parameter. Once a reasonably complete picture of the system's possible behaviors is in hand, it is then possible to interpret these results to draw conclusions about the most likely behavior of the system.

To illustrate this novel application of BFB methods to atomistic multiscale problems, some representative problems will be presented including the results for a small "simple" atomic column subjected to axially compressive displacements. The set of possible equilibrium states found is much more complex than first expected and is a vivid illustration of the complex behavior these systems are capable of. These results will be described and some suggestions for "new" simulation/interpretation procedures will be discussed.

Influence of interatomic potential on the atomistic fracture in iron

C. H. Ersland^{1*}, C. Thaulow¹, D. Farkas² and E. Østby³

¹Department of Engineering Design and Materials,
Norwegian University of Science and Technology, NO-7491 Trondheim, Norway

²Department of Materials Science and Engineering,
Virginia Tech, Blacksburg, VA24061, USA

³SINTEF Materials and Chemistry, NO-7465 Trondheim, Norway

*christer.h.ersland@ntnu.no

Brittle fracture of metals can have catastrophic consequences, both for humans and for the environment. In order to prevent such events it is of importance to study the mechanisms taking place close to the crack-tip in a fracture process. By using atomistic modeling it is possible to investigate fracture mechanisms at length- and timescales previously unreachable by experiments and continuum models.

When doing atomistic simulations, the function describing the forces between the atoms is a crucial point for getting trustworthy results. A variety of such functions, or interatomic potentials, exist for iron. These include the embedded atom method (EAM) potentials of Ruda et al. [1] and Mendeleev [2], the Finnis-Sinclair (FS) potential of Lau et al. [3] and the analytic bond-order potential (ABOP) of Müller et al. [4]. The Ruda and Lau potentials are created for use in Fe-C systems, and include descriptions of the forces between iron and carbon atoms, but the formalism is such that they can also be used for pure iron systems.

The Griffith criterion in fracture mechanics predicts that cleavage will follow the direction of lowest surface energy. However, experiments and simulations have shown that this generally not the case. The most likely cleavage plane of iron is the (1 0 0) plane, but most potentials for pure Fe ranks the (1 1 0) plane as having slightly lower energy. Plastic deformations [5] and lattice trapping [6] have been discussed as causes for this ambiguity.

In this study, comparison of the above interatomic potentials has been performed by conducting molecular dynamics simulations of mode I fracture in bcc iron. This comparison could be used to determine the "best" candidate for use in further work. A simulation cell with an edge crack has been set up, and results by using the four different potentials have been compared. Different crack directions and temperatures have been used, to find the influence of this on the resulting crack behavior. Surface energy calculations have been performed in order to validate the crack plane ranking of the potentials, and the stress-intensity K_{Ic} at fracture has been compared with the corresponding fracture toughness predicted by fracture mechanics.

References

- [1] M. Ruda, D. Farkas, and G. Garcia, "Atomistic simulations in the Fe-C system," *Computational Materials Science*, vol. 45, no. 2, pp. 550–560, 2009.
- [2] M. I. Mendeleev and D. Farkas, "Unpublished EAM potential for α -Fe."
- [3] T. T. Lau, C. J. Först, X. Lin, J. D. Gale, S. Yip, and K. J. van Vliet, "Many-body potential for point defect clusters in Fe-C alloys," *Physical Review Letters*, vol. 98, no. 21, p. 215501, 2007.
- [4] M. Müller, P. Erhart, and K. Albe, "Analytic bond-order potential for bcc and fcc iron - comparison with established embedded-atom method potentials," *Journal of Physics: Condensed Matter*, vol. 19, p. 326220, 2007.
- [5] M. J. S. Spencer, A. Hung, I. K. Snook, and I. Yarovsky, "Density functional theory study of the relaxation and energy of iron surfaces," *Surface Science*, vol. 513, no. 2, pp. 389–398, 2002.
- [6] Y.-F. Guo and C.-Y. Wang, "Atomistic study of lattice trapping behavior for brittle fracture in bcc-iron," *Computational Materials Science*, vol. 40, no. 3, pp. 376–381, 2007.

Cohesive zone model for intergranular slow crack growth in ceramics: influence of the process and the microstructure

R. Estevez¹, M. Romero de la Osa^{1,2}, C. Olagnon¹, J. Chevalier¹, C. Tallaron²

¹Université de Lyon, INSA-Lyon, MATEIS CNRS UMR 5510, 25 avenue Jean Capelle,
F-69621 Villeurbanne cedex, France

²CEA Le Ripault, Laboratoire Microstructure et Comportement
37260 Monts, France
Rafael.Estevez@insa-lyon.fr

Ceramic polycrystals are prone to Slow Crack Growth (SCG) that is also environmentally assisted, similarly to what is observed for glasses. The kinetics of fracture are known to be dependent on the load level, the temperature and also on the Relative Humidity (RH). However, evidences are available on the influence of the microstructure on the SCG rate with an increase in the crack velocity with decreasing the grain size, crack propagation taking place beyond a load threshold that is also grain size dependent.

A cohesive zone is proposed for the intergranular failure process. The methodology accounts for an intrinsic opening that governs the length of the cohesive zone and ultimately allows the investigation of grain size effects. A rate and temperature dependent cohesive zone is proposed [1] to mimic the reaction-rupture mechanism that is inspired by Michalske and Freiman's picture [2] together with a recent study by Zhu et al. [3] of the reaction-rupture mechanism. The present investigation extends a previous work [4] in which the problem is formulated. Here, we explore the influence of initial thermal stresses originating from the sintering process on the crack growth under a static load. We show that these are responsible for the grain size dependence reported experimentally for the crack velocity. In addition, account for initial stresses enable the prediction of a load threshold below which no crack growth is observed: a crack arrest takes place when the crack path meets a region locally in compression.

1. Romero de la Osa M., Estevez R., Chevalier J., Olagnon C., Charles Y., Vignoud L., Tallaron C., *J. Mech. Adv. Mat. Struct.*, 16 :623-631, 2009.
2. Michalske T. A., Freiman S. W. *J. Am. Ceram. Soc.*, 66:284-288, 1983.
3. Zhu T., Lib J., Linc X., Yip S., *J. Mech. Phys. Sol.*, 53:1597-1623, 2005.
4. Romero de la Osa M., Estevez R., Chevalier J., Olagnon C., Charles Y., Vignoud L., Tallaron C., *Int. J. Fract.*, 158(2) :157-167, 2009.

Influence of texture evolution on the plastic deformation of commercial sheet steels under bi-axial loading conditions

G. Falkinger^{1,2}, A. Prakash¹ and H. Riedel¹

¹Fraunhofer Institute for Mechanics of Materials IWM, Woehlerstr. 11, 79108 Freiburg, Germany

²Voestalpine Stahl GmbH, Voestalpine Strasse 3, 4020 Linz, Austria

Email: georg.falkinger@iwm.fraunhofer.de

The purpose of this contribution is to study the influence of the evolution of crystallographic texture on the plastic deformation of commercial sheet steels under bi-axial loading conditions. To this end deep-drawing tests with a hemispherical punch were carried out for a low-carbon steel and a dual-phase steel. Using different specimen geometries, a broad variety of bi-axial loading conditions from uni-axial to equi-bi-axial was achieved. Preliminary results show that phenomenological models, e.g. Hill [1948], fail to predict the strain path of the specimens during deformation, indicating a strong influence of the evolving texture. Texture simulations of the experiments have been performed using a commercial finite element software employing a material model based on crystal plasticity [Huang 1991, Prakash et al. 2009] with a homogenization scheme based on the assumptions of Taylor [1938]. The crystallographic texture for the simulations was determined using electron backscatter diffraction (EBSD) techniques on the materials in the as-received state. Optical methods have been used to determine the strain field evolution during deformation. We compare the simulated texture as well as the evolving strain fields with those from the experiments. Additionally, we also discuss the parameter identification as well as the optimization of the computational performance.

References:

R. Hill [1948], *Proc. Roy. Soc. Lond. A* **193**, 281 – 297

Y. Huang [1991], *Technical Report MECH-178*, Harvard University

A. Prakash, S.M. Weygand and H. Riedel [2009], *Comput. Mater. Sci.* **45**, 744 – 750

G. I. Taylor [1938], *Journal of Institute of Metals* **62**, 307 – 327

Assessment of Interfaces in Electronic Packages using a Combination of Molecular Dynamics and Fracture Mechanics

Thomas Fellner, Jürgen Wilde

University of Freiburg
IMTEK - Department of Microsystems Engineering
Laboratory for Assembly and Packaging
Georges-Koehler-Allee 103, 79110 Freiburg, Germany
fellner@imtek.de, wilde@imtek.de

ABSTRACT

One of the aims of our study was the estimation of representative fracture-mechanic interface properties like the critical energy release rate or the crack resistance. Therefore we developed a concept which combines the information gained from molecular dynamics simulations with fracture-mechanics computations. To that purpose the crack tip stress-strain behaviour of the interface is analysed using finite element simulations.

This paper focuses on the modelling of copper-epoxy interfaces with a commercial Molecular Dynamics (MD) software. Primarily, the interaction between the adhesive partners in terms of adhesion was computed. Therefore copper surfaces with pure epoxy resins as well as a combination with thiol-based adhesion promoters leading to covalent bonding were examined. From the MD simulations information like the bonding energy per area and the stress-strain fracture-behaviour on bonding sites was extracted and transferred to a fracture-mechanics FEM simulation. The results were compared with measurements from crack propagation tests conducted in parallel. Moreover the effect of chemical modifications by use of adhesion promoters was evaluated qualitatively and quantitatively. The fracture toughness has been proven to be an effective parameter for characterisation of copper-moulding-compound interfaces by other authors. In our experiments we were able to confirm the high suitability of appropriate fracture-mechanic tests in assembly and packaging technology (A&P).

1. Introduction

A&P is a very large and important field in electronics and microsystems technology. Due to an increasing variety of materials, the reliable interconnection of different materials is one of its principal engineering challenges. Metal-plastic compound parts, and especially those consisting of a copper structure encapsulated in an epoxy resin are a characteristic feature of almost all present-day's packaging solutions.

In order to characterize the quality of composites, material parameters like the breaking strength or the fracture toughness are commonly used as evaluation criteria. For this purpose, a comprehensive number of tests such as peel, shear, pull or fracture-mechanics tests has to be performed on a large scale. Unfortunately, these tests will not reveal direct information on the phenomena which basically determine the adhesive strength on the molecular and interface scale. Among these are the number of chemical bonds per area, the strength of these bonds and the cohesive strength of the material adjacent to the interface. In order to design better interfaces, the knowledge about effective parameters near the interface is indispensable. In this regard, molecular dynamics simulations can make a major contribution to a better understanding and a faster characterization of interfaces and to evaluate the quality of different modifications to the composites even before performing tests.

2. Experiments

2.1 Specimens & surface preparations

To investigate the adhesion of copper-epoxy interfaces a shear test and a fracture-mechanical test were performed respectively. In these tests the investigated copper substrates were polished with 3 μm diamond suspension in order to obtain equivalent surface roughness. Subsequently, the copper substrates were degreased electrochemically in a hot alkaline bath to remove organic contaminations. Finally the copper substrates were finished in an aqueous CAROAT® etching solution for 15 s to gain a representative control sample. CAROAT® is typically used for printed circuit boards and leads to a reproducible degree of oxidation and thus to a strong metal epoxy-bond.

2.2 Used functional group

A new thiol-based molecule was synthesized and used as an adhesion promoter for copper-epoxy interfaces. First of all, the commercially available and low-cost cystamin dihydrochloride (Fig. 1, left) was deprotonated with sodium hydroxide in an aqueous solution. Following, the water insoluble cystamin ($\text{C}_4\text{H}_{12}\text{N}_2\text{S}_2$) was transferred to dichloromethane and isolated by using a rotary evaporator. The disadvantage of the unprotonated cystamin molecule is the poor stability during room temperature storage. In favor of gaining a higher stability and an easy handling, the free amino end-groups were saturated by Bisphenol-A-Diglycidylether (BADGE) (Fig. 1, right). This modified thiol-based molecule (THIOL-BADGE) can be solved in acetone before the application onto the substrates. Now, it contains two functional groups. In the center there is a disulphide bridge which reacts with the copper surface to form a strong chemical bond [1]. The second functional end group is the free oxirane ring of the BADGE to form a chemical bond to an overlaid epoxy resin.



Figure 1. Cystamin dihydrochloride (left), Bisphenol-A-Diglycidylether (right).

2.3 XPS – surface analysis

Confirming the covalent bond of the THIOL-BADGE three different copper samples were characterized by XPS surface analysis. Before the analysis, the samples were degreased electrochemically in a hot alkaline bath. Additionally, Control A was immersed into a pure acetone solvent for 1 h. Control B was immersed into a 10 mM BADGE acetone solution for 1 h. Finally the third sample was immersed into a 10 mM THIOL-BADGE acetone solution. Afterwards, the samples were tempered at 100 °C in pure nitrogen for 10 min before being rinsed thoroughly in two steps with acetone and ultrasound to remove unbonded molecules.

Table 1. Atomic concentration on copper surface

Element	Control A [%]	Control B [%]	THIOL-BADGE [%]
C1s	19.86	25.10	43.54
N1s	0.18	1.42	3.84
O1s	26.05	25.60	21.64
S2p	0.32	0.29	1.47
Cu2p3	53.59	47.59	29.51

Table 1 illustrates the atomic concentration of the different treated surfaces. Compared to the two control samples the THIOL-BADGE shows a significantly higher concentration of

carbon and hence a lower concentration of copper and oxygen. This suggests an increase of molecules mainly consisting of carbon atoms onto the surface. Additionally, as well documented in the literature the increasing S2p peak indicates chemisorbed sulfur [2].

2.4 Shear test & results

To verify the bonding mechanism of the THIOL-BADGE several button shear tests were performed using a DAGE 4000 shear tester. Therefore, simple wire end sleeves were filled with an epoxy resin and were applied to the different treated copper substrates. The used epoxy system is a pure BADGE resin cured with a diamin hardener (4,4'-Diaminodiphenylmethan) at 120 °C for 12 h in pure nitrogen ambiance. The mixing ratio of about 20 wt-% hardener and 80 wt-% BADGE was well-elected after preliminary investigations to obtain only adhesive fractures. The Control A substrate was just rinsed with acetone and dried with nitrogen after the cleaning as described in chapter 2.1. The cleaned Control B substrate was dipped into an acetone BADGE solution and the THIOL-BADGE substrate was dipped into an acetone THIOL-BADGE solution for a few seconds each. After the dipping, they were tempered for 1 h at 140 °C in pure nitrogen ambiance and rinsed thoroughly in two steps with acetone and ultrasound to remove unbonded molecules. Table 2 shows the shear test results for both the THIOL-BADGE and the two control samples. Obviously the THIOL-BADGE leads to an increase of the bonding energy for the used epoxy.

Table 2. Shear test results (shear height: 50 μm ; test speed: 85 $\mu\text{m/s}$)

Shear strength:	Control A	Control B	THIOL-BADGE
Mean value [MPa]	14.00	16.54	22.26
Standard deviation [MPa]	5.45	3.18	7.35
Number of samples	220	74	87

2.5 Fracture mechanics test

To determine the fracture toughness at the epoxy copper interface a tapered double cantilever beam (TDCB) consisting of copper was used. For this purpose, the two beams were treated as described in chapter 2.4 and joined with the already introduced epoxy system. The thickness of the epoxy layer was held constant at 65 μm by the means of spacers. The TDCB and its further dimensions are shown in Fig. 2.

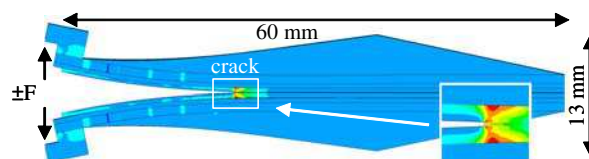


Figure 2. Tapered double cantilever beam specimen (width: 30 mm)

3. Multi-scale simulation

A molecular dynamics model was built using the Accelrys Materials Studio to evaluate the interaction energies for both a physisorbed and a chemisorbed epoxy resin. Therefore it was used a Cu_2O unit cell with a surface dimension of 25.6 \AA x 25.6 \AA . Above the surface the amine cross-linked epoxy system was set with an initial density of 1.2 g/cc. In the case of the chemisorbed epoxy the Cu-Thiol bond was modelled with a bonding energy of 276 kJ/mol [3]. When exceeding this value the covalent bond opens. During the MD simulation the cross-linked molecule was stepwise pulled upwards (Fig. 3). Between each step the model was equilibrated for 100 ps and the interface energies were calculated. The progression of these energies E'_{surf} versus the displacement d obtained from MD simulations

was fitted to the Morse potential model (Fig. 4 left). In the following step, the derivation of this fit was normalized to the surface area of the unit cell to get the tensile fracture strength σ_f at nanoscale (Fig. 4 left). The maximum of σ_f is used as a failure criterion and was transferred to the macroscale FEM simulation of the TDCB.

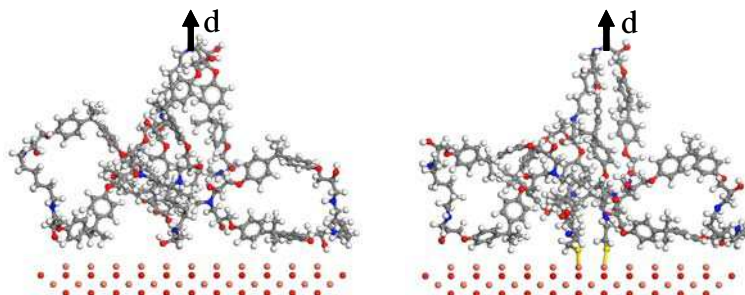


Figure 3. Diamin cross-linked BADGE displaced ($d = 17.5 \text{ \AA}$) from the Cu_2O surface, physisorbed (left) and with one THIOL-BADGE chemisorbed (right).

4. Results – fracture mechanics measurement vs. multi-scale simulation

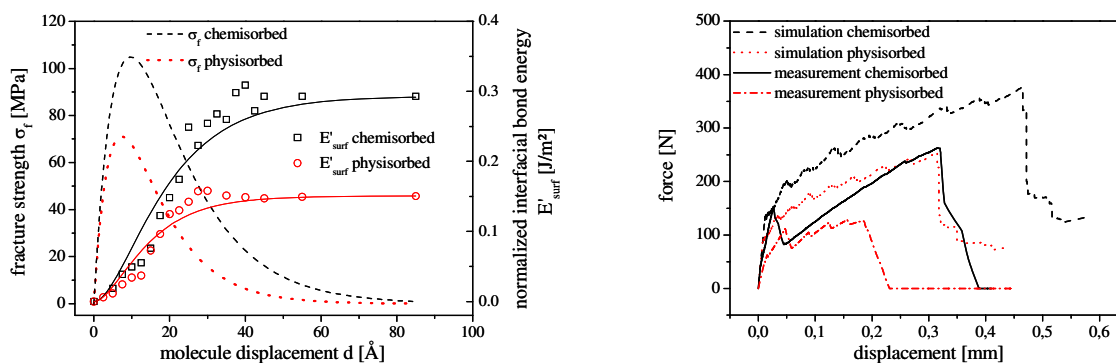


Figure 4. Left: MD-Simulated bond energies vs. displacement, Morse potential model fit (solid lines) and the derivative of this fit σ_f (dotted lines). Right: Results of the fracture mechanic measurement compared to the multi-scale simulation for different treated TDCBs.

Figure 4 (right) shows the force displacement diagram for both the multi-scale simulation and the fracture-mechanic measurement for the chemisorbed and for the physisorbed specimen, respectively. A good agreement of the interrelations between the chemisorbed and physisorbed cases as well as between simulation and measurement is observed. In general, the absolute values of the simulated fracture forces are a little higher than these obtained from the measurements. Furthermore, the maximum forces increase by a factor of 1.5 for the simulation and a factor of 2.0 for the measurement if performing the covalent linkage. This suggests that there could be more than two covalent bonds to the surface per unit cell if compared to the measurement.

Concluding, a new synthesized thiol-based adhesion promoter leads to a crack resistance which is by a factor of 4.4 higher (24 J/m^2 to 105 J/m^2) than that of the control sample. The crack propagation and hence material properties were computed with a multi-scale simulation and well predicted for both the covalent and the non-covalent linked interface, respectively.

References

- [1] Cell K. Y. Wong, Haibo Fan, Matthew M. F. Yuen, “Interfacial adhesion study for SAM induced covalent bonded copper-EMC interfaces by molecular dynamics simulation”, IEEE Transactions on Components and Packaging Technologies, Vol. 31, No. 2, pp. 297, 2008.
- [2] T. P. Ang, T. S. A. Wee, W. S. Chin, “Three-dimensional self-assembled monolayer of n-alkanethiols on copper nanoclusters”, J. Phys. Chem. B 2004, 108, 11001-11010.
- [3] G. Loepf, S. Vollmer, G. Witte, Ch. Wöll, “Adsorption of heptanethiol on Cu(110)”, Langmuir, Vol. 15, No. 11, 3767-3772, 1999.

Construction of Cauchy and polar equivalent continua from discrete homogenization techniques. Application to foams and biological membranes

Jean-François Ganghoffer¹, Francisco Dos Reis²

¹LEMETA. 2, Avenue de la Forêt de Haye. BP 160. 54504 Vandoeuvre Cedex. France.
Jean-Francois.Ganghoffer@ensem.inpl-nancy.fr

²LEMETA. 2, Avenue de la Forêt de Haye. BP 160. 54504 Vandoeuvre Cedex. France.

Architected materials such as polymeric and metallic foams have attracted the interest of many researchers in the last decade, due to their specific mechanical properties, which make them suitable materials adopted for their high crash absorbing capacity. The derivation of the mechanical properties of foams with a regular architecture (in the sense of endowed with a quasi periodic network) in relation to the topology of the cellular material and the bulk mechanical properties is especially interesting, in order to understand the observed behavior and to possibly tune the foam architecture to achieve certain properties at the structural level.

The derivation of the effective mechanical properties of 2D and 3D lattices made of beams is herewith investigated, relying on the asymptotic homogenization technique to get closed form expressions of the equivalent properties vs. the geometrical and mechanical micro parameters. In order to analyze the respective roles of flexion and extension at both the micro and macro scales, a mixed lattice able to account for both extensional and flexional effects in a versatile manner has been conceived. The scaling law of its effective traction modulus versus density shows a complex nonlinear evolution, with a drastic decrease when flexional modes become dominant over extensional ones. Extending next the present methodology towards 3D geometries, the effective mechanical behavior of Kelvin foams under compression is obtained, which agrees with both the literature and F.E. simulations. The symmetries of the effective compliance matrix do however not exhibit some of the required material symmetries under shear when the edge node rotations are prevented. A classification of lattices is then proposed with respect to the choice of the equivalent continuum model, according to the nature of the boundary conditions.

An extension of the asymptotic homogenization to micropolar continua is next performed, considering microrotations as additional d.o.f. at both the micro and macro scales. As an illustration of the method, the Poisson's ratio of the re-entrant hexagonal lattice shows very negative values, for moderate values of the angle between the re-entrant bars of the unit cell. The homogenized behavior of chiral lattices also exhibiting negative Poisson's ratio shows a coupling between micromoments and deformations. The effective mechanical behavior of planar biological membranes is further calculated.

Plasticity of Nano- and Micro-pillars

Nasr M. Ghoniem⁽¹⁾, Anthony Brown⁽¹⁾, and Jaafar El-Awady⁽²⁾

⁽¹⁾ Department of Mechanical and Aerospace Engineering, University of California, Los Angeles, Los Angeles, CA, 90095, ghoniem@seas.ucla.edu

⁽²⁾ Department of Mechanical Engineering, Johns Hopkins University, Baltimore, MD 21218, jelawady@jhu.edu

ABSTRACT

We review unique mechanisms of plastic deformation in nano- and micropillars. At the nano-scale, it is shown that plastic deformation is asymmetric with respect to direction of mechanical loading, as a result of specific relationships between the normal and resolved shear stress on active slip planes. This is attributed to the dependence of shear wave speed on the stress state acting on slip planes. Plastic deformation of nano-twinned copper pillars show a mechanism transition from dislocation nucleation to twin boundary migration. The flow strength σ_f of micropillars is shown to be size-dependent, and scales with the diameter, D as: $\sigma_f \propto D^{-0.69}$, in agreement with experiments. For micropillars of diameter larger than ≈ 100 nm, a ‘weakest-link’ dislocation activation mechanism accounts for the size effect. Aspects of work-hardening in discrete steps can be explained to result from cross-slip and sub-division of screw segments.

1. Introduction

At the atomic level, plastic deformation is facilitated by several basic mechanisms involving grain boundary sliding, diffusional creep, slip through dislocation motion, and twin boundary migration. It is generally associated with the irreversible deformation of solid crystals, because processes such as atomic diffusion and defect nucleation require an energy barrier, and as such, atomic motion cannot be reversed. The mechanical deformation of nanopillars beyond the elastic regime shows unusual characteristics that are not observed in bulk materials. Recent Molecular Dynamics (MD) simulations show that the primary yielding mechanism under uniaxial compression is by nucleation of Shockley partial dislocations from the surface. However, when considering polycrystalline nanopillars, the interaction of grain boundaries and dislocations produces a yet more complex picture. Deformation mechanisms in nanopillars containing multiple grains can be accommodated by either grain boundary migration, grain boundary sliding, motion of existing dislocations, and nucleation of new dislocations from surfaces and grain boundaries. The preferred mechanism can depend on a variety of conditions ranging from the orientation and direction of the crystallography relative to the deformation, the availability of slip planes, or the lattice energies of the respective defects. The effects of free surfaces on yielding was studied by Li and Ghoniem¹ for twinned copper. For micro-pillars, one of the key issues discussed in the literature recently is the dependence of the flow strength on the pillar size, and the mechanisms that control work hardening

One objective of the present work is to explore conditions that control two important modes of plastic deformation in copper nanopillars: dislocation nucleation from the surface and twin boundary migration. The main aim here is to show that a transition from reversible to irreversible plastic flow can be induced in axially loaded nano-pillars, and that a tension-compression asymmetry is inherent in plastically deforming nanopillars. A second objective is to investigate the effect of size on the strength of micropillars, and the nature of work hardening. The present

review is based on the recent work of Brown & Ghoniem², and El-Awady et. al.³.

2. Computational Method

Atomic interactions in MD simulations here were modeled using an Embedded Atom Method (EAM) potential for copper using the Mishin potential. A twin boundary was then constructed by performing 180° rotation of the half-grain above a selected slip plane (111) relative to the other half. For each simulation, the angle θ formed between the load axis and the twin boundary normal controls the shear load ratio, R , defined as the ratio between the resolved shear stress and normal stress acting on the slip plane. In addition to the rotation, in-phase shifts lateral to the rotation plane were also performed on the half-grains. Finally, all atoms outside a cylinder with a diameter of 9 nm and of a height between 27 and 30 nm were removed from the simulation block, thus leaving an atomically smooth cylindrical surface behind.

The computational method adopted for micropillars follows the formulation developed by El-Awady et al.³. In this formulation, the Boundary Element Method (BEM) is coupled with the 3-D Parametric Dislocation Dynamics (PDD) to incorporate the influence of free and internal interfaces on dislocation motion, and hence to describe microscopic plastic flow in finite volumes. In this methodology, the effects of surfaces and boundary conditions are modeled with the BEM, while the computational structure of the PDD is unchanged. In the PDD, all dislocation loops are discretized into curved parametric segments and the elastic field, forces, and motion of the dislocation segments in an infinite medium are computed.

3. Reversible-Irreversible Plasticity Transition

Plastic deformation of twinned fcc crystals has been shown by Li and Ghoniem to proceed via two main channels: (1) nucleation and propagation of dislocations; and (2) twin boundary migration¹. Nucleation of Shockley partial dislocations takes place at free surfaces⁴, or at twin boundaries themselves¹, and as such, will lead to irreversible plastic deformation. On the other hand, if surface dislocation nucleation is somehow prevented, and twin boundaries are subjected to sufficient shear displacement, twinning dislocations can form at these boundaries allowing them to migrate normal to the shear plane displacement. The atomic mechanisms of this twin boundary motion (TBM) “coupled” to shear deformation have recently been described within the framework of stick-slip dynamics⁴. Hu, Li and Ghoniem found that the “stick” phase of the dynamics is associated with accumulated strain in the crystal, and that such strain is suddenly released by the nucleation of 1/6[112]-type twinning partial dislocations⁴.

The yield locus for twinned copper nanopillars is shown in Fig. 1. When the local shear stress is below about 1 GPa, and the normal stress on twin planes is very large (e.g. above ≈ 2.5 GPa), TBM cannot be sustained anymore, and another plastic deformation channel opens up in the form of dislocation nucleation from the surface. We select here the two stress components, $\langle \sigma_R \rangle$ and $\langle \sigma_N \rangle$, to depict the yield surface of copper nano-pillars loaded in tension and in compression. The state of plastic reversibility at local shear stresses in the range $0.5 \leq \langle \sigma_R \rangle \leq 1$ GPa can be attained with a corresponding increase in the compressive normal stress, up to ≈ 2.5 GPa. Beyond these limits, twinned copper nanopillars make a transition to a state of plastic irreversibility attained by surface dislocation nucleation and TBM. The critical transition from reversible to irreversible plasticity is demonstrated in Fig. 2, where it is clearly shown that below a strain of about 3.3%, twinned copper nanopillars prefer to deform plastically by TBM, and thus the deformation is reversible since it is not associated with any surface dislocations.

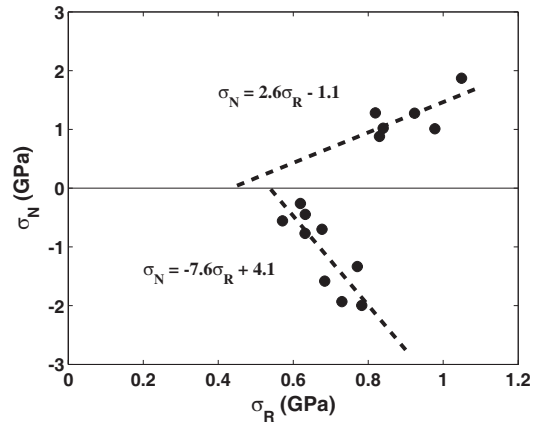


Figure 1: Yield locus for reversible plasticity for twinned nanopillars ($\langle \sigma_N \rangle$ versus $\langle \sigma_R \rangle$).

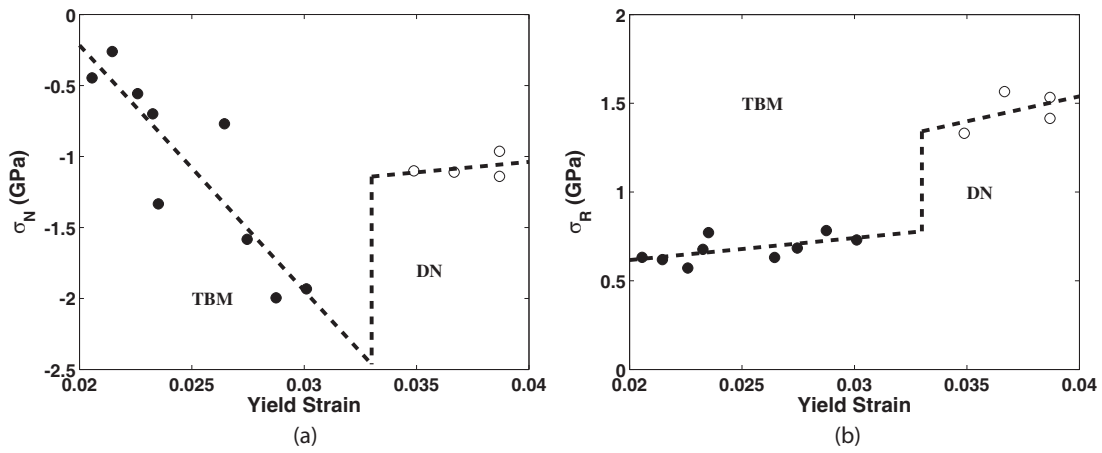


Figure 2: The normal stress, $\langle \sigma_N \rangle$, (a) and the critical resolved shear stress, $\langle \sigma_R \rangle$, (b) plotted as a function of the yield strain for twinned copper nanopillars under compression.

At larger values of strain, plastic deformation becomes irreversible.

4. Tension-Compression Asymmetry

A tension-compression asymmetry is observed² in simulations of nanopillars. Fig. 1 shows the yield locus for reversible plasticity controlled by TBM. Under compression, a lower value of the local shear stress is needed to initiate yield by TBM, as compared to the same conditions under tension. Twinning dislocation nucleation and motion is facilitated when the twin boundary is under compression, as compared to being under tension. However, and in both cases, a larger value of local shear is required to initiate TBM when any normal stress is additionally operating on the twin plane. Analysis of the simulations show that the speed of dislocation motion on twin boundaries is reduced whether the normal stress is tensile or compressive.

5. Flow Strength Size Dependence of Micro-pillars

To develop scaling laws for the strength of micropillars, PDD computer simulations coupled with a statistical analysis have been performed on the range of diameters from 0.25 to 5.0 μm . For each of the micropillar sizes, the initial dislocation density was statistically varied in the range $\rho = 1 - 50 \times 10^{12} \text{ m}^{-2}$. The scaling relationship for the flow strength, σ_f , with the

micropillar diameter is seen to be of a power law type, with an exponent of -0.69. This is in close agreement with the exponent produced by the experimental results³. A best fit of simulated results for Ni micropillars is $\sigma_f \approx 222 D^{-0.69}$, where D (μm) and σ_f (MPa). Plastic deformation beyond the yield point of micropillars shows work-hardening that has two characteristics: (1) it shows nearly perfect plasticity, with intermittent steps in the stress-strain relationship, and (2) large deformation results in geometric instabilities. The work-hardening in discrete steps can be explained in the simulations³ to result from cross-slip and sub-division of screw segments

6. Summary & Conclusions

Plastic deformation of twinned copper nanopillars shows behavior that is not observed in the deformation of bulk copper. The unique features of this deformation stem from the small size and the ability to control the type and nature of dislocation nucleation and motion inside these nano-systems. The yield locus for twinned copper nanopillars is an approximate linear relationship between the shear and normal components of the average atomic stress on twin planes. The critical transition from reversible to irreversible plasticity is shown to take place at a strain of $\approx 3.3\%$. We also show here that reversible plastic yield under tension is not the same as under compression, which indicates a clear “tension-compression asymmetry” in the reversible plasticity of twinned nanopillars. The reversible-irreversible plasticity transition is found to be the result of a competition between the nucleation and growth of twinning dislocations for reversible plasticity, versus dislocation emission from free surfaces for irreversible plasticity. For micropillars, the probability of a single pinned or double pinned dislocation of length $0.1 \mu\text{m}$ existing in a micropillar is found to be very small. Thus, for a micropillar having a diameter $D \leq 0.16 \mu\text{m}$, most pre-existing dislocations would be close to the surface, and also junction formation would be very unlikely because of the low initial dislocation density. Thus, surface-nucleated dislocations would escape from the pillar leaving it dislocation free, giving rise to a possible dislocation-exhaustion mechanism. For larger micro-pillars, however, there is a higher probability of having pinned dislocations, and thus a ‘weakest link’ mechanism would control the strength and work-hardening of the pillar.

References

- [1] L. Li, N. Ghoniem, Twin-size effects on the deformation of nanotwinned copper, *Phys. Rev. B* 79(7) (2008) 075444.
- [2] J.A. Brown, N.M. Ghoniem, Structure and Motion of Junctions Between Coherent and Incoherent Twin Boundaries in Copper, *Acta Materialia*, 57 (2009) 4454.
- [3] J. A. El-Awady, S. B. Biner, N.M. , A Self-Consistent Boundary Element, Parametric Dislocation Dynamics Formulation of Plastic Flow in Finite Volumes, *Journal of the Mechanics and Physics of Solids*, 56(5) (2008) 2019.
- [4] Q. Hu, L. Li, N. Ghoniem, Stick-slip dynamics of coherent twin boundaries in copper, *Acta Materialia*, 57(15) (2009) 4454.

Acknowledgements

Work is supported by the U.S. NSF grants: 0506841 and 0625299, and the U.S. AFOSR, grant: FA9550-07-1-0396.

A 3D Atomistic-Continuum Foliation Model For Multiwalled Carbon Nanotubes

Susanta Ghosh¹, Marino Arroyo²

[1susanta.ghosh@upc.edu](mailto:susanta.ghosh@upc.edu) [2marino.arroyo@upc.edu](mailto:marino.arroyo@upc.edu)

LaCàN, Departament de Matemàtica Aplicada 3,
Universitat Politècnica de Catalunya (U.P.C.), Barcelona, E-08034, Spain

Multiwalled carbon nanotubes (MWCNTs) have the potential to greatly contribute to nano-scale devices and nanostructured materials. Predictive simulations have become one of the focal points in current carbon nanotube research. A recently developed atomistic-based continuum model for surface of mono-layer lattices (Arroyo and Belytschko, 2004, International Journal for Numerical Methods in Engineering) is quite accurate and can significantly reduce the computational cost of atomistic simulations via continuum approximation. However, this approach is also computationally expensive, since each and every wall needs to be modeled, and the interactions between them need to be resolved. Indeed, a large fraction of computational effort of this approach is used to compute the van der Waals (VDW) interactions. Contrary to the short-range covalent bond potential, the non-bonded potential requires the computation of a large number of pair interactions, with neighbor lists that need to be updated as the system deforms. The objective of the present research is to extend this atomistic-continuum scheme, as well as other related single layer models, in order to obtain a computationally efficient 3D continuum model for MWCNTs. In the proposed model the energy density (hyper-elastic potential) of the bulk 3D continuum is composed of elastic potential of a stack of layers and energy of interlayer VDW interactions per unit volume. The resulting 3D continuum model is different from standard anisotropic elastic models, in that the important kinematical quantities are those of foliation rather than the usual ones. Our results show that the proposed model reduces computational effort dramatically, since it completely obviates the pairwise calculation of VDW force. The present approach may have a broad range of applications in the analysis and design of MWCNTs, particularly when the overall behaviour is insensitive to precise details of pairwise VDW potential, such as registry effects.

Coarse implicit time integration of a cellular scale particle model for plant tissue deformation

**P. Ghysels¹, G. Samaey¹, P. Van Liedekerke²,
E. Tijskens², H. Ramon² and D. Roose¹**

¹K.U.Leuven – Department of Computer Science, Celestijnenlaan 200A - bus 2402,
B-3001 Heverlee – Belgium,
pieter.ghysels@cs.kuleuven.be, Tel.: +32-16-327700

²K.U.Leuven – Department of Biosystems, Kasteelpark Arenberg 30 - bus 2456,
B-3001 Heverlee - Belgium

Plant tissue is a material with a distinct multiscale nature, in which properties at the (fine) cellular level influence the (coarse) tissue behavior in a highly non-trivial way. A computational model is developed that appreciates the fine scale by modeling the plant cell walls as thin viscoelastic shells using Discrete Elements (DEM) and the internals of the cells as a viscous fluid using Smoothed Particle Hydrodynamics (SPH). This Lagrangian particle model is used as the fine scale model in a Representative Volume Element (RVE) based computational multiscale method. A coarse material description for a simple fading memory viscoelastic solid is derived from the fine scale model using Generalized Mathematical Homogenization and is solved by standard Finite Elements (FEM). A constitutive equation is never explicitly derived, instead the FEM computes the stress tensor from the underlying fine scale model inside an RVE centered around the FEM quadrature points.

A class of algorithms, called constrained runs iterations, is presented to consistently initialize the many degrees of freedom inside an RVE simulation. An RVE is initialized consistently only when its coarse observables, such as the volume averaged deformation and velocity gradients agree with the corresponding coarse-scale variables at the coarse coordinate, and when the RVE state is consistent with the fine scale dynamics. This procedure allows initialization of the RVE with both coarse scale deformation and velocity gradients, which would not be possible with a simple relaxation of the internal RVE state, since either deformation or velocity would change.

Computation of the Cauchy stress from an RVE is straightforward by volume averaging over the RVE. We use forward finite differencing of the objective Truesdell stress rate to estimate both the fourth order elasticity and viscosity tensors. This requires fine scale RVE simulations with slightly perturbed deformation and velocity gradients. The elasticity and viscosity tensors are then used to construct the coarse scale stiffness and damping matrices respectively. These allow implicit time integration of the coarse scale FEM model using much larger time steps than would be possible using explicit time integration methods for the FEM model. Note that when only the fine scale model is used, explicit integration with very small time steps must be used. So besides exploiting the spatial separation in scales by only simulating inside the RVEs, we also exploit the separation in temporal scales.

Multiscale approach of interaction between hydrogen and plasticity in AA 5083 aluminum alloy. Experimental and numerical investigations

Edouard Pouillier¹, Esteban P. Busso¹, and Anne-Francoise Gourgues-Lorenzon¹

¹MINES ParisTech, Centre des Matriaux, CNRS UMR 7633, B.P. 87, 91003 Evry Cedex, France.

ABSTRACT

To investigate crystal plasticity effects on intergranular cracking of a 5083 aluminum alloy after hydrogen charging, tensile specimens charged with hydrogen over a depth of several μm were used to quantify the effect of inelastic strains at the grain scale. The evolution of strain fields at various scales and the local microtexture were recorded in the same region at various stages of an in-situ tensile test in the scanning electron microscope. The first boundaries to crack, after only a few percents of strain, were all located between two grains that were little deformed, inside a cluster of more heavily deformed grains. To derive a local fracture criterion, a strain gradient crystal plasticity model was employed in finite element (FE) simulations of the experiments. A threshold value of the local opening stress needed to intergranular crack nucleation was determined to be about 250 MPa.

1. Introduction

Al-5Mg based alloys, such as AA5083, are sensitive to intergranular stress corrosion cracking and hydrogen-induced embrittlement (HIE) when the major part (but not all) of Mg atoms are in solid solution. Intergranular fracture is due to a close interaction between hydrogen, crystal plasticity and grain boundary [1]. Nevertheless, the role of micro plasticity is not well established yet. The main objective of this study is to quantitatively investigate the effect of crystal plasticity on intergranular crack initiation of a hydrogen-charged 5083 aluminum alloy, during tensile testing. A representative region containing 500 grains was chosen in the central part of the tensile specimens. It was characterized by electron backscatter diffraction (EBSD) at the initial state. During in-situ tensile tests, local strain fields and crack nucleation events were investigated. The same region was also meshed as a crystal aggregate for mechanical analysis of the test with a crystal plasticity model [2]. From stress and strain analysis, intergranular crack initiation conditions were investigated and a fracture criterion was eventually derived.

2. Experimental work

2.1 Material and specimen preparation

The AA5083 alloy under study was provided as an extruded rod end bar with a diameter of 15 mm, which had been hammered up to 30% of strain. Specimens were solution treated, quenched and aged for 7 days at 150 °C to get a high sensitivity to HIE. EBSD analyses revealed a textureless microstructure with a mean grain size of 27 μm . The regions characterized by EBSD (≈ 500 grains) were thus assumed to be representative of the material. EBSD scans were also acquired after deformation to investigate local orientation changes due to plastic deformation. HIE was obtained over a depth of 5 μm by cathodic charging in a boric acid solution, leading to hydrogen trapping at grain boundaries next to Al_3Mg_2 nano-precipitates [1]. Only the re-

gion of interest, in the central part of tensile specimens, was charged with hydrogen, preventing from premature fracture (due to cracking initiated out of the observed region) during the tensile test. The charging conditions also led to local pitting corrosion, allowing getting surface heterogeneities to optimize DIC results.

2.2 In-situ tensile test inside the scanning electron microscope (SEM)

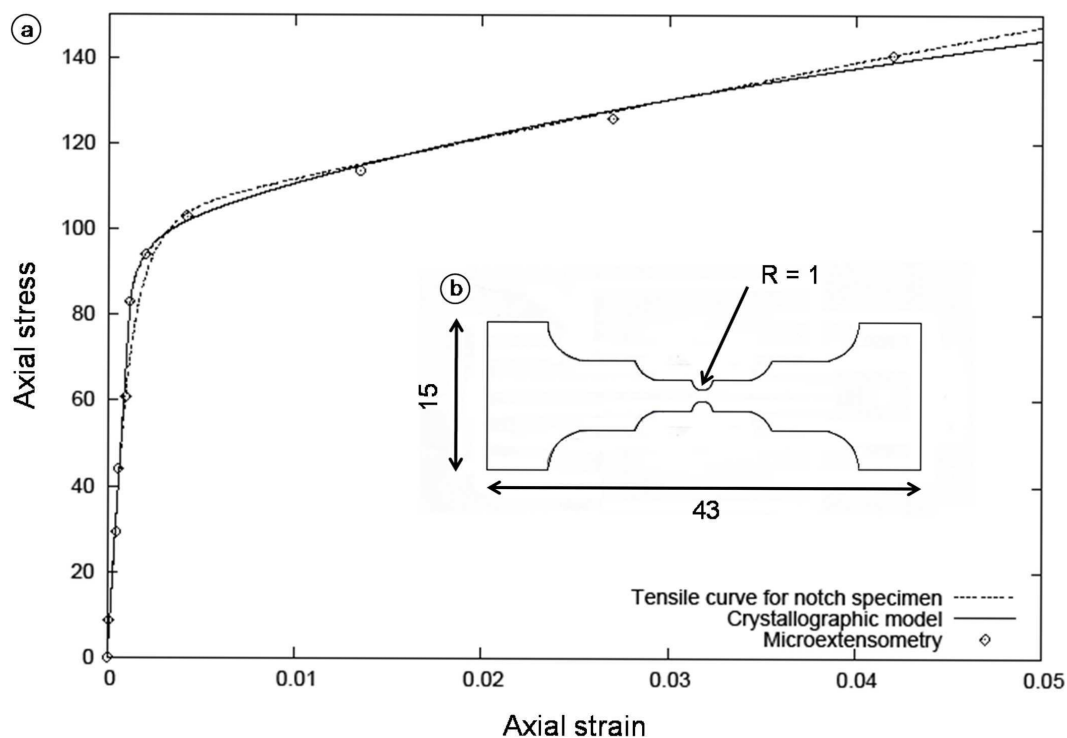


Figure 1: Axial stress-local average elongation curve in the central part of the notched tensile specimen: experimental tensile curve; model prediction for an aggregate of 450 grains in the studied region; "microextensometry" from displacement of indentation marks.

One-mm-thick flat tensile specimens with two notches at the center of the gage part were used in order to localize strain within the studied region (Figs 1-2). A mini-tensile machine was used for in-situ testing in the SEM with a prescribed load line displacement rate of $0.36 \text{ mm} \cdot \text{min}^{-1}$. The upper surface of the specimen together with fiducial indentation marks were first imaged at three magnification levels, with a spatial resolution of $0.5\text{-}50 \mu\text{m}$. The test was interrupted several times up to a local average elongation of 5% and digital images of the region of interest were acquired at the same three magnification levels. An optimized digital image cross-correlation technique was used to compute surface strain fields from recorded images. Processing DIC data by strain averaging over areas of $200 \mu\text{m}$ up to 1 mm in size provided fine-scale strain fields, as well as boundary conditions to be applied to crystal aggregates in the modeling part of the study.

2.3 Results and discussion

DIC computations at large scale (Fig. 2b) revealed that microcracks first nucleate within large deformation bands, after less than 1% of average plastic strain. Cracks first nucleate between grains that are less deformed compared to their neighbors (Fig. 2c). At finer scale, strain field

computations and local study of crystal orientation evolution by using EBSD confirmed that e.g. grain 2 and grain 3 of Fig. 2d were less deformed than their neighbors, such as grain 1. Complementary X-Ray tomography and serial sectioning measurements showed that cracked grain boundaries were perpendicular to the applied load. This suggests that local stresses have to be determined to derive a fracture criterion for the present case.

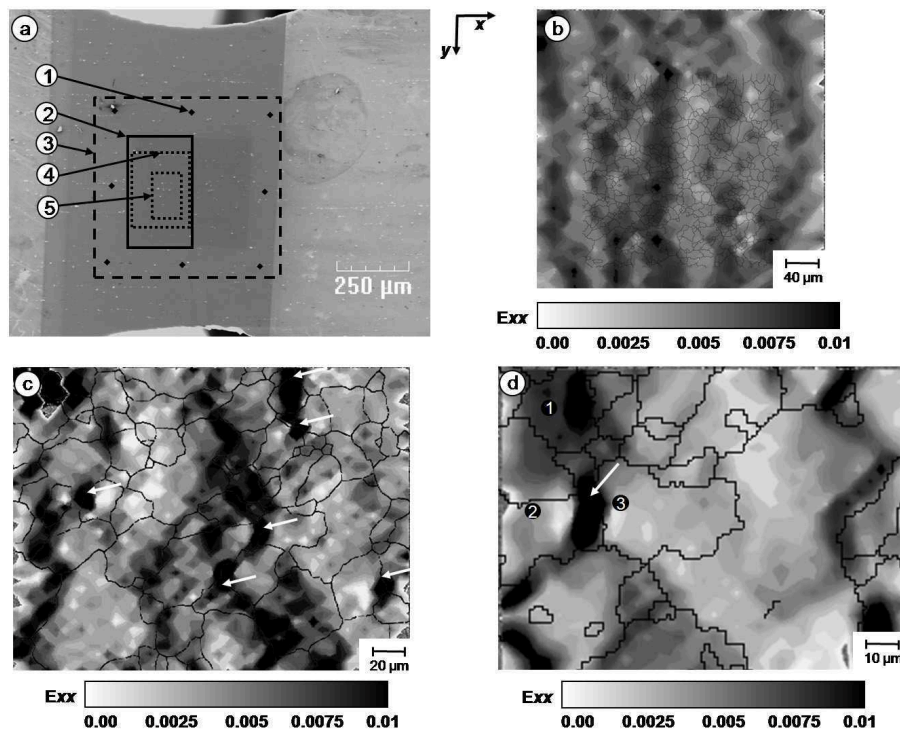


Figure 2: (a) SEM image: 1) indentation marks, 2) region analyzed with EBSD; DIC studied zones at 3) large, 4) medium and at 5) small scale. Axial strain fields measured by DIC after 0.5% of average elongation at (b) large, (c) medium and (d) small scales.

3. Mechanical analysis of the test and determination of a fracture criterion

3.1 Numerical procedures

The measured microtexture was used in finite element (FE) simulations with an in-house automated FE meshing method. The 2D FE mesh was obtained from initial EBSD grain color maps by using a local gradient detection method. First, triple junctions were detected. Grain boundaries were then identified as detected segments between triple junctions. The length scale used to divide these segments allowed the wavy shape of grain boundaries to be taken into account (lines in Fig. 3a). The measured displacements of each node of the mesh edges, obtained by DIC and generalized plane strain, were applied as boundary conditions to take the influence of the neighboring grains of the simulated aggregates into account.

Material constitutive equations were based on a generalized non-local rate-dependent crystallographic formulation for finite strains [2]. Additional solid solution strengthening by Mg atoms was modeled as an increase in the critical resolved shear stress by ≈ 37 MPa. Constitutive equation parameters were first calibrated from macroscopic stress-strain curves of smooth tensile specimens cut from the same material. For the mechanical analysis of the test at various scales, EBSD maps of 400 grains down to 40 grains in the initial state (typically, areas 3, 4, 5 in Fig. 2a) were meshed as crystal aggregates for FE simulations.

3.2 Results

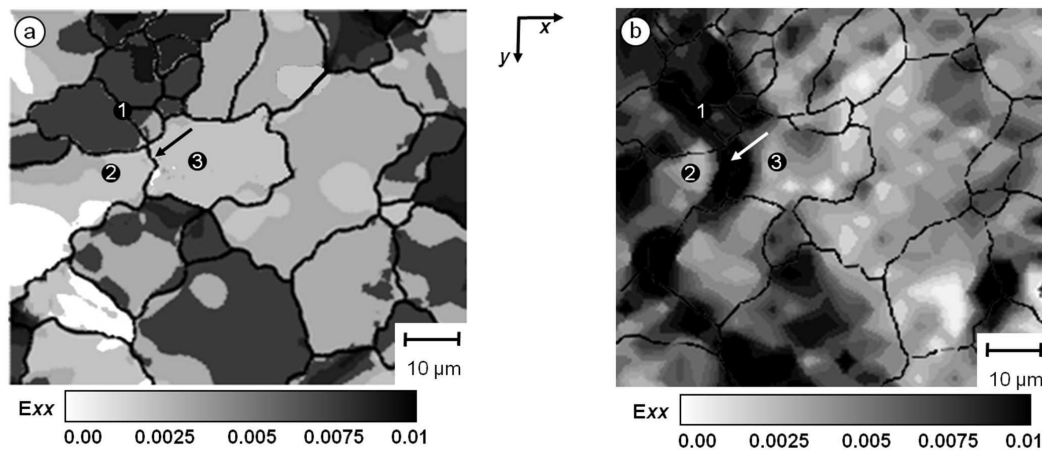


Figure 3: Axial strain field E_{xx} : (a) measured by DIC (b) predicted with the model.

The good agreement between experimental and numerical results both concerning average behavior (Fig. 1) and small scale (Fig. 3) validates the proposed model. From local stress fields, the normal stress in cracked GB was then calculated. An average value of 250 MPa was determined for an intergranular crack to nucleate. This value was confirmed on 3 specimens by analyzing more than 50 cracked all in the same configuration (i.e. boundaries between "hard" grains within a region of "softer" grains).

4. Conclusions

For the studied material and hydrogen charging conditions, intergranular crack nucleation is not a direct consequence of strain incompatibility across the grain boundary. All intergranular cracks initiate between grains that little deform, within a more severely deformed cluster of grains. Local strains are satisfactorily predicted by using FE simulation with a crystal plasticity model based on the actual microtexture. From local stress analysis, a local fracture criterion (250 MPa opening stress) was derived.

Acknowledgements

This research was supported by the French National Agency of Research (ANR), under the contract H-Inter.

References

- [1] Tanguy D., Bayle B., Dif R., Magnin T.. Hydrogen effects during IGSCC of pure Al-5Mg alloy in NaCl media. *Corrosion Science*, **44**, 1163–1175, 2002.
- [2] Cheong K.S., Busso E.P.. Effects of lattice misorientations on strain heterogeneities in FCC polycrystals. *Journal of the Mechanics and Physics of Solids*, **54**, 671–689, 2006.

A continuum approach applied to a strongly confined Lennard-Jones fluid.

R.M. Hartkamp, S. Luding

**Multiscale Mechanics, Faculty of Engineering Technology, University of Twente
P.O. Box 217, 7500 AE, Enschede, The Netherlands
r.m.hartkamp@utwente.nl**

ABSTRACT

Results from molecular dynamics simulations are analyzed with a continuum approach. It is shown that for strongly confined fluids the Navier-Stokes equations for incompressible, Newtonian fluids are not applicable over the whole channel. Near the walls, a Knudsen layer is formed and interesting oscillatory structures are seen, the fluid behaves non-Newtonian in these regions.

1. Introduction

Molecular dynamics simulations have become an important tool for the study of microscopic fluid properties. A channel geometry is often used to study the inhomogeneous behavior of strongly confined fluids (Koplik & Banavar⁶, Bitsanis *et al.*¹, Travis & Gubbins⁷) which behave different from Newtonian fluids. Our understanding of these non-Newtonian fluids is still very limited, while gaining a deeper insight is becoming increasingly important with the rise of microfluidic and nanofluidic applications, such as lab-on-a-chip devices. Similar phenomenology (i.e. layering, anisotropy) is observed in many particle systems (van Gunsteren *et al.*³, Ghosh *et al.*²). In this study, liquid argon is confined between two walls with normal in the x -direction (Fig. 1). When an atom leaves the system in y - or z -direction, it re-enters at the opposite side due to periodic boundary conditions. Both walls consist of two layers of argon atoms (each layer containing 128 atoms) fixed in a 001-face centered cubic (fcc) lattice. The fluid-wall interaction is equal to the fluid-fluid interaction and the number density of the system is $\rho^* = 0.8$ (corresponding to a volume fraction of $\nu = 0.415$ based on atom diameter σ). Physical quantities are nondimensionalized by using the length, energy and mass scales of liquid argon, which are $\sigma = 3.405 \times 10^{-10}$ m, $\epsilon = 1.67 \times 10^{-21}$ J and $m = 6.626 \times 10^{-26}$ kg respectively. A constant body force f^* acts on the fluid in negative z -direction, causing it to flow. The mutual interaction of the neutral spherically symmetric argon atoms is modeled via a two-body Lennard-Jones (LJ) potential. From the interaction potential, the force between two atoms can be calculated:

$$F_{LJ}(r) = -\frac{\partial U}{\partial r} = 24\frac{\epsilon}{\sigma} \left(2 \left(\frac{\sigma}{r} \right)^{13} - \left(\frac{\sigma}{r} \right)^7 \right), \quad (1)$$

with r the distance between two atom centers. The force is truncated at $r_c = 2.5\sigma$ in order to reduce calculation time for pair interactions. Furthermore, the force is shifted with $F_{LJ}(r_c)$ in order to maintain a continuous force at the location of truncation $F(r) = F_{LJ}(r) - F_{LJ}(r_c)$ and $F_{LJ}(r \geq r_c) = 0$.

From the positions, velocities and interatomic forces, other physical scalar or tensorial quantities can be calculated (e.g. shear rate, stress and viscosity) (Hartkamp *et al.*⁴). The position and momentum of each atom are used to calculate the forces acting on them and then their position and velocity after an increment (Δt) in time via the Velocity Verlet algorithm. The body force

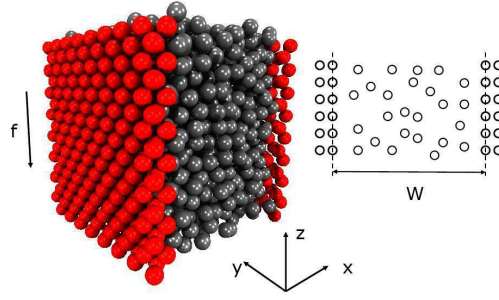


Figure 1: Liquid argon (grey, 2304 atoms) confined between solid argon walls (red, 512 atoms). The width of the channel is defined as shown on the right.

leads to an acceleration of the fluid, while viscous effects retard the flow until a steady state is reached. Local thermostats near the walls keep the energy (and thus the temperature) constant in time ($T^* = 1.0$ for the simulations presented here, which is equal to a temperature of $T = 121$ K for argon) (Ghosh *et al.*²). Atoms are initially positioned on a 001-fcc lattice. The lattice melts during the equilibration, followed by a steady state flow. The steady-state simulation results are averaged by means of 4000 snapshots over a period of time of 4000τ . Furthermore, spatial averaging is employed over the directions parallel to the solid walls, whereas, the x -direction (perpendicular to the solid walls) is divided into equally spaced bins of width $b = 0.083$. The channel is $W = 16.245\sigma$ in width and $H = 13.68\sigma$ in length and height. The fluid in the channel consists of $N = 2304$ argon atoms.

The Knudsen number of the flow, which is the ratio between the mean free path λ and the characteristic length scale $L_W = W/3$, is $\text{Kn} = (\sqrt{2}\pi\sigma^2\rho^*L_W)^{-1} = 0.052$. Typically, flows with a Knudsen number in the regime $0.001 \leq \text{Kn} \leq 0.1$ can be analyzed with conventional fluid dynamics equations such as the Navier-Stokes equations. However, the no-slip boundary condition does not hold if $\text{Kn} \geq 0.01$. A region forms near the wall, called the Knudsen layer, where the flow can not be analyzed by the conventional approach, an additional slip boundary condition is needed. The thickness of this layer depends on the Knudsen number, but is typically of the same order of magnitude as the mean free path.

Section 2 treats the conservation of momentum, applied to the system which is considered here. In section 3, the computational results are compared to the Newtonian theory and the results are briefly discussed.

2. Equations of fluid motion

The equations of fluid motion for an incompressible and Newtonian fluid are given by:

$$\rho \left(\frac{\partial \mathbf{v}}{\partial t} + \mathbf{v} \cdot \nabla \mathbf{v} \right) = -\nabla p + \mu \nabla^2 \mathbf{v} + \mathbf{f}, \quad (2)$$

with ρ being the density, \mathbf{v} the velocity vector, p the pressure, μ the shear viscosity and \mathbf{f} the external force on the fluid per unit volume.

For the system discussed here, the equations of motion can be simplified considerably. The system properties are (kept) constant in the y - and z -direction and the fluid is confined in x -direction. The force vector is: $\mathbf{f} = \{0, 0, -f\}$, with $f = \rho^* f^*$, where ρ^* is the number density and f^* is the body force on each particle. The body force on the fluid causes a streaming velocity profile in the negative z -direction.

After substituting the force vector and the velocity field, all the terms in the conservation of

x - and y -momentum drop out¹, leaving only the z -component of the momentum conservation Eqn. (2), which reduces to a Poisson equation:

$$\frac{\partial^2 v_z}{\partial x^2} = \frac{f}{\mu}. \quad (3)$$

The macroscopic fields are obtained from molecular dynamics simulations in the canonical ensemble (NVT). The averaged results satisfy Eqn. (3) if the fluid in the nanochannel behaves indeed incompressible and Newtonian. Velocity is an almost parabolic function of the x -location, due to the boundary conditions, besides wall effects.

3. Results and discussion

Fig. 2 shows the streaming velocity in z -direction as function of x and the first and second derivative with respect to the x -direction. The derivatives are obtained from the velocity profile via a central difference scheme. The velocity profile is approximately quadratic in the bulk, corresponding to linear and constant first and second derivatives respectively. However, the fluid deviates from this behavior near the walls of the channel. The predicted Knudsen layer can be identified where the trend in the streaming velocity deviates from a quadratic profile. This region is especially clear from looking at the first and second derivative of the velocity profile. The apparent slip in velocity corresponds to a slow decay to a zero shear rate at the sides of the channel. In addition to the Knudsen layer, oscillatory structures are seen in each of the profiles. The magnitude of these oscillations are maximal near the walls and decay towards the bulk.

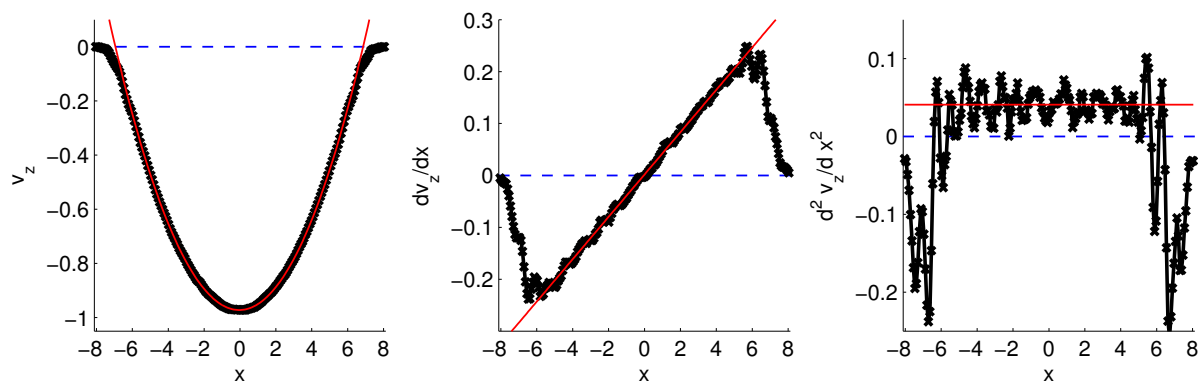


Figure 2: (left) Velocity profile in negative z -direction across the channel and (middle) first and (right) second derivatives with respect to x . The red solid lines represent the parabolic velocity profile with $f/\mu = 0.0408$ [(ms)⁻¹].

Fig. 3 shows the right-hand side of Eqn. (3) (left) and the difference between the right- and left-hand sides (right). The shear viscosity is defined as the ratio between the shear stress and the shear rate. The ratio between the force per volume and the shear viscosity (Fig. 3 (left)) forms a plateau in the bulk of the fluid and clearly deviates from this plateau near the walls of the channel. The strong oscillations in the center of the channel are an artefact due to the calculation of the shear viscosity; the shear rate is approximately zero in the center of the channel, leading to unphysical results for the shear viscosity, which should be ignored.

¹This is true for a homogeneous fluid, which is not necessarily in agreement with the outcome of the molecular dynamics simulations.

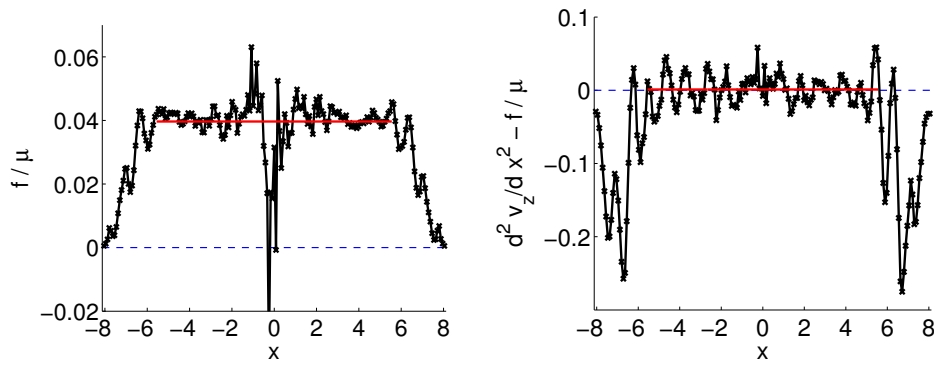


Figure 3: (left) The ratio between force and shear viscosity. (right) The difference between the left- and right-hand side of the conservation of z -momentum.

The difference between both terms in the conservation of momentum (Fig. 3 (right)) is a measure for the error that is made by treating the fluid as Newtonian. In the bulk region, the difference between both terms fluctuates around zero, which indicates that the fluid behavior is Newtonian in the bulk region, apart from statistical noise. The deviation from zero near the walls is larger in magnitude and opposite in sign compared to the average value of both individual terms in the bulk, indicating that the made assumptions do not hold in this region due to the Knudsen layer and the oscillatory structures close to the wall. The behavior of the curvature near the wall can not be compensated by a positive viscosity. This indicates that important contributions to the constitutive relation are missing, as will be studied in future work (Hartkamp *et al.*⁴). The Navier-Stokes equations with a slip boundary condition are also questionable near the walls due to the layering which extends a few σ into the fluid, see Hartkamp & Luding⁵.

Acknowledgements

This work was financially supported by MicroNed grant 4-A-2.

References

- [1] Bitsanis I., Vanderlick T.K., Tirrell M. and Davis H.T., A tractable molecular theory of flow in strongly inhomogeneous fluids, *Journal of Chemical Physics*, Vol. 89, pp. 3152, 1988
- [2] Ghosh A., Paredes R. and Luding S., Poiseuille flow in a nanochannel - use of different thermostats, *International Congress of Particle Technology*, CD Proceedings, pp. 1-4, 2007
- [3] van Gunsteren W.F., Berendsen H.J.C., Postma J.P.M., DiNola A. and Haak J.R., Molecular Dynamics with Coupling to an external bath, *Journal of Chemical Physics*, Vol. 81, pp. 3684, 1984
- [4] Hartkamp R.M., Ghosh A. and Luding S., Anisotropy of a fluid confined in a nanochannel, In preparation, 2010
- [5] Hartkamp R.M. and Luding S., Anisotropic Lennard-Jones fluids in a nanochannel., *International Conference on Multiphase Flow*, Tampa, Florida, pp. 1-7, CD Proceedings, 2010
- [6] Koplik J. and Banavar J.R., Molecular dynamics simulation of microscale poiseuille flow and moving contact lines, *Physical Review Letters*, Vol. 60, pp. 1282, 1988
- [7] Travis K.P. and Gubbins K.E., Poiseuille flow of Lennard-Jones fluids in narrow slit pores, *Journal of Chemical Physics*, Vol. 112, pp. 1984, 2000

Atomic-scale simulations of extended defects in strontium titanate

Pierre Hirel^{1,2}, Matous Mrovec^{1,2} and Christian Elsässer^{1,2}

¹Institut für Zuverlässigkeit von Bauteilen und Systemen (IZBS), Karlsruher Institut für Technologie, Kaiserstr. 12, 76131 Karlsruhe, Germany

²Fraunhofer-Institut für Werkstoffmechanik IWM, Wöhlerstr. 11, 79108 Freiburg, Germany
pierre.hirel@izbs.uni-karlsruhe.de

Plastic deformation, which depends on extended defects in the crystal structure, can have dramatic influences on the electronic, optical and mechanical behaviors of materials. In perovskite-type ceramics, which are functional components of electroactive devices, lattice dislocations are known to have an important influence on the devices' performance and lifetime. In the case of confined systems like, e.g., epitaxial thin films, superlattices or nanoparticles, the influence of lattice dislocations, stacking faults, or interfacial misfit dislocations is even more pronounced. HRTEM studies have shown that the strain fields surrounding dislocations can significantly perturb the ferroelectric properties of the materials. Therefore, the determination of properties for extended defects in these materials is of high relevance.

This study investigates the structure and energetics of extended defects in perovskite materials by means of atomistic and electronic calculations. The simulations are based on a multi-scale approach that uses both quantum-mechanical first-principles calculations, and classical atomistic simulations with rigid-ion or shell-model potentials. Planar defects are investigated, and the accuracy of the interatomic potentials is probed, through the computation of generalized stacking-fault energies (γ -surfaces). The core structures of dissociated dislocations in strontium titanate are also addressed in comparison to results from experimental HRTEM and the elasticity theory of dislocations.

Computational Multiscale Mechanics of Inelastic Cohesive Interfaces with Size Effects

Britta Hirschberger

Leibniz Universität Hannover, Institute of Continuum Mechanics,
Appelstr. 11, 30167 Hannover, Germany, hirschberger@ikm.uni-hannover.de

It is well known that for small-scale specimens, standard continuum mechanics descriptions particular fail to represent size effects arising due to a relatively large microstructure. Micromorphic continuum models remedy for this shortcoming by means of additional micro kinematic degrees of freedom and balance relations and the introduction of an internal length parameter to mimic a typical microstructural size.

A challenge is the modeling of cohesive failure zones, in which the underlying microstructural properties govern the macroscopically observed failure behavior. In previous works [Hirschberger, Sukumar, Steinmann, *Phil. Mag.*, 88:3603, 2008], we introduced a computational homogenization framework (FE^2) for thin cohesive material layers with both a meso-heterogeneous and a microstructured substructure. The material layers are represented with a cohesive interface on the macro level, whereas we used a micromorphic continuum to model locally periodic representative volume elements (RVEs) of finite height on the meso and micro scale. While the method was presented in a hyperelastic setting, the current work proposes the necessary extension to inelastic material layers. To this end, inelastic constitutive models are incorporated in the micromorphic representative volume element. For the sake of simplicity, we here employ an *inelastic micropolar RVE* [Steinmann. *Int. J. Numer. Meth. Engng.*, 38:583, 1995; Forest and Sievert, *Acta Mech.*, 160:71, 2003.], being a special case of the micromorphic continuum.

With inelastic micromorphic material models in the RVE, typical inelastic macroscopic responses in the cohesive material interfaces can be predicted based on their microstructural constitution. This feature makes the present contribution relevant for the modeling of cohesive failure in small-scale specimens consisting of microstructured materials. Moreover, this versatile framework can be transferred to other coupled problems on the RVE level.

Dislocation fluxes and line length changes in averaged descriptions of dislocations

Thomas Hochrainer^{1,2}, Stefan Sandfeld², Peter Gumbsch^{1,2} and Michael Zaiser³

¹Fraunhofer IWM, Wöhlerstr. 11, 79108 Freiburg, Germany

²Karlsruhe Institute of Technology, izbs, Kaiserstr. 12, 76131 Karlsruhe, Germany

³Centre for Materials Science and Engineering, The University of Edinburgh, King's Buildings, Sanderson Building, Edinburgh EH93JL, United Kingdom
Thomas.Hochrainer@kit.edu

Crystal plasticity is the result of the motion and interaction of dislocations. There is, however, still a major gap between our knowledge of the behavior of individual dislocations and continuum crystal plasticity models. Earlier averaged descriptions of dislocations failed to reflect at least the averaged kinematics of a dislocation system [1]. Only recently a higher dimensional dislocation density tensor was defined which overcomes essential drawbacks of earlier dislocation density measures and their evolution equations [2] in that dislocation fluxes and line length changes are correctly described. By introducing assumptions on the dislocation velocity and curvature we partially integrate the evolution equation of the higher dimensional tensor to develop simpler formulations which evolve the total dislocation density and the average curvature of the dislocations. Together with the evolution of the classical dislocation density tensor this governs a faithful representation of the dislocation kinematics without the use of extra dimensions or the intricacies of screw–edge representations [3, 4]. The kinematics are illustrated at simple example cases and compared to predictions of the underlying higher dimensional theory.

References

- [1] E. Kröner, Benefits and shortcomings of the continuous theory of dislocations, *International Journal of Solids and Structures* 38, 1115-1134 (2001)
- [2] T. Hochrainer, M. Zaiser, P. Gumbsch, A three-dimensional continuum theory of dislocations: kinematics and mean-field formulation, *Philosophical Magazine* 87, 1261-1282 (2007)
- [3] A. Arsenlis, D. Parks, R. Becker, and V. Bulatov, On the evolution of crystallographic dislocation density in non-homogeneously deforming crystals, *Journal of the Mechanics and Physics of Solids* 52, 1213-1246 (2004)
- [4] M. Zaiser and T. Hochrainer, Some steps towards a continuum representation of 3D dislocation systems, *Scripta Mater.* 54, 717-721 (2006)

Multiscale Modeling of Nanocrystalline Pillars

Daniel E. Hurtado¹ and Michael Ortiz²

¹California Institute of Technology
1200 E California Blvd. MC104-44, Pasadena, CA 91125, USA
dhurtado@caltech.edu

²California Institute of Technology
1200 E California Blvd. MC105-50, Pasadena, CA 91125, USA.
ortiz@aero.caltech.edu

Experimental observations in nanocrystalline materials with grain size below ~100 nm show a transition in deformation mechanisms – from subgrain dislocation-driven to grain-boundary dominated – as the specimen size decreases^[1]. These findings set new challenges on the constitutive modeling of nanomaterials as they introduce new mechanisms not considered by traditional crystal-plasticity models. The development of computational models that are capable of incorporating these relevant mechanisms plays a fundamental role in the design of novel engineered materials.

Direct numerical simulations of nanopillars using a continuum finite element model with a multiscale constitutive model are performed. The polycrystalline domain is generated from an initial coarse mesh by using a robust two-step algorithm capable of dealing with non-trivial geometries^[2] which leads to the definition of grain domains with a smooth grain boundary. At the subgrain level, a non-local elasto-viscoplastic constitutive model developed within the framework of variational constitutive updates^[3] is employed, where the crystallographic nature of the material is explicitly considered and the anisotropic material response is adequately represented. The consideration of the self-energy of the dislocations renders the constitutive model non-local, and introduces a length scale into the model. Results from numerical simulations for different diameters and grain sizes will be presented.

REFERENCES

- [1] J.R. Greer, D. Jang, J. Kim, M.J. Burek. Emergence of New Mechanical Functionality in Materials via Size Reduction. *Adv. Func. Materials* 19, 2009.
- [2] J.J. Rimoli, M. Ortiz. A method for generating geometric representations of polycrystals. Submitted, 2009.
- [3] Ortiz, M., Stainier, L. The variational formulation of viscoplastic constitutive updates. *Comp. Methods Appl. Mech. Engrg.* 171, 1999.

Structure-Property Relations Based on Non-Equilibrium Statistical Mechanics

Author: Markus Hütter^{1,2}

Affiliations: ¹ETH Zurich, Department of Materials, Polymer Physics, HCI H 529, Wolfgang-Pauli-Str. 10, CH-8093 Zurich, Switzerland. markus.huetter@mat.ethz.ch.
²Eindhoven University of Technology, Mechanical Engineering, Materials Technology, PO Box 513 , WH 4.136, 5600 MB Eindhoven, The Netherlands

ABSTRACT

Two modeling approaches are used to tackle the formulation of structure-property relations with respect to the mechanical behavior. On the one hand, a “multiscale” strategy examines the evolution of macroscopic and simultaneously meso- or microscopic variables. On the other hand, the “coarse graining” approach is concerned with deriving coarser dynamics as based on the knowledge about the fine-scale dynamics. Both of these distinct tasks are greatly helped by modern nonequilibrium thermodynamics. Particularly, we consider the nonequilibrium thermodynamics framework General Equation for the Non-Equilibrium Reversible-Irreversible Coupling (GENERIC). As specific illustrations for the multiscale and coarse-graining strategies, respectively, we consider (i) kinetic theory in polymer rheology, (ii) statistical dislocation dynamics in metal visco-plasticity, and (iii) the modeling of amorphous solids.

1. Introduction

While the crucial importance for structure-property relations is manifest, there are at least two fundamentally different ways to formulate them in modeling. First, in analogy to the classical formulation of macroscopic phenomenological relations, one can make an ad-hoc ansatz for the macroscopic effect of the microstructure. In order to study dynamic effects, one thus requires studying the evolution of some microstructural variables in parallel to some macroscopic fields, therefore this is called “multiscale approach” (Fig. 1). For formulating both the structure-property relation and the microstructure evolution, nonequilibrium thermodynamics provides invaluable tools. Certainly, such thermodynamic methods are empty before they are applied to concrete examples. However, exactly for that same reason, they are powerful devices to *check* the healthiness of the equations, i.e., their thermodynamic consistency. The second approach to formulate structure-property relations is based on “coarse graining”. In distinction to the previous scenario, the goal is not to study the dynamics on multiple scales simultaneously, but rather one intends to *derive* static and dynamic properties on the coarser scale, e.g., to address the structure-property relation from a fundamental perspective (Fig. 1). Two prominent examples of coarse graining are (a) (static) equilibrium statistical mechanics, and (b) the so-called fluctuation-dissipation theorems, e.g., the relation between the viscosity and the time-correlation of the stress fluctuations. As will be shown below, there are methods that allow to coarse grain both static and dynamic properties.

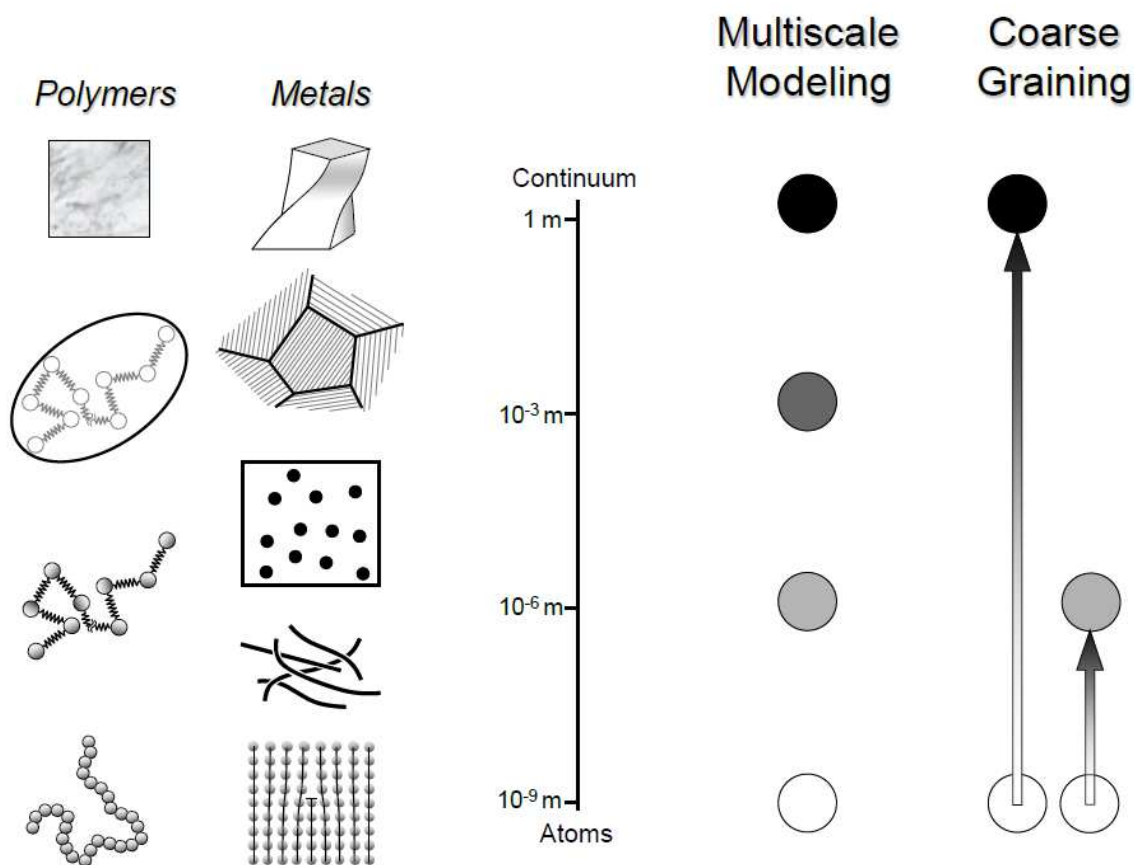


Figure 1. Illustration of different levels of description for polymers and metals. While we understand “multiscale modeling” as studying the evolution on multiple levels at the same time, “coarse graining” rather is concerned with establishing the transition from a fine level to a coarser level.

In order to reconcile both strategies, “multiscale” and “coarse graining”, from a single perspective, the nonequilibrium thermodynamics framework called General Equation for the Non-Equilibrium Reversible-Irreversible Coupling (GENERIC) is discussed. In the following, we give a concise summary of that method (Sec. 2), followed by a discussion of specific illustrative examples in Sec. 3, namely, (i) kinetic theory in polymer rheology, (ii) statistical dislocation dynamics in metal visco-plasticity, and (iii) the modeling of amorphous solids.

2. Method

With reference to the distinction between multiscale and coarse graining discussed in the introduction, we now are going to present the key aspects of the method of choice. For more details, the reader is referred to [1-6].

2.1 Single- and multiscale strategy

As a guideline for modeling materials with microstructure we use the GENERIC formalism [1-3]. In the following, only a concise summary of the method is given; the reader is referred to the original literature for more details. Let us denote by \mathbf{x} the set of dynamic variables which describes the given nonequilibrium system to the desired detail. According to the

framework, the time evolution of the variables \mathbf{x} of an isolated system can be written in the form

$$\dot{\mathbf{x}} = \mathbf{L} \cdot \frac{\delta E}{\delta \mathbf{x}} + \mathbf{M} \cdot \frac{\delta S}{\delta \mathbf{x}}, \quad (1)$$

where the two generators E and S are the total energy and entropy functionals in terms of the state variables \mathbf{x} , and \mathbf{L} and \mathbf{M} are certain matrices (operators). The two contributions to the time evolution of \mathbf{x} generated by the total energy E and the entropy S are called the reversible and irreversible contributions, respectively. The notation $\delta / \delta \mathbf{x}$ typically implies functional rather than partial derivatives.

The GENERIC structure also imposes certain conditions on the building blocks in Eqn. (1). First, the Poisson operator \mathbf{L} must (i) be antisymmetric, (ii) fulfill the Jacobi identity, and (iii) satisfy the degeneracy condition

$$\mathbf{L} \cdot \frac{\delta S}{\delta \mathbf{x}} = \mathbf{0}. \quad (2)$$

In contrast, the friction matrix \mathbf{M} must (i) be Onsager-Casimir symmetric, (ii) be positive semi-definite, and (iii) satisfy the degeneracy condition

$$\mathbf{M} \cdot \frac{\delta E}{\delta \mathbf{x}} = \mathbf{0}, \quad (3)$$

which altogether ensure the conservation of total energy and a non-negative entropy production. In this sense the, general principles are accounted for. However, the framework needs to be filled with further physics, namely with the knowledge about the specific system of interest. This will be discussed in Sec. 3.

2.2 Coarse graining

A particular feature of the GENERIC framework in contrast to other methodologies in this field is that it applies to different levels of description, e.g. reversible Hamiltonian mechanics and dissipative macroscopic field theories. Obviously, the four building blocks E , S , \mathbf{L} , and \mathbf{M} differ between the different levels. However, there are abstract coarse-graining procedures to relate them [3-6].

The first step in coarse graining consists of establishing the two levels of description that one attempts to link. The variables on the finer level we shall denote by \mathbf{z} , which for a microscopic many-particle system could be the collection of all particle positions and momenta, $\mathbf{z} = (\mathbf{r}_1, \dots, \mathbf{r}_N, \mathbf{p}_1, \dots, \mathbf{p}_N)$. On the other hand, one needs to specify the variables of interest on the coarser level, \mathbf{x} . To be more precise, the choice of coarser variables actually defines the coarser level. For example, for a solid material described in purely macroscopic terms, \mathbf{x} may contain a strain tensor as well as a temperature field. When considering more details, for example of a crystalline metal, the densities of various dislocation types are additional variables, on the mesoscopic level.

The concept of ensembles is crucial for establishing the relation between both levels of description. Similar to equilibrium thermodynamics, for a given ensemble, the key player is

the distribution function of microstates \mathbf{z} in agreement with a macrostate \mathbf{x} , $\rho_{\mathbf{x}}(\mathbf{z})$. In particular, we have apart from the normalization $\int \rho_{\mathbf{x}}(\mathbf{z}) d\mathbf{z} = 1$ the important relation

$$\mathbf{x} = \int \rho_{\mathbf{x}}(\mathbf{z}) \hat{\mathbf{x}}(\mathbf{z}) d\mathbf{z} = \langle \hat{\mathbf{x}}(\mathbf{z}) \rangle_{\mathbf{x}}, \quad (4)$$

where $\hat{\mathbf{x}}(\mathbf{z})$ is the instantaneous value of \mathbf{x} expressed in terms of the microstate \mathbf{z} . For example, for \mathbf{x} the macroscopic mass density, $\hat{\mathbf{x}}(\mathbf{z})$ is a sum of Dirac delta functions that are located at the actual particle positions. In analogy to equilibrium thermodynamics, there are different ensembles, according to whether the coarse grained variables are to be represented exactly without fluctuations (“microcanonical”) or if fluctuations are permitted and only the averages of the coarse variables are controlled with Lagrange parameters (“canonical”).

Once, the variables on both levels as well as the statistical ensemble have been chosen, one proceeds with the specification of the generating functionals as required in the evolution equation (1),

$$E(\mathbf{x}) = \langle E_0(\mathbf{z}) \rangle_{\mathbf{x}}, \quad (5)$$

$$S(\mathbf{x}) = S[\mathbb{Z}], \quad (6)$$

where the entropy $S[\mathbb{Z}]$ is a functional of the partition function \mathbb{Z} related to the distribution of microstates $\rho_{\mathbf{x}}(\mathbf{z})$ [3]. The specific form of the entropy, which is omitted here, depends on the chosen ensemble. The entropy is related to the number of microstates \mathbf{z} that correspond to a given macrostate \mathbf{x} . Both the energy and the entropy contain purely static information about the system. Therefore, if one attempts to access them with computer simulations, (static) Monte Carlo simulations is the ideal tool. In general, apart from the fact that the state space on the coarse-grained level is larger than the equilibrium state space, the conceptual idea behind and the techniques of calculation for the energy and entropy are closely related to the well-known equilibrium counterpart.

To finally arrive at the coarse-grained evolution equations, the Poisson operator and the friction matrix must be determined, as required for the reversible and irreversible dynamics, respectively. As a general comment, one observes that irreversible effects are absent on the atomistic level, while from an increasingly coarser perspective on the same system there emerge irreversible effects. For example, water on the level of atoms obeys Newton’s reversible equations of motion, while on the macroscopic level viscous effects play a crucial role in our everyday experience with water. Upon systematic coarse graining, the emergence of irreversibility becomes clear: The coarser (i.e., the less accurate and less explicit) the description of the material, the less is the dynamics “under control”. Since the variables on the coarse level should account for the slowest modes of deformation, what is left “un-controlled” can be considered to represent more rapid motions. If those left-out rapid motions are significantly faster than the controlled processes, one speaks of time-scale separation, and hence, from the viewpoint of the coarse level, they are considered fluctuations. In more technical terms, one can show that the Poisson operator and the friction matrix are given by (see also the projection operator formalism [9])

$$\mathbf{L}(\mathbf{x}) = \left\langle \frac{\partial \hat{\mathbf{x}}(\mathbf{z})}{\partial \mathbf{z}} \cdot \mathbf{L}_0(\mathbf{z}) \cdot \frac{\partial \hat{\mathbf{x}}(\mathbf{z})}{\partial \mathbf{z}} \right\rangle_{\mathbf{x}}, \quad (7)$$

$$\mathbf{M}(\mathbf{x}) = \frac{1}{k_B} \int_0^{\tau} \left\langle \dot{\hat{\mathbf{x}}}^f(\mathbf{z}(t)) \dot{\hat{\mathbf{x}}}^f(\mathbf{z}(0)) \right\rangle_{\mathbf{x}} dt, \quad (8)$$

if time-scale separation holds. Here, $\mathbf{L}_0(\mathbf{z})$ denotes the Poisson operator on the fine level, k_B is the Boltzmann constant, τ is the time scale separating slow from fast processes, and $\hat{\mathbf{x}}^f$ is the fluctuating part of the time-evolution of the instantaneous value $\hat{\mathbf{x}}$. In other words, reversible terms are transferred from the fine to the coarse level. In contrast, irreversible contributions arise as a result of fluctuations, in particular, from the time-correlations between them, leading to the notion of fluctuation-dissipation relations. For example, the time-correlation of the fluctuations in the shear stress gives rise to a shear viscosity, while the fluctuations in the flux of energy amounts to the thermal conductivity [7,8]. Since the friction matrix involves the dynamics on the fine scale, dynamic simulation methods are required for numerical studies. Particularly, if the fine scale level consists of microscopic discrete particles, molecular dynamics simulations are adequate.

It can be shown that all requirements of the GENERIC framework are met by Eqns. (5-8), with the notable exception of the Jacobi identity.

3. Illustrations

3.1 Kinetic theory of polymer rheology

The complex viscoelastic behavior of polymeric fluids is a prime example for discussing the relation between structure and mechanical behavior. The modeling of polymer rheology in relation to microstructural quantities has a long tradition [10]. For example in unentangled polymer melts, the deformation of the overall polymer coil and the entropic force to restore the spherical shape of the coil are considered the most relevant modes of deformation. Hence, either a conformation tensor $\mathbf{c} = \langle \mathbf{R}\mathbf{R} \rangle$ of the polymer end-to-end vector or radius of the gyration \mathbf{R} , or the corresponding distribution function $p(\mathbf{R})$ are often used to describe viscoelasticity.

The multiscale approach to such a system thus must encompass, e.g. the conformation tensor \mathbf{c} describing the overall distortion of the chain. On the other hand, one is interested in the macroscopic deformation and thermal behavior. To that end, one can choose as the full set of field variables (all functions of time t and position \mathbf{r})

$$\mathbf{x} = (\mathbf{u}, \rho, e, \mathbf{c}) , \quad (9)$$

with the first three variables being the densities of momentum, mass, and internal energy of the melt. Note that e accounts only for the local energy contributions, while energetic effects on the scale of the entire chain are not included in e . Under the assumption that energetic effects of the chain conformation are negligible [11], the energy of the system consists of the kinetic ($u^2 / (2\rho)$) and internal energy (e) contributions of the melt-continuum, while the entropy consists of the melt-continuum entropy $s(\rho, e)$ and of the conformational entropy (\mathbf{c} -dependent contribution). Having control of the conformation tensor, the entropy is highest for a spherical coil, and is decreased for distorted coils. Using the conformation tensor (or even the distribution function) in combination with the macroscopic hydrodynamic fields underlines the multiscale nature of this (admittedly very simplistic) modelling effort.

The form of the Poisson operator \mathbf{L} can be determined based on the behaviour of the variables under affine deformations on the following way. For example, if the polymer coil deforms affinely with the macroscopic flow field $\mathbf{v} = \mathbf{u} / \rho$, then $\dot{\mathbf{R}} = (\partial \mathbf{v} / \partial \mathbf{r}) \cdot \mathbf{R}$. From this,

one infers the advection behaviour of the conformation tensor, which is found to be of upper-convected type. Similarly, one can proceed with the other variables in \mathbf{x} . By way of the GENERIC properties of the Poisson operator (antisymmetry, degeneracy, Jacobi identity), the remaining elements of the Poisson operator can be determined. The main result of this procedure is that the stress tensor, which is part of the reversible evolution equation of the momentum density, is determined in terms of the polymer conformation. In other words: Understanding the effect of the macroscopic flow field on the polymer chain and using nonequilibrium thermodynamics amounts to specifying the back-effect of the polymer chains on the macroscopic flow field.

The irreversible dynamics for this specific example consists primarily of the thermal conduction and of the relaxation of the chain conformation. Both of these contributions are to be accounted for in the friction matrix \mathbf{M} . Educated ansatzes can be made for the chain-relaxation contribution in this multiscale approach, and the reader is referred to [3] for an overview. In the following, however, we rather wish to comment on the coarse-graining strategy as applied to this specific example.

The application of systematic coarse-graining to polymeric fluids has been beautifully exemplified by Ilg et al. [12,13]. Ilg [12] has shown technically how to coarse grain from an atomistic description to the level as specified in Eqn. (9). Doing so, microscopic justification was provided for equations derived previously on phenomenological grounds. Particularly, we point out that in this example the specification of the instantaneous coarse-grained structural variable is straightforward. For a single chain,

$$\hat{\mathbf{c}}(\mathbf{r}) = \left[\frac{1}{N} \sum_{i=1}^N (\mathbf{r}_i - \mathbf{r}_{CM})(\mathbf{r}_i - \mathbf{r}_{CM}) \right] \delta(\mathbf{r} - \mathbf{r}_{CM}), \quad (10)$$

where N is the number of beads, and \mathbf{r}_{CM} denotes the center of mass as given by the positions \mathbf{r}_i of the individual beads. In [13], Ilg et al. exploit coarse graining to present a thermodynamically guided, low-noise, time-scale-bridging, and pertinently efficient strategy for the dynamic simulation of microscopic models for complex fluids. This strategy allows for studying the structural and mechanical response of the material beyond the regime of linear response, also in general (mixed) flow situations.

3.2 Statistical dislocation dynamics

Understanding, and tailoring, the viscoplastic deformation behaviour of metals is of paramount technological importance. To that end, the discovery of the lattice defects, i.e. dislocations, as mediators of irrecoverable deformation was a major breakthrough. With respect to modelling, this opens a completely new world as there is a concrete proposition for structural variables on the mesoscopic scale. Dislocations can be accounted for in different ways. For example, one could consider the distribution of dislocation line orientations (see discrete dislocation dynamics [14]), leading to a rather detailed description, with some analogy to the so-called reptation models in polymer melt rheology. However, since the viscoplastic deformation is governed to a large degree by how different dislocations interact, such a detailed description would be rather involved conceptually, and numerical difficult to handle for reasonable system sizes. In contrast, one can go one step coarser, and consider (line) densities of dislocations as the quantities of interest [15-18].

It is most natural to study the dynamics of dislocations jointly with a macroscopic description of viscoplasticity. The latter has been examined e.g. in [19] by using as dynamic (Eulerian) field variables

$$\mathbf{x}' = (\mathbf{u}, \mathbf{F}^e, e) , \quad (11)$$

with \mathbf{u} and e the densities of linear momentum and internal energy, defined earlier. \mathbf{F}^e denotes the elastic contribution to the deformation gradient, with material time-derivative

$$\dot{\mathbf{F}}^e = (\nabla \mathbf{v})^T \cdot \mathbf{F}^e - \boldsymbol{\kappa}^p \cdot \mathbf{F}^e , \quad (12)$$

where $\boldsymbol{\kappa}^p$ is the plastic strain rate tensor, for which a constitutive relation in terms of the dislocation processes is needed. For studying the system from a multiscale perspective, the full set of variables is proposed as

$$\mathbf{x} = (\mathbf{u}, \mathbf{F}^e, e, \rho) , \quad (13)$$

with ρ symbolizing several dislocation densities, e.g., mobile/immobile, edge/screw/mixed, for different glide systems. Preliminary attempts in this direction indicate the following [20]. First, implementing the Peach-Koehler force due to the macroscopically applied stress as a contribution in the evolution of the dislocation densities automatically results (without any further assumptions) in the tensorial Orowan relation for the plastic strain rate tensor. In contrast, mutual interactions between dislocations have no effect on the plastic strain rate tensor. And second, the diffusion-type equation for the dislocation densities does not only contain a drift term in the form of dislocation interactions and Peach-Koehler forces due to externally applied stresses. There is also a diffusional contribution, which is often missed when deriving the density evolution with non-thermodynamic techniques. The relevance of the diffusion term is two-fold. One the one hand, it indicates that in the absence of any dislocation interactions, the dislocations would attain a homogeneous distribution simply for entropic reasons. On the other hand, if the diffusion equation is transformed into the corresponding trajectory-wise interpretation, the diffusion terms stands for random fluctuations (noise) [21], as one would expect for mesoscopic objects as the dislocations are.

The procedure for coarse graining, as compared to the multiscale approach, is less clear. The following contrasts sharply with the example of polymeric fluids presented above. One of the main problems in coarse graining from an atomistic description to the level of dislocations (and their densities) concerns the proper definition of the instantaneous variables $\hat{\mathbf{x}}(\mathbf{z})$ (see Eqn. (4)). What is the problem? Eqn. (10) for the instantaneous tensor of gyration is expressed exclusively in terms of the current particle positions. It is however, less clear how such an instantaneous expression should look like for either the (elastic part of the) deformation gradient or for the identification of dislocation. In order to define the deformation gradient based on particle positions, different methods have been proposed, among them the best-fit uniform deformation gradient [22,23], and a method based on quadruples of particles [6]. In any case, all of these methods rely on comparing two snapshots of the many-particle system, and as such they fundamentally differ from Eqn. (10). Further, if the deformation gradient had been identified on a particle-level, one could then use the compatibility condition to introduce on local scales the derivative of the deformation gradient, and hence invoke the concept of a microscopic Nye tensor [23,24]. Apart from the complications associated with the definition of the deformation gradient, the extraction of dislocation densities is even more cumbersome. So, for strained systems with dislocations, already the proper definition of the coarse-grained variables in terms of atomistic configuration is complicated.

3.3 Deformation of amorphous solids

Amorphous solids are a particularly challenging class of materials. On the one hand, they exhibit a predominantly elastic regime at small deformations, with a transition to (rate-dependent) plastic behaviour at larger deformations, as crystalline solids do. On the other hand, they show aging and more importantly, one is unclear about the structural signature most relevant for the mechanical behaviour. One prominent idea consists in monitoring regions that rearrange nonaffinely upon deformation. This can be viewed in terms of the inherent structures, as elaborated in [26,27], or in a coarser sense in terms of the so-called shear transformation zones (STZ) [22,28]. While [26,27] are important steps towards coarse graining in amorphous solids, in the following we rather comment on a multiscale strategy related to the STZ-model.

In the tensorial version of the STZ-model [28], the dynamic microstructural variables consist of the number density of zones n , as well as an average orientation tensor \mathbf{N} . The fundamental mechanism underlying viscoplastic deformation is (a) the orientation of the existing zones, as well as (b) the generation of zones. Similar to the procedure in Sec. 3.2, it is tempting to search for a unified description of macroscopic elasto-viscoplasticity with STZ-dynamics. In other words, the relevant set of variables is

$$\mathbf{x} = (\mathbf{u}, \mathbf{F}^e, e, n, \mathbf{N}) , \quad (14)$$

with the evolution equation for the elastic deformation gradient of the form (12). The main goal of such a multiscale approach is to better resolve the physics behind the plastic strain rate tensor $\boldsymbol{\kappa}^p$. As a first result, one can show the following. Knowledge about the effect of zone orientation in the different evolution equations in \mathbf{x} leads to the identification of the driving force for the orientation process. This is direct result of thermodynamic consistency. Admittedly, the method presented here imposes only rather general (and weak) conditions on the kinetic processes involved in the zone orientation process.

Discussion

The mechanical behaviour of three types of materials have been studied by way of a multiscale approach, i.e. by following the time-evolution in terms of a macroscopic continuum field theory unified with a mesoscopic structural variable. In contrast to the identification of the structural variable for the polymer melt and the crystalline metals, it is considerably more complicated to make a good choice for the amorphous solids. Two choices have been considered, however, this point still open for discussion.

With regard to coarse graining, it became clear that there are features distinctive to solid systems. First, and most importantly, strain measures such as the deformation gradient on the atomistic level cannot be defined purely in terms of the current particle positions; rather the comparison of two configurations is needed. And second, an analytic (rather than based on by-eye inspection or based on an energy-criterion) expression for the identification of dislocations is highly complicated.

Acknowledgements

The author likes to thank Hans Christian Öttinger, Patrick Ilg, Theo Tervoort, Lambert van Breemen, and Erik van der Giessen for stimulating discussions.

References

- [1] M. Grmela, H. C. Öttinger, *Phys. Rev. E* 56, 6620--6632 (1997).
- [2] H. C. Öttinger, M. Grmela, *Phys. Rev. E* 56, 6633-6655 (1997).
- [3] H. C. Öttinger, *Beyond Equilibrium Thermodynamics* (Wiley, Hoboken, N.J., 2005).
- [4] H. C. Öttinger, *Phys. Rev. E* 57, 1416-1420 (1997).
- [5] H. C. Öttinger, *MRS Bull.* 32, 936-940 (2007).
- [6] M. Hütter, T.A. Tervoort, *Adv. Appl. Mech.* 42, 253-317 (2008).
- [7] S. R. de Groot, P. Mazur, *Non-Equilibrium Thermodynamics* (North-Holland, Amsterdam, 1962).
- [8] R. Kubo, M. Toda, N. Hashitsume, *Statistical Physics, Vol. 2: Nonequilibrium Statistical Mechanics* (2nd ed.) (Springer, Berlin, 1991).
- [9] H. Grabert, *Projection Operator Techniques in Nonequilibrium Statistical Mechanics* (Springer, Berlin, 1982).
- [10] R. B. Bird, C. F. Curtiss, R. C. Armstrong, O. Hassager, *Dynamics of Polymeric Liquids, vol. 2: Kinetic Theory* (2nd ed.) (Wiley, New York, 1987)
- [11] M. Hütter, C. Luap, H. C. Öttinger, *Rheol. Acta* 48, 301-316 (2009).
- [12] P. Ilg, *Physica A* 387, 6484-6496 (2008).
- [13] P. Ilg, H.C. Öttinger, M. Kröger, *Phys. Rev. E* 79, 011802 (2009).
- [14] D. Raabe, *Computational Materials Science: The Simulation of Materials, Microstructures and Properties* (Wiley-VCH, Weinheim, 1998).
- [15] U. F. Kocks, *J. Eng. Mater.-T ASME* 98, 76-85 (1976).
- [16] U. Essmann, H. Mughrabi, *Philos. Mag. A* 40, 731-756 (1979).
- [17] H. Mecking, U. F. Kocks, *Acta Metal.* 29, 1865-1875 (1981).
- [18] Y. Estrin, Y., Ch. Dislocation density-related constitutive modeling (pp. 69-106), in *Unified Constitutive Laws of Plastic Deformation* (Academic Press, San Diego, 1996).
- [19] M. Hütter, T. A. Tervoort, *J. Non-Newtonian Fluid Mech.* 152, 53-65 (2008).
- [20] M. Hütter, unpublished work (2009).
- [21] H. C. Öttinger, *Stochastic Processes in Polymeric Fluids* (Springer, Berlin, 1996).
- [22] M. L. Falk, J. S. Langer, *Phys. Rev. E* 57, 7192-7205 (1998).
- [23] J. A. Zimmerman, D. J. Bammann, H. Gao, *Int. J. Solids Struct.* 46, 238-253 (2009).
- [24] C. S. Hartley, Y. Mishin, *Mater. Sci. Eng. A* 400-401, 18-21 (2005).
- [25] M. Hütter, L. C. A. van Breemen, manuscript in preparation (2010).
- [26] E. Del Gado, P. Ilg, M. Kröger, H.C. Öttinger, *Phys. Rev. Lett.* 101, 095501 (2008).
- [27] M. Mosayebi, E. Del Gado, P. Ilg, H.C. Öttinger, *Phys. Rev. Lett.* 104, 205704 (2010).
- [28] J. S. Langer, *Phys. Rev. E* 77, 021502 (2008).

Inverse Analysis Applied to the Investigation of Composite Materials

Sandra Ilic and Klaus Hackl

Institute of Mechanics, Ruhr-University of Bochum
Bochum, Germany
sandra.ilic@rub.de
klaus.hackl@rub.de

Recently, the study of component materials of composites on the basis of data on the effective material behavior has become very intensive. This, of course, belongs to the group of inverse problems which are in general solved by minimizing the error induced by introducing an approximation function for the experimentally identified data. Depending on the purpose different types of error functions can be assumed. However, the root-mean-square error has been used as the standard method in many contributions. The reasons for this are that this approach leads to a computationally efficient solution and can clearly be substantiated. It is a result obtained by maximization of the probability that some sets of parameters appearing in the approximation function is correct if the set of experimental data is given. In our approach, the approximation is the displacement function obtained by minimizing the total potential corresponding to the nonlinear composite materials and given external load. Since the requirements for statistically uniform materials are met, the multiscale FEM is chosen for the solution of the forward problem and the determination of the displacements. Finally, the combination of the root-mean-square error with the multiscale FEM results in the nonlinear least square method for whose solution the Levenberg-Marquardt method is used.

The illustrative examples serve to investigate two- and three-phase composite materials, each phase having two characteristic parameters. Special attention is given to the analysis of the computer effort needed to solve the problem. In this context, it can be observed that the number of iterations increases significantly by increasing of the number of phases. However, in the case of two-phase materials, different starting iteration vectors yield the same results while, the problem of detecting global minima appears for three- and more phase materials.

Effect of phosphorus impurities on grain boundary-related plasticity of nanocrystalline bcc-Fe using molecular dynamics simulation

Jong-Bae Jeon, Byeong-Joo Lee and Young Won Chang

Department of Materials Science and Engineering, POSTECH, San-31 Hyoja-dong
Nam-gu Pohang, Republic of Korea
blizzard@postech.ac.kr

Phosphorus impurities in bcc-Fe are reported to aggregate at grain boundaries, leading to a decrease in the grain boundary cohesion and consequent embrittlement of the material. This deterioration of the plasticity is closely related with the interaction of the atoms located at grain boundaries, so that atomic level research is essential to understand the problem in fundamental way. The atomic level interaction of Fe-P atoms at grain boundary and its effect on plasticity can be revealed more distinctly in nanocrystalline material whose mechanical property is greatly governed by grain boundary characteristics. In the present research Fe-P binary system is modeled by embedded atomic model (EAM) potential and nanocrystalline samples are built using Voronoi technique which allows for the construction of three-dimensional (3-D) grain boundary networks with desired crystallographic orientation. BCC nanocrystalline Fe-P specimens having three different phosphorus concentrations with same average grain diameter of 5nm are fabricated and then tempered in 500K in order to make phosphorus atoms to be distributed at grain boundaries. Compressive loading is applied to the specimen in 300K with constant strain rate condition. Atomic level analysis is focused on the relationship between the distribution and the concentration of phosphorus atoms at grain boundary, and the atomic level process of grain boundary-related plasticity.

Deformation behaviors of nanocrystalline bcc-Fe during compressive loading using molecular dynamics simulation

Jong-Bae Jeon, Byeong-Joo Lee and Young Won Chang

Department of Materials Science and Engineering, POSTECH, San-31 Hyoja-dong
Nam-gu Pohang, Republic of Korea
blizzard@postech.ac.kr

Nanocrystalline (nc) material generally exhibits excellent yield and fracture strength, and has potential to be further applied in structural and functional materials by optimizing mechanical properties but its deformation mechanism still remains unclear. Most recent atomistic simulations on the deformation behavior of nc materials have provided valuable insight on the deformation mechanisms of bulk nc materials, which can be hardly obtained through experimental investigations: even in the nc materials, the deformation behavior is still to a major extent governed by dislocations nucleated at grain boundary ledges not via classical Frank-Read sources within grain interior. Most of simulation researches, however have been carried out on fcc materials (Ni, for example) and besides the deformation behavior of bcc materials is remarkably different from fcc in general so that the atomistic modeling approaches to nc bcc materials are necessary to solve the remained ambiguity of the deformation behavior of bcc nc materials. Here we perform compressive tests on three-dimensional nc samples of bcc-Fe in temperature range from 0K to 300K with constant strain rate condition. BCC-Fe is modeled by embedded atomic model (EAM) potential and nc samples are built using Voronoi technique which allows for the construction of three-dimensional grain boundary networks with desired crystallographic orientation. Detailed analysis for the deformation behaviors based on the atomistic process correlates the stress-strain response with deformation mechanisms including dislocation nucleation/propagation and mechanical twinning, which significantly depend on the grain boundary networks and the deformation temperature.

Atomistic modeling of strength and stability in nano-twinned structures in fcc metals

Yashashree Kulkarni

Department of Mechanical Engineering, University of Houston, Houston, TX 77204, USA
ykulkarni@uh.edu

Although nanocrystalline metals and alloys are known to possess attractive combinations of properties such as ultra-high strength and superior fatigue and wear resistance, it is well established that the large excess energy associated with grain boundaries leads to structural instability in the grain structure. In particular, under conditions of suitably high stress, grains grow and the high-strength characteristic of nanocrystalline metals decreases. Furthermore, it has also been shown that loss of fracture toughness and a transition towards brittle behavior are critical issues associated with nanostructuring. On the other hand, studies over the past few years have revealed that properties of ultra-fine grained fcc metals may be further enhanced by the presence of nanoscale twins as an alternative to nanocrystalline structures. These attractive properties include ultra-high yield strength, high ductility, good electrical conductivity and high strain-rate sensitivity.

The talk will present our investigations of the strength and structural stability of nano-twinned fcc metals by way of atomistic simulations. Our results show that owing to the symmetric, low energy structure and very high shear strength of coherent twin boundaries, nano-twinned metals are more stable even with decreasing twin lamella thickness. However, in agreement with experiments, our simulations also exhibit a loss of strength below a critical twin spacing due to interaction of twin boundaries containing defects. Thus, the aim of this work is to address whether nano-twinned structures represent an optimal motif as compared to their nanocrystalline counterparts with respect to strength, stability, and the role of twin boundaries in the ductile versus brittle response of these nanostructured metals.

Deformation of gold nanowires: elongation mechanisms, electronic structure, and quantum conductance

Lyle Levine, Francesca Tavazza, Anne Chaka, Douglas Smith, Jon Pratt

National Institute of Standards and Technology, Gaithersburg, Maryland, 20899-8553, USA; Lyle.Levine@nist.gov

Metallic nanowires have attracted considerable attention over the past decade due to their enormous potential as interconnects in nanoelectronics and their often unique physical and chemical properties. Research into gold nanowires has been particularly rewarding since this ductile noble metal can be drawn into wires of atomic dimensions and simultaneous electrical measurements exhibit quantum conductance behavior.

We will first describe a new surface probe instrument capable of sustaining single-atomic-bond junctions in the electronic quantum-conduction regime for tens of minutes. The instrument measures and controls the gap formed between a probe and a flat surface with better than 5 pm long-term stability in a high-vacuum chamber at 4 K using a fiber-optic interferometer that forms a Fabry-Perot cavity immediately adjacent and parallel to the probe.

To model the experiment, semistatic density functional theory is used to explore and compare the evolution of [110] and [111] gold nanowires during tensile deformation under a wide range of conditions. Different tensile axes, nanowire shapes and effective strain rates are probed. A rich diversity of deformation pathways is uncovered, that converge to only two final local configurations with reproducible breaking strengths, in agreement with experimental results. Large structural rearrangements are often observed during the elongation; such rearrangements are often followed by significant self-ordering of the wire. Four highly ordered intermediate structures were identified and investigated.¹ The accessibility of these structures and their stability under load for forward and reverse loading are found to be key factors governing the morphological evolution of the nanowire. Finally, electronic properties and quantum conductance are computed for several of the observed deformation pathways and intermediate structures. Good agreement is found between the quantum conductance calculations and experimental results.²

¹F. Tavazza, L.E. Levine and A.M. Chaka, J. Appl. Phys. **106**, 043522 (2009)

²D.T. Smith, J.R. Pratt, F. Tavazza, L.E. Levine, and A.M. Chaka, J. Appl. Phys. (in press)

Solutions to the periodic Eshelby inclusion problem in two dimensions

Liping Liu

Department of Mechanical Engineering, University of Houston
Houston, TX 77004, liuliping@uh.edu

We solve the homogeneous Eshelby inclusion problem on a finite unit cell with periodic boundary conditions. Using the Fourier method we first establish the relations between the periodic Eshelby inclusion problem and two simpler problems concerning harmonic and biharmonic equations. Restricted to two dimensions, we employ the complex-variable method, in particular, the Plemelj formulas, the Cauchy integral and the Weierstrass elliptic functions, to construct solutions to the periodic Eshelby inclusion problem. The main result is a representation formula of the strain field which is reminiscent of the familiar Green's representation formula. The formula is valid for any smooth inclusion and divergence-free eigenstress. Also, the number of inclusions in the unit cell is not limited.

Using the obtained representation formula, we establish a necessary and sufficient condition for a simply-connected inclusion to be a Vigdergauz structure. Interior solution is exceptionally simple for a Vigdergauz structure with constant eigenstress, which enable us to show that the induced strain is not uniform if the uniform eigenstress is symmetric but not dilatational and the inclusion is not a laminate. These results are expected to be extended to inhomogeneous Eshelby inclusion, which will have wide applications in micromechanics.

Discrete dislocation study of the effect of grain boundaries on the plastic deformation of bicrystals

Xiaoming Liu¹, Lucia Nicola², Erik Van der Giessen¹

¹Zernike Institute for Advanced Materials, University of Groningen, The Netherlands
Corresponding author: Xiaoming Liu xiaoming.liu@rug.nl
University of Groningen, Zernike Institute for Advanced Materials, Nyenborgh 4, 9747 AG
Groningen, The Netherlands.

²Department of Materials Science and Engineering, Delft University of Technology,
2628 CD Delft, The Netherlands.

Grain boundaries (GBs) can play an important role in plastic deformation since they can lead to dislocation pile ups, or to the nucleation, absorption, and transmission of dislocations. There is a large sizescale gap between the understanding of these phenomena at the atomic scale (e.g., [1]) and the modeling of the effect of GBs in polycrystals. At the crystal sizescale, the collective behavior of dislocations is mainly implemented through constitutive laws involving the dislocation density as an independent field variable (e.g., [2]).

In this paper we propose to connect these scales using the superposition method [3] for Discrete Dislocation Plasticity inside grains that are connected with a Cohesive Surface model [4] representing the GB. The properties of such a cohesive law, relating the relative displacement across the GB to the transmitted traction, can be derived from classical molecular simulations.

More specifically, we consider a bi-crystal specimen, as shown in Figure 1. Periodic boundary conditions are applied in the direction parallel to the GB, and deformation is imposed by prescribed displacements along the top and bottom boundary. The height of the strip is varied so as to investigate size effects. Particular emphasis is given to the absorption of dislocations and their spreading in the GB as a function of GB properties. The results will be presented in a form that allows for transfer to continuum plasticity models.

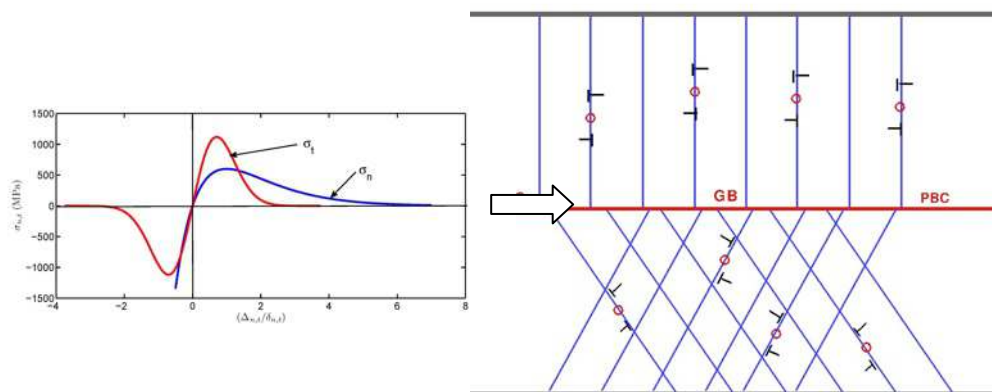


Figure 1. Sketch of the model comprising two grains. The red circles represent nucleation sites for dislocations (denoted by \perp symbols). The inset shows the cohesive law from [4] that is adopted for the GB.

- [1] V. Yamakov, D. Wolf, S. R. Phillpot, A. K. Mukherjee and H. Gleiter, *Nature Materials* 1 (2002) 45.
- [2] C. J. Bayley, W. A. M. Brekelmans and M. G. D. Geers, *International journal of solids and structures* 43 (2006) 7268.
- [3] E. Van der Giessen and A. Needleman, *Modelling and Simulation in Materials Science and Engineering* 3 (1995) 689.
- [4] X. P. Xu and A. Needleman, *Journal of the Mechanics and Physics of Solids* 42 (1994) 1397.

Micromechanics of polypropylene non-woven felts: experimental characterization and numerical modelling

Álvaro Ridruejo¹, Carlos González^{1,2} and Javier LLorca^{1,2}

¹Departamento de Ciencia de Materiales, Universidad Politécnica de Madrid.
E.T.S. de Ingenieros de Caminos. 28040 – Madrid, Spain.

²Instituto Madrileño de Estudios Avanzados de Materiales (IMDEA-Materiales)
C/ Profesor Aranguren s/n. 28040 Madrid, Spain.
Email address: jllorca@mater.upm.es (Javier LLorca)

Nonwoven felts are materials manufactured from a set of disordered fibers consolidated by bonds of different nature, such as simple entanglement, local thermal fusion or chemical binders, depending on the particular material or processing technique. The interest in these materials is increasing due to lower processing costs (as compared to woven fabrics) and they are used today in a number of applications, including ballistic protection, thermal insulation, liquid-absorbing textiles, fireproof layers, or geotextiles for soil reinforcement. The mechanical behavior of non-woven fabrics is very different from that of woven materials. Their stiffness and strength are lower than their woven counterparts, but they are far superior in terms of their deformation capability and energy absorption during deformation. In addition, the deformation and failure processes of non-woven felts are highly complex because they involve different micromechanisms which act simultaneously: straightening, large deformation and rotation of the fibers as well as bond breakage, fiber sliding and fracture.

There is a lack of sound physically-based micromechanical models to represent the mechanical behavior of these materials and this was the main objective of this investigation. The material studied was a non-woven felt made up of polypropylene fibers consolidated by thermal bonding. Tensile tests were performed on unnotched samples, showing that the deformation of this material involved complex mechanisms including fiber reorientation and plasticity. Bond breakage and fiber fracture were the main damage mechanisms. Damage was spread over a large area before localization. In addition, the post-peak behavior showed either a sudden failure of a large amount of fibers with a sharp drop of the measured force, or a further extension of damage with a gradual decay of load. In both cases the unraveling of fibers allows the felt to keep a certain load-carrying capability up to large strains. The experiments also examined the role of defects by inserting central notches with different sizes. These tests confirmed the notch-insensitive behavior of the felt.

The felt behavior was modeled by means a continuum-based finite element computational model. The model was implemented by a VUMAT (user-material) subroutine for ABAQUS Explicit. The boundary conditions controlled the deformation gradient tensor for each element, which in turn allowed the calculation of the elongation of a fiber with an arbitrary orientation. Taking a set of isotropic, non-interacting fibers, the stress tensor was obtained as the angular integral of the constitutive equation for one fiber. The constitutive equation for the fibers was fitted to an elastic-plastic behavior according to experimental data and included damage by fiber fracture. Finally, the ability of the model to reproduce the

macroscopic behavior of the felt as well as the micromechanisms of deformation and fracture is demonstrated by comparison with the experimental results.

Rejuvenation Effects in Polymer Glassy Dynamics

Alexey V. Lyulin¹, Dmitri Hudzinsky^{1,2}, Eric Janiaud^{2,3} and Antoine Chateauinois³

¹Theory of Polymers and Soft Matter, Department of Applied Physics, Eindhoven University of Technology, P.O.Box 513, 5600 MB Eindhoven, The Netherlands

a.v.lyulin@tue.nl

²Dutch Polymer Institute, P.O.Box 902, 5600 AX, The Netherlands,

d.hudzinsky@tue.nl

³Laboratoire PPMD-SIMM, UPMC, CNRS UMR 7615, Ecole Supérieure de Physique et Chimie Industrielles (ESPCI), 10, rue Vauquelin, 75231 Paris Cedex 05, France,

antoine.chateauinois@espci.fr

ABSTRACT

We use massive united-atoms molecular-dynamics (MD) simulations and an original lateral contact experiment to explore the influence of mechanical history on polymer mechanical behaviour and segmental mobility. Two typical glassy polymers are considered: bulk acrylate (experiments) and atactic polystyrene (aPS) (simulations). Cyclic shear strains lead to mechanical rejuvenation process and enhanced physical ageing rate. This experimentally observed mechanical rejuvenation of a polymer has been for the first time connected to the drastic increase in the simulated segmental mobility.

1. Introduction

Polymer glasses are characterized by very broad spectrum of relaxation times. Polymer segmental mobility and polymer mechanical properties characterized by this spectrum are influenced by many factors, as physical aging, external mechanical deformation, spatial nanoconfinement, and many others. The main goal of the present study is to shed light on the influence of some of these factors on polymer segmental dynamics and its mechanical behaviour.

Polymer glasses age with time. The concept of the physical ageing of polymer materials was introduced by Struik long ago [1]. At that time Struik suggested that the large deformations in glassy polymers influence the physical ageing process, mainly by creating the additional free volume. Since ageing is supposed to occur due to some relaxation (decrease) in free volume, the free volume created by the deformation erases some part of the ageing, and rejuvenation takes place. McKenna recently [2] showed that after the application of deformation the polymer glasses end up into a new thermodynamic state which is different from that after thermal rejuvenation above T_g , meaning that some amorphous-amorphous transition takes place. This suggestion is supported by the concept of the potential energy landscape of the glassy state [3].

Computer-simulation studies of the changes in polymer dynamics under the influence of the deformation have been scarce. Capaldi et al. [4] showed the increased conformational transition rate upon the application of the uniaxial compression in molecular-dynamics (MD) simulations of a polyethylene-like chain. Using direct atomistic simulations of (bis)phenol-A-polycarbonate glass Lyulin et al. also showed [5] that the partitioning of the internal energy is completely different for thermally and mechanically rejuvenated polymers: the thermal rejuvenation is for more than 80% due to weaker van der Waals interactions, while the

difference after a mechanical rejuvenation is for about 40% due to increased torsion of the polymer chains.

In the present manuscript our aim is to understand how mechanical deformation influences the polymer ageing phenomenon and its dynamics, by doing both atomistic modelling and mechanical experiments on typical polymer glass formers. Cyclic shear experiments in the plastic regime have been carried out using a lateral contact method where a crosslinked glassy acrylate film is cyclically sheared within a contact between two elastic (glass) substrates [6]. As compared to more conventional mechanical experiments using bulk polymer specimens, this contact method presents the advantage of preventing the formation of macroscopic defects such as cracks within the glassy polymer when large strain cyclic strains are applied. Atactic polystyrene, aPS, is chosen for MD simulations. We will show how the mechanical rejuvenation influences the whole spectrum of segmental relaxation times in a polymer glass. For this purpose not only orientational dynamical autocorrelation functions are simulated, but the whole distribution function of polymer relaxation times is calculated as well, for both non-rejuvenated and rejuvenated samples.

2. Simulational and Experimental Details

The united-atom representation of aPS is chosen for the MD simulations, no explicit hydrogen atoms are present. The aPS model is described in detail by Lyulin *et al.* [7]. In short, the *NPT* MD simulations have been performed for 8 aPS polymer chains consisting of $N_p = 80$ monomers each (molecular weight ≈ 8300 Da, below one entanglement length) and its periodic images.

After the equilibration at $T=540\text{K}$ the continuous cooling was performed with a constant cooling velocity of 0.01 K/ps down to the room temperature, 300 K , which is well below the known glass transition temperature (about 380 K) for this polymer. In order to simulate the effects of the rejuvenation, a $50\text{ \AA} \times 50\text{ \AA} \times 50\text{ \AA}$ box containing aPS bulk cooled down to $T=300\text{K}$ is submitted to a cycle of uniaxial extension-compression. aPS samples are stretched for about 30 % (well above the yield point) and compressed back with a deformation velocity of 0.001 \AA /ps .

Cyclic shear experiments on a glassy acrylate polymer were carried out using a lateral contact method. In this experiment, a crosslinked acrylate film (about $50\text{ }\mu\text{m}$ in thickness) is cyclically sheared within a circular macroscopic contact (about $660\text{ }\mu\text{m}$ in diameter) between a glass flat and a spherical glass lens under a constant applied normal load (30 N). From a measurement of the lateral contact stiffness, the complex shear modulus can be determined both in the linear (viscoelastic) and in the non linear regimes. Full details regarding the experimental methodology and data analysis are provided in references [6,8].

3. Results and Discussion

The local orientational mobility in both non-rejuvenated and rejuvenated aPS bulk at $T=300\text{ K}$ has been simulated with the help of Legendre polynomials of the second order (autocorrelation functions, ACFs)

$$P_2(t) = \langle 3/2(\mathbf{b}(0)\mathbf{b}(t))^2 - 1/2 \rangle, \quad (1)$$

where \mathbf{b} is the unit vector directed along the phenyl side group and brackets denote the averaging over positions and over time. After the rejuvenation the local segmental mobility is changed. Rejuvenation drastically increases the relaxation rate, especially in the latest stage of the relaxation. The standard KWW fit [9] can not be used to describe the whole relaxation

process. It means that different relaxation mechanisms contribute differently to the orientational mobility. To take this into account, each ACF is analyzed using the CONTIN [10] method

$$P_2(t) = \int_{-\infty}^{+\infty} F(\ln \tau) \exp(-t/\tau) d(\ln \tau), \quad (2)$$

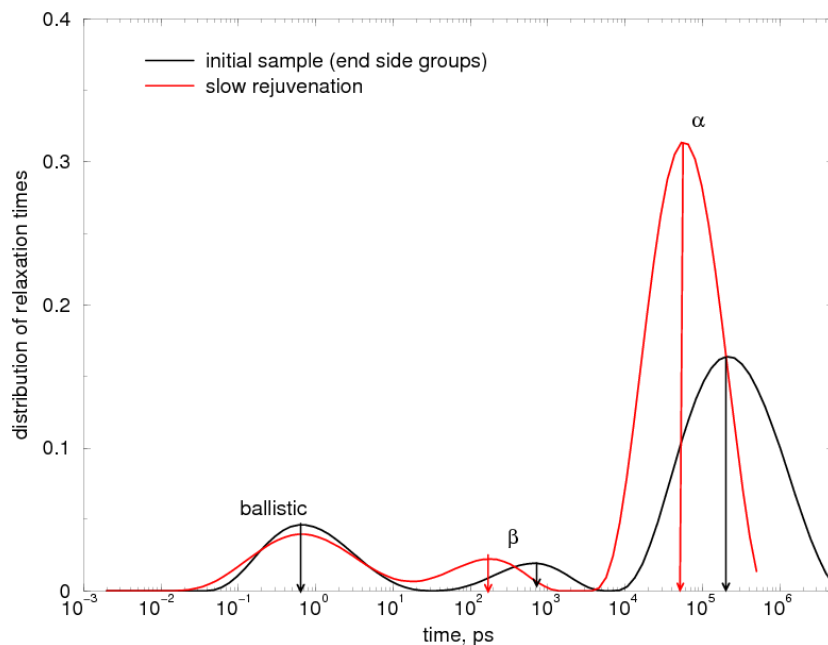


Figure 1. Simulated distribution function of the relaxation times for P_2 ACF of the average side bond vector at the chain ends for both initial and rejuvenated samples.

where $F(\ln \tau)$ is a normalized distribution function of relaxation times. The distribution function of the relaxation times is shown in Fig. 1 for the end phenyl groups averaged over all aPS chains. Three relaxation processes are clearly seen. The magnitude of the long-time α process increases after the rejuvenation, and its position is clearly shifted to the shorter times. Ballistic process at very short times is not affected by the rejuvenation at all. Such a ballistic motion can describe only one percent of the total relaxation of the P_2 ACF. The clear shift of the in-cage β relaxation takes place, also to shorter times. We noticed also that initially the density of the rejuvenated samples is higher as compared to the initial density for the aged polymer. The faster in-cage β relaxation is probably associated with this initial increase of the density. Finally, the increased ageing rate after the rejuvenation is definitely explained by the faster α process for the rejuvenated material.

Prior to the application of cyclic shear in the yield regime, the complex linear viscoelastic modulus, G^* , of the acrylate film is first measured in its reference state at low strain (0.5 %) and for frequencies ranging from 0.05 to 10 Hz. No significant time dependent change in this modulus is observed after a contact time of more than one hour, which means that physical aging processes of the virgin film are not detectable within this time frame. Sixty shear cycles at large strain amplitude (6.4 %) and at a frequency of 1 Hz are subsequently applied to the film in order to induce plastic deformation. Then, the dynamics of the yielded polymer glass is probed from a continuous measurement of its linear viscoelastic properties at low strain (0.5 %). As compared to the initial (i.e. before yield) viscoelastic modulus (G' =1100 MPa, G'' =67±3 MPa), the storage modulus at 1 Hz is decreased by about 15 % and the loss modulus is increased by about 80% immediately after cyclic yield (Fig. 2). However, a progressive recovery of these linear viscoelastic properties is observed as a function of time. Such a recovery may be viewed as evidence of enhanced physical aging rate of the mechanically rejuvenated glass. The time dependent viscoelastic spectra recorded immediately after cyclic

yield are consistent with the occurrence of a mechanical “rejuvenation” effect. Accordingly G' is depressed and G'' is increased. From these data, one can speculate on a shift of the G^* spectra to higher frequencies as a result of cyclic plastic deformation.

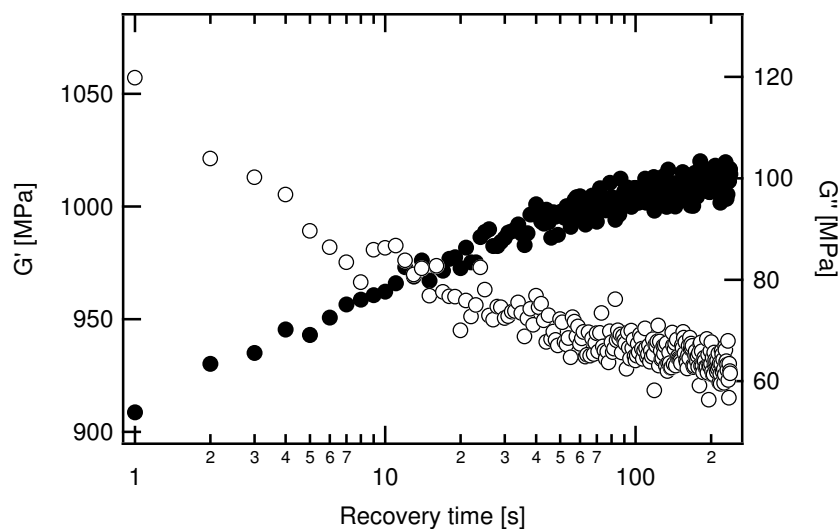


Figure 2. Recovery of storage (G') and loss (G'') components of the linear viscoelastic modulus ($\gamma_0=0.5\%$, 1Hz) after the application of 60 shear cycles in the yield regime ($\gamma_0=6.4\%$, 1Hz). (●) G' ; (○) G'' . Before cyclic yield, the initial values of the components of the linear viscoelastic modulus are $G'=1066 \pm 9$ MPa and $G''=67 \pm 3$ MPa.

Although the timescales are completely different, this hypothesis is supported by the MD simulations which show that mechanical rejuvenation shift the relaxation times distribution – both in α and β transition zones - to shorter times. As a result of the increased segmental mobility within the post-yield mechanically stimulated glass, ageing is reinitiated as indicated by the progressive recovery of the viscoelastic properties.

Acknowledgements

This study is a part of a Dutch Polymer Institute research program, project #654. This work was also sponsored by the Stichting Nationale Computerfaciliteiten (National Computing Facilities Foundation, NCF) for the use of supercomputer facilities, with financial support from the Nederlandse Organisatie voor Wetenschappelijk Onderzoek (Netherlands Organization for Scientific Research, NWO).

References

- [1] L. C. E. Struik, *Physical Aging in Amorphous Polymers and Other Materials*, Elsevier, Amsterdam, 1978).
- [2] G.B. McKenna, *J.Phys.: Condens. Matter*, 15, 737 (2003).
- [3] F.H. Stillinger, *Science*, 267, 1935 (1995).
- [4] F. M. Capaldi, M. C. Boyce, G. C. Rutledge, *Phys. Rev. Lett.*, 89, 175505 (2002).
- [5] A. V. Lyulin, M. A. J. Michels, *Phys. Rev. Lett.*, 99, 085504 (2007).
- [6] Gacoin, E., A. Chateauminois, C. Fretigny, *Tribology Letters*, 21, 245 (2006).
- [7] A. V. Lyulin, N. K. Balabaev and M. A. J. Michels, *Macromolecules*, 35, 9595 (2002).
- [8] Gacoin, E., A. Chateauminois, and C. Fretigny, *Polymer*, 45, 3789 (2004).
- [9] G. Williams, D.C. Watts, *Trans. Faraday Soc.*, 66, 80(1970).
- [10] S. Provencher, *Comput. Phys. Commun.*, 27 213 (1982).

Combining ab initio calculations and classical concepts in solid solution strengthening

Duancheng Ma¹, Martin Friák¹, Johann von Pezold¹, Dierk Raabe¹, and Jörg Neugebauer¹

¹Max-Planck-Institut für Eisenforschung GmbH, Max-Planck-Strasse 1, 40237, Düsseldorf, Germany, d.ma@mpie.de

Solid solution strengthening is one of the most important strengthening mechanisms in soft metallic systems. Over the centuries of materials research, a combination of three mechanisms was revealed as decisive for the solid-solution strengthening phenomena: (i) the size mismatch of components (Nabarro's parrelastic concept), (ii) the elastic modulus mismatch of atoms (Fleicher's dielastic contribution), and (iii) the concentration of solutes (statistical concept of Friedel and Labush). Employing a multi-descriptive modeling approach combining density functional theory calculations (resolving atomic structure of materials) and linear-elasticity theory (based on continuum description) the key parameters essential for the classical theories are determined. In this way, the strengthening capability of the solute elements can be precisely quantified, the classical concepts can be tested and their possible validity limits identified. As an example, selected binary Al systems are studied and an attempt is made to explain the hardening effect of the solute elements in terms of the underlying electronic structure and charge densities.

A Micromechanical Numerical Analysis for Triaxial Compression of Granular Materials

Vanessa Magnanimo^{1*}, Luigi La Ragione² and Stefan Luding¹

¹M.S.M. University of Twente, Enschede – The Netherlands

²D.I.C.A. Politecnico di Bari, Bari – Italy

* M.S.M. University of Twente, 7500 Enschede (NL) email: v.magnanimo@utwente.nl

It has been consistently observed that two specimens of a granular soil, prepared by different methods in the laboratory, may exhibit quite different responses to applied loading under otherwise identical conditions [1][2]. Similar results have been obtained measuring wave velocity in granular assemblies by means of numerical simulations [3]. While there is abundant evidence of the impact of the previous history (preparation procedure) on granular soils behavior, it remains a challenging task how to describe and take it in account in mechanical analysis.

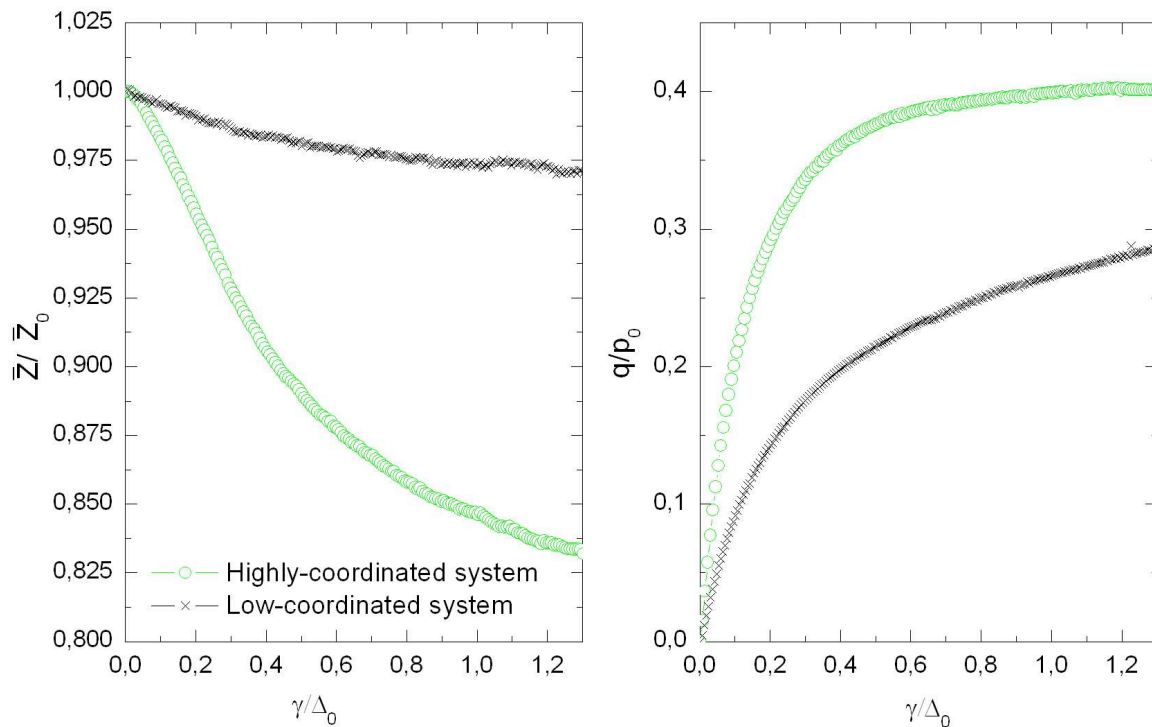


Fig.1 Evolution of the coordination number and the deviatoric stress with respect to the deviatoric strain (normalized on the initial volumetric strain).

In the present work the case of axial-symmetric compression with constant mean-stress of a dense granular assembly is studied. The analysis is conducted performing molecular dynamic simulations [4][5] on aggregates of 10.000 dry frictional spheres. For specimens with same density ϕ and subjected to the same initial confining pressure p_0 and same loading path, the difference in the response

can be considered directly associated with the different microstructure. That is, the microstructure in the granular sample can play the role of a *descriptor* in the reference state of the history of the material before to reach such a configuration. Particularly, we focus on the average number of contacts per particle, i.e. the coordination number, in the reference state. The results show that, when a deviatoric strain is applied, the deviatoric stress and the volumetric strain strongly depend on the initial coordination degree of the sample. Interestingly the evolution of the microstructure itself and the effective stiffness of the assembly even are related to the initial contact network of the sample.

- [1] F. Tatsuoka et al. *Soils Found.* **26** (3), 23, 1986.
- [2] Z.X. Yang et al. *Géotechnique* **58** (4), 237, 2008.
- [3] V. Magnanimo et al. *Europhys. Lett.* **81**, 34006, 2008.
- [4] P.A. Cundall and O.D.L. Strack. *Géotechnique* **29** (1), 4765, 1979.
- [5] S. Luding. In *The Physics of Granular Media*, 299, Weinheim, 2004.

Driving forces for moving inclusion and inhomogeneity boundaries with transformation strain

Xanthippi Markenscoff and Luqun Ni
Dept of MAE 0411, UCSD, La Jolla, CA 92093, USA

ABSTRACT

The radiated fields of expanding Eshelby inclusions and inhomogeneities with transformation strain (eigenstrain) are obtained based on a formula of Willis (1965) [1], and the “driving forces” are evaluated for a plane moving inclusion boundary. They consist of a self-force and a Peach-Koehler type force associated with external loading. The total “driving force” (dynamic J integral) equaling zero, or to a dissipative term, yields the kinetic relation between loading and boundary velocity.

1. Introduction: Expanding Eshelby Inclusions.

The analysis of an expanding spherical inclusion with transformation strain (eigenstrain) is formulated in Markenscoff and Ni (2010a) [2] on the basis of the dynamic Green’s function for an infinite elastic solid; they obtained the radiated fields from a spherical (Eshelby) inclusion with constant dilatational eigenstrain, initially at rest, and expanding radially non-uniformly according to $R(t) = R_0 + I(t)$. It followed the analysis of Willis (1965) [1], with the difference that Willis (1965) [1] studied the radiated field from a spherical inclusion with time dependent dilatational eigenstrain, but not changing in volume. The radiated fields were evaluated [2] on the basis of the dynamic Green’s function according to

$$u_i(\mathbf{x}, t) = \int_{-\infty}^{+\infty} dt' \int_{V(t')} C_{jklm} \varepsilon_{lm}^*(\mathbf{x}'; t') \frac{\partial G_{ij}(\mathbf{x} - \mathbf{x}', t - t')}{\partial x_k} dV' \quad (1a)$$

$$= \int_{-\infty}^{+\infty} dt' \int_{S(t')} C_{jklm} \varepsilon_{lm}^*(\mathbf{x}'; t') n_k(\mathbf{x}) G_{ij}(\mathbf{x} - \mathbf{x}', t - t') dS \quad (1b)$$

with the eigenstrain $\varepsilon_{ij}^*(\mathbf{x}; t)$ in a finite region $V(t)$ with boundary $\partial V(t) = S(t)$; they were shown to satisfy the Hadamard jump conditions.

By a limiting process from the spherical solution (Fig. 1), in which the radius of the spherical inclusion tends to infinity so as the inclusion to remain constrained, the radiated fields of a half-space inclusion with dilatational eigenstrain moving from rest non-uniformly in the x_1 direction were obtained [2].

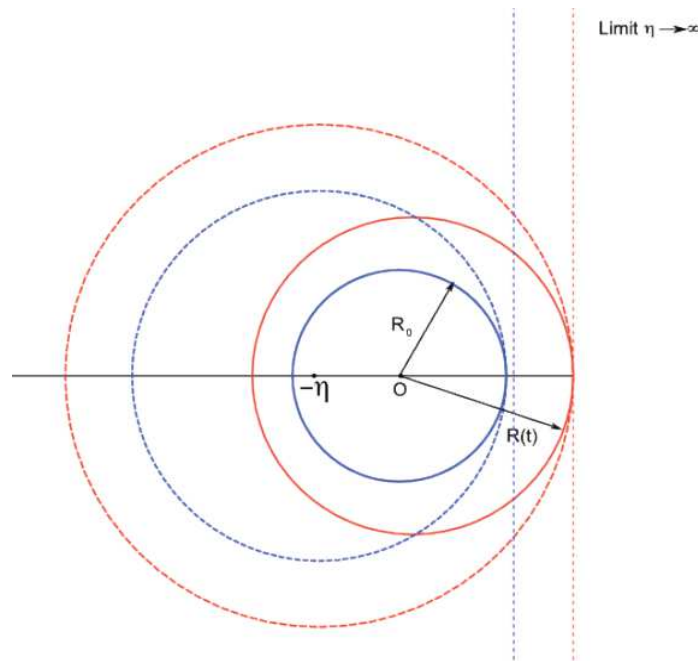


Figure 1. A plane boundary as a limit of a spherical one

For a static circular inclusion, the limit that yields the half-plane inclusion has been obtained by Dundurs and Markenscoff (2009) [3], and the resulting stress field, which requires applied tractions at infinity to sustain the eigenstrain, coincides, indeed, with the Eshelby solution (1957) [4] for the interior, and outside the boundary, with the one determined by the Hill (1961) [5] jump conditions. Analogously is treated the 3-dimensional limit of a spherical inclusion to yield a half-space inclusion, and this limit is the initial condition for the dynamic problem of the half-space inclusion. This static limit is the minimum energy solution for a half-space constrained inclusion, since, superposing self-equilibrated tractions at infinity (that keep the interface compatible) increases the total energy of the system. It may be noted that Eqn(1), when integrated from time minus infinity to zero, gives the static Eshelby solution[4].

2. Driving Forces on Inclusion Boundaries

For a plane boundary (of a constrained inclusion) moving from rest in general motion $l(t)$, “the driving force” (e.g. [6], [2])

$$f = \left[\left[W \right] \right] - \langle \sigma_{ij} \rangle \left[\left[\frac{\partial u_i}{\partial x_j} \right] \right] \quad (2)$$

was calculated by Markenscoff and Ni (2010) [7] from the limiting fields of the spherical one as the radius tends to infinity (see Figure 1), so that the plane constrained boundary moves according to: $R(t) = R_0 + l(t)$. The driving force is derived from the dynamic J integral (Noether’s theorem), and is equal to the energy-release rate (the mechanical rate of work) needed to create an incremental volume of (dilatational here) eigenstrain (due to whatever source), as the boundary moves dynamically:

$$-\frac{2\mu(3\lambda+2\mu)\varepsilon^{*2}}{(\lambda+2\mu)} - \frac{(3\lambda+2\mu)^2\varepsilon^{*2}}{2(\lambda+2\mu)} \left[\frac{a\dot{l}(t)}{(a^2 - \dot{l}^2(t))} \right]. \quad (3)$$

The above expression for the self-force consists of two terms: the first static one, coinciding with Eshelby (1977) [8] and Gavazza(1977) [9], and the second one due to inertia [2]. If an

externally are applied field σ_{ij}^{appl} is superposed, and all the interaction terms are included in Eqn (3), then an additional Peach-Koehler type term appears in Eqn (3), of the form

$$\langle \sigma_{k\ell}^{appl} \rangle \left[\left[\varepsilon_{k\ell}^*(\mathbf{x}, t) \right] \right]. \quad (4)$$

Considering that the total dynamic J integral (from which the “driving force” is derived) has to vanish in the absence of dissipation, we have the “equation of motion“, or “kinetic relation” for a plane boundary with dilatational eigenstrain under σ_{11}^{appl} external loading:

$$\begin{aligned} -\frac{2\mu(3\lambda+2\mu)\varepsilon^{*2}}{(\lambda+2\mu)} - \frac{(3\lambda+2\mu)^2\varepsilon^{*2}}{2(\lambda+2\mu)} \left[\frac{a\dot{l}(t)}{(a^2-\dot{l}^2(t))} \right] + \sigma_{11}^{appl}\varepsilon^* &= 0 \text{ (no dissipation)} \\ &= F(\dot{l}(t)) \text{ (dissipation)} \end{aligned} \quad (5)$$

This expression reveals that the fundamental structure of the energy-release rate, or the “driving-force” on the boundary of an expanding inclusion, is analogous to the one for a moving dislocation [10]: a self-force and a Peach-Koehler force, and no cross terms of the applied loading with the motion, thus allowing for the unified treatment of the energetics of moving defects. In the case of the dislocation the self-force depends on the acceleration (and hence, there is an effective mass), while, in the moving plane boundary, only on the velocity.

For a plane moving half-space inclusion boundary with general eigenstrain the radiated fields have been evaluated in [11] on the basis of Eqn (1a) with initial condition the limiting fields of the spherical inclusion. The driving force for general eigenstrain was calculated to be [11]:

$$f = f_0 - \frac{1}{2} \frac{\left[(\lambda+2\mu)\varepsilon_{11}^* + \lambda(\varepsilon_{22}^* + \varepsilon_{33}^*) \right]^2}{(\lambda+2\mu)} \frac{c_1\dot{l}(t)}{c_1^2 - \dot{l}^2(t)} - \frac{2\mu c_2\dot{l}(t)}{c_2^2 - \dot{l}^2(t)} \left[(\varepsilon_{12}^*)^2 + (\varepsilon_{13}^*)^2 \right] \quad (6a)$$

with the latter terms being due to inertia, while the first one, f_0 , is the static self-force [11]:

$$\begin{aligned} f_0 &= -\frac{32\mu(\lambda+\mu)}{15(\lambda+2\mu)} (\varepsilon_{11}^*)^2 - \frac{2\mu(\lambda+\mu)}{15(\lambda+2\mu)} \left((\varepsilon_{22}^*)^2 + (\varepsilon_{33}^*)^2 \right) - \frac{4\mu(7\lambda+2\mu)}{15(\lambda+2\mu)} \varepsilon_{11}^* (\varepsilon_{22}^* + \varepsilon_{33}^*) \\ (6b) &+ \frac{2\mu(\lambda-4\mu)}{15(\lambda+2\mu)} \varepsilon_{22}^* \varepsilon_{33}^* - \frac{4\mu(9\lambda+14\mu)}{15(\lambda+2\mu)} \left((\varepsilon_{12}^*)^2 + (\varepsilon_{13}^*)^2 \right) - \frac{2\mu(3\lambda-2\mu)}{15(\lambda+2\mu)} (\varepsilon_{23}^*)^2 \end{aligned}$$

Any superposed applied loading will add a term given by Eqn (4), and an analogous to (5) equation of motion.

3. Moving boundaries of inhomogeneities with eigenstrain.

The radiated fields obtained by Markenscoff and Ni (2010b) [11] can be used in order to obtain the inhomogeneous (of different elastic constants C_{ijkl}^*) moving boundary by the Eshelby equivalent eigenstrain method extended to dynamics [7] (e.g. Mura[12], Eqn (24.2)):

$$C_{ijmn} \varepsilon_{mn}^{*equiv}(\mathbf{x}, t; \dot{l}(t)) - \Delta C_{ijmn} \varepsilon_{mn}(\mathbf{x}, t; \dot{l}(t)) = \sigma_{ij}^{appl} - C_{ijmn}^* \varepsilon_{mn}^{appl} \quad (7)$$

with $\varepsilon_{mn}(x, t; \dot{l}(t))$ being related to the equivalent eigenstrain by the solutions for the strain of the radiated fields of the moving inclusion boundary, obtained in [11], as a function of the eigenstrain and the boundary velocity.

The total equivalent $\varepsilon^{**equiv}(\mathbf{x}', t'; \dot{l}(t'))$ is due to the eigenstrain itself in the half-space moving boundary plus the equivalent one due to the inhomogeneity (e.g. [12])

$$\varepsilon_{ij}^{**equiv} = \varepsilon_{ij}^{*equiv} + \varepsilon_{ij}^* \quad (8)$$

so that the radiated fields for the moving boundary of an inhomogeneity with eigenstrain can be evaluated from Eqn (1a) with the total equivalent eigenstrain:

$$u_i(\mathbf{x}, t) = \int_{-\infty}^{+\infty} dt' \int_{V(t')} C_{jklm} \varepsilon_{lm}^{**equiv}(\mathbf{x}', t'; \dot{l}(t')) \frac{\partial G_{ij}(\mathbf{x} - \mathbf{x}', t - t')}{\partial x_k} dV' \quad (9)$$

Subsequently, from these, the driving force can be calculated.

References

- [1] Willis, J.R. (1965) "Dislocations and Inclusions", *J. Mech. Phys. Sol.*, 13, 377-395
- [2] Markenscoff, X. and Ni, L. (2010) a. "The energy-release rate and self-force of dynamically expanding spherical and plane inclusion boundaries with dilatational eigenstrain" *J. Mech. Phys. Sol.* 58, 1-11.
- [3] Dundurs, J. and Markenscoff, X. (2009) Stress fields and Eshelby forces on half-plane inhomogeneities and strip inclusions meeting a free surface" *Int. J. Sol. Str.* 46, 2481-2485.
- [4] Eshelby, J.D. (1957) The determination of the elastic field of an ellipsoidal inclusion and related problems, *Proc. Roy. Soc. London*, A241, 376-396.
- [5] Hill, R. (1961) "Discontinuity relations in mechanics of solids", in *Progress in Solid Mechanics*, I.N.Sneddon and Hill, R. eds, North-Holland, Amsterdam.
- [6] Eshelby, J.D. (1970), "Energy relation of the energy-momentum tensor in continuum mechanics" in *Inelastic Behavior of Solids*, eds Kanninen, M.F. *et al*, pp77-115.
- [7] Markenscoff, X. (2010) "Driving forces on moving inhomogeneities with transformation strain", *J.Elast.* (invited paper for the D. Carlson volume, in preparation)
- [8] Eshelby, J.D. (1977) Lecture on the elastic energy-momentum tensor, in *Collected Works of J.D. Eshelby: The Mechanics of Defects and Inhomogeneities*, pp 907-931, Markenscoff, X. and Gupta, A. editors, Springer, Netherlands (2006)
- [9] Gavazza, S.D. (1977) "Forces on pure inclusion and Somigliana dislocations" *Scripta Metallurgica*, 11,979-981.
- [10] Eshelby, J.D. (1953), "The equation of motion of a dislocation", *Phys. Rev.*90, 248-255
- [11] Markenscoff, X. and Ni, L. (2010), b. "Driving forces and radiated fields for expanding/shrinking half-space and strip inclusions with general eigenstrain" *Quart. Appl. Math.* (in press)
- [12] Mura, T.,(1982) *Micromechanics of Defects in Solids*, Martinus Nijhoff Publishers, The Hague, 1982

Microstructurally motivated grain boundary model for strain gradient crystal plasticity

**G.J. McShane¹, P.R.M. van Beers²,
V.G. Kouznetsova², M.G.D. Geers²**

¹University of Cambridge, Engineering Department,
Trumpington Street, Cambridge, CB2 1PZ, UK

²Department of Mechanical Engineering, Eindhoven University of Technology,
P.O. Box 513, 5600 MB Eindhoven, The Netherlands
e-mail: gjm31@cam.ac.uk

Interfaces play an important role in the mechanical behaviour of polycrystalline and multi-phase materials. Grain and phase boundaries in metals locally constrain plastic deformation. For fine-grained materials, or metallic devices with dimensions approaching that of the material grain size, interface behaviour has a particularly strong influence. In these cases, modelling efforts have to consider the multi-scale nature of the problem: an accurate prediction of the continuum level response depends on accurately accounting for the interface micromechanics. The complex interactions between dislocations and grain boundaries have been revealed by a number of experimental investigations and, more recently, atomic scale numerical calculations. These studies help to identify the key parameters influencing the extent to which an interface obstructs the propagation of slip. Crystallographic misorientation, the dislocation type and its orientation relative to the interface all appear to be important.

In this work, we present a microstructurally motivated continuum level model which aims to capture grain boundary behaviour within a strain gradient crystal plasticity framework. Strain gradient theories are able to capture size dependent plasticity by accounting for the presence of geometrically necessary dislocations. Most models of this type require additional, non-standard boundary conditions to be specified at interfaces. We discuss these higher order boundary conditions in the context of recent microstructurally motivated frameworks. We proceed to develop thermodynamically consistent constitutive relationships which govern slip at a grain boundary. The interface model accounts for the local microstructure and its evolution, consistent with experimental observations. Finally, the numerical implementation is discussed.

Multiscale simulation of the curing of particle-filled polymers

Julia Mergheim

Chair of Applied Mechanics, University of Erlangen-Nuremberg,
Egerlandstr. 5, 91058 Erlangen; email: julia.mergheim@itm.uni-erlangen.de

The curing of polymers is a complex process involving the transition of a viscous fluid, i.e. the liquid monomer solution, into a viscoelastic solid. This phase transition is accompanied by increases in stiffness and viscosity as well as a volume shrinkage which may lead to residual stresses or strains.

Polymeric materials are frequently enriched with different reinforcements like nanoparticles or glass fibres to enhance their properties. The resulting improvement of the stiffness or the fracture properties depends in particular on the interaction between the reinforcements and the polymeric matrix, i.e. on the strength of the bonding between particles and matrix. When the curing process proceeds the bond between matrix and particles is developed, but the concurrent shrinkage of the polymer matrix can lead to a degradation of the interfacial stiffness or even to debonding.

A multiscale framework based on computational homogenisation, i.e. on the FE^2 scheme [1], is developed to analyse the influences that the curing process has on the overall mechanical properties of nanoparticle filled polymers. On the mesoscopic scale both the matrix material and the particles are explicitly modelled within an RVE. The curing of the polymer matrix is governed by a phenomenological hypoelastic constitutive equation which includes the temporal evolution of the stiffness and the volume shrinkage [2]. Furthermore, a cohesive law is introduced to model the interaction between matrix and particles. It governs the development of the interfacial stiffness during the curing process as well as its degradation due to the appearance of shrinkage stresses. The macroscopic response is computed by homogenising the stress response of the RVE for a prescribed deformation. The macroscopic stress-strain behaviour for different load cases is considered to elucidate the influences of the curing process on the overall material properties of the compound.

[1] J.M. Guedes, N. Kikuchi: Preprocessing and postprocessing for materials based on the homogenization method with adaptive finite element methods, *Comput. Methods Appl. Mech. Engrg.* Vol. 83, pp. 143–198, 1990.

[2] M. Hossain, G. Possart, P. Steinmann: A finite strain framework for the simulation of polymer curing. Part I: elasticity. *Comput. Mech.*, Vol. 44, pp.621-630, 2009.

Multiscale Modelling of Nano Tensile Tests for Different Cu-Precipitation States in α -Fe

David Molnar^{1,2}, Peter Binkele¹, Stephen Hocker¹, Siegfried Schmauder^{1,2}

¹ **Institute for Materials Testing, Materials Science and Strength of Materials (IMWF), University of Stuttgart, Pfaffenwaldring 32, 70569 Stuttgart, Germany, e-mail: david.molnar@imwf.uni-stuttgart.de;** ² **Stuttgart Research Centre for Simulation Technology (SRC SimTech), SimTech Cluster of Excellence, University of Stuttgart**

ABSTRACT

Copper-containing iron changes its material behaviour during its ageing process, especially when operated at higher temperatures of approximately 340°C . In that case, copper precipitates, with a mean radius of about one nanometer, form on a relatively large time scale (days) within the iron matrix, yielding first a precipitation strengthening of the material. However, as the precipitates grow further in time, the material strength decreases again. The growth of precipitates is due to vacancy jumps, a process that can be accounted for by Monte-Carlo (MC) simulations. Unfortunately, the rigid lattice model (RLM) which is applied within this MC method does not permit the application of forces onto the simulation box, which would be necessary for performing e.g. tensile tests. On the other hand, with Molecular Dynamics (MD) simulations, tensile tests can be simulated. Transferring a precipitation state from MC to MD allows the performance of tensile tests throughout the precipitation process and hence on relevant time scales. In the framework of Multiscale Materials Modelling (MMM), this can be understood as a multi-time-scale approach in a sequential way in which the transferred parameter is given by a realistic distribution of the precipitates. Thus, combining the above mentioned methods, the short time scale of MD is bridged with the larger time scale which is accessible with MC simulations. In this way, a computational modelling of tensile tests depending on a realistic precipitation distribution throughout the ageing process of copper-containing iron is achieved.

1. Introduction

In the recent past, multiscale approaches have been bridging more and more the gaps between atomistic and continuum modelling techniques in order to expand knowledge of the influence of atomistic interactions onto the macroscopic material behaviour and consequently to use them for material design. Combining different simulation methods hierarchically, i.e. in a sequential way, each method is applied on its appropriate length and time scale and coupled via an adequate parameter transfer. With MC simulations, the process of precipitation of copper-containing iron has been described for different temperatures¹. The formation velocity of precipitates and their increase in size over time strongly depends on the annealing temperature. Molecular Dynamics simulations have been carried out in order to investigate the tensile behaviour of pure iron² and the interaction of a dislocation with a single Cu-precipitate in an iron matrix and the resulting change of the critical resolved shear stress³. In this study, the changing material behaviour of copper-containing iron is investigated by combining kinetic Monte Carlo (MC) with Molecular Dynamics (MD) simulations sequentially (Fig.1). At certain times, i.e. states of precipitation, the field of precipitates is transferred from MC to MD. With this more realistic distribution of copper clusters, tensile tests are performed, neglecting defects in order to unravel the sole influence of the precipitate distribution on the tensile behaviour and, in detail, on the tensile

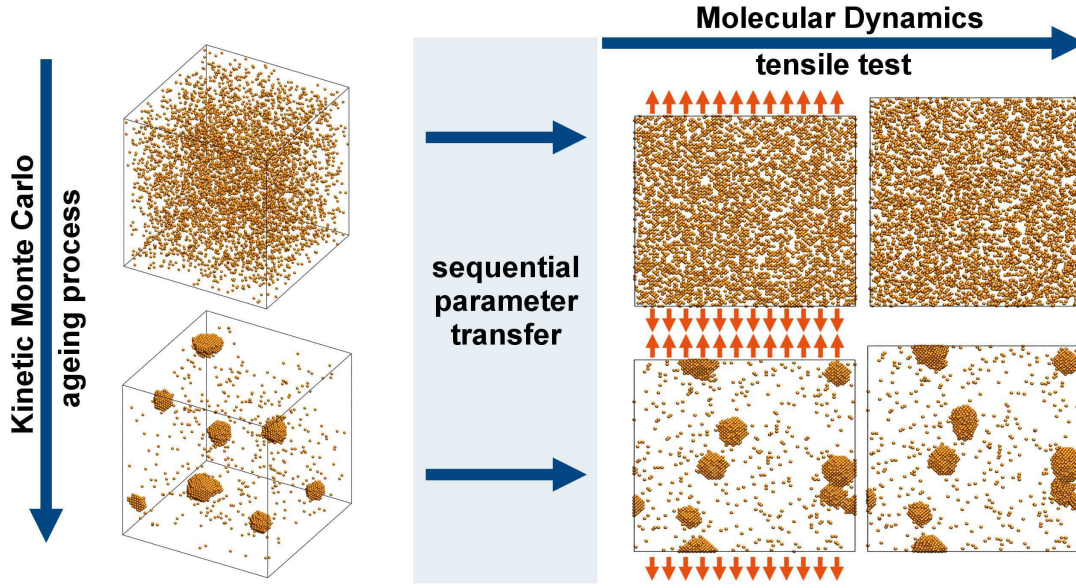


Figure 1: Scheme of the sequential modelling approach. With Monte Carlo simulations the relatively slow process of precipitation is simulated. Molecular Dynamics simulations allow for the deformation of the structure and thus for the performance of tensile tests.

strength of the material.

2. Modelling Scheme

First, the growth of precipitates is simulated, using a kinetic Monte Carlo approach, which is based on a code developed by Soisson et al.⁴. After transferring the precipitation field to Molecular Dynamics, computational tensile tests on a nanoscale are performed. A fixed body-centered cubic (bcc) and rigid lattice (Rigid Lattice Model, RLM) for α -Fe can be assumed during the whole precipitation process as the copper precipitates are embedded coherently in the α -Fe lattice for small precipitate radii⁵. The box size is $L = 64$ lattice constants, i.e. $N = 2 L^3 = 524288$ atoms are considered for two supersaturated configurations (1 at.% Cu, 10 at.% Cu). Periodic boundary conditions are applied within both methods.

2.1 Monte Carlo (MC) Method

The chemical binding between atoms is described by first- and second-neighbour interaction energies. A vacancy within the simulation box allows the movement of an atom by site exchange between the vacancy (V) and a neighbouring atom (Fe, Cu). This thermally activated change is given by the transition rates

$$\Gamma_{Fe,V} = \nu_{Fe} \exp\left(-\frac{\Delta E_{Fe,V}}{k_B T}\right), \quad \Gamma_{Cu,V} = \nu_{Cu} \exp\left(-\frac{\Delta E_{Cu,V}}{k_B T}\right), \quad (1)$$

where $\nu_{Fe/Cu}$ denote attempt frequencies and $\Delta E_{Fe/Cu,V}$ the activation energies which depend on the local atom configuration. For each neighbour of the vacancy V , the jump frequencies $\Gamma_1, \dots, \Gamma_8$ are calculated. By applying a rejection-free residence time algorithm, one of these eight possibilities is selected. Typically, over 10^{11} vacancy jumps are performed during the simulation of precipitation. The time scale is adjusted according to the number of Monte Carlo steps and the vacancy concentration. As the RLM of the MC code does not permit the simulation of any deformation, the whole atomic configuration is transferred from MC to MD.

2.2 Molecular Dynamics (MD) Simulations

MD tensile tests are carried out using the IMD code⁶ and an Embedded Atom Method (EAM) potential by Bonny et al.⁷. First, the transferred configuration from MC is relaxed uniaxially to achieve an equilibration of the sample. Tensile loading is then applied at room temperature by straining the sample at a constant strain rate of 10^{-6} in each MD step in [001] direction. By using npT pressure control, the pressure is kept zero in directions perpendicular to the tensile direction.

3. Simulation Results

With an advancement factor of precipitation $\xi(t) = \frac{c_{Cu}^m(t=0) - c_{Cu}^m(t)}{c_{Cu}^m(t=0) - c_{Cu}^m(t \rightarrow \infty)}$, where c_{Cu}^m denotes the concentration of Cu within the matrix, the deviation from thermal equilibrium is estimated. The process of precipitation is presented in Fig.2A for $350^\circ C$ and $500^\circ C$ and two Cu-concentrations.

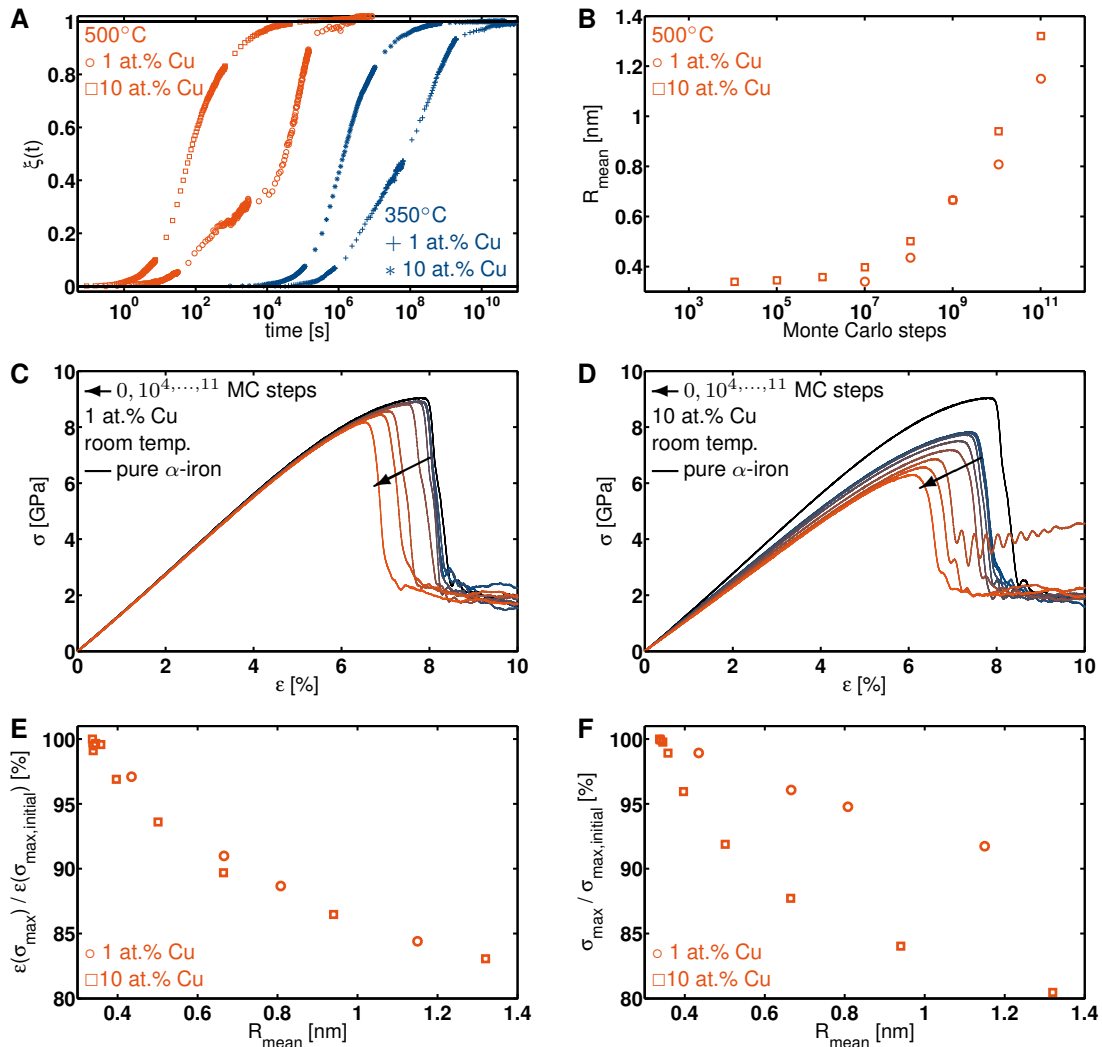


Figure 2: Simulation Results: (A) Development of precipitation, (B) Mean radius as a function of MC steps, (C) Stress-strain curves 1 at.% Cu, (D) Stress-strain curves 10 at.% Cu, (E) The fracture strain decreases during precipitation depending on the mean radius of the precipitates, (F) The tensile strength decreases as well with increasing precipitate sizes but additionally depends on the concentration, i.e. the number of precipitates. (+ $350^\circ C$, 1 at.% Cu, * $350^\circ C$, 10 at.% Cu, \circ $500^\circ C$, 1 at.% Cu, \square $500^\circ C$, 10 at.% Cu).

$\xi = 0$ corresponds to a solid solution, whereas for $\xi = 1$ the ideal (for thermal equilibrium) amount of copper has precipitated. Fig.2B shows the increase of the mean radius of the precipitates, i.e. the growth process. After each of the nine states ($0, 10^4, \dots, 11$ MC steps) of Fig 2B, the atomic configuration is transferred to MD, and after relaxing the sample, tensile loading is applied. The obtained stress-strain curves for 1 at.% Cu (Fig.2C) and 10 at.% Cu (Fig.2D) at different states of precipitation are compared to the tensile behaviour of pure α -Fe. As copper is a more ductile material than iron, the curves of the Fe-Cu alloy lie below the pure iron stress-strain curve. With growing mean radius of the precipitates, the fracture strain $\epsilon(\sigma_{max})$ decreases (Fig.2E). However, the concentration of Cu, i.e. the number of precipitates, does not have an additional effect. In contrast, the tensile strength, showing a similar decreasing behaviour with increasing precipitate sizes, notably depends on the concentration of Cu (Fig.2F). The decrease in both quantities can be explained since during precipitation, the number of Cu-Cu bonds which possess a lower binding energy as compared to those of Fe-Cu bonds or Fe-Fe bonds, increases and thus the material is weakened. On the other hand, the fracture strain hardly depends on the Cu-concentration. After reaching fracture strain, dislocations are generated within the whole Fe-Cu crystal.

4. Conclusion and Outlook

In this study, two methods (MC and MD) have been successfully combined in order to obtain information of the influence of a realistic copper precipitation field on the tensile behaviour of supersaturated Fe-Cu alloys. The sequential multiscale modelling approach applied here allows to benefit from the advantages of MC simulations, i.e. the access of larger time scales on which precipitation occurs while MD is restricted to very short time scales. Furthermore, the MD simulations allow the performance of computational tensile tests circumventing the restriction of the RLM. Growing precipitates result in a decrease of the tensile strength as well as of the fracture strain in the absence of dislocations. As in reality no defect free single crystals exist, dislocations will be implemented into the analysis in the future. This will change the tensile behaviour dramatically due to interactions between dislocations and precipitates. Nevertheless, the multiscale modelling approach presented here allows the separation of the influence of Cu-precipitates on the tensile strength of Fe-Cu alloys from the influence of dislocation-particle interactions which will be analyzed in the future.

Acknowledgements

The authors D. Molnar and S. Schmauder would like to thank the German Research Foundation (DFG) for financial support of the project within the Cluster of Excellence in Simulation Technology (EXC 310/1) at the University of Stuttgart.

References

- [1] S. Schmauder and P. Binkele. Atomistic Computer Simulation of the Formation of Cu-Precipitates in Steels. *Comp. Mat. Sci.*, **24** (9), 42–53, 2002.
- [2] D. Saraev, P. Kizler, and S. Schmauder. The Influence of Frenkel Defects on the Deformation and Fracture of α -Fe Single Crystals. *Modelling Simul. Mater. Sci. Eng.*, **7** (6), 1013–1023, 1999.
- [3] C. Kohler, P. Kizler, and S. Schmauder. Atomistic Simulation of Precipitation Hardening in

- α -Iron: Influence of Precipitate Shape and Chemical Composition. *Modelling Simul. Mater. Sci. Eng.*, **13** (1), 35–45, 2005.
- [4] F. Soisson, A. Barbu, and G. Martin. Monte Carlo Simulations of Copper Precipitation in Dilute Iron-Copper Alloys During Thermal Ageing and under Electron Irradiation. *Acta Mat.*, **44** (9), 3789–3800, 1996.
- [5] P. J. Othen, M. L. Jenkins, and G. D. W. Smith. High-Resolution Electron Microscopy Studies of the Structure of Cu Precipitates in α -Fe. *Phil. Mag. A*, **70** (1), 1–24, 1994.
- [6] J. Stadler, R. Mikulla, and H.-R. Trebin. IMD: A Software Package for Molecular Dynamics Studies on Parallel Computers. *Int. J. Mod. Phys. C*, **8**, 1131–1140, 1997.
- [7] G. Bonny, R. C. Pasianot, N. Castin, and L. Malerba. Ternary Fe-Cu-Ni Many-Body Potential to Model Reactor Pressure Vessel Steels: First Validation by Simulated Thermal Annealing. *Phil. Mag.* (34-36), **89**, 3531–3546, 2009.

Quantum-accurate multiscale modelling of stress corrosion: the origin of hydrogen-induced nm-smooth cleavage in silicon crystals

Gianpietro Moras^{1*}, Lucio Colombi Ciacchi², Christian Elsässer¹, Peter Gumbsch¹ and Alessandro De Vita³

¹Karlsruhe Institute of Technology, Institute for Reliability of Components and Systems, D-76131 Karlsruhe and Fraunhofer Institute for Mechanics of Materials IWM, Woehlerstr. 11 D-79108 Freiburg, Germany

²University of Bremen, Faculty of Engineering and BCCMS, D-28359 Bremen and Fraunhofer Institute for Manufacturing Technology and Applied Materials Research IFAM, D-28359 Bremen, Germany

³King's College London, Physics Department, WC2R 2LS London, United Kingdom
*gianpietro.moras@iwm.fraunhofer.de

Silicon crystals can be sliced efficiently by hydrogen implantation followed by thermal annealing, yielding nm-smooth cleavage surfaces. The process has long been thought to be driven by H₂ internal pressure, powering the creation of a network of micron-sized cracks, which eventually connect splitting the crystal samples. However, cleavage is initiated by sub-micrometric disk-shaped “platelet” defects whose growth mechanism has remained elusive as it is inaccessible to direct experimental probing, and far beyond the limits of full quantum-mechanical modelling.

Here we present a study of the thermal evolution of a *hydrogen-induced platelet*, made possible by the “*Learn on the Fly*” hybrid quantum/classical atomistic technique, which is specially suited for investigating tightly coupled chemo-mechanical processes. The scheme allows us to monitor with quantum accuracy the complete repertoire of chemical activity of a realistically sized, 35000-atom platelet system in a unique simulation. This unveils a series of causally linked chemical steps occurring in different regions of the system, which add up to a complete stress-corrosive cycle, thus revealing that *stress corrosion* is the fundamental mechanism of platelet growth. We observe that H₂ molecules form by associative desorption from the internal platelet surfaces, after which they diffuse until they reach the platelet perimeter. There the molecules dissociate back, stabilizing the breaking-up of highly stressed silicon bonds and thus yielding irreversible platelet growth. A build-up of H₂ internal pressure is neither needed for nor allowed by this process, which rules out pressure-induced catastrophic platelet growth, and allows for the remarkably nm-smooth cleavage surfaces observed experimentally. This is revealed by a mesoscale model based on our atomistic results, which further discloses the theoretical kinetic limits of the *ion-cut* process.

Plastic Deformation of Gold Microparticles on a Sapphire Substrate

Dan Mordehai¹, Eugen Rabkin¹, and David Srolovitz^{2,3}

¹Department of Materials Engineering, Technion - Israel Institute of Technology, 32000 Haifa, Israel. Email: danmord@tx.technion.ac.il

²Department of Physics, Yeshiva University, New York, NY 10033, USA.

³Institute of High Performance Computing, A*STAR, 1 Fusionopolis Way, 16-16 Connexis, Singapore 138632, Singapore.

We report a combined experimental/molecular dynamics study of the indentation and compression of faceted Au microparticles on a sapphire surface. The particles were created via the dewetting of a polycrystalline Au film on sapphire substrate (Fig. 1a). Nanoindentation was also performed in Au films of similar dimensions. Experiments show that the larger microparticles are softer, i.e. the strength is size dependent. Simulations show that deformation is controlled by dislocation nucleation near the tip, followed by fast dislocation glide toward the surface. Well defined pile-ups were observed near the indents in thin films, while no such pile-ups were observed in the particles. The Molecular Dynamics simulations supply us with insights of the dislocation mechanisms within the microparticles during deformation and aide in rationalizing the size effect observed experimentally (Fig. 1b). We present a comparison of post-deformation particle shapes from high resolution AFM and the simulations.

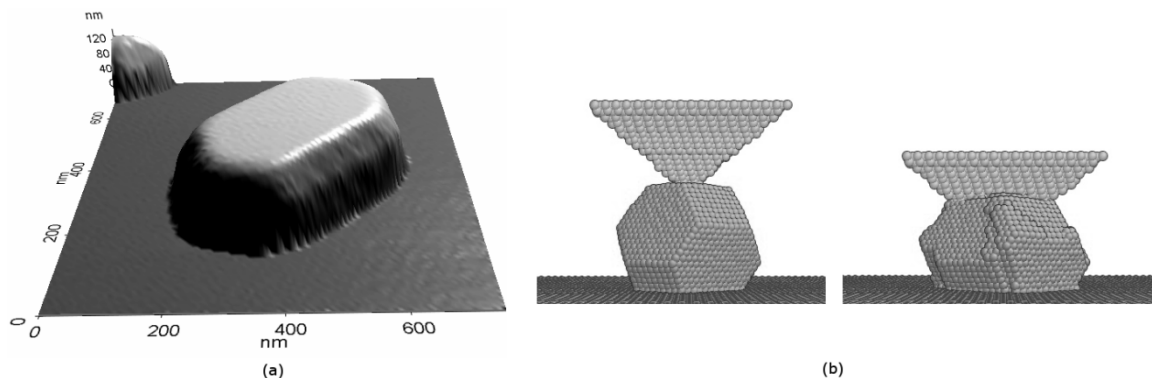


Figure 1: (a) An SFM image of one elongated Au microparticle on sapphire substrate. (b) MD simulation of the indentation of a faceted microparticle with a cube corner punch.

Influence of Initial Dislocation Structure and Boundary Conditions on Micro Tensile Tests Studied by 3-D Discrete Dislocation Dynamics

Christian Motz¹, Jochen Senger², Daniel Weygand² and Peter Gumbsch^{2,3}

¹Erich Schmid Institute, Austrian Academy of Sciences, Jahnstrasse 12, 8700 Leoben, Austria, christian.motz@oeaw.ac.at

²IZBS, University of Karlsruhe (TH), Kaiserstrasse 12, 76131 Karlsruhe, Germany

³iWM, Fraunhofer Institut für Werkstoffmechanik, Wöhlerstrasse 11, 79108 Freiburg, Germany

The ongoing miniaturization of components and devices in many modern technologies (e.g. microelectronics, medical devices, etc.) requires the knowledge of mechanical properties in these small dimensions. Size effects in the mechanical properties prohibit the usage of macroscopic properties. Hence, numerous efforts were undertaken in the past to measure small-scale properties. However, the initial material conditions as well as the boundary conditions are usually not completely known, which is caused by the preparation method (may cause damage to the material) and possible misalignment of the testing equipment (may induce additional bending and torsion loading).

To investigate the influence of the initial dislocation structure in terms of initial dislocation density and additional bending loading on the mechanical response of micro tensile samples 3-D discrete dislocation dynamics simulations (3-D DDD) were performed. Tensile samples with square cross-sections from 0.5×0.5 to $2.0 \times 2.0 \mu\text{m}^2$ and aspect ratios of 1:1:3 and 2:2:3, respectively, were simulated. The material properties of aluminium were used. For the study of the influence of the initial dislocation structure on the mechanical response a special relaxation method was utilized to obtain more realistic initial dislocation structures for the subsequent tensile test. For the superimposed tension and bending tests, which should mimic an imperfect tensile test, Frank-Read sources were used as initial structure. The displacement controlled tests showed a strong dependence of the mechanical response on both, the initial dislocation structure (density) as well as the boundary conditions. The scaling exponent of the size effect varies from -0.5 to -0.9 in the investigated size regime depending on the initial conditions. Finally, the impact of these material and boundary conditions on micro mechanical experiments and the derived mechanical properties will be discussed.

Imperfection and size dependent fracture of thin metallic films

T. Pardoën^{1,3}, M. Coulombier^{1,3}, A. Boe⁴, C. Brugger¹, M.S. Colla^{1,2}, L. Delannay¹, S. Dancette¹, H. Idrissi⁵, B. Wang⁵, D. Schrijvers⁵, T.J. Massart⁶, and J.P. Raskin^{2,3}

¹Institute of Mechanics, Materials and Civil Engineering, Université catholique de Louvain, Place Sainte Barbe 2, B-1348 Louvain-la-Neuve, Belgium (thomas.pardoën@uclouvain.be)

²Information and Communication Technologies, Electronics and Applied Mathematic Université catholique de Louvain, B-1348 Louvain-la-Neuve, Belgium

³CeRMiN, Research Center in Micro and Nanoscopic Materials and Electronic Devices, Université catholique de Louvain, B-1348 Louvain-la-Neuve, Belgium

⁴IEMN UMR CNRS8520, IRCICA FR CNRS3024 Université de Lille, 59651 Villeneuve d'Ascq, France

⁵EMAT, University of Antwerp, Groenenborgerlaan 171, 2020 Antwerpen, Belgium

⁶BATir CP 194/2, Building Architecture & Town Planning, Université Libre de Bruxelles, Belgium

The resistance of thin metallic films to plastic localization and fracture is an important issue in flexible electronics, thin coatings on deformable substrates, and several types of MEMS. The resistance to plastic localization is controlled by the strain hardening, strain rate sensitivity, and presence of imperfections. The resistance to fracture is controlled by the resistance to damage. Experimental results obtained using a nanomechanical lab-on-chip technique on Al and Pd films with thickness between 50 and 500 nm show several types of size effects affecting the ductility and fracture. A strong statistical dependence of the ductility on the overall size of the sample is also observed. The two materials exhibit different mechanisms of plastic localization and fracture. The objective is to discuss the similarities and differences between the two systems based on transmission electron microscopy characterization and on a multiscale modeling approach relying on a strain gradient plasticity FE model with evolving higher order boundary conditions at the interfaces.

The Al films, with 100- 200nm grain size, show a stable necking process followed by localized shear banding. The strain hardening capacity is moderate. Damage takes place by void nucleation at triple junctions. Plasticity is dominated by the interactions between the dislocations and grain boundaries. Strain gradient effects tend to stabilize the necking process while imperfections do the opposite. Stress driven grain grow within the necking region also contributes to stabilizing the localization process.

The Pd films involve 20-30 nm grain sizes containing a high density of fine coherent 2nm thick growth twins offering multiple barriers to dislocation motion, and sources for dislocation storage and multiplication. The very high strain hardening capacity coming from the dislocation/twin boundary interactions does not lead to large ductility due to failure mechanisms initiating after 2 to 4 % strain.

Micro and meso analysis of two-dimensional dislocation pile-up

Ron HJ Peerlings, Tom de Geus and Marc GD Geers

Department of Mechanical Engineering, Eindhoven University of Technology
PO Box 513, 5600 MB Eindhoven, The Netherlands
R.H.J.Peerlings@tue.nl

Classical crystal plasticity theory cannot properly capture phenomena such as dislocation pile-up and dislocation patterning. To remove this limitation, higher-order crystal plasticity theories have been proposed in the literature. The higher-order terms in these theories have been connected to the short-range interaction of individual dislocations, e.g. by Groma and co-workers on the basis of statistical arguments. In the present contribution we study this relationship from a deterministic perspective.

We consider an idealised pile-up situation in which walls of edge dislocations are pushed towards a barrier by an externally applied stress. Whereas discrete, microscopic analyses clearly show a pile-up of dislocations against the barrier, the conventional, mesoscopic crystal plasticity theory predicts a collapse into a wall of super-dislocations at the barrier. The reason for this pathological behaviour is that short-range interactions between the individual dislocations, which in reality prevent such a collapse, are not accounted for in the conventional theory.

A back-stress term can be introduced to account for the nearest-neighbour interactions. However, a comparison of predictions made with the higher-order theory thus obtained and the discrete simulations shows that the back-stress term only partially repairs the shortcoming of conventional crystal plasticity theory. For the idealised problem considered, a finite sized pile-up is now obtained, but the dislocation density distribution within the pile-up is still quite different from that of the discrete simulations.

The response in a thin boundary layer near the barrier can be captured by the conventional continuous theory for a single pile-up. In this contribution we develop a similar understanding of the remaining part of the pile-up, in which interactions between the different slip planes as well as between all walls within a certain range play a crucial role.

Atomistic Simulations of Cross-Slip Nucleation at Screw Dislocation Intersections in Face-Centered Cubic Nickel and Copper

Satish Rao¹, Dennis Dimiduk², Jaafar El-Awady³, Triplicane Parthasarathy¹, Michael Uchic², Christopher Woodward²

¹ UES Inc. 4401 Dayton-Xenia Road OH 45432 Dayton, United States

² Air Force Research Laboratory AFRL/RXLM, Bldg 655, 2230 Tenth Street, OH 45433, WPAFB, United States

³ UTC 2977 Hobson Way, OH 45433, WPAFB, United States

The Escaig model for thermally activated cross-slip in Face-Centered Cubic (FCC) materials assumes that cross-slip preferentially occurs at obstacles that produce large stress gradients on the Shockley partials of the screw dislocations. However, it is unclear as to the source, identity and concentration of such obstacles in single-phase FCC materials. In this talk, we describe embedded atom potential, molecular-statics simulations of screw character dislocation intersections with forest dislocations in FCC Ni and Cu to illustrate a mechanism for cross-slip nucleation. The simulations show how such intersections readily produce cross-slip nuclei and thus may be preferential sites for easy cross-slip. Simple 3-dimensional dislocation dynamics simulations accounting for Shockley partials are shown to qualitatively reproduce the atomistically-determined core structures for the same dislocation intersections. It is also shown that there exists a finite activation barrier for the screw dislocation to transfer from the fully glide plane or the fully cross-slip plane state to the partially cross-slipped state at these intersections, which is a factor of 2 - 5 lower than that in the bulk. The activation barrier for cross-slip at these intersections is shown to be linearly proportional to $(d/b)\ln(1.732d/b)0.5$, as in bulk, where 'd' is the Shockley partial spacing of the partial dislocations and 'b' is the Burger's vector of the screw dislocation. The activation energies are determined as a function of the line orientation and Burger's vector of the intersecting dislocations. These results suggest that cross-slip should be preferentially observed at selected screw dislocation intersections in FCC materials.

Coupled Micro-Macro-Scale Finite-Element-Simulation Of Mechanically Induced Residual Stresses

B. Regener^{1,*}, T. Taxer², R. Wesenjak¹, C. Krempaszky¹ and E. Werner²

¹Christian Doppler Laboratory of Materials Mechanics of High Performance Alloys, Institute of Materials Science and Mechanics of Materials, Technische Universität München, Boltzmannstraße 15, 85748 Garching, Germany,

²Institute of Materials Science and Mechanics of Materials, Technische Universität München, Boltzmannstraße 15, 85748 Garching, Germany

*regener@wkm.mw.tum.de

A coupled finite element based model on two different length scales is introduced in order to predict mechanically induced residual stresses in metallic components possessing heterogeneous microstructures. Each integration point of the macroscopic model is connected with a model on the micro-scale featuring the micro topology. The microscopic model is based on a periodic micro field approach employing individual parameter sets for each phase optionally taking into account crystal plasticity or classical continuum theory. Whereas boundary conditions are applied to the macroscopic model, the microscopic one serves as implicit constitutive law based on the modeling of all considered physical effects.

The coupling of the macro and micro scale is based on a large strain framework utilizing an updated corrotational lagrangian integration scheme. The deformation gradient increment at each macroscopic integration point is applied as boundary condition to the microscopic model which provides the stress update and the stiffness through homogenization and differentiation of the homogenized stress-strain-curve. In order to simulate macroscopically complex load paths accurately, for each integration point the microscopic load history is stored individually.

To generate industry-oriented micro topologies efficiently, mathematical models from stochastic geometry are combined with metallurgical and stereological insight. For dual and complex phase steels as well as various titanium alloys the utilization of Voronoï and Johnson-Mehl-tessellation is appropriate. For nickel-based superalloys, stochastic distributions of characteristic micro heterogeneities are employed.

To grant appropriate description of micro field variables an extensive validation was carried out. To achieve so called representative volume elements, a convergence study of apparent mechanical properties and mesh fineness was conducted.

Multiscale Model of Deformation Twinning in Tantalum

David Richards, James Belak, Kyle Caspersen, Luis Sandoval, Michael Surh

Condensed Matter and Materials Division
Lawrence Livermore National Laboratory
PO Box 808, L-045
Livermore, CA 94550 USA
richards12@llnl.gov

Efforts to understand plasticity in BCC metals have focused mostly on the role of dislocations. For example, recent work at LLNL has produced a multiscale constitutive model for Ta based on molecular dynamics (MD) and dislocation dynamics (DD) simulations of slip. However, recovered Ta samples from high strain rate experiments clearly show that twin formation also serves as an important strain relief mechanism. Since experiments at the National Ignition Facility will access conditions where twinning is known to occur it is necessary to extend the current LLNL constitutive model by adding the effects of deformation twinning to the existing multiscale framework. Accurate modeling and analysis of experimental results will only be possible when the continuum level materials models include all of the deformation mechanisms that are known to occur. To this end we have performed MD simulations to investigate the nucleation and growth properties of twin boundaries and to determine the threshold stress for twinning as a function of pressure, temperature, and strain rate in the presence of various microstructures. We report progress on using these MD results to determine parameters for a continuum scale constitutive model for tantalum that includes the effect of deformation twinning.

This work performed under the auspices of the U.S. Department of Energy by Lawrence Livermore National Laboratory under Contract DE-AC52-07NA27344.

First-principles study of superhard SiN_x /TiN nanocomposites

Pawel Rodziewicz, Bernd Meyer

Interdisziplinäres Zentrum für Molekulare Materialien ICMM
and Computer-Chemie-Centrum CCC, Universität Erlangen–Nürnberg, Germany
pawel.rodziewicz@chemie.uni-erlangen.de

Nanocomposite materials based on TiN nanocrystalites embedded in an amorphous silicon nitride matrix with thickness of only a few atomic layers and composition close to Si₃N₄ show a superhardness similar to that of diamond. To elucidate the chemical origin of the material hardness and the exceptional strength of the SiN_x /TiN interfaces we have used DFT calculations in combination with Car-Parrinello molecular dynamics (CPMD) simulations to create and to investigate model SiN_x /TiN interface structures. As the first step we studied the initial stages of SiN_x layer formation on TiN(001) by adding successively silicon and nitrogen atoms to the TiN surface to form up to two monolayer thick SiN_x films with different composition. For a selected set of configurations, chosen on the basis of thermodynamic stability, we then applied a stepwise procedure based on heating, quenching and final geometry optimization to search for stable and energetically favorable amorphous structures of SiN_x films and stacks of SiN_x /TiN multilayers. The relative stability of the different model interface structures is analyzed in terms of Ti, Si and N coordination numbers, and the mechanical strength of the interfaces is assessed by the calculation of stress–strain curves to determine the ideal decohesion strengths which will serve as input parameters for finite element simulations of fracture and materials failures.

Stability and mobility of hydrogen in the vicinity of point and extended defects in bcc-Fe

Jutta Rogal¹, Yaojun A. Du¹ and Ralf Drautz¹

¹Interdisciplinary Centre for Advanced Materials Simulation
Ruhr-Universität Bochum, 44780 Bochum, Germany
email: jutta.rogal@rub.de

Hydrogen embrittlement of iron and steels has been studied extensively in experiment and theory, but due to the complexity of the mechanisms involved it is still not fully understood. Two of the most discussed mechanisms for hydrogen embrittlement are hydrogen enhanced decohesion (HEDE) and hydrogen enhanced local plasticity (HELP). To address these mechanisms from a microscopic point of view it is important to obtain a detailed understanding of the stability and mobility of hydrogen in the vicinity of point and extended defects.

On an atomistic scale the diffusion of hydrogen in iron can be considered as a rare event compared to the time scale of molecular vibrations. This requires to study the dynamical evolution over an extended time scale up to seconds or longer going beyond the limits of classical molecular dynamics. Here we employ kinetic Monte Carlo (kMC) simulations with energetics based on density functional theory (DFT).

To investigate hydrogen diffusion close to vacancies and interfaces in bcc-Fe we use an adaptive kMC approach where the stable states and energy barriers are determined on-the-fly during the simulation and an a priori mapping to a lattice is not required. In our simulations we study the evolution of the local hydrogen concentration around these defects. In the case of vacancies we also consider the formation of H-vacancy clusters and the influence of hydrogen on the mobility of the vacancy itself.

A 3D multiscale framework for computing the deformation and adhesion of gecko setae

Roger A. Sauer¹

¹Graduate School AICES, RWTH Aachen University, Templergraben 55, 52056 Aachen, Germany

Recently, a 3D multiscale model has been published that describes the adhesion and deformation of a gecko foot-hair, the so-called seta [1]. Here we present an overview of this model and focus on current modelling improvements. The chosen multiscale approach combines three models at different length scales: At the top level, on the order of several micrometers, a nonlinear finite element beam model is chosen to capture the branched microstructure of the gecko seta. At the intermediate level, on the order of several nanometers, a second finite element model is used to capture the detailed behavior of the seta tips, the so-called spatulae. At the lowest level, on the order of a few Angstroms, a molecular interaction potential is used to describe the van der Waals adhesion forces between spatulae and substrate. The molecular interaction forces are coarse-grained into an effective continuum contact formulation at the spatula level [2]. The overall spatula adhesion behavior in turn is inserted as a contact formulation at the seta level. The model allows for a detailed, yet efficient simulation of the mechanical seta behavior. To illustrate and validate the proposed gecko seta model, dynamic pull-off simulations are shown and compared to experimental data from the literature.

References

- [1] R. A. Sauer, *Multiscale modelling and simulation of the deformation and adhesion of a single gecko seta*, *Comp. Meth. Biomech. Biomed. Engng.*, 12 (6) (2009), 62
- [2] R. A. Sauer and P. Wriggers, *Formulation and analysis of a 3D finite element implementation for adhesive contact at the nanoscale*, *Comput. Methods Appl. Mech. Engng.*, 198 (2009), 3871

Parameter Identification over Multiple Scales

Ulrike Schmidt, Julia Mergheim and Paul Steinmann

Chair of Applied Mechanics, University of Erlangen-Nuremberg,
Egerlandstr. 5, 91058 Erlangen, Germany,
ulrike.schmidt@ltm.uni-erlangen.de, julia.mergheim@ltm.uni-erlangen.de,
paul.steinmann@ltm.uni-erlangen.de

ABSTRACT

In this work a method to identify small scale material parameters used in computational homogenization is presented. Based on the multi-scale simulation technique known as FE² or ML-FEM the large scale response is calculated using the solution of a boundary value problem on the small scale. The simulated response is compared to the experimental results in the objective function, its sensitivities are derived and used in gradient-based optimization algorithms for the identification of linear elastic material parameters.

1. Introduction

Modeling of materials with a periodic heterogeneous micro-structure, e.g. laminates, has been a topic in research for quite a while. In this work we focus on the numerical homogenization approach called FE² method to simulate mechanical material behavior of said materials, see [1-2]. Experimental parameter identification on the finer scale can be very time consuming, costly and difficult. Thus, an alternative is explored: identifying the small scale parameters through large scale experiments, cmp. [3-4]. To this end a new concept for multi-scale parameter identification using the FE² method is investigated.

2. Direct Problem

The FE² method is used to calculate a mechanical response of a component with a heterogeneity at a much finer scale than the dimensions of the component itself. This scale separation makes a computation with fully resolved heterogeneities far too expensive. Therefore the strategy of homogenization is employed. Assuming a periodic media described by a known representative volume element (RVE), its large scale elasticity tensor is determined as the tangent of the homogenized stress w.r.t. the large scale strain in each large scale integration point.

The geometry on the large scale is described by $\bar{\Omega}$, its boundary by $\partial\bar{\Omega}$. We investigate the stationary mechanical equilibrium without body forces together with appropriate boundary conditions modeling the experimental setup. At the Neumann boundary $\partial\bar{\Omega}^N$ tractions $\bar{\mathbf{t}}_p$ are prescribed, whereas at the Dirichlet boundary $\partial\bar{\Omega}^D$ the displacements $\bar{\mathbf{u}}_p$ are prescribed:

$$\bar{\nabla} \cdot \bar{\boldsymbol{\sigma}} = \mathbf{0} \text{ in } \bar{\Omega}, \quad \bar{\mathbf{t}} = \bar{\mathbf{t}}_p \text{ on } \partial\bar{\Omega}^N \quad \text{and} \quad \bar{\mathbf{u}} = \bar{\mathbf{u}}_p \text{ on } \partial\bar{\Omega}^D, \quad (1)$$

where the large scale stresses $\bar{\boldsymbol{\sigma}}$ are determined by homogenization of the small scale stresses. On the small scale domain Ω we consider the stationary mechanical equilibrium

$\nabla \cdot \boldsymbol{\sigma} = 0$ and complement it by a boundary condition, which is consistent with the homogenization theory, e.g. the linear displacements boundary condition (linear BC)

$$\mathbf{u}(\mathbf{x}) = \bar{\boldsymbol{\varepsilon}} \cdot \mathbf{x} \quad \forall \mathbf{x} \in \partial\Omega^c \quad (2)$$

or the periodic fluctuations and anti-periodic tractions boundary condition (periodic BC):

$$\mathbf{u}(\mathbf{x}^+) - \mathbf{u}(\mathbf{x}^-) = \bar{\boldsymbol{\varepsilon}} \cdot (\mathbf{x}^+ - \mathbf{x}^-), \quad \forall \mathbf{x}^+ \in \partial\Omega^+, \mathbf{x}^- \in \partial\Omega^-, \quad (3)$$

$$\mathbf{t}(\mathbf{x}^+) + \mathbf{t}(\mathbf{x}^-) = \mathbf{0}, \quad \forall \mathbf{x}^+ \in \partial\Omega^+, \mathbf{x}^- \in \partial\Omega^-. \quad (4)$$

The small scale stresses are determined by Hooke's law $\boldsymbol{\sigma} = \mathbb{C} : \boldsymbol{\varepsilon}$ with elasticity tensor \mathbb{C} .

After employing the finite element method to the small scale problem, the resulting stiffness matrix \mathbf{K} can be used to determine the homogenized discrete elasticity tensor \mathbb{C}^d :

$$\bar{\mathbb{C}}^d = \frac{1}{|\Omega|} \sum_{a,b=1}^{\text{npn}} \left(\mathbf{x}_a \otimes \tilde{\mathbf{K}}_{ab} \otimes \mathbf{x}_b \right)^{\top \ell}, \quad (5)$$

where $\tilde{\mathbf{K}}_{ab}$ is a 3×3 sub-matrix of the matrix $\tilde{\mathbf{K}}$, corresponding to the pair of nodes a, b with $\tilde{\mathbf{K}}$ itself being the small scale condensed stiffness matrix (or Schur complement) and npn is the number of nodes with prescribed displacements. The left transposed of a fourth order tensor is denoted by $(\cdot)^{\top \ell}$ and defined as $(C_{ijkl})^{\top \ell} = C_{jikl}$ in index notation. Since the small scale stiffness matrix is independent of the applied large scale strain at the boundary of the RVE, it suffices to compute the homogenized elasticity tensor once. Then the large scale problem reduces to a standard finite element problem with the large scale elasticity tensor given by the homogenization procedure.

3. Inverse Problem

The task of the inverse problem is to determine small scale material parameters, such that the simulated data fits the experimental data. We want to extend this idea over multiple scales, i.e. we want to identify small scale material parameters with large scale, but no small scale experimental data. Therefore large scale geometry, loading and deformation are known, as well as the geometry and the constitutive model on the small scale. The small scale material parameters are to be obtained and are contained in the vector $\boldsymbol{\alpha}$. The parameter identification over multiple scales yields the following least square minimization problem:

$$\min_{\boldsymbol{\alpha}} f(\bar{\mathbf{u}}_m, \bar{\mathbf{u}}, \boldsymbol{\alpha}), \text{ such that } \boldsymbol{\alpha} \text{ is admissible.} \quad (6)$$

The large scale displacements $\bar{\mathbf{u}}_m(\bar{\mathbf{x}}_i)$ are measured at M points $x_i, i = 1, \dots, M$. For the sake of simplicity, these points are assumed to coincide with the nodes of the discretization. The simulated displacements $\bar{\mathbf{u}}(\bar{\mathbf{x}}_i)$ are computed by means of FE². The objective function is then given as

$$f(\bar{\mathbf{u}}_m, \bar{\mathbf{u}}, \boldsymbol{\alpha}) := \frac{s}{2} \sum_{i=1}^M \|\bar{\mathbf{u}}(\bar{\mathbf{x}}_i) - \bar{\mathbf{u}}_m(\bar{\mathbf{x}}_i)\|_{\mathbb{R}^3}^2, \quad (7)$$

where s is a scaling factor, e.g. $s^{-1} = \sum_{j=1}^M \|\bar{\mathbf{u}}_m(\bar{\mathbf{x}}_j)\|_{\mathbb{R}^3}^2$. In order to ensure that the direct problem can be solved, the material parameters must be feasible, e.g. shear modulus μ and bulk modulus K must be positive: $K > 0, \mu > 0$. Not only the feasibility condition,

but also additional information, if available, can be incorporated in the constraints. If, for examples, a particle reinforced material is considered, the inclusion is usually stiffer than the matrix resulting in the inequality: $E_{\text{incl}} > E_{\text{mat}}$. Optimization algorithms can handle different classes of constraints and must be chosen accordingly. We consider the function `lsqnonlin` (`lsqn`) from the MATLAB's optimization toolbox, which can handle box constraints and secondly an algorithm called `TRESNEI`, which can handle nonlinear inequality constraints. Consistent analytical sensitivities of the discrete problem are used by the optimization algorithms employed to solve the least square problem. The large scale derivative w.r.t. the material parameters is linked to the small scale by the term involving the large scale elasticity tensor, as can be seen by differentiating Eqn (5):

$$\frac{d}{d\alpha_i} \bar{\mathbb{C}}^d = \frac{1}{|\Omega|} \sum_{a,b=1}^{\text{npn}} \left(\mathbf{x}_a \otimes \frac{d}{d\alpha_i} \tilde{\mathbf{K}}_{ab} \otimes \mathbf{x}_b \right)^{\top \ell}. \quad (8)$$

4. Examples

Periodic and linear displacement boundary conditions on the small scale are considered. The algorithms are tested for artificial data, where the solution of the direct problem for given material parameter sets $\boldsymbol{\alpha}_A$ and $\boldsymbol{\alpha}_B$ replaces the measured data in the objective function. The optimization was then conducted for a set of 15 random starting points in the interval $[\frac{1}{2}\boldsymbol{\alpha}_A, \frac{3}{2}\boldsymbol{\alpha}_A]$. The RVE consists of a matrix material with a stiffer spherical inclusion at the center. We considered two different large scale geometries, a plate and a punched disk. Both are fixed at the bottom and a surface tension of -0.5 GPa is applied on the top surface.

Results are depicted in Tab 1 and Tab 2, where N_{err} counts the number of starting points for which the algorithms failed to converge to the reference material parameters within the tolerance of 10^{-4} . N_{it} describes the mean number of iterations over the set of 15 random starting points. In addition to the mentioned loading scenarios 'plate' and (punched) 'disk', another, combined scenario denoted as 'multi' is investigated. There the parameters are identified for both 'plate' and 'disk' simultaneously, i.e. the sum of the individual objective functions is minimized. As can be seen from Tab 1 the problem is solved by all algorithms and for all starting points in case of the material $\boldsymbol{\alpha}_A$. The `TRESNEI` algorithm needs less averaged iterations. For the second material $\boldsymbol{\alpha}_B$, where

Table 1: results for $\boldsymbol{\alpha}_A$

algorithm		lsqn	TRESNEI	lsqn	TRESNEI	lsqn	TRESNEI	lsqn	TRESNEI	
problem		min g $\boldsymbol{\alpha}$		min f $0 < \boldsymbol{\alpha}$		min g $\boldsymbol{\alpha}$		min f $0 < \boldsymbol{\alpha}$		
plate	N_{err}	0	0	0	0	0	0	0	0	
	N_{it}	35	15	34	19	10	8	29	13	
disk	N_{err}	0	0	0	0	0	0	0	0	
	N_{it}	13	12	35	17	6	7	56	11	
multi	N_{err}	0	0	0	0	0	0	0	0	
	N_{it}	19	10	38	13	6	7	15	11	
					periodic BC		linear BC			

the particular parameters corresponding to different phases are closer together, the performance decreases. Tab 2 shows the poor performance for the single scenarios 'plate'

Table 2: results for α_B

algorithm	lsqn	TRESNEI	lsqn	TRESNEI	lsqn	TRESNEI	lsqn	TRESNEI	
problem	$\min_{\alpha} g$		$\min_{0 < \alpha} f$		$\min_{\alpha} g$		$\min_{0 < \alpha} f$		
plate	N_{err}	8	0	1	0	8	1	3	2
	N_{it}	365	41	69	72	235	127	114	185
disk	N_{err}	1	3	5	0	5	2	1	1
	N_{it}	31	25	221	35	269	17	92	22
multi	N_{err}	0	0	1	0	0	0	1	0
	N_{it}	15	20	26	23	30	19	35	15
	periodic BC				linear BC				

and 'disk', but satisfactory results for the 'multi' problem. This indicates, that one scenario alone does not yield enough information for a good and stable identification. The differences between linear and periodic BC are insignificant.

5. Conclusion

A multi-scale parameter identification concept has been presented, based on a computational homogenization scheme and gradient based least-square solvers. The set of small scale material parameters is calculated in a two-scale parameter identification procedure. The performance of two gradient-based algorithms was tested using a set of random starting points and artificial data from numerical experiments. The excerpt of numerical examples presented here indicates good performance for composites of phases with strongly differing material parameters. But for material phases with similar parameters a good performance is only received, when the data of different large scale tests is combined. In the future the focus will be on stability, choice of experiments and questions of modeling nonlinear problems.

Acknowledgments

The authors gratefully acknowledge the funding of the German Research Council (DFG), which, within the framework of its "Excellence Initiative" supports the Cluster of Excellence "Engineering of Advanced Materials" (www.eam.uni-erlangen.de) at the University of Erlangen-Nuremberg.

References

- [1] F. Feyel and J.-L. Chaboche (2000), *Comput. Meth. Appl. Mech. Eng.*, Vol. 183 (3-4), pp. 309-330
- [2] C. Miehe and A. Koch (2002), *Arch. Appl. Mech.*, Vol. 72 (4), pp. 300-317
- [3] T. Burczynski and W. Kuś (2008), *J. Phys. Conf. Ser.*, Vol. 135 (1), pp. 012025
- [4] C. Oskay and J. Fish (2008), *Comput. Mech.*, Vol 42 (2), pp. 181-195
- [5] U. Schmidt, J. Mergheim and P. Steinmann, "Multi-Scale Parameter Identification", submitted 2010

A finite element implementation of a polycrystalline material based on the viscoplastic self-consistent model

Javier Segurado¹, Javier LLorca¹ and Ricardo Lebensohn²

¹ *Departamento de Ciencia de Materiales, Universidad Politécnica de Madrid & Instituto Madrileño de Estudios Avanzados en Materiales (IMDEA-Materiales) ETS de Ingenieros de Caminos, 28040 Madrid, Spain. jsegurado@mater.upm.es*

² *Los Alamos National Laboratory, Los Alamos, USA*

The mechanical response of polycrystals depends on the behavior of the constituent single crystal grains, as well as on their orientation (texture) and its evolution with the loading history. An accurate simulation of a deformation process of these materials should be sensitive to their microstructure and its evolution. Single crystal anisotropy requires the use of polycrystal models that account for inhomogeneous deformation depending on grain orientation. In particular, visco-plastic self-consistent (VPSC) models have been successfully used for describing strongly anisotropic aggregates.

The polycrystal mechanical behavior can be implemented inside a finite element (FE) code to simulate the deformation of polycrystalline materials undergoing complex deformation. In this study, the VPSC formulation has been implemented in an implicit FE code. Here, VPSC is used as a macroscopic physically-based viscoplastic model that provides the plastic strain rate in an implicit elasto-viscoplastic FE material subroutine (programmed here using a UMAT subroutine in the implicit FE code ABAQUS). Each integration point of the FE model is considered as a polycrystal with a given initial texture. Within this framework, for each point and time increment VPSC calculations driven in stress (creep) are carried out iteratively to obtain the actual stress increment consistent with the FE total strain increment. This integration is fully implicit and based in a Newton-Rapson scheme. The implementation is efficient because the viscoplastic tensor computed internally by VPSC for homogenizing is, in turn, used for evaluating the derivatives of the residual, as well as the consistent tangent stiffness matrix for the FE global non linear scheme. This strategy provides a very robust elasto-viscoplastic model, which allows simulating deformation processes with relative large deformation increments.

As a benchmark analysis of the current model, the three-dimensional deformation of zirconium bars deforming under four-point bending is simulated. Results are compared with experimental results and simulations performed with a FE explicit implementation of VPSC

Void growth in polycrystals using 2D dislocation dynamics

Javier Segurado¹ and Javier LLorca¹

¹ *Departamento de Ciencia de Materiales, Universidad Politécnica de Madrid & Instituto Madrileño de Estudios Avanzados en Materiales (IMDEA-Materiales) ETS de Ingenieros de Caminos, 28040 Madrid, Spain. jsegurado@mater.upm.es*

The overall ductility of metals is mainly controlled by the ability of the material to withstand the growth of micron-sized voids up to the point in which fracture is triggered by the sudden coalescence of neighbor voids into a crack. Although microvoids normally appear within a grain (single crystal), in further stages voids are frequently located in the interface between two, three or more grains. The growth of these voids is driven by the plastic flow of the grains surrounding them.

Most of the models developed to quantify and understand the void growth process did not take into account two important factors: the anisotropic nature of plastic flow in single crystals and the size effects that appear when plastic flow is confined into very small regions. These limitations can be overcome using discrete dislocation dynamics, which includes naturally both effects, but up to this moment this technique has only been applied to study voids growing inside single crystals [1].

In this investigation, the mechanical response and void growth process of FCC polycrystalline metals with voids located at the grain boundaries was studied by means of discrete dislocation dynamics. The simulations were based on the methodology developed by Van der Giessen and Needleman [2], which was extended by the authors to non-convex domains through the use of finite elements with embedded discontinuities [3].

A wide range of simulations were carried out to ascertain the influence of grain size respect to initial void size (in the order of microns): from grains much larger than initial voids leading to void surrounded by a polycrystal, to grains of size in the order of microns.

[1] Segurado J, LLorca J. *Acta Materialia* 2009, 57:1427

[2] Van der Giessen E, Needleman A. *Modell Simul Mater Sci Eng* 1995;3:689.

[3] Romero I, Segurado J, LLorca J. *Modell Simul Mater Sci Eng* 2008;16:035008.

Dislocation microstructure evolution in cyclically twisted micro samples simulated with discrete dislocation dynamics techniques

J. Senger¹, D. Weygand¹, O. Kraft^{1,2} and P. Gumbsch^{1,3}

Karlsruhe Institute of Technology (KIT), Kaiserstr. 12, 76131 Karlsruhe, Germany,

¹Institut für Zuverlässigkeit von Bauteilen und Systemen

²Institut für Materialforschung II

³Fraunhofer IWM, Wöhlerstr. 11, 79108 Freiburg, Germany

jochen.senger@kit.edu

Ongoing miniaturization in technical devices requires a better comprehension of the material behavior at small scales. Experiments and simulations have shown that metallic samples in micro meter range are stronger than the corresponding bulk material. This behavior was first observed in torsion experiments on polycrystalline copper [1] and later also for nominally uniform compressed micro-samples [2]. The latter micro-pillar deformation experiments have been extensively studied by discrete dislocation dynamics simulations, whereas rather limited information on the evolving microstructure obtained by discrete dislocation dynamics studies is available for the torsion experiments.

In this study single crystalline metallic wires with quadratic cross section and random dislocation structure (Frank-Read sources) [3] are twisted cyclically. The resulting normalized torsion moment is determined for different sample diameters. The overall trend, an increasing normalized torsion moment with decreasing sample diameter is similar to experimental observations on polycrystalline copper. Furthermore, the influences of the strain amplitude, crystallographic orientation and aspect ratio on the plastic deformation will be discussed.

A detailed analysis reveals that a continuous increase of the dislocation density occurs, which corresponds well the generation of geometrically necessary dislocations. Small samples show a stair-case like increase of the dislocation density since plastic flow is controlled by the limited dislocation source statistic. In contrast to tension or compression tests, strain gradients hinder mobile dislocations to escape through the surface. The constrained dislocation motion results in higher dislocation densities with increasing loading cycles.

References:

- [1] N. A. Fleck et al., *Acta Metallurgica* 42 (1994), 475-487
- [2] M. Uchic et al, *Science* 305 (2004), 986-989
- [3] C. Motz et al., *Acta Materialia* 57 (2009) 1744-1754

Multiscale Modeling of Polycrystal Deformation with Grain Boundary Sliding

A. Shaban, A. Ma and A. Hartmaier

Micromechanical Modeling of Macroscopic Material Behavior
Interdisciplinary Centre for Advanced Materials Simulation (ICAMS)
Ruhr-Universität Bochum, Germany
ahmed.shaban@rub.de

In ultra-fine grained and nanocrystalline materials dislocation glide becomes increasingly difficult. Hence, to describe the deformation of such materials, it is important to understand grain boundary sliding and damage accumulation near triple junctions and to formulate valid constitutive relations.

For this purpose we have built a representative volume element (RVE) where a cohesive zone model has been developed in which the normal and tangential behavior for special grain boundaries are parameterized based on ab-initio calculations for bi-crystals. This model has been coupled with a dislocation density based crystal plasticity model for the bulk material in order to study the plastic deformation of polycrystalline material in the presence of grain boundary sliding. With the RVE simulations we study competing mechanisms between dislocation slip and grain boundary sliding. Furthermore, we also investigate micro crack nucleation near grain boundary triple junctions.

The simulation results reveal that the normal and tangential interface strengths, both, are necessary to obtain a good load carrying capacity of crystal aggregate. Furthermore, grain boundaries with higher interface strength tend to produce stress concentrations and strain heterogeneities and even change the local deformation patterns. This study also finds that grain boundaries with larger misorientations can stably increase the global material strength during the deformation process.

Flexoelectricity in Nanostructures

Pradeep Sharma¹

¹University of Houston, Department of Mechanical Engineering and Department of Physics, Houston, TX 77204
psharma@uh.edu

Crystalline piezoelectric dielectrics electrically polarize upon application of uniform mechanical strain. Inhomogeneous strain, however, locally breaks inversion symmetry and can potentially polarize even non-piezoelectric (centrosymmetric) dielectrics. Flexoelectricity--the coupling of strain gradient to polarization-- is expected to show a strong size-dependency due to the scaling of strain gradients with structural feature size. The existence and importance of flexoelectricity has been experimentally confirmed in several materials especially ferroelectrics. In this presentation, I present an introduction to flexoelectricity and discuss its ramifications for the design of multifunctional materials, size-dependent piezoelectricity and energy storage. Specifically, I present results (based on a combination of atomistic and theoretical approaches) that provide insights into the "effective" size-dependent piezoelectric and elastic behavior of inhomogeneously strained non-piezoelectric and piezoelectric nanostructures. I will argue, through computational examples, the tantalizing possibility of creating "apparently piezoelectric" nano-composites without piezoelectric constituents. I will also present experimental evidence based upon nanoindentation of ferroelectrics. Finally, I propose that flexoelectricity is an important and essential contributor to the intrinsic dead-layer effect in high permittivity ferroelectric based nanocapacitors used for energy storage.

Discrete dislocation dynamics modeling of screw dislocations in bcc metals: linking local atomistic information to the mesoscale

K. Srivastava¹, R. Groeger², D. Weygand¹ and P. Gumbsch^{1,3}

Karlsruher Institut für Technology (KIT), Kaiserstr. 12, 76131 Karlsruhe, Germany,

¹Institut für Zuverlässigkeit von Bauteilen und Systemen

²Institute of Physics of Materials, Academy of Sciences of the Czech Republic, Žitkova 22, 61662 Brno, Czech Republic

³Fraunhofer IWM, Wöhlerstr. 11, 79108 Freiburg, Germany

kinshuk.srivastava@kit.edu

In bcc metals, the mobility of screw and edge dislocations is very different at low-temperatures. Furthermore screw dislocations show the so called non Schmid behavior, which necessitates to take into account the local stress state in a mesoscopic mobility law for screw dislocations.

In this contribution, an atomistically informed mesoscopic model of plastic flow in bcc metals incorporating the effect of non-glide stresses and orientation of applied loading on the $1/2\langle 111 \rangle$ screw dislocation in a three-dimensional discrete dislocation dynamics framework is presented. Mobility of screw dislocations is governed by the thermally activated motion via the kink pair nucleation mechanism. The activation enthalpy for kink-pair nucleation is obtained from results of atomistic studies and takes into account the non Schmid effects.

Studies on single dislocation on Tungsten under tension and compression show the experimentally observed tension-compression asymmetry and at higher temperatures a trend towards the experimentally observed wavy slip. The anomalous slip which has been observed in various experiments in various bcc metals at low temperatures, is also shown to be a consequence of the effect of non-glide components of the stress tensor.

Keywords: Body centered cubic metals; Activation enthalpy; Non-schmid; Discrete Dislocation Dynamics; Anomalous slip

Dislocation Dynamics Model for the Loss of Interface Coherency

David J. Srolovitz¹, S. S. Quek¹, and Yang Xiang²

¹Institute of High Performance Computing, 1 Fusionopolis Way, #16-16 Connexis, SINGAPORE 138632

²Department of Mathematics, Hong Kong University of Science and Technology, Clear Water Bay, Kowloon, HONG KONG

The conversion of a two phase interface from coherent to semicoherent or incoherent can have a profound effect on the microstructure of a material, second phase particle morphology and size, misfit stresses, dislocation-particle interactions, yield strength, ... The process of coherency loss can occur as a natural consequence of phase transformations or particle coarsening. On the other hand, loss of coherency can occur most readily through the interaction of the second phase particle with lattice dislocations – especially during plastic deformation. We report the results of a dislocation dynamics study of the interaction of lattice dislocations with coherent and semicoherent particles in the presence of an applied stress. The simulations are performed through a combination of continuum elasticity and a level set method for dislocation dynamics in three spatial (and one time) dimensions. The results show that a dislocation interacting with a spherical coherent particle tends to leave dislocation loops in the particle-matrix interface during the bypass process. Subsequent dislocations on the same slip plane lead to more and more loops being formed at the particle-matrix interface. This process continues until sufficient loops are added to the interface to cancel the particle misfit in the direction of the dislocation Burgers vector. Once the interface is rendered semicoherent in this manner, the nature of dislocation-particle interactions change and the particle becomes a more effective barrier to dislocations. In this limit, the dislocations that become an integral part of the particle-matrix interface and the matrix dislocations react during the bypass process. From a modeling perspective, these simulations show the importance of describing the interface structure and the matrix dislocations in exactly the same framework such that the matrix dislocations are capable of modifying the interface structure and *vice versa*.

Effect of atomistic surface steps on the brittle to ductile transition of silicon

Christian Thaulow*, Dipanjan Sen** ***, and Markus J. Buehler**

* Department of Engineering Design and Materials, The Norwegian University of Science and Technology, NO-7491 Trondheim, Norway
christian.thaulow@ntnu.no

**Laboratory for Atomistic and Molecular Mechanics, Department of Civil and Environmental Engineering, Massachusetts Institute of Technology, 77 Massachusetts Ave. Cambridge, MA, USA

*** Department of Materials Science and Engineering, Massachusetts Institute of Technology, 77 Massachusetts Ave. Cambridge, MA, USA

ABSTRACT

We employ atomistic models of single crystal silicon with up to 200,000 atoms to examine the influence of crack tip heterogeneities on the brittle-to-ductile transition (BDT) and the competition between brittle bond-breaking and emission of dislocations. We first examined the crystallographic orientations most widely known to exhibit fracture, e.g. failure on the $\{111\}$ and $\{110\}$ planes, but could not generate dislocations. Even at the very high temperature of 1500K, the material behaved in a completely brittle manner. In contrast, when the failure plane was changed to the $\{100\}$ plane, dislocation loops were observed. The formation of these loops could be linked to the geometrical ledges at the crack tip with favourable orientations for slip on the $\{111\}$ planes. The dislocations caused the cracks to arrest, but re-initiation took place.

1. Introduction

The failure of components made of silicon is an important issue in the electronic- and nano-technological developments. The functioning of these components relies on a detailed understanding of the properties on the atomistic level, and the last decades have seen a vast amount of research efforts to unlock the mechanisms and take benefits in the further product developments.

The mechanisms responsible for the failure of silicon have been investigated experimentally and theoretically. The experiments clearly demonstrate a sharp transition from brittle to ductile behavior at a temperature above about 870K, [1]. The BDT phenomenon is explained as a shift in mechanism from the breaking of covalent brittle bonds between the atoms to nucleation and propagation of dislocations. The emission of dislocations shield the crack and trigger plastic deformation, hence the crack tip stresses are relieved and make further breaking of bonds difficult.

There have been many attempts to explain the transition and gain insight in the detailed mechanisms. But despite all efforts, the interactions at the crack tip responsible for the generation of dislocations have not been understood. Atomistic simulations offer genuine possibilities for examining the crack tip failure interactions. The most correct atomistic description is obtained by quantum mechanics DFT, but because of the very restricted volume that can realistically be treated; a few hundreds of atoms, the 3D nature of dislocation loops can not be examined. But with the emergence of new, quantum mechanics informed force field interatomic potentials, we now have tools available for examining material volumes of sufficient dimensions.

In a previous study by the authors we were able to model the BDT with models containing about 27.000 atoms [2]. The three main factors contributing to the BDT are proposed to be:

- 1) The brittle crack advance with a stepwise brittle fracture - arrest - re-initiation mechanism.
- 2) Bond rotation at the crack tip that lead to the formation of new covalent bond structures, most typically the 6-member rings are transformed to five- and seven-member rings. The shift in bond structure relieves the stresses, and induces additional lattice trapping.
- 3) Formation of small geometrical ledges at the crack tip with orientation in the preferred $\{111\}$ slip plane for dislocation emission. The ledges are either caused by crack tip micro cracks on the $\{111\}$ plane or by crack tip stretching/deformation by blunting. The dominating tensile stresses acting on the macro-crack will tentatively decompose and exhibit shear components on the slant oriented ledges. It has theoretically been shown that even very small amounts of shear loading, in the order of 10% of the tensile, will stimulate emission of dislocations [3].

The three mechanisms work together and an efficient interplay is important in order to generate dislocations. Fig. 1 visualizes the crack tip mechanisms.

These findings stimulated to explore the 3D nature of the dislocations, and new models with maximum thickness of 100 Å and a total number of atoms of up to 200,000 were prepared.

2. Atomistic model

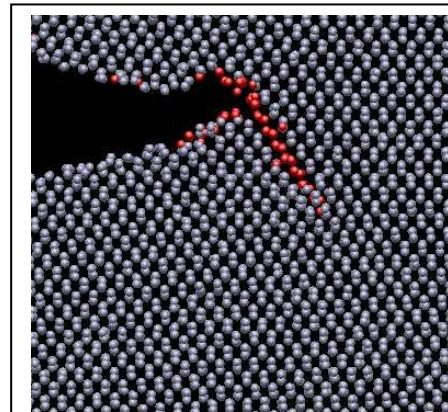


Figure 1. Slip vector plot of formation of a ledge at the crack tip of silicon and the subsequent emission of dislocation at 1200K, adapted from [2]. The brittle fracture was completely arrested after the emission of a dislocation on a $\{111\}$ slip plane

The system set up was the same as described in [2]. We apply the first principles based ReaxFF reactive force field, which retains nearly the accuracy of quantum mechanics, even for bond breaking events [4].

A perfect crystal with an edge crack was loaded by displacing the boundaries. The model geometry is approximately 200\AA by 180\AA , with a thickness of 50\AA for the $\{111\}$ and $\{110\}$ orientations and 100\AA for the $\{100\}$ orientation, and a crack length of 40\AA , Fig. 2. We use periodic boundary conditions in the loading- and thickness directions (x- and z-directions respectively). Before the loading the model is relaxed at the relevant temperature. Each time step is 0.2fs . After relaxation the model was loaded $200,000$ time steps at a strain rate of $2 \times 10^9 \text{ s}^{-1}$.

3. Results

Brittle crack jump followed by emission of dislocations was observed in the model with crack orientation $x100y011$ at 1200K . We section the model in the thickness direction and observe that the tendency to formation of dislocations varies along the crack front. Two dislocation loops were observed on the $\{111\}$ planes in the period of arrest before the brittle crack continued through the model. The emission of dislocations coincided with formation of ledges. We also analysed the dislocations with the slip line vector and found a good agreement with the observations, Fig. 3. We find that the slip directions are $\langle 211 \rangle$ and the slip vector is 2.3\AA . This is in accordance with the partial Burgers vector on the glide plane for silicon with lattice constant of 5.4\AA .

4. Discussion

Even though we have proven the origin and the nature of dislocation loops, Fig. 3, it still remains to explain why the crack does not come to a complete arrest as was the case for the smaller 15\AA thick model [2]. This question is of special interest since the BDT temperature observed between 880K and 890K for the thin models coincided very well with the observed experimental results. We ask if there is a thickness effect. One explanation could be that the local loop can arrest the crack for a moment, but

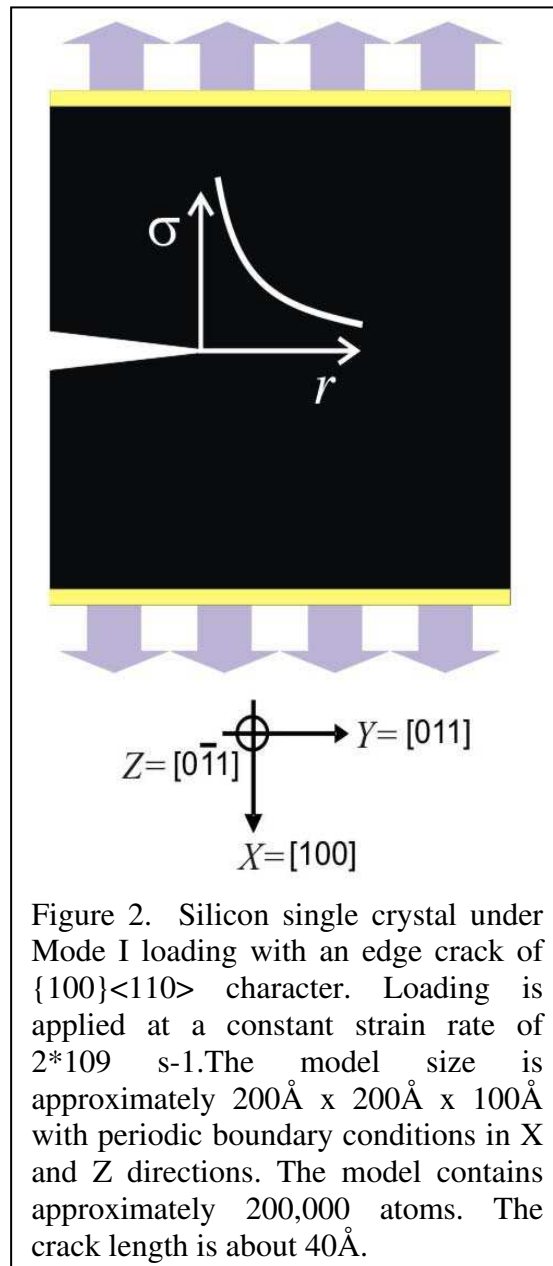


Figure 2. Silicon single crystal under Mode I loading with an edge crack of $\{100\}\langle 110 \rangle$ character. Loading is applied at a constant strain rate of $2 \times 10^9 \text{ s}^{-1}$. The model size is approximately $200\text{\AA} \times 200\text{\AA} \times 100\text{\AA}$ with periodic boundary conditions in X and Z directions. The model contains approximately $200,000$ atoms. The crack length is about 40\AA .

since no ledges are formed on the adjacent crack front segments, the brittle fracture will dominate and over-rule the ductile island. If this is the case, an array of nucleation sites will be necessary in order to secure arrest along a substantial fraction of the crack front. In contrast, the 15Å model is totally dominated by the dislocation, and hence comes to a complete arrest. The critical distance between the nucleation points is probably also related to how effective the sources are and how dominating the dislocations become.

One interesting source for creating dense patterns of ledges could be the response from surface waves, [5]. The well known mirror-mist-hackle instability phenomenon, where dynamical instability leads to an increase roughening of the fracture surface as the crack speed increases, could also be a source for ledges.

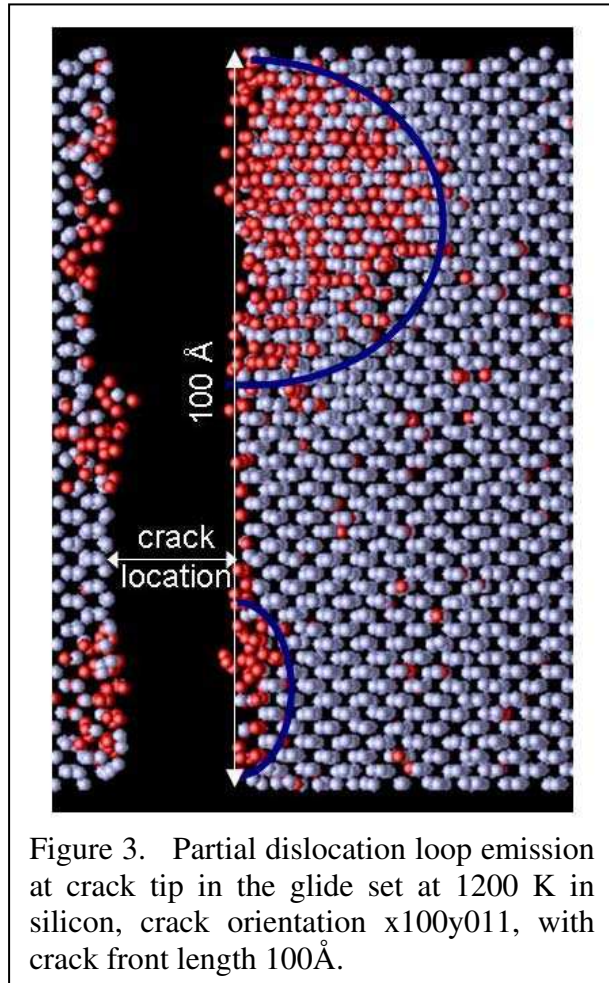


Figure 3. Partial dislocation loop emission at crack tip in the glide set at 1200 K in silicon, crack orientation $x100y011$, with crack front length 100\AA .

Acknowledgements

We acknowledge the support from the Arctic Materials project at SINTEF and from NOTUR (Norwegian High Performance Computing).

References

1. Samuels, J. and S. Roberts, *The brittle-ductile transition in silicon. I. experiments*. Proceedings of the Royal Society of London. Series A, Mathematical and Physical Sciences, 1989. **421**(1860): p. 1-23.
2. Sen, D., et al., *Atomistic study of crack-tip cleavage to dislocation emission transition in silicon single crystals*. Physical Review Letters 2010. **PACS numbers: 62.20.mt**.
3. Rice, J., *Dislocation nucleation from a crack tip: an analysis based on the Peierls concept*. Journal of the Mechanics and Physics of Solids, 1992. **40**(2): p. 239-271.
4. Buehler, M., et al., *Threshold crack speed controls dynamical fracture of silicon single crystals*. Physical Review Letters, 2007. **99**(16): p. 165502.
5. Bouchaud, E., et al., *Can crack front waves explain the roughness of cracks?* Journal of the Mechanics and Physics of Solids, 2002. **50**(8): p. 1703-1725.

Discrete and continuum micromechanical models of transformation-induced plasticity in multiphase steels.

Sergio Turteltaub

Delft University of Technology
Faculty of Aerospace Engineering
Kluyverweg 1, 2629 HS Delft
The Netherlands
s.r.turteltaub@tudelft.nl

Among the class of high-strength, high-ductility materials, multiphase steels occupy a prominent position. The microstructure of multiphase steels consists of grains of retained austenite embedded in a ferrite-based matrix. Upon mechanical loading, retained austenite may transform into martensite, as a result of which plastic deformations are induced in the surrounding phases. This solid-state martensitic transformation has been experimentally identified as the underlying mechanism responsible for the improvement of the overall yield strength and ductility. A detailed understanding of these mechanisms is essential in order to optimize the properties of these materials.

The microscopic mechanisms controlling the macroscopic properties are studied by means of numerical simulations of aggregates of grains of retained austenite embedded in a ferrite-based matrix. Two approaches are used to simulate the phase transformation and plastic deformation, namely applying a *discrete* and a *continuum* model. In the discrete model, plasticity is accounted for using discrete dislocations and the transformation is explicitly modelled through evolving transformation regions inside grains of retained austenite. The evolution of the martensitic regions is governed by a kinetic relation that relates the phase boundary velocity to the corresponding driving force. The continuum model is based on crystal plasticity coupled to a transformation model where the transforming regions are represented through internal variables (volume fractions). The driving forces for transformation and plasticity are derived from thermodynamical principles and include lower length-scale contributions from surface and defect energies. Both discrete and continuum models provide valuable insight, at somewhat different length scales, on the interaction between plastic deformation and transformation. The simulations are used to study the effect of various microstructural parameters, such as crystal orientation, austenitic volume fraction and grain size, on the effective response of an aggregate of multiphase grains.

This presentation is based on joint work with A. Suiker, D. Tjahjanto, J. Shi and E. van der Giessen.

Quasicontinuum simulation of mixed mode fracture in bcc-Fe

Authors: Inga Vatne¹, Erling Østby², Christian Thaulow¹

Affiliations: ¹ Department of Engineering Design and Materials, NTNU, 7491 Trondheim, Norway; ²SINTEF Materials and Chemistry, 7034 Trondheim, Norway

ABSTRACT

In this paper the use of modified boundary layer (MBL) approach in multiscale model of fracture in bcc-Fe has been investigated. The method used is the Quasicontinuum (QC) method with an EAM interatomic potential. Mixed mode fracture and the influence of different T-stress level on this has been investigated. The analyses have been carried out assuming different crystallographic orientations. The results show that the behavior at the crack tip is sensitive to both the crystallographic orientation, the mode of loading and the applied T-stress level. Phenomena like cleavage crack propagation, twinning, and dislocation emission are observed in the analyses.

1. Introduction

Multiscale and atomistic modeling of materials is developing rapidly and represent interesting tools to investigate the mechanisms taking place at the crack tip. In FE simulations the modified boundary layer approach is sometimes used to change the constraint by changing the stress in x-direction, the T-stress. Beltz and Machova¹ where the first to systematically control the T-stress in an atomistic simulation and concluded that it will influence the crack tip stability and result in a transition from ductile to brittle behavior for a $(\bar{1}10)[110]$ orientation. In² it is investigated how the T-stress will affect the crack tip behavior on nano-scale, in the present paper this same approach is applied for mixed mode loading.

2. The quasicontinuum method

The quasicontinuum method was developed by Tadmor et. al.³. The method couples a continuum and an atomistic description of the material. The continuum description uses the Cauchy-Born rule to calculate the energy and the properties of the nodes. The material behavior is then calculated from these properties. The atomistic domain uses a molecular static description. The interaction between the atoms are modeled with an EAM potential developed by Mendeleev et. al.⁴. In this work, a OK static approach is used. The coupling between the continuum and atomistic domains is done by refining the continuum mesh to atomistic size in a transition region, so that every atom is represented. In this way the atoms can use the nodes in the continuum domain as atomistic neighbors to calculate their energy due to interatomic reactions. The total energy is then calculated by summing over all atoms and nodes, and the equilibrium is found by minimizing this energy.

3. Modified Boundary Layer

The modified boundary layer is a continuum mechanical approach where the analytic solution for the stress field around a crack tip is used as boundary conditions, and the stress in x-direction, the T-stress, can be used to change the constraint. The anisotropic formulation for mixed mode

MBL without the T-stress term and with w as a weighting factor for the degree of mode II loading, so that $k_1 = (1 - w)k$ and $k_2 = wk$, implemented as given by⁵:

$$\begin{aligned}
 u(r, \theta) &= k_1 \sqrt{(2r)} \operatorname{Re} \left[\frac{1}{\mu_1 - \mu_2} (\mu_1 p_2 \sqrt{\cos\theta + \mu_2 \sin\theta} - \mu_2 p_1 \sqrt{\cos\theta + \mu_1 \sin\theta}) \right] \\
 &\quad + k_2 \sqrt{(2r)} \operatorname{Re} \left[\frac{1}{\mu_1 - \mu_2} (p_2 \sqrt{\cos\theta + \mu_2 \sin\theta} - p_1 \sqrt{\cos\theta + \mu_1 \sin\theta}) \right] \\
 v(r, \theta) &= k_1 \sqrt{(2r)} \operatorname{Re} \left[\frac{1}{\mu_1 - \mu_2} (\mu_1 q_2 \sqrt{\cos\theta + \mu_2 \sin\theta} - \mu_2 q_1 \sqrt{\cos\theta + \mu_1 \sin\theta}) \right] \\
 &\quad + k_2 \sqrt{(2r)} \operatorname{Re} \left[\frac{1}{\mu_1 - \mu_2} (q_2 \sqrt{\cos\theta + \mu_2 \sin\theta} - q_1 \sqrt{\cos\theta + \mu_1 \sin\theta}) \right]
 \end{aligned} \tag{1}$$

Where p_1, p_2, q_1, q_2 and μ_j are constants calculated from s_{ij} which are the components of the compliance matrix⁵.

The displacement due T-stress can be given by an expression corresponding to the anisotropic expressions for MBL

$$u(r, \theta) = T \cdot \left(S_{11} - \frac{S_{13}}{S_{33}} S_{13} \right) \cdot r \cos\theta, v(r, \theta) = T \cdot \left(S_{12} - \frac{S_{13}}{S_{33}} S_{13} \right) \cdot r \cos\theta$$

or by an isotropic formulation given as:

$$u(r, \theta) = T \cdot \left(\frac{1 + \nu^2}{E} \right) \cdot r \cos\theta, v(r, \theta) = -T \cdot \left(\frac{\nu(1 + \nu)}{E} \right) \cdot r \cos\theta$$

4. Model

A square model with a size of about $1500\text{\AA} \times 1500\text{\AA}$ is used, with a crack size of about 750\AA . At the crack tip a domain of nonlocal atomistic description is applied. Further away a local domain with finite element description is applied, while a modified boundary layer formulation is used as boundary conditions. Three crystallographic orientations has been investigated, 1 - (010)[101], 2 - (1 $\bar{1}$ 0)[001] and 3 - (01 $\bar{1}$)[011], given by the crack plane and the crack front.

5. Mixed mode loading

Simulations with mixed mode loading is done for all of the four orientations. The objective is to see how the crack behavior change as the mode of loading change. The mode of loading is characterized by w given in eq. 1. The dislocation emission and fracture behavior was analyzed with a common neighbor analysis (cna) where blue is bcc structure, green is fcc structure, red is twinning and white is no specific crystallographic structure,⁶. Orientation 1 is the so called easy twinning orientation. It shows crack growth straight ahead in pure mode I loading, see fig. 1(a). As the mode II contributes the crack grows in a direction 35° to the original crack plane normal, corresponding a $\{121\}$ plane, see fig. 1(b). As the mode II contributions increases twinning occurs in a $\{121\}$ plane, see fig. 1(c). When the mode II contribution increases even more, edge dislocations that moves along a $\{121\}$ plane are created, see fig. 1(d). Also note that with low degree of mode II loading there is a creation of a small fcc area at the crack tip.

Orientation 2 has crack growth straight ahead on a $\{110\}$ plane with the creation of a small fcc area at the sides of the crack tip, see fig. 2(a) and 2(b). When $w = 0.4$, the fcc area at the crack

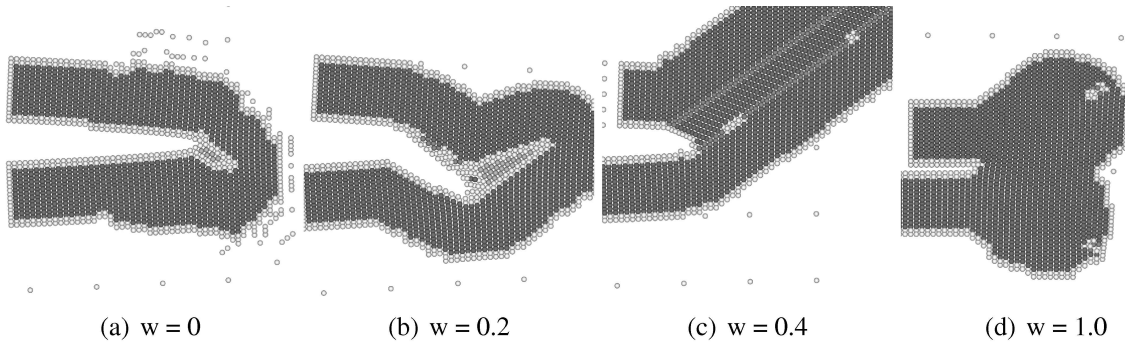


Figure 1: Orientation 1, $(010)[101]$. With w characterizing the mixed mode, where $w = 0$ corresponds to pure mode I loading and $w = 1$ corresponds to pure mode II loading.

tip gets larger and slip is created straight ahead of the crack tip, and 90° s on the crack tip, which both are $\{110\}$ planes. At a high degree of mode II loading this slip and also the fcc area turns to only go straight ahead from the crack tip.

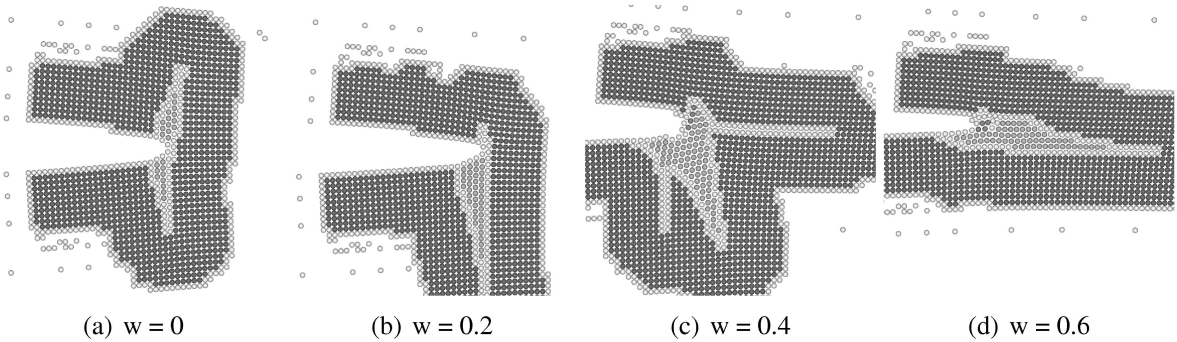


Figure 2: Orientation 2, $(1\bar{1}0)[001]$. With w characterizing the mixed mode, where $w = 0$ corresponds to pure mode I loading and $w = 1$ corresponds to pure mode II loading.

Orientation 3 has edge dislocation creation on $\{121\}$ planes when $w < 0.3$ and twinning on the same planes with higher w . This orientation is the so called hard twinning orientation. However, as shown in fig. 3, with increasing mode II loading, twinning does occur. Emission of edge dislocation backwards along a $\{121\}$ plane is observed with $w > 0.7$. Also at $w = 0.7$ crack growth down along a $\{100\}$ plane is observed together with twinning and dislocation emission on $\{121\}$ planes.

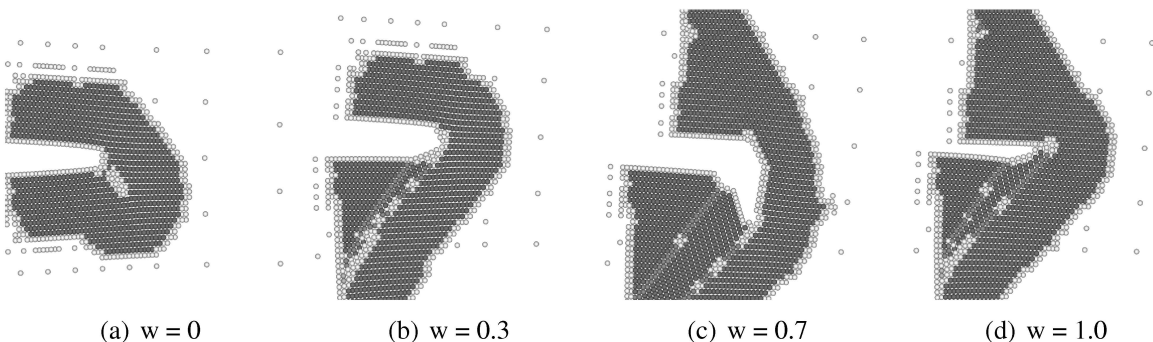


Figure 3: Orientation 3, $(01\bar{1})[011]$. With w characterizing the mixed mode, where $w = 0$ corresponds to pure mode I loading and $w = 1$ corresponds to pure mode II loading.

6. Effect of T-stress

In² the effect of T-stress on the critical stress intensity factor and the crack tip behavior is discussed. Most of the simulations in² are done with an isotropic version of MBL. The anisotropic formulation of the T-stress given in eq. 2 is here compared with an isotropic formulation of the T-stress, eq. 2. In fig. 4, the critical stress intensity factor is plotted against the T-stress for both isotropic and anisotropic formulations of the T-stress, but both has anisotropic formulations for MBL. As the figure shows, there is no large difference between the two different formulations. Mixed mode loading however, seems to cause significantly different behavior. The close to linear trend is no longer observed. This is due to the fact that both the T-stress and mode II loading is in the same direction and will influence each other. The difference is that mode II is shear while the T-stress is normal stresses.

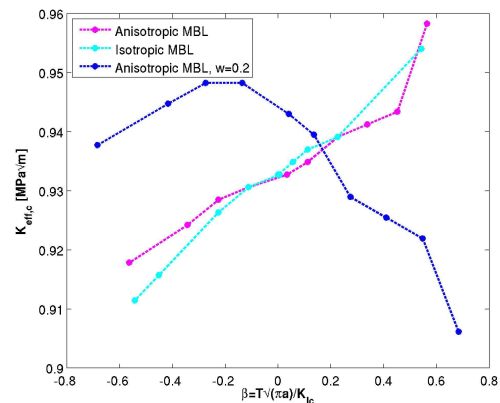


Figure 4: Critical stress intensity factor plotted against the T-stress for isotropic and anisotropic formulation of the T-stress.

7. Conclusion

Multiscale simulations predict that the crack tip behave more ductile as the mode II load increase. With increased T-stress on mode I formulations the stress intensity factor increases, but with mixed mode simulations another relationship is observed.

References

- [1] G. E. Beltz and A. Machová. Effect of T-stress on dislocation emission in iron. *Scripta Materialia*, 50(4):483–487, 2004.
- [2] I. Vatne, E. Østby, and C. Thaulow. Multiscale materials modeling of fracture in fe using modified boundary layer (mbl), 2010.
- [3] R. E. Miller and E. B. Tadmor. The quasicontinuum method: Overview, applications and current directions. *Journal of computer-aided materials design*, 9(3):203–239, 2002.
- [4] M. I. Mendeleev, S. Han, D. J. Srolovitz, G. J. Ackland, D. Y. Sun, and M. Asta. Development of new interatomic potentials appropriate for crystalline and liquid iron. *Philosophical Magazine*, 83(35):3977–3994, 2003.
- [5] G. Sih and H. Leibowitz. *Mathematical theories of brittle fracture*, volume Vol. II. Mathematical Fundamentals of *Fracture - An Advanced Treatise*. Academic Press, New York, 1968.
- [6] A. Stukowski. Visualization and analysis of atomistic simulation data with ovito—the open visualization tool. *Modelling and Simulation in Materials Science and Engineering*, 18:015012, 2010.

Strength of single crystal superalloys: from dislocation dynamics simulations to continuum micromechanics

Vattré Aurélien¹, Fedelich Bernard², Arjen Roos³ and Benoit Devincre³

¹DMSE, Massachusetts Institute of Technology, 77 Massachusetts Avenue, Cambridge
MA 02139, United States
avattre@mit.edu

²BAM, Federal Institute for Materials Research and Testing, Under den Eichen 87
12205 Berlin, Germany

^{3,4}ONERA - The French Aerospace Lab, 29 Avenue de la Division Leclerc, BP 72
92322 Châtillon Cedex, France

The present work deals with crystal plasticity of single crystal nickel-base superalloys. In this context, a scale transition of transferring information from mesoscale towards a physically justified micromechanical model is shown.

A numerical coupling between dislocation dynamic simulations and the finite element method, the so-called Discrete-Continuous Model (DCM) is used in order to take into account the mutual interactions between dislocations and precipitates.

A set of calculations addresses the anisotropic mechanical response of single crystal superalloys. Analyses of dislocation interactions show the crucial role of one active slip system and its collinear system in the strain localization in the form of slip bands. Furthermore, screening of long-range elastic interactions associated to the interfacial dislocation network explain the origin of the low hardening rate observed in $\langle 111 \rangle$ -oriented specimens at high temperatures.

A new interpretation of the cubic slip phenomenon is also suggested by essentially determining by the nature of the dislocation network at the interfaces.

These main results are taken into account in a continuum micromechanical model to improve the estimation of kinematical hardening. A key role is played by the combination of the activated octahedral slip systems as function of the crystal orientation. It is shown that for the systems activated in $\langle 111 \rangle$ orientation, the contributions to kinematical hardening compensate, while kinematical hardening remains high for $\langle 001 \rangle$ specimens, which explains the experimental dependence of plastic flow on the orientation. Results are presented for the alloy CMSX-4 in several orientations.

Micromechanics based failure predictions of fibre reinforced composites

Ted Vaughan, Conor McCarthy

Materials and Surface Science Institute (MSSI) and the Department of Mechanical and Aeronautical Engineering, University of Limerick, Limerick, Ireland.

Ted.Vaughan@ul.ie, Conor.Mccarthy@ul.ie

ABSTRACT

A micromechanics damage model is presented which predicts the failure locus of a unidirectional carbon fibre reinforced epoxy composite in the transverse plane. A Mohr-Coulomb material model is used to predict the onset and evolution of matrix plasticity, while a cohesive zone model is used to examine the effects of interfacial decohesion in a number of statistically equivalent representative volume elements. Combined transverse tensile and shear loading is used to generate a failure surface for the material, which was found to show good agreement with the predictions of the Hashin failure theory. The micromechanical model developed also provides novel insight into the interaction of microscopic damage mechanisms during the fracture process and could prove useful in identifying optimum parameters for composite material systems development.

1. Introduction

Fibre reinforced composites exhibit a gradual damage accumulation to failure with a multitude of hierarchical dissipative mechanisms responsible for the deterioration of mechanical properties. The anisotropic nature of each individual composite ply means that failure, and the interaction of damage mechanisms during the failure process, is highly dependant on the direction of loading. Many failure theories currently available are phenomenological based [1] and their performance under certain multiaxial loading configurations has been found to be poor as they do not consider the microscopic development of failure. As a result, virtual testing through computational micromechanics is emerging as an alternative approach to failure based predictions for multiaxial stress states [2, 3]. This paper discusses a micromechanics damage model, developed in ABAQUS [4], which predicts the effects of matrix non-linearity, fibre-matrix debonding and local fibre distribution. The Nearest Neighbour Algorithm [5] is used to create statistically equivalent fibre distributions for the micromechanical models allowing for an accurate representation of the microscopic stress state. Combined transverse tensile and shear loading is applied to a number of representative volume elements and the failure locus obtained is compared against the predictions from the Hashin failure theory [6].

2. Finite Element Modelling

2.1 Microstructure Generation

The fibre distribution for the HTA/6376 material has been recently characterised and the Nearest Neighbour Algorithm (NNA) has been developed [5] which enables statistically equivalent fibre distributions to be generated. The NNA uses experimentally measured nearest neighbour distribution functions to define the inter-fibre distances allowing the short range interaction of fibres in the microstructure to be reproduced enabling an accurate representation of the local microscopic stress state. A typical geometry produced by the NNA is shown in Fig. 1(a). The fibre and matrix regions were meshed using 4-noded, full integration plane strain elements (CPE4). Cohesive elements (COH2D4) were introduced

between the fibre and the matrix to predict the onset of fibre-matrix debonding. Periodic boundary conditions, similar to those used by [7], were applied to the micromechanical models to ensure a macroscopically uniform stress/displacement field existed across the boundaries of each RVE.

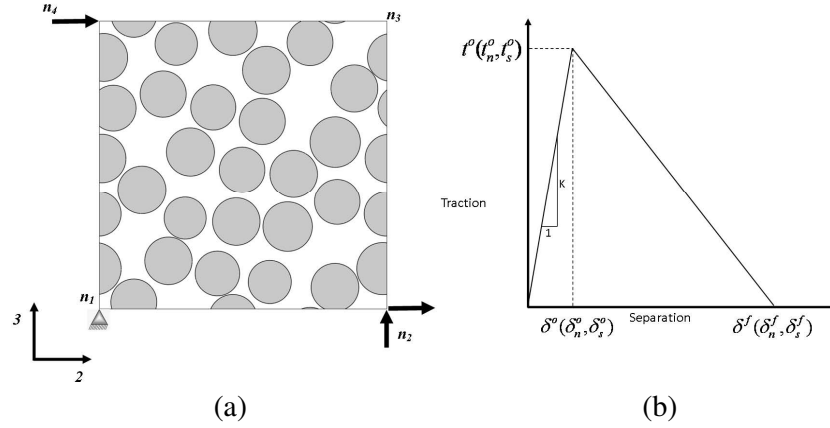


Figure 1: (a) Boundary conditions applied to RVE to simulate combined transverse tensile and shear loading (b) Traction-separation law governing behaviour of cohesive elements

2.2 Material Behaviour

The HTA fibres are assumed here to be linear elastic while the 6376 matrix is assumed to behave as an elastic-plastic solid. The elastic properties of the HTA fibres and the 6376 matrix can be found in [5]. The behaviour of the matrix phase is sensitive to the hydrostatic stress and as a result the Mohr-Coulomb yield criterion is employed. The Mohr-Coulomb criterion states that yielding will occur on a given plane when the shear stress (τ) exceeds the cohesive stress of the material plus the frictional force acting along the failure plane, such that,

$$\tau = c - \sigma_n \tan \phi \quad (1)$$

Where c is the cohesion yield stress, σ_n is the normal stress acting on the failure plane and ϕ is the angle of internal friction. For the 6376 epoxy matrix the internal friction angle and cohesion stress for the 6376 epoxy matrix are, $\phi = 26^\circ$ and $c = 82$ MPa, respectively. A non-associative flow rule is used to compute the direction of plastic flow, meaning that the dilatant angle, φ , is assumed to be zero. The behaviour of the fibre-matrix interface was modelled using cohesive elements available in ABAQUS [4]. Their constitutive response is defined in terms of a standard traction-separation law which relates the separation displacement between the top and bottom faces of the element to the traction vector acting upon it, as shown in Fig. 1(b). The initial linear response is followed by the initiation of damage, based on the maximum stress criterion, which is followed by linear softening. This effective displacement at failure of the cohesive elements determines the rate of damage in the element and this was defined in terms of the fracture energy, Γ , which corresponds to the area under the traction separation curve. For simplicity, it was assumed that the interfacial normal strength was equal to the interfacial shear strength ($t_n = t_s = 60$ MPa) and the fracture energies were the same for Mode I and Mode II type failures ($\Gamma = 25$ J/m²).

3. Results

3.1 Transverse Tensile Deformation

Figure 4 (a) shows the stress strain response of an RVE subject to transverse tensile loading. The initial linear response is followed by non-linear behaviour due to fibre-matrix debonding

initiating in a number of locations, as shown by micromechanical model in Fig. 2. These interfacial cracks tend to develop between neighbouring fibres with a small inter-fibre spacing. These interfacial cracks grow and small regions of the matrix ‘bridge’ the debonded fibres. Upon further loading the matrix undergoes intense plastic deformation allowing the interfacial cracks to coalesce resulting in final fracture which occurs at a transverse tensile stress of 66MPa. This sequence of damage is very similar to observed by Hobbiebrunken *et al.* [8] in a carbon fibre/epoxy composite with a low cure temperature.

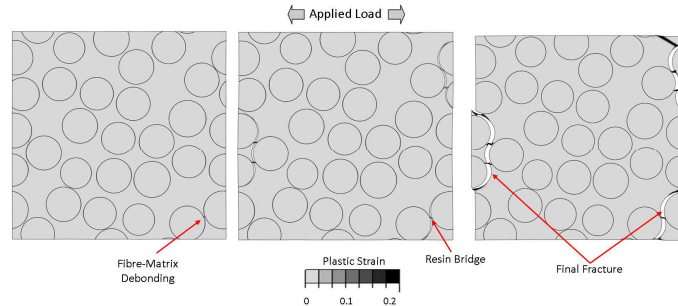


Figure 2. Microstructural damage evolution for transverse tensile loading

3.2 Transverse Shear Deformation

Figure 4 (a) also shows the stress strain response of an RVE subject to transverse shear loading. Here, the initial linear response is followed by non-linear behaviour due to a combination of fibre-matrix debonding and matrix yielding, as shown in Fig. 3. For the shear case interfacial cracks initiate around closely neighbouring fibres which are aligned at +45° to the horizontal shear loading direction. These interfaces fail due to the interfacial normal stress being exceeded and are aligned with the main tensile loading axis of the RVE. As the fibre-matrix bond fractures, stress is redistributed meaning the shear load is taken up by the matrix region immediately adjoining the interfacial crack. As a result of this stress intensification, slip occurs almost parallel to one of the shear loading axes, in this case the vertical shear loading axis. Hence, there is intense shear yielding of the matrix in this region. These regions of highly yielded matrix allow for neighbouring interfacial cracks to coalesce and a fracture path develops due to a combination of both intra-ply damage mechanisms. This occurs at a transverse shear stress of 57MPa.

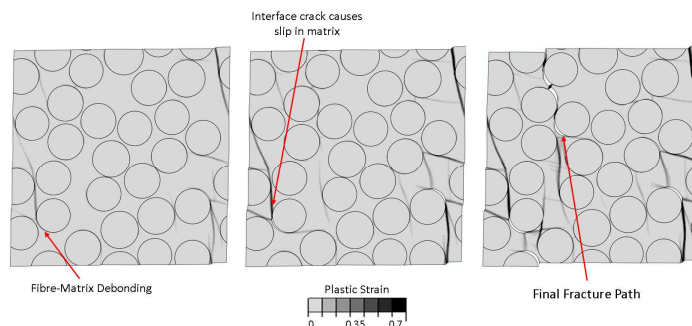


Figure 3. Microstructural damage evolution for transverse shear loading

3.3 Combined Transverse Tensile and Shear Loading

To generate the failure locus of the carbon fibre composite, combined transverse tensile and shear loading was applied to an RVE, as shown in Fig. 1 (a). The ratio of shear strain (γ_{23}) to transverse strain (ϵ_{22}) applied was varied such that a resulting failure locus could be interpreted. This is shown in Fig. 4(b) where each response curve corresponds to a particular $\gamma_{23}/\epsilon_{22}$ loading ratio. Also shown is the prediction of the Hashin model, which assumes a

quadratic interaction of the transverse shear and tensile strengths [6]. Failure predictions from the micromechanics damage model show good correlation with the Hashin failure theory.

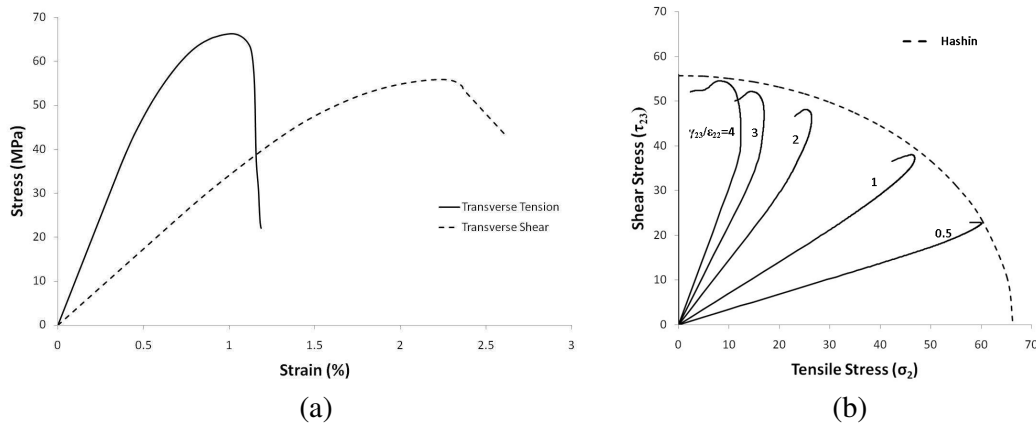


Figure 4. (a) Mechanical response of an RVE for both transverse shear and transverse tensile load cases (b) Micromechanical prediction of failure surface in the transverse plane using combined transverse tensile and shear loading

4. Concluding Remarks

A micromechanics damage model has been developed which predicts the failure locus of a unidirectional carbon fibre reinforced epoxy composite using combined transverse tensile and shear loading. The failure locus was found to show good agreement with the predictions of the Hashin failure theory. Further development of this type of model should allow for a range of stress states to be examined enabling accurate predictions of three dimensional failure envelopes in fibre reinforced composites.

Acknowledgements

This authors wish to acknowledge the funding provided by the Irish Research Council for Science, Engineering and Technology (IRCSET) and Science Foundation Ireland (SFI). Computational work was carried out using the MSSSI AMPS cluster, enabled under the framework of the INSPIRE programme, funded by the Irish Government's Programme for Research in Third Level Institutions, Cycle 4, National Development Plan 2007-2013.

References

- [1] Soden PD, Hinton MJ, Kaddour AS. A comparison of the predictive capabilities of current failure theories for composite laminates. *Compos. Sci. Technol.* 1998; 58(7): 1225-1254.
- [2] González C, Llorca J. Virtual fracture testing of composites: A computational micromechanics approach. *Eng. Fract. Mech.* 2007; 74(7): 1126-1138.
- [3] Totry E, González C, Llorca J. Failure locus of fiber-reinforced composites under transverse compression and out-of-plane shear. *Compos. Sci. Technol.* 2008; 68(3-4): 829-839.
- [4] ABAQUS, Version 6.7. HKS., 2007.
- [5] Vaughan TJ, McCarthy CT. A combined experimental-numerical approach for generating statistically equivalent fibre distributions for high strength laminated composite materials. *Compos. Sci. Technol.* 2010; 70(2): 291-297.
- [6] Hashin Z. Failure criteria for unidirectional composites *Journal of Applied Mechanics* 1980; 47:329-335.
- [7] Van der Sluis O, Schreurs PJG, Brekelmans WAM, Meijer HEH. Overall behaviour of heterogeneous elastoviscoplastic materials: effect of microstructural modelling. *Mech. Mater.* 2000; 32(8): 449-462.
- [8] Hobbiebrunken T, Hojo M, Adachi T, De Jong C, Fiedler B. Evaluation of interfacial strength in CF/epoxies using FEM and in-situ experiments. *Composites Part A: Applied Science and Manufacturing* 2006; 37(12): 2248-2256.

Dislocation loops in nanocrystalline metals

M Velasco¹, C Brandl¹ and H Van Swygenhoven¹

¹Paul Scherrer Institute, NUM/ASQ, Materials Science and Simulation, CH-5232 Villigen
PSI, Switzerland
mario.velasco@psi.ch

In a nanocrystalline grain boundary (GB) network dislocations usually nucleate at ledge structures in the GB and propagate throughout the grain, depositing dislocation line sections at the GBs. Recent simulations of nc-Al deforming at a constant strain rate have shown that the propagation of dislocations along GBs can be a rather complex process involving multiple cross-slip events to avoid depositing edge dislocation segments into locally compressive regions of the GB. Thus via cross-slip the dislocation is able to propagate along more favourable regions such as triple lines under tension.

Here we use the atomistic simulation methodology published in [MSMSE 17(2009)055008] to implement well-defined dislocation loops in a grain having well defined misorientations with its nanocrystalline environment. This allows to study the reaction of GBs when bombarded with several dislocations and this as function of their tilts and twist component.

MMM 2010, October 4-8, Freiburg, Germany

Dislocation Dynamics and Plasticity in Micro-Pillars and Thin Films

Wei Cai

Mechanical Engineering Department, Stanford University, CA 94305-4040

Understanding plasticity and strength of crystalline materials in terms of the dynamics of microscopic defects has been a goal of materials research in the last seventy years. The size-dependent yield stress observed in recent experiments of sub-micrometer metallic pillars provides a unique opportunity to test our theoretical models, allowing the predictions from defect dynamics simulations to be directly compared with mechanical strength measurements.

The balance between the dislocation multiplication rate and depletion rate (at the surface) may be the key to understand the observed size effect in flow stress. Here we report two counterintuitive observations concerning dislocation multiplication in small volumes from Molecular Dynamics and Dislocation Dynamics simulations. In body-centered-cubic (BCC) metals, the surface itself can induce dislocation multiplication as a single dislocation moves across the pillar. In face-centered-cubic (FCC) metal pillars and thin films, however, even jogs of the Lomer-Cottrell type are not strong enough pinning points to act as permanent dislocation sources. These results highlight the need for better calibration of Dislocation Dynamics models against the more fundamental atomistic models.

A Numerical and Experimental Analysis of the Competition between Transgranular and Intergranular Fracture in Rolled Tungsten

Daniel Rupp¹ and Sabine M. Weygand²

¹Karlsruhe Institute of Technology, Institute for Materials Research II, Herrmann-von-Helmholtz-Platz 1, D-76344 Eggenstein-Leopoldshafen, Germany

²Karlsruhe University of Applied Sciences, Department of Mechanical Engineering and Mechatronics, Moltkestrasse 30, D-76133 Karlsruhe, Germany
sabine.weygand@hs-karlsruhe.de

To characterize the potential of tungsten as a structural material in future fusion reactors we have performed a thorough investigation of the fracture behavior of textured polycrystalline tungsten in a large temperature range for different crack orientations. The fracture mechanical tests, conducted in three point bending, exhibit that the anisotropic microstructure has a significant impact on the fracture mode as well as on the absolute toughness values. In the present paper special attention is drawn to the specimen orientation extracted in the rolling direction as they switch from transgranular to intergranular fracture at elevated temperatures resulting in a drastic change of their macroscopic fracture pattern. The aim is to present a fracture criterion which allows to interpretate and predict this change in fracture mode.

Our performed in situ SEM fracture test reveals that secondary cracks ahead of the notch propagate. They are located normal to the notch direction and lead to crack deflection. Based on this experimental observation an energy criterion stemming from layered materials is adapted. In this proposed criterion the ratio of the energy release rate of the notch to the one of the secondary crack is determinant. This ratio is calculated with a finite element model where secondary cracks of various lengths were positioned in different distances ahead of the notch.

With this energy criterion a temperature for the fracture mode change is predicted which agrees very well to the one observed experimentally.

Self-multiplication of Dislocation under High Strain Rate Deformation

D S Xu¹, H Wang¹, R Yang¹ and P Veyssi re²

¹Institute of Metal Research, Chinese Academy of Sciences, 72 Wenhua Road, Shenyang 110016, China, E-mail: dsxu@imr.ac.cn

²LEM, CNRS-ONERA, BP 72, Chatillon, France

The nucleation and multiplication of dislocations in some fcc metals and TiAl during high strain rate deformation were investigated using molecular dynamics simulation. The lattice was shear deformed along the primary slip system at various temperatures and strain rates from 10^6 to 10^{10} s^{-1} . It was shown that at higher strain rates many dislocations nucleated almost simultaneously at different places, while at the lower strain rates, only one primary loop nucleates. Secondary loops were found to nucleate after the primary loop has reached a critical size. Nucleation takes place at specific sites near the line of the primary dislocation loop, either on the same plane as the primary dislocation or on nearby planes depending on the materials investigated. The loops expand and react with each other and form point defects of various types, including vacancy and their clusters in the form of short vacancy rows, interstitial loops of different lengths and heights. The structural evolutions of the defects formed are investigated and the implications to the mechanical properties discussed.

A Calculation Approach Considering the Shape and Arrangement Effects of the Spherical Inhomogeneity on the Elastic Constants

Safak Yilmaz

Faculty of Mechanical Engineering
Technical University of Istanbul
Inonu Cad. No. 81. Taksim Beyoglu
34437 Istanbul
TURKIYE
yilmazsaf@itu.edu.tr

In this work, a numerical calculation approach considering the shape and arrangement of inhomogeneity was proposed to estimate the elastic constants of heterogeneous materials having a continuous matrix, including spherical inhomogeneity. The results were discussed by comparison with MTM and FEM results.

For a composite domain having perfectly bounded double constituents, the properties lie in the upper bound-parallel loading model [1] and lower bound-serial loading model values [2]. Hence, it would be plausible to estimate the composite behavior as a weighted average of the upper and lower bounds. A matrix region including a reinforcement having a volume fraction of V_f can be built up by a collection of a nested sequence of skins. For the components of stiffness tensor, it was assumed that the stiffness tensor components of the i^{th} heterogeneous domain was calculated using the following equations;

$$C_i = (1 - Gf)C_i^{UB} + Gf C_i^{LB} \quad (1)$$

where C_i^{UB} , C_i^{LB} and C_i are the upper bound values, lower bound values and weighted average values for the i^{th} heterogeneous domain, respectively. Gf is the weighted constant for the lower bound values. In the present work, the ratio of the projection area to the surface area of the inhomogeneity was considered for calculating the weighted constant, Gf . The proposed numerical calculation approach for the projection area is named PAA in the text for simplicity.

The case of spherical shaped inhomogeneity was considered for the geometry of inhomogeneity. The staggered (ST) and transversely aligned (TA) arrangement cases were considered for geometry of inhomogeneity arrangement. The elastic moduli of different heterogeneous systems calculated by MTM [3] and FEM [4] were compared with the results of the PAA proposed in Fig 1. As seen from Fig. 1, the agreement between the PAA results and MTM and FEM findings were very good. The agreement between elastic moduli calculated with PAA and with MTM and FEM indicates the success of the PAA proposed in the current study. The numerical calculation method proposed in this work allows the systematic and parametric investigation of the effects of microstructural geometry on the elastic behavior of heterogeneous materials including spherical inhomogeneity.

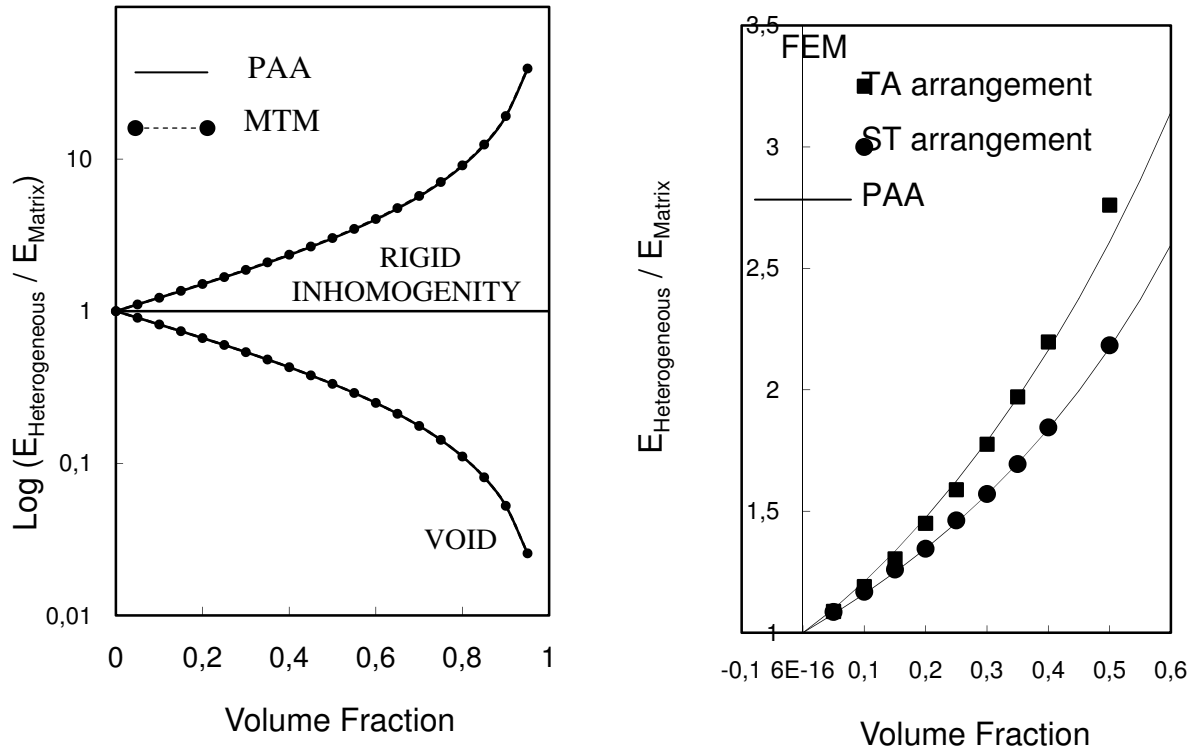


Figure 1. Normalized elastic moduli versus volume fraction. (a) Al matrix including rigid inhomogeneity and void, (b) Al matrix including SiC particulates.

References

- [1] W. Voight, Lehrbuch Der Kristallphysik. Teubner Verlag, Berlin-Leipzig, 1928.
- [2] A. Reuss A, Berechnung der fließgrenzen von mischkristallen auf grund der plastiizitätsbedingug fur einkristalle. Zeitschrift fur angewandte mathematik und mechanik, **9** (1929) 49-58.
- [3] T. Mori, K. Tanaka, Average stress in the matrix and average elastic energy of materials with misfitting inclusions. Acta Metall. Mater., **21**, 571-574, 1973.
- [4] S. Yilmaz, A. Aran, Finite element analysis of deformation behavior in ductile matrix containing hard particles. Mate. Sci. Tech. **14**, 1154-1162, 1998.

Modeling the transition from toughening to embrittlement by grain boundaries in tungsten

X.H. Zeng¹, D. Rupp², S.M. Weygand³ and A. Hartmaier¹

¹Interdisciplinary Centre for Advanced Materials Simulation, Ruhr-University Bochum, Stiepel Str. 129 (UHW), 44801 Bochum, Germany, E-Mail: xiaohui.zeng@rub.de

²Forschungszentrum Karlsruhe, Institute for Material Research II, Herrmann-von-Helmholtz-Platz 1, D-76344, Eggenstein-Leopoldshafen, Germany

³Karlsruhe University of Applied Sciences, Department of Mechanical Engineering and Mechatronics, Moltkestrasse 30, D-76133 Karlsruhe, Germany

Fracture toughness of commercially pure polycrystal tungsten was investigated by means of mechanical testing and numerical simulations. The material was produced in a powder metallurgical route followed by hot rolling leading to an elongated grain structure. Notched samples prepared in three orthogonal directions with respect to the rolling direction were subjected to three-point-bending tests at different loading rates in a wide range of temperatures from 120 to 1200 K. The measured fracture toughness is compared to the results of single crystal. We found that the fracture toughness of the polycrystal exhibits much smaller temperature dependence such that the polycrystal is significantly tougher at low temperatures, but more brittle than the single crystal above 300 K. We consider that the opposite effects of toughening and embrittlement due to grain boundaries originate from temperature-dependent interactions between grain boundaries and dislocations. At low temperature grain boundaries introduce additional dislocation sources along the crack front so that more shielding dislocations can be produced than in a single crystal. At elevated temperature however grain boundaries limit the dislocation mobility and confine the plastic zone by hindering dislocation motion. This idea is verified by performing dislocation dynamics simulations for polycrystals with different dislocation generation models and different grain sizes. The numerical analysis qualitatively agrees with the experimental findings.

Chemomechanics of Nanoparticle Uptake by Living Cells

Sulin Zhang¹, Hongyan Yuan¹, Ju Li², and Gang Bao³

¹Department of Engineering Science and Mechanics, The Pennsylvania State University, University Park, PA 16802

²Department of Materials Science and Engineering, University of Pennsylvania, 3231 Philadelphia, PA 19104

³Department of Biomedical Engineering, Georgia Institute of Technology and Emory University, Atlanta, GA 30332
Email: suz10@psu.edu

Tumor-specific drug delivery has long been desired in chemotherapeutic cancer treatment for achieving enhanced therapeutic efficacy and for mitigating adverse side effects. Most existing anticancer agents are incapable of distinguishing between benign and malignant cells, and consequently they cause systematic toxicity during chemotherapy. Owing to their small size, ligand-coated NPs can be efficiently directed toward, and subsequently endocytosed by tumor cells through ligand-receptor recognition and interaction, thereby offering an effective approach for specific targeting of tumor cells. In the present work, we present a thermodynamic model for receptor-mediated endocytosis of ligand-coated NPs. Through thermodynamic arguments, we reveal that, unlike the adhesion between two inanimate objects, the adhesion strength between an NP and a living cell is a non-local, variable quantity that depends on not only the particle size and the ligand density, but also the receptor density that is actively regulated by the cell. The cellular uptake depends interrelatedly on the particle size and ligand density, featuring a two-dimensional phase diagram in the particle size and ligand density space. The variable adhesion strength specifies a lower and an upper phase boundary beyond which the cellular uptake vanishes. The design principles of the NPs obtained from our studies are validated by comparisons to the characteristics of viruses. Our findings are not only important for understanding the biological behaviors and evolutionary design of cells, but also for engineering NP-based therapeutic and diagnostic agents.

Twist grain boundary migration by molecular-dynamics simulation

J. Zhou¹, V. Mohles² and G. Gottstein³

¹ Institut für Metallkunde und Metallphysik, RWTH Aachen University, Kopernikusstrasse 14, D-52056 Aachen, Germany. zhou@imm.rwth-aachen.de

² Institut für Metallkunde und Metallphysik, RWTH Aachen University, Kopernikusstrasse 14, D-52056 Aachen, Germany

³ Institut für Metallkunde und Metallphysik, RWTH Aachen University, Kopernikusstrasse 14, D-52056 Aachen, Germany

Molecular dynamics simulations have been used to study grain boundary migration of [001] twist grain boundaries (GBs) in pure Al described by an EAM. A newly proposed driving force being able to drive flat GBs with different misorientations was applied to all twist GBs. It is found that the twist GBs remain stable during migration. The special GBs with a high density of coincidence sites always move much faster than the more random GBs. The temperature dependence of the GB mobility indicates that GB migration is a thermally activated process. The simulated activation enthalpies with respect to the migration processes are in good agreement with the ones obtained in real experiments. For the first time, cross slip of screw dislocations is shown as the mechanism of low-angle GBs.

Nanomechanics of Plasticity in Ultra-Strength Materials

Ting Zhu¹

¹Woodruff School of Mechanical Engineering
Georgia Institute of Technology, Atlanta, GA 30332, USA
Email: ting.zhu@me.gatech.edu

Recent experiments on nanostructured materials, including nanowires, nanopillars, nanoparticles, nanofilms, nanotwins, and nanocrystals, have revealed a host of “ultra-strength” phenomena, defined by stresses in the material generally rising up to a significant fraction ($>1/10$ th) of the ideal strength—the highest achievable strength of a defect-free crystal. This talk describes the mechanics and deformation mechanisms in ultra-strength materials with flow defect-limited characteristics.

Nano-twinned copper exhibits an unusual combination of ultrahigh strength and high ductility, along with increased strain-rate sensitivity. We develop a mechanistic framework for predicting the rate sensitivity and elucidating the origin of ductility in terms of the interactions of dislocations with interfaces. Using atomistic reaction pathway calculations, we show that slip transfer reactions mediated by twin boundary are the rate-controlling mechanisms of plastic flow. We attribute the relatively high ductility of nano-twinned copper to the hardening of twin boundaries as they gradually lose coherency during plastic deformation. We have further studied the nanostructural evolution including the twin-size dependent exhaustion of mobile dislocation density and the orientation effects of twin textures based on crystal plasticity modeling. These findings provide new insights into possible means of optimizing strength and ductility through the creation of coherent internal boundaries [1,2].

Dislocation nucleation is essential to the plastic deformation of small-volume crystalline solids. The free surface may act as an effective source of dislocations to initiate and sustain plastic flow, in conjunction with bulk sources. Here we develop an atomistic modeling to address the probabilistic nature of surface dislocation nucleation. We show the activation volume associated with surface dislocation nucleation is characteristically in the range of $1-10b^3$, where b is the Burgers vector length. Such small activation volume leads to sensitive temperature and strain-rate dependence of the nucleation stress, providing an upper bound to the size-strength relation in nanopillar compression experiments [3].

- [1] L. Lu, T. Zhu, Y. Shen, M. Dao, K. Lu, S. Suresh, “Stress relaxation and the structure size dependence of plastic deformation in nanotwinned copper,” *Acta Materialia*, 57, 5165-5173 (2009).
- [2] T. Zhu, J. Li, A. Samanta, A. Leach and K. Gall, “Temperature and strain-rate dependence of surface dislocation nucleation”, *Physical Review Letters*, 100, 025502 (2008).
- [3] T. Zhu, J. Li, A. Samanta, H. G. Kim and S. Suresh, “Interfacial plasticity governs strain rate sensitivity and ductility in nanostructured metals”, *Proceedings of the National Academy of Sciences of the USA*, 104, 3031-3036 (2007).

Continuum model for the long-range elastic interaction on stepped epitaxial surfaces in 2+1 dimensions

Xiaohong Zhu¹ and Yang Xiang¹

¹Department of Mathematics, Hong Kong University of Science and Technology, Clear Water Bay, Kowloon, Hong Kong, Email: xhzhu@ust.hk

In heteroepitaxy, the mismatch of lattice constants between the crystal film and the substrate causes misfit strain and stress in the bulk of the film, driving the surface of the film to self-organize into various nanostructures. Below the roughening transition temperature, an epitaxial surface consists of facets and steps, and changes its morphology by lateral motion of steps. In this paper, we present a $2+1$ -dimensional continuum model for the long-range elastic interaction on stepped surface of a strained film. The continuum model is derived rigorously from the discrete model for the interaction between steps; thus it incorporates the discrete features of the stepped surfaces. Examples show that our continuum model is much more accurate as an approximation to the discrete model than the traditional continuum approximation. Moreover, in the linear instability of a planar surface, our continuum model gives the transition from step bunching instability to step undulation instability as the distance between adjacent steps increases, which agrees with the experimental observations and the results of discrete models and is missing using the traditional continuum approximation. Numerical simulations of the surface evolution using our model in the nonlinear regime show several different surface morphologies, including the morphology of step bunching which cannot be obtained using the traditional continuum approximation.

Multi-scale Simulations of Solidifying Foams

G. Zikos¹, D. K. Mahajan¹, F. Varnik^{1,2}, A. Hartmaier¹ and I. Steinbach¹

¹ Interdisciplinary Center for Advanced Materials Simulations, Ruhr-Universität Bochum
Stiepelers Strasse 129, 44801 Bochum, Germany

² Max-Planck Institut für Eisenforschung - Max-Planck Str. 1, 40237 Düsseldorf,
Germany

georgios.zikos@rub.de

The low density and the richness of mechanical properties of polymer foams make these materials of great industrial importance. In this work, we investigate phenomena that arise from the different length scales of a solidifying polymer foam via molecular dynamics and the lattice Boltzmann method. We use values for the local fluid viscosity, inspired by molecular dynamics for the case of a gas bubble inside a polymer melt, as input to our lattice Boltzmann simulations. These simulations then resolve the evolution of a liquid foam, whose viscosity increases with time (in order to take account of solidification), in the presence of a moving wall boundary. For this purpose, we combine a recently proposed mid-range repulsion force in the lattice Boltzmann method [Chibbaro, Falcucci, Chiatti, Chen, Shan and Succi PRE 2008] (allowing us to slow down the bubble-coalescence process) with the results of molecular dynamics calculations for the local viscosity. These simulations show how the competing effects of solidification and shear affect the structural properties and thereby the mechanical stability of solid foams.

2D and 3D Stress Fields Analysis Based on Direct Mapping of the Dual-Scale Porous Network of Plasma-Sprayed Tungsten

A.Zivelonghi¹, A.Larrue² and T.Weitkamp² and J.H.You¹

¹ Max-Planck-Institut für Plasmaphysik, Boltzmannstr.2, 85748 Garching, Germany

²ESRF Grenoble, 6 rue Jules Horowitz, B.P. 220, 38043 Grenoble, France

Corresponding Author: [A.Zivelonghi](mailto:A.Zivelonghi@ipp.mpg.de) adz@ipp.mpg.de

In this work two- and three-dimensional simulated stress fields including damage initiation across the complex dual-scale random porous network of Plasma-Sprayed Tungsten (PS-W) are presented and compared. Both classical and extended Finite Element (XFEM) analysis have been used to model crack initiation under tensile and shear loading.

Influence of dimensionality as well as complementarity of the two approaches is shown. Morphological characterization of inclusions and analysis of statistical representativity (RVE) for the calculated stress fields is also presented. 3D models have been generated from high resolution microtomography (1.4 $\mu\text{m}/\text{voxel}$) performed at the ESRF beamline ID-19. Due to high absorbance of tungsten, segmentation was a challenging task requiring to apply special segmentation filters. After that, adaptive meshing has been applied on the reconstructed microstructure. Planar models have been generated from high resolution SEM Images (0.2 $\mu\text{m}/\text{px}$). Numerical solution was calculated with Abaqus v6.9EF2 with extended XFEM capability for damage mechanics. Details of the demanding computational tasks are provided.

PS-W is a porous coating with promising thermomechanical properties for fusion applications [1]. Applied on surfaces directly exposed to a fusion plasma, it has to withstand high heat-flux and thermomechanical stress. An accurate micromechanical modelling is required to understand the complex mechanisms governing damage and failure of the coating.

[1] R. Neu et al. / Journal of Nuclear Materials 363–365 (2007) 52–59

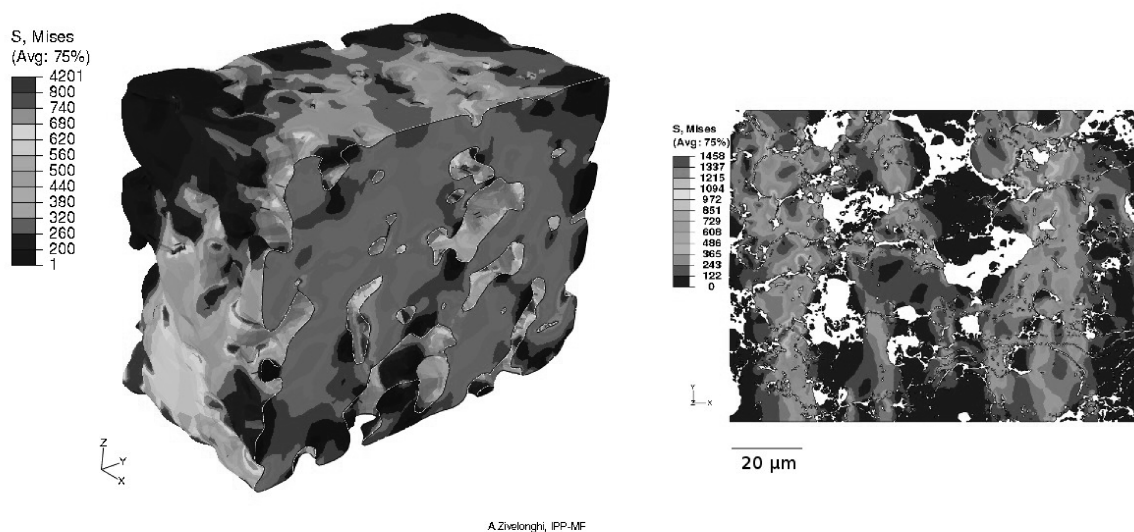


Fig. 1 Left: Calculated stress fields on a 3D region of VPS-W reconstructed from a tomographic measurement. Right: the same field calculated on a planar model derived from a high resolution SEM image of a polished cross-section

The Mechanism of Plastic Deformation Localization in Metals

Lev B. Zuev and Svetlana A. Barannikova

Institute of Strength Physics and Materials Science, SB RAS,
2/4 Akademichesky Ave., 634021 Tomsk, Russia
E-mail: lbz@ispms.tsc.ru; bsa@ispms.tsc.ru

ABSTRACT

An attempt is made at introducing into plasticity physics of quantum mechanics principles, which were developed on the base of evidence obtained in plastic flow localization investigations carried on for a range of metals and alloys that differ in chemical bond and crystal lattice type (BCC/FCC/HCP), structural state (single-crystal/polycrystalline) and deformation mechanisms (dislocation glide/twinning).

1. Introduction: Autowave plastic deformation

In the recent two decades exhaustive experimental investigations of plastic flow were carried out. It has been found that the plastic flow is prone to localization [1]. The process of plastic flow would exhibit this distinctive feature at the micro-, meso- and macro-scale levels. The macro-scale level is the most interesting and informative one for plastic flow physics.

For macro-scale plastic flow localization the following main relationships are established: (i) the plastic flow would exhibit a localization behavior from yield point to failure; (ii) a specific localized flow pattern would emerge at each plastic flow stage; (iii) the localization patterns occurring in the deforming solid are regarded as autowave processes (self-excited autowaves); (iv) the autowaves in question are related to processes involving self-organization of defects.

Using a specially developed speckle-photography technique [1], the kinematics of plastic flow localization autowaves was established. This is suggestive of the phenomenon having an intriguing nature. Evidently, the autowave characteristics, i.e. propagation velocities $10^{-5} < V_{aw} < 10^{-4} \text{ m}\cdot\text{s}^{-1} \ll V_{sound} \approx 3\cdot 10^3 \text{ m}\cdot\text{s}^{-1}$, wavelength $\lambda \approx 10^{-2} \text{ m}$ and frequency $10^{-3} < \omega < 10^{-2} \text{ Hz}$, differ in principle from those of elastic (ultrasound) waves [2] and plasticity waves [3].

2. Dispersion relation for localized plastic flow autowaves: experimental results

To gain a better understanding of the nature of autowave processes involved in plastic flow localization, one must consider the dispersion relation $\omega(k)$ (see Fig. 1), which was derived in [4] for the stages of easy glide and linear work hardening, i.e.

$$\omega(k) = \omega_0 \pm \alpha(k - k_0)^2, \quad (1)$$

where α , ω_0 and k_0 are constants, which depend on work hardening stage and kind of material. Note that for easy glide, $\alpha < 0$ and for linear work hardening, $\alpha > 0$. By substituting $\omega = \omega_0 \cdot \tilde{\omega}$ and $k = k_0 + \tilde{k} \cdot (\text{sign } \alpha \cdot \alpha / \omega_0)^{-1/2}$ into Equation (1), the latter is reduced to the canonical form $\tilde{\omega} = 1 \pm \tilde{k}^2$ (see Fig. 2); here $\tilde{\omega}$ is dimensionless frequency, \tilde{k} is

dimensionless wave number and $\text{sign}\alpha = +1$ for $\alpha > 0$ is a signum function of the

coefficient α . The dispersion relation of quadratic form satisfies the Schrödinger nonlinear equation [5] that is applied to self-organization processes occurring in nonlinear media. This is an undeniable proof that the process of plastic flow localization is involved in the self-organization of the deforming medium.

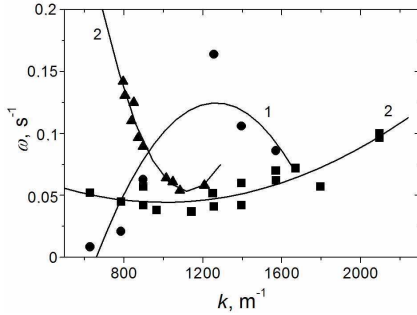


Figure 1. Dispersion relation $\omega(k)$ obtained for easy glide (1) and linear work hardening stages (2): single Cu, Sn, Fe (●), γ -Fe (■) crystal, polycrystalline Al (▲)

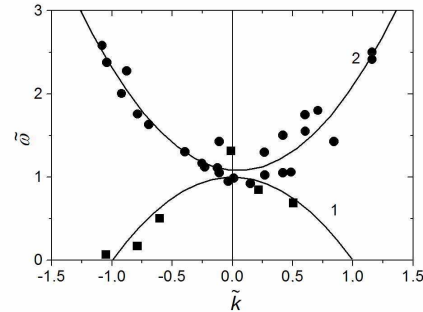


Figure 2. A generalized relation $\tilde{\omega}(\tilde{k})$ for easy glide (1) and linear work hardening stages (2): single γ -Fe crystal, polycrystalline Al

3. A correspondence between the localized plastic flow autowave and effective mass

Effective mass is conventionally found [6] from the dispersion law $\omega(k)$ as

$$m_{aw} = \hbar \left(d^2 \omega / dk^2 \right)^{-1}, \quad (2)$$

where $\hbar = h/2\pi$ is the Planck constant. The effective masses obtained for single γ -Fe crystals and polycrystalline Al are $m_{aw}^{(Fe)} = 0.6$ amu and $m_{aw}^{(Al)} = 0.1$ amu. Note that effective masses of the same magnitude can be calculated from the de Broglie equation [6] as

$$m_{aw} = h / \lambda V_{aw}. \quad (3)$$

Similar calculations were performed by addressing autowaves [7]. To test the validity of this idea, m_{aw} values were calculated from (3), using the autowave characteristics obtained for a number of metals and alloys [1]; the results obtained are listed in the Tab. 1. Apparently, the resulting values have about the same scale, i.e. $m_e \ll m_{aw} \approx 1$ amu (here m_e is the rest mass of electron; 1 amu = $1.67 \cdot 10^{-27}$ kg is atomic mass unit). The average mass calculated from (3) for the same metals is $\langle m_{aw} \rangle = (2.2 \pm 0.3) \cdot 10^{-27}$ kg = 1.32 ± 0.2 amu.

Now volume is calculated as $\Omega = m_{aw} / \rho$ (here m_{aw} is effective mass and ρ is metal density); hence effective size $d_\Omega = \Omega^{1/3}$ (see the Table). The results obtained are close to the ion radii, r_{ion} , of the investigated metals [8], which is validated by the ratios d_Ω / r_{ion} listed in the Tab. 1. For all the investigated metals and alloys, the average $\langle d_\Omega / r_{ion} \rangle = 0.51 \pm 0.1$. Normalization of m_{aw} values was performed in atomic masses, M_{at} ; then dimensionless mass $s = m_{aw} / M_{at} \ll 1$ was introduced for a range of metals. As is seen from Fig. 3, the latter quantity grows linearly with increasing electron concentration n [9] as

$$s = s_0 + \kappa \cdot n = 1.6 \cdot 10^{-2} + 0.17 \cdot 10^{-2} \cdot n. \quad (4)$$

On the base of the above the existence of a certain quasi-particle is hypothesized, which corresponds to localized plastic deformation autowaves generated in the deforming solid; the quasi-particle has macro-scale mass $0.5 \leq m_{aw} \leq 2$ amu and effective size $d_\Omega \approx r_{ion}$ as

determined from (3) using localized deformation macrocharacteristics. The above approach is traditionally used in condensed-state physics [10]. This enables one to unambiguously relate the macroparameters of the localization process to crystal lattice characteristics of the deforming metal.

Table 1. Microscopic characteristics calculated from the data on localized plastic flow autowaves

Metal	$\lambda \cdot 10^3$	$V_{aw} \cdot 10^5$	m_{aw}	M_{at}	$s \cdot 10^2$	n	$\rho \cdot 10^{-3}$	$\Omega \cdot 10^{27}$	$d_{\Omega} \cdot 10^9$	$r_{ion} \cdot 10^9$	d_{Ω}/r_{ion}
	(m)	(ms ⁻¹)	(amu)	(amu)			(kgm ⁻³)	(m ³)	(m)	(m)	
Cu	4.5	8.0	1.1	63	1.74	1	8.9	0.21	0.059	0.128	0.46
Al	7.2	11	0.50	27	1.87	3	2.7	0.31	0.068	0.143	0.48
Zr	5.5	3.5	2.05	91	2.24	4	6.5	0.53	0.081	0.16	0.50
Ti	7.0	5.0	1.1	48	2.3	4	4.5	4.2	0.075	0.146	0.51
V	4.0	7.0	1.42	51	2.81	5	6.1	0.33	0.069	0.135	0.51
γ -Fe	5.0	5.1	1.76	56	2.81	8	7.9	0.33	0.069	0.127	0.54
α -Fe	4.3	5.2	1.77	56	3.0	8	7.9	3.75	0.072	0.127	0.57
Ni	3.5	6.0	0.89	59	3.24	10	8.9	0.32	0.068	0.125	0.54

4. A two-component model of plastic flow

The macro- and micro-scale quantities under discussion might differ crucially in spatial scales in the range $10^6 < \lambda/r_{ion} < 10^7$. Nonetheless, it is established that *the product of the macro-characteristics of autowave processes, i.e. $\lambda \cdot V_{aw}$, and that of the micro-characteristics of a respective metal, i.e. $r_{ion} \cdot V_{\perp}$, are related linearly as*

$$\lambda \cdot V_{aw} \approx \zeta_{Me} \cdot r_{ion} \cdot V_{\perp}, \quad (5)$$

where V_{\perp} is the rate of transverse elastic waves [11]. The numerical factor differs in the range $0.52 \leq \zeta_{Me} \leq 0.82$ for various metals, with the average $\langle \zeta \rangle \approx 0.62$. The physical meaning of the latter factor might be deduced from (5) represented as

$$m_{aw} = h/\lambda V_{aw} \approx \zeta_{Me}^{-1} \cdot h/r_{ion} V_{\perp}, \quad (6)$$

where $h/r_{ion} V_{\perp} \equiv m_{ph}$ is phonon mass. From Fig. 4 follows that $m_{aw} \approx 1.6m_{ph}$, i.e.

$$1.5m_{ph} \leq m_{aw} \leq 2m_{ph}. \quad (7)$$

It corresponds to the mechanism of dislocation generation due to the superposition of phonons, which was proposed in [12]. Thus a significant role is assigned to the lattice characteristics in the evolution of localized plastic flow autowaves.

The above is not a mere formalization of the relationship between the parameters of plastic flow localization on the one hand and the acoustic characteristics of the deforming medium on the other. This places emphasis on the role of the phonon subsystem in the evolution of localized plastic deformation, which involves (i) relaxation acts due to the motion of dislocations, dislocation ensembles and localized plastic flow autowaves and (ii) generation of elastic waves due to acoustic emission, i.e. elastic strain redistribution involving large- and small-scale relaxation events.

Generally, the above phenomena are studied independently. However, on the base of the concept proposed in [13] these might be grouped together to consider a system undergoing self-organization and resultant separation into related subsystems, i.e. an information and a dynamic one. Acoustic emission signals serve as deformation carriers in the deforming system. These are generated by relaxation shears, thereby initiating redistribution of elastic strain fields to cause new shears in the dynamic subsystem of mobile defects.

Apparently, relation (6) formalizes the connection between the kinetic characteristics of the information and dynamic subsystems, i.e. elastic wave propagation velocity and dislocation motion rate in the vicinity of stress concentrators, respectively. In the frame of the proposed

model, acoustic emission impulses would control localized plastic flow development, while acoustic impulses having sufficiently high energy would activate new plasticity events.

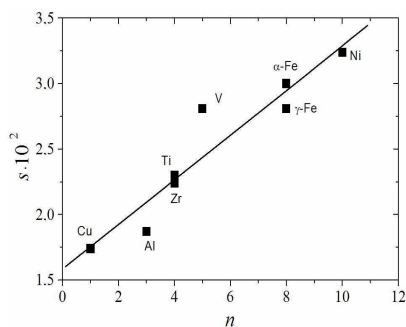


Figure 3. Dimensionless mass s as a function of electron concentration n ; correlation coefficient ~ 0.95

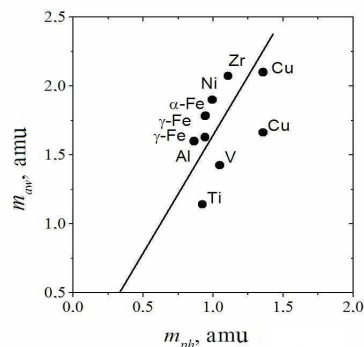


Figure 4. A correlation the masses of a quasi-particle of localized plastic flow and a phonon; correlation coefficient ~ 0.95

5. Conclusion

When considered in the context of the proposed model, the relation between localized deformation nuclei is attributed to the exchange phonon interaction. In this scenario it appears reasonable to assume that to the autowave of localized deformation corresponds a quasi-particle whose characteristics are determined by autowave parameters.

Further development of the proposed concept would enable one to group localized plastic flow together with such phenomena as superfluidity and superconductivity, which are taken to be macro-scale manifestations of the medium's quantum properties.

Acknowledgements

This work was partly supported by the grant of the RFBR (09-08-00213-a).

References

- [1] Zuev L. B., Danilov V. I. and Barannikova S. A. *Plastic Flow Macrolocalization Physics* (Novosibirsk, Nauka Publishers, 2008).
- [2] Newnham R. E. *Properties of Materials* (Oxford, University Press, 2005).
- [3] Kolsky H. *Stress Waves in Solids* (New York, Dower Publications, 2003).
- [4] Barannikova S. A. and Zuev L. B. *Technical Physics* **35**, 558-562 (2009).
- [5] Scott A. *Nonlinear Science* (Oxford, University Press, 2003).
- [6] Landau L. D. and Lifshits E. M. *Quantum Mechanics* (London, Pergamon Press, 1977).
- [7] Zuev L. B. *International Journal of Solids and Structures* **42**, 943-949 (2005).
- [8] Pearson W. B. *The Crystal Chemistry and Physics of Metals and Alloys* (New York, Wiley, 1972).
- [9] Cracknell A. P. and Wong K. C. *The Fermi Surface* (Oxford, Clarendon Press, 1973).
- [10] Kaganov M. I. and Lifshits I. M. *Quasiparticles* (Moscow, Mir Publishers, 1979).
- [11] Anderson O. L. in: *Physical Acoustic III*, Part B, 62-121 (New York, Academic Press, 1965).
- [12] Umezawa H. and Matsumoto H. *Thermo Field Dynamics and Condensed States* (Amsterdam, North-Holland Publ. Comp., 1982).
- [13] Kadomtsev B. B. *Physics-Uspekhi* **165**, 967-981 (1995).